



# **Rejection of organic micropollutants with high pressure membranes (NF/RO)**

**A.R.D. Verliefde**



# Table of Contents

1. Introduction	1
2. Rejection of uncharged organic solutes (Influence of steric and solute-membrane (hydrophobic) interactions)	25
3. Rejection of charged organic solutes (Influence of electrostatic interactions)	84
4. Rejection in full-scale plants	136
5. Influence of membrane fouling	178
6. Practical applications	230
Conclusions and recommendations	277
List of publications	285
Curriculum vitae	289



# **Chapter 1:**

## **Introduction**

Parts of this chapter were based on:

A.R.D. Verliefde, E.R. Cornelissen, G.L. Amy, B. Van der Bruggen and J.C. van Dijk, Priority organic micro pollutants in water sources in Flanders and The Netherlands, and assessment of removal possibilities with nanofiltration, *Environmental Pollution*, 146 (1) (2006) 281.

## **1. The issue of organic micropollutants in drinking water sources**

During the last few decades, the drinking water industry has become increasingly concerned about the occurrence of organic micropollutants in source waters for the drinking water supply. The term micropollutants is used, since the concentrations of the pollutants in the source waters are often in the ng/l up to the µg/l-range. In the 1980's, Dutch and Flemish drinking water companies were faced with increasing pesticide concentrations in surface waters, due to high levels of use by farmers (but also private use – often excess doses are used, unregulated) and consequent run-off from farmlands. A two-track approach was used to solve this problem: pressure was exerted by the government on farmers and producers to develop alternatives to the use of pesticides, and drinking water barriers were improved by implementing activated carbon filtration.

In the late 1990's, however, attention shifted from pesticides towards other organic micropollutants: pharmaceuticals, hormones, personal care products, plasticizers, flame-retardants, fuel additives and other industrial organic pollutants (e.g. bisphenol-A) were being found in increasing concentrations in ground- and surface water. This was partly due to the improving methods of analysis and the lower detection limits, but also due to an increased production and consumption. Some of the pollutants mentioned above are classified as “endocrine disrupting compounds (EDCs)”, because of their adverse effect on the hormonal system of human and animal life [1]. Others are known (or suspected) carcinogens. Therefore, ingestion of these substances might be harmful. Even though the World Health Organization (WHO) and/or the U.S. Environmental Protection Agency (E.P.A.) have issued guidelines for humanly safe drinking water concentrations for several pollutants, health effects

related to the consumption of drinking water containing a cocktail of organic micropollutants are still unknown, or difficult to predict. Therefore, removal of these pollutants in the drinking water treatment is desirable. However, measurements have indicated that removal of these pollutants in the current drinking water treatment is not always effective [2,3], partly because several newly detected pollutants are small and polar, making them very water soluble, very mobile in the environment, and extremely difficult to remove in the treatment [4-6].

Table 1.1 lists some selected micropollutants, which are found (in relatively high concentrations) in surface waters in the Netherlands, Belgium and the European Union. The table shows maximum incidental concentrations found in surface water and drinking water. For some compounds, a guideline or the statutory value for the human health limit are also given. This limit corresponds to the maximum concentration allowable in drinking water without any risk to human health, based on an average consumption of 2 liters of bottled water per day for a life-span of 60 years.

As can be seen from Table 1.1, concentrations of several pollutants in surface water exceed the human health limits, indicating the necessity of a robust drinking water treatment to safeguard the consumer from potential health risks.

It is also apparent that concentrations of most organic micropollutants in the drinking water are indeed much lower than the concentrations found in the surface water. However, some micropollutants (e.g. some pharmaceuticals [3]) are still found in trace amounts in the finished drinking water.



Compound	Surface water (ng/l)			Drinking water (ng/l)	
	Flanders	the Netherlands	EU	the Netherlands	HHL (ng/l)
<b>Hormones</b>					
17 $\beta$ -estradiol	2.3	1.0	2.3	<0.4	7
17 $\alpha$ -ethinylestradiol	-	0.4	<1	<0.4	7
estrone	21.7	3.4	21.7	<0.4	-
<b>Industrial chemicals</b>					
bisphenol-A	580	22 000	22 000	<10	100 000
phthalates	10 300	200 000	200 000	2100	-
PCBs	<7	20	80	<10	-
nonylphenolpolyethoxylates	-	2600	2600	1500	-
MTBE	-	62 000	62 000	<1000	9 x 10 <sup>6</sup>
NDMA	-	<10	<10	2	12
<b>Pesticides</b>					
atrazine	13 000	400	13 000	30	600
simazine	19 000	50	19 000	<10	1000
glyphosate	-	450	1000	> 100	10000
carbendazim	> 2000	1480	> 2000	u.d.	200
<b>Pharmaceuticals</b>					
sulfamethoxazole	-	90	1700	40	75 000
carbamazepine	-	500	2000	90	50 000
acetylsalicylic acid	-	65	-	122	25 000
iopamidol	-	470	470	69	415 x 10 <sup>6</sup>
amidotrizoic acid	-	290	300	83	250 x 10 <sup>6</sup>

Table 1.1 - Maximum incidentally measured concentrations in surface and drinking water of selected organic micropollutants (u.d.: under detection limit; - : no data; HHL= human health limit) [2, 6, 7-12]

In an attempt to counter the unwanted presence of organic micropollutants in the source waters for the drinking water production, the European Water Framework Directive (WFD) [13] was adopted in the year 2000. The WFD is the most substantial piece of legislation on European waters yet. It requires that all inland and coastal waters within defined river basin districts must reach at least a “good status” by 2015 and defines how this should be achieved through the establishment of environmental objectives and ecological targets for surface waters. The WFD sets ambitious goals

for the surface and ground waters, consisting of strict standards for chemical and ecological parameters. These standards also include the presence of certain organic micropollutants and are generally based on the survival/sustainability of aquatic life. This is important since several studies have shown the causal effect of endocrine disrupting compounds on e.g. deformation of aquatic animals and feminization of male fish in certain rivers (Figure 1.1).

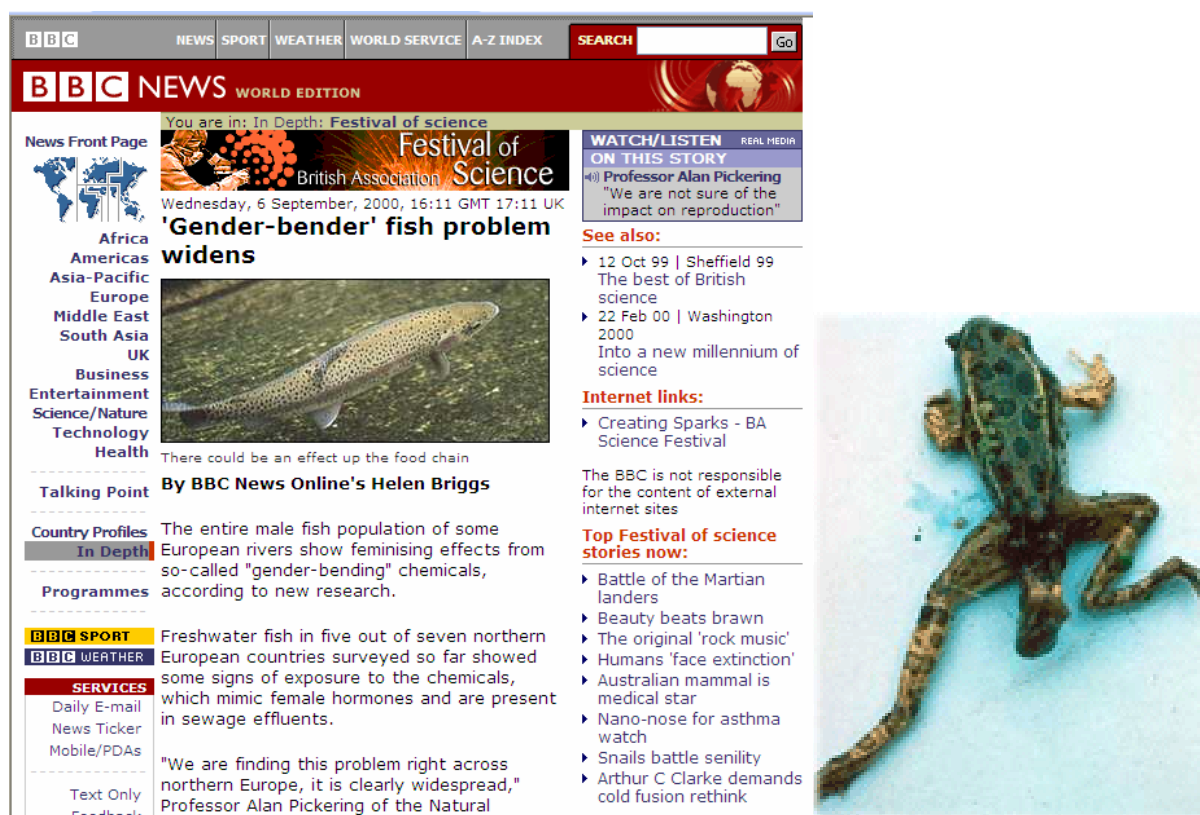


Figure 1.1 – Problems arising due to endocrine disrupting chemicals in the aquatic environment (left: “gender-bender” (i.e. feminization) of male fish; right: a baby frog with 3 legs)

However, it has to be duly noted that ground- and surface water are not only ecologically important, but they also play an important role as source waters for the production of drinking water. Serious lobbying is going on at the moment to incorporate this aspect (which is now underrepresented) into the WFD. It also has to

be noted that, even though the WFD provides an admirable and essential first step in handling the problem of organic micropollutants in the environment, it is faced with an enormous amount of information, and an enormous amount of substances involved (ranging from pesticides, to pharmaceuticals and EDCs). Therefore, it will become a necessity to make priorities and focus attention on the most dangerous or most omnipresent pollutants.

In order to better represent the importance of the drinking water function of surface and ground waters in the WFD, it is essential to narrow the field down to the most urgent problems.

For the presence of organic micropollutants in ground- and surface waters for the production of drinking water, for example, prioritization will have to be based on the presence of the pollutants, but also on the effects of the pollutants (e.g. suitability for human consumption), and on the effectiveness of their removal. One possible scheme for this prioritization is given in Figure 1.2.

This scheme is thus focused on four essential aspects: the human toxicity of the pollutants, their removal in the current drinking water treatment, their occurrence in and discharge towards the environment, and the public opinion on their presence (i.e. people prefer not to have any pharmaceutical residues in their drinking water, even though there is not always a direct risk to human health).

Toxicology of the pollutants can not be changed and a decrease in their occurrence can only be realized through governmental measures. Changing the public opinion through campaigns is not an option, since the consumer's confidence in the quality of the drinking water is a priority for drinking water companies.

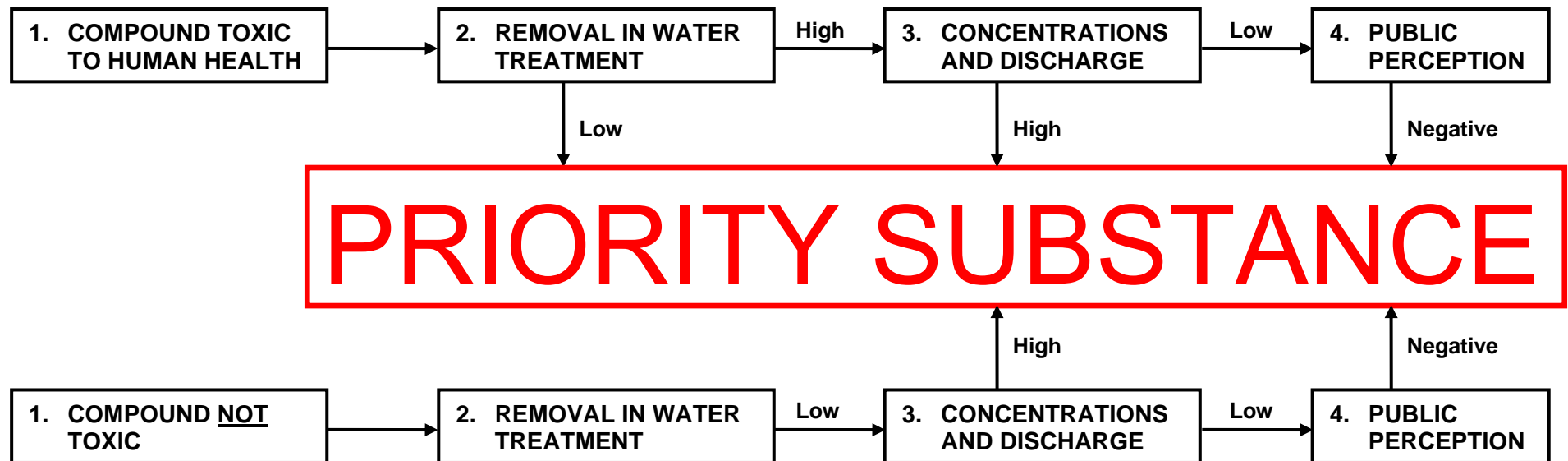


Figure 1.2 – Possible scheme for prioritization of organic micropollutants in surface- and groundwaters for drinking water production

Therefore, research on the removal of organic micropollutants in the drinking water treatment becomes a necessity.

As was shown before, the present drinking water treatment is not flawless, and (studies on) new and advanced treatment techniques are necessary.

## **2. Nanofiltration (NF) and reverse osmosis (RO)**

One of the new and advanced techniques in drinking water treatment is membrane filtration. Membranes can be seen as highly efficient, nano-engineered sieves. Membrane processes in drinking water treatment are used when water of high quality is desired. A membrane process can be defined as a separation process where a feed stream (containing pollutants that have to be removed), is split into a clean water stream (the permeate) and a concentrated stream (the concentrate) (Figure 1.3). According to the driving force that is used to produce the clean water, several membrane processes can be distinguished. However, in drinking water treatment, pressure is mostly used as driving force. When a pressure difference is applied over the membrane, the feed stream is partly “pushed” through the membrane. This results in the removal of certain solutes, and the type of solutes that is removed depends on the “pore size” of the membrane. The clean water stream (the permeate) that is thus produced is the desired stream in drinking water treatment applications. However, the removal of the solutes results in an accumulation of these solutes on the feed side of the membrane, resulting in a concentrated stream that still has to be disposed of. This is one of the major drawbacks of membrane processes: pollutants

are not destroyed, they are only separated from the product, and the concentrated stream can not always be discharged to the environment.

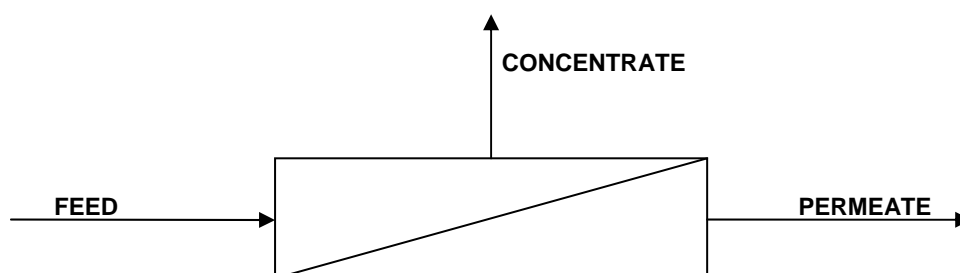


Figure 1.3 – Schematic representation of a membrane process: the feed stream is split into a “clean” stream (the permeate) and a “concentrated” stream (the concentrate)

Depending on the “pore size” of the membranes, four different pressure-driven membrane processes can be distinguished. The membranes with the smallest pore size are called reverse osmosis membranes, and they can even separate dissolved salts from water molecules. Therefore, they are often used for the desalination of seawater.

If the size of the organic pollutants in Table 1.1 is compared to the pore sizes of the membrane processes in Table 1.2, it can be concluded that only nanofiltration and reverse osmosis can be applied to remove organic micropollutants. The molecular weight (or, more appropriate, the molar mass) values of organic micropollutants are often around 200-300 g/mol, whereas the Molecular Weight Cut-Off (MWCO, the molar mass of a solute that is removed for 90% by the membrane) of NF and RO membranes is also in that region. Therefore, NF/RO membranes should provide high removal efficiencies for organic micropollutants.

	Applied pressure	Permeate flux range (l/(m <sup>2</sup> .h.bar))	pore size (nm)	Application
<b>Microfiltration (MF)</b>	0.1 – 2 bar	> 50	> 100	Particle removal
<b>Ultrafiltration (UF)</b>	< 5 bar	10 – 50	5 – 100	Particle removal, virus removal, removal of macromolecules
<b>Nanofiltration (NF)</b>	3 – 15 bar	1.4 – 12	0.5 – 5	Removal of multivalent salts and small organic molecules
<b>Reverse osmosis (RO)</b>	7 – 100 bar	0.05 – 4	0.1 – 1	Removal of all salts and small organic molecules

Table 1.2 – Different pressure driven membrane processes (often used in drinking water treatment)

However, research shows that removal of some organic micropollutants still seems to be incomplete and traces may still be detected in the permeate of NF and RO installations [14].

In order to incorporate the effects of NF/RO treatment in the drinking water treatment on the removal of organic micropollutants in the prioritisation scheme in Figure 1.2, it would be ideal if the removal of any given micropollutant by NF/RO could easily be predicted, based on the simple information of the chemical structure of the micropollutants.

Removal of solutes by NF/RO is usually referred to as rejection. Rejection of a given solutes is defined as:

$$R_i = 1 - \frac{c_{p,i}}{c_{f,i}} \quad (1.1)$$

where  $R_i$  is the rejection of the solute  $i$  (in %) and  $c_{p,i}$  and  $c_{f,i}$  are the concentrations of solute  $i$  in the permeate and the feed, respectively.

Gradually, some understanding of organic micropollutant rejection mechanisms on NF/RO has begun to emerge, which now includes the perspective of solute-membrane interactions. In general, three major solute-membrane interactions are distinguished: steric hindrance (sieving effect), electrostatic interactions and hydrophobic-hydrophobic/adsorptive interactions. These solute-membrane interactions are determined by *solute properties* (e.g., molecular weight/size, charge, and hydrophobicity), *membrane properties* (e.g. molecular weight cut-off, pore size, surface charge and hydrophobicity), *operating conditions* (e.g., pressure, flux, and recovery) and *feed water composition* (e.g. pH, temperature, inorganic balance). In addition, membrane fouling by natural organic matter (NOM) or particulate matter may alter the membrane surface properties and thus the solute-membrane interactions.

Even though numerous studies have been carried out to study transport mechanisms of organic solutes through NF and RO membranes and it is known that the solute-membrane interactions all contribute to the eventual rejection of organic solutes, less knowledge is available on the development of models that convey a fundamental understanding and a simple quantification of these governing phenomena. This thesis will contribute to the construction of such models, by gaining more insight in the governing removal mechanisms. Ideally, this type of models should be based on readily available knowledge about solute- and membrane properties that affect them [14]. As indicated above, it would be ideal if the removal of any given micropollutant by NF/RO could easily be predicted, based on the simple information of the chemical structure of the micropollutant.



### 3. Rejection mechanisms for organic micropollutants in NF/RO

Most studies on the rejection of organic micropollutants have focused on neutral solutes (and in particular pesticides) [15-28].

For uncharged solutes, the literature mentions two main solute-membrane interactions that may influence solute rejection: a steric hindrance (~ sieving) effect between large solutes and the membrane matrix, and hydrophobic (Van der Waals) interactions between hydrophobic solutes and hydrophobic membrane surfaces [29-37].

Steric hindrance is mainly determined by the size of the solute and the size of the membranes pores: solutes larger than the membrane pores (or with a molar mass above the MWCO) are well rejected; solutes smaller than the membrane pores (or with a molar mass lower than the MWCO) can permeate through the membrane more easily (Figure 1.4). This generally leads to a typical S-shaped curve if rejection is plotted as a function of the solute molar mass or the solute size.

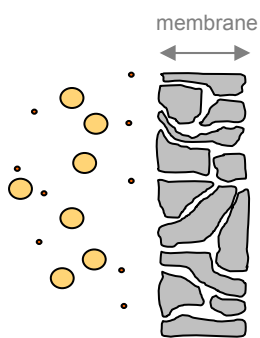


Figure 1.4 – Size exclusion effect on rejection of organic micropollutants with NF/RO membranes

For hydrophobic solutes with hydrophobic membranes, hydrophobic-hydrophobic (Van der Waals) interactions between the solutes and the membranes may also have

an influence on the rejection, in addition to the steric hindrance. Experiments have shown [31] that hydrophilic molecules are better rejected compared to hydrophobic molecules of similar size. This is explained by the hydrophobic-hydrophobic interactions: hydrophobic solutes can partition into the membrane matrix more easily (a.o. by the formation of H-bonds), and consequently diffuse to the permeate side. Hydrophobic solutes are thus transported to the permeate side of the membrane more easily, explaining the lower rejection values.

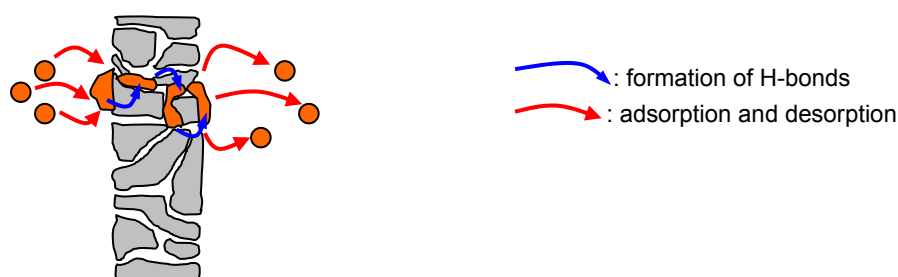


Figure 1.5 – Influence of hydrophobic-hydrophobic (Van der Waals) interactions between solute and membrane on rejection of organic micropollutants with NF/RO membranes

Hydrophobic solutes can also adsorb onto hydrophobic membranes and into the membrane pores [35, 38-41]. This adsorption can affect solute rejection: several studies have shown that adsorption of hydrophobic compounds onto hydrophobic membranes can lead to a temporary overestimation of the observed rejection [42-44]. To obtain an accurate evaluation of membrane performance, saturation of the membrane with the compound of interest must be accomplished: initial rejection values of hydrophobic solutes can be high due to adsorption, but rejection generally decreases to an equilibrium value when saturation of the membrane is reached (i.e. breakthrough is observed). After saturation of the membranes is complete, the lower rejection for hydrophobic solutes compared with hydrophilic solutes is observed, which is due to the higher partitioning of the hydrophobic solutes, as mentioned

above. Hydrophobicity of organic molecules is usually expressed as the logarithm of the octanol-water partition coefficient,  $\log K_{ow}$ . Molecules with  $\log K_{ow} > 2$  are usually referred to as hydrophobic. Hydrophobicity of NF/RO membranes is usually characterized by the contact angle ( $\theta$ ) with a water droplet on the membrane surface. Studies have shown that membranes with larger contact angles could adsorb more mass per unit area of organic compound than membranes with smaller contact angles, and hydrophobic molecules are more adsorbed than hydrophilic molecules [45].

Even though plenty of literature data exist that explain the lower observed rejection values of hydrophobic solutes by increased solute-membrane affinity, this effect was never quantified and the separate contributions of steric and hydrophobic interactions to the rejection have never been distinguished.

This thesis will present different new concepts to distinguish the contributions of steric and hydrophobic interactions on rejection. Moreover, a mathematical model will be presented and validated that is able to quantify the influence of both interactions.

Most NF/RO membranes are negatively charged at neutral pH due to the dissociation of acidic functional groups on the membrane surface. Therefore, in addition to separation mechanisms for neutral solutes, electrostatic interaction between charged organic solutes and the charged membrane surface can also influence rejection of organic micropollutants. Most studies on electrostatic interactions have reported an increase in rejection of negatively charged organic solutes due to electrostatic repulsion between the negatively charged membrane and the negatively charged organic solute [29, 32-35]. This high rejection, however, is dependent on feed water pH, since both membrane surface charge (through the dissociation of the functional

groups on the membrane surface as a function of their  $pK_a$ ) and organic solute charge (as a function of the solute  $pK_a$ ) vary with varying pH [34].

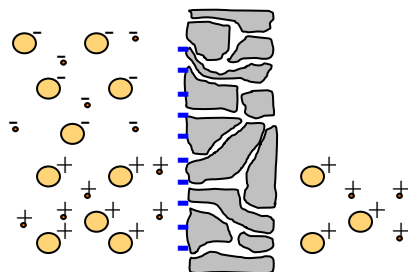


Figure 1.6 – (Hypothetical) influence of electrostatic interactions on rejection of organic micropollutants with NF/RO

Several numerical models have been suggested to explain the electrostatic effects on the rejection of inorganic ions [46-48]. These models always account for the Donnan exclusion effect: if the co-ion of a certain salt (the ion with a charge similar to the membrane surface charge) can not pass the membrane due to electrostatic repulsion, then the counter-ion is also rejected in order to counteract the potential difference that would arise between the different sides of the membrane if the counter-ion would not be rejected. One of the innovative hypotheses in this thesis states that this Donnan exclusion mechanism does not play a role in rejection of organic solutes, and that rejection of positively charged organic solutes will be lower than for negatively charged organic solutes, due to charge attraction between the negatively charged membrane surface and the positively charged organic solute. This has never been studied before in literature, since most studies have focused, as mentioned before, only on effects of electrostatic repulsion between the membrane and organic ions carrying a similar charge. A simplified tool to model the effect of

electrostatic interactions on the rejection of both positively and negatively charged organic solutes will be constructed in this thesis and validated with experimental data.

#### **4. Goal and overview of the thesis**

This thesis will critically review the previous work on rejection of organic micropollutants with NF/RO and will compare this with new insights, gathered during this study. The final goal is the construction of a simple model that can explain nanofiltration/reverse osmosis rejection of organic micropollutants, based on their chemical structure (and thus their physico-chemical parameters).

In the second chapter of this thesis different rejection models for uncharged solutes will be developed. In contrast to previous models constructed in literature, the models constructed in this thesis will incorporate not only the effect of solute size (and thus the effect of steric hindrance), but also the influence of solute-membrane affinity (solute-membrane hydrophobic-hydrophobic (Van der Waals) interactions) on rejection.

The third chapter of this thesis will address the effects of electrostatic interactions on the rejection of charged organic micropollutants with (charged) NF/RO membranes.

The hypothesis that attraction of positively charged organic solutes towards the membrane surface leads to a decrease in rejection of these positively charged solutes will be tested. Moreover, a simple tool to predict the influence of charge interactions on rejection of positively and negatively charged organic solutes will be constructed and validated. The influence of selected feed water parameters will also be investigated.

In the fourth chapter, both models for uncharged and charged organic solutes will be combined into a general transport model for organic solutes on NF/RO membranes. This model will be expanded to a model for full-scale installations. The full-scale rejection model that is thus constructed, is then validated by comparing modelled rejection values to experimentally obtained rejection values on a 2-stage pilot nanofiltration unit, consisting of 18 4-inch membrane modules.

In a fifth chapter, the influence of the feed water matrix and membrane fouling on NF/RO rejection of organic micropollutants will be investigated. By using different types of pre-treatment before the nanofiltration of surface water, different types of membrane fouling will be realised, and the influence of these fouling layers on rejection of organic micropollutants will be compared with rejection values obtained on unfouled membranes, to gain more insight in how fouling can affect rejection. This is important, since NF/RO installations in full-scale applications are usually susceptible to membrane fouling.

The last chapter of this thesis will deal with practical applications of NF/RO treatment for the removal of organic micropollutants. For different surface waters, the effect of NF/RO treatment, followed by an activated carbon filtration for the removal of organic micropollutants will be tested and explained. NF/RO and activated carbon filtration are expected to be complimentary, since the removal of hydrophobic solutes on NF/RO is usually lower than for hydrophilic solutes, whereas activated carbon filtration usually offers a higher removal efficiency for more hydrophobic solutes and a lower removal of hydrophilic solutes. Moreover, it is expected that the combination of NF/RO with subsequent activated carbon filtration will result in less competition of natural organic matter (NOM) with organic micropollutants for adsorption sites on the

activated carbon since the NOM is removed by the NF/RO step, making the activated carbon process more efficient.

In the second part of the last chapter, some novel membrane materials will be tested for their removal capabilities for organic solutes. These novel membranes were initially developed to increase the water fluxes through the membrane. This was done by making the membranes more hydrophilic, by the incorporation of nano-engineered super-hydrophilic particles in the top layer. This thesis will investigate and discuss whether the increased hydrophilicity also results in an improved rejection of hydrophobic solutes (since less solute-membrane affinity is expected).

## References

- [1] S. Barlow, R.J. Kavlock, J.A. Moore, S.L. Schantz, D.M. Sheehan, D.L. Shuey and J.M. Lary, Teratology society public affairs committee position paper: Developmental toxicity of endocrine disruptors to humans, *Teratology* 60 (1999) 365.
- [2] M. Mons, A.C. Hoogenboom, and T.H.M. Noij, Pharmaceuticals and drinking water supply in the Netherlands, BTO report 2003.040 (2003) Kiwa Water Research, Nieuwegein, the Netherlands.
- [3] J.F.M. Versteegh, N.G.F.M. van der Aa and E. Dijkman, Geneesmiddelen in drinkwater en drinkwaterbronnen – Resultaten van het meetprogramma 2005/2006, RIVM rapport 703719016/2007 (2007), RIVM, Bilthoven, the Netherlands
- [4] W. Siegers, Verwijdering van NDMA in de drinkwaterzuivering, BTO-report 2004.034 (2004), Kiwa Water Research, Nieuwegein, the Netherlands
- [5] F. Soroushian, Y. Shen, and M. Wehner, Evaluation and pilot testing of advanced treatment processes for NDMA removal and reformation prevention, Annual Conference Proceedings (2001), American Water Works Association, Denver CO, USA.
- [6] G.A. van den Berg and L.M. Puijker, Voorkomen van MTBE in het Nederlandse oppervlaktewater, KWR-report 04.099 (2005) Vewin/Kiwa Water Research, Nieuwegein, the Netherlands.
- [7] G.A. van den Berg, S. de Rijk, A. Abrahamse, L.M. Puijker, Bedreigende stoffen voor drinkwater uit de Maas, KWR-report 07.043 (2007), Kiwa Water Research, Nieuwegein, the Netherlands.
- [8] GWRC, 2003. Occurrence of EDC in water systems. Global Water Research Coalition, London.
- [9] Mons, M., Samenvatting informatie geneesmiddelen, BTO-report 2004.004 (2004), Kiwa Water Research, Nieuwegein.
- [10] [www.rivm.nl](http://www.rivm.nl)
- [11] Vlaamse Milieumaatschappij, Jaarrapport Water 2006 (2007) Vlaamse Milieumaatschappij, Erenbodegem, Belgium
- [12] Witters, H., Berckmans, P., Vangenechten, C., Comhaire, F., Dhooge, W., Hens, L., Verspecht, A., De Wit, J., Hoebeeck, A., Lafère, J., Opsporen van de verspreiding en effecten van stoffen met hormoonverstorende werking in Vlaamse waters (2003), Vlaamse Gemeenschap/Vlaamse Milieumaatschappij



- [13] [http://ec.europa.eu/environment/water/water-framework/index\\_en.html](http://ec.europa.eu/environment/water/water-framework/index_en.html)
- [14] C. Bellona, J.E. Drewes, P. Xu and G. Amy, Factors affecting the rejection of organic solutes during NF/RO treatment – a literature review. *Water Research*, 38 (2004) 2795.
- [15] Y. Kiso, A. Mizuno, R.A. Adawiah binti Othman, Y.-J. Jung, A. Kumano and A. Arijji, Rejection properties of pesticides with a hollow fiber NF membrane (HNF-1). *Desalination*, 143 (2002) 147.
- [16] S.-S. Chen, J.S. Taylor, L.A. Mulford and C.D. Norris. Influences of molecular weight, molecular size, flux, and recovery for aromatic pesticide removal by nanofiltration membranes. *Desalination*, 160 (2004) 103.
- [17] K. Kosutic, L. Furac, L. Sipos and B. Kunst. Removal of arsenic and pesticides from drinking water by nanofiltration. *Separation and Purification Technology*, 42 (2005) 137.
- [18] P. Berg, G. Hagmeyer and R. Gimbel. Removal of pesticides and other micropollutants by nanofiltration. *Desalination*, 113 (1997) 205.
- [19] B. Van der Bruggen, J. Schaep, W. Maes, D. Wilms and C. Vandecasteele. Nanofiltration as a treatment method for the removal of pesticides from ground waters. *Desalination*, 117 (1998) 139.
- [20] J.A.M.H. Hofman, E.F. Beerendonk, H.C. Folmer and J.C. Kruithof. Removal of pesticides and other micropollutants with cellulose-acetate, polyamide and ultra-low pressure reverse osmosis membranes. *Desalination*, 113 (1997) 209.
- [21] K.M. Agbekodo, B. Legube and S. Dard. Atrazine and simazine removal mechanisms by nanofiltration: influence of natural organic matter concentration. *Water Research*, 30 (11) (1996) 2535.
- [22] Y. Zhang, C. Causserand, P. Aimar and J.P. Cravedi. Removal of bisphenol A by a nanofiltration membrane in view of drinking water production. *Water Research*, 40 (2006) 3793.
- [23] C. Causserand, P. Aimar, J.P. Cravedi and E. Singlande. Dichloroaniline retention by nanofiltration membranes. *Water Research*, 39 (2005) 1594.
- [24] Y. Zhang, B. Van der Bruggen, G.X. Chen, L. Braeken and C. Vandecasteele. Removal of pesticides by nanofiltration: effect of the water matrix. *Separation and Purification Technology*, 38 (2004) 163.
- [25] K. Majewska-Nowak, M. Kabsch-Korbutowicz and M. Dodz. Effects of natural organic matter on atrazine rejection by pressure driven membrane processes. *Desalination*, 145 (2002) 281.

- [26] Y.J. Jung, Y. Kiso, R.A. Adawih binti Othman, A. Ikeda, K. Nishimura, K.-S. Min, A. Kumano and A. Arijj. Rejection properties of aromatic pesticides with a hollow-fiber NF membrane. *Desalination*, 180 (2005) 63.
- [27] E.C. Devitt, F. Duceillier, P. Cote and M.R. Wiesner. Effects of natural organic matter and the raw water matrix on the rejection of atrazine by pressure-driven membranes. *Water Research*, 32 (9) (1998) 2563.
- [28] K.V. Plakas, A.J. Karabelas, T. Wintgens and T. Melin. A study of selected herbicides retention by nanofiltration membranes – The role of organic fouling. *Journal of Membrane Science*, 284 (2006) 291.
- [29] Y. Yoon, P. Westerhoff, S.A. Snyder and E.C. Wert. Nanofiltration and ultrafiltration of endocrine disrupting compounds, pharmaceuticals and personal care products. *Journal of Membrane Science*, 270 (2006) 88.
- [30] K. Kimura, S. Toshima, G. Amy and Y. Watanabe. Rejection of neutral endocrine disrupting compounds (EDCs) and pharmaceutical active compounds (PhACs) by RO membranes. *Journal of Membrane Science*, 245 (2004) 71.
- [31] L. Braeken, R. Ramaekers, Y. Zhang, G. Maes, B. Van der Bruggen and C. Vandecasteele. Influence of hydrophobicity on retention in nanofiltration of aqueous solutions containing organic compounds. *Journal of Membrane Science*, 252 (2005) 195.
- [32] L.D. Nghiem, A.I. Schäfer and M. Elimelech. Role of electrostatic interactions in the retention of pharmaceutically active contaminants by a loose nanofiltration membrane. *Journal of Membrane Science*, 286 (2006) 52.
- [33] W. Pronk, H. Palmquist, M. Biebow and M. Boller. Nanofiltration for the separation of pharmaceuticals from nutrients in source-separated urine. *Water Research*, 40 (2006) 1405.
- [34] C. Bellona and J.E. Drewes. The role of membrane surface charge and solute physico-chemical properties in the rejection of organic acids by NF membranes. *Journal of Membrane Science*, 249 (2005) 227.
- [35] K. Kimura, G. Amy, J.E. Drewes, T. Heberer, T.-U. Kim and Y. Watanabe. Rejection of organic micropollutants (disinfection by-products, endocrine disrupting compounds and pharmaceutically active compounds) by NF/RO membranes. *Journal of Membrane Science*, 227 (2003) 113.

- [36] Y. Yoon, G. Amy, J. Cho, N. Her and J. Pellegrino. Transport of perchlorate ( $\text{ClO}_4^-$ ) through NF and UF membranes. *Desalination*, 147 (2002) 11.
- [37] L.D. Nghiem and S. Hawkes. Effects of membrane fouling on the nanofiltration of pharmaceutically active compounds (PhACs): Mechanisms and role of membrane pore size. *Separation and Purification Technology*, 57 (2007) 182.
- [38] K.O. Agenson, J.I. Oh and T. Urase, Retention of a wide variety of organic pollutants by different nanofiltration/reverse osmosis membranes: controlling parameters of process, *Journal of Membrane Science*, 225 (2003) 91.
- [39] Y. Kiso, T. Kon, T. Kitao and K. Nishimura, Rejection properties of alkyl phthalates with nanofiltration membranes, *Journal of Membrane Science*, 182 (2001) 205-214.
- [40] Y. Kiso, Y. Sugiura, T. Kitao and K. Nishimura, Effects of hydrophobicity and molecular size on rejection of aromatic pesticides with nanofiltration membranes, *Journal of Membrane Science*, 192 (2001) 1.
- [41] L.D. Nghiem and A.I. Schäfer, Adsorption and transport of trace contaminant estrone in NF/RO membranes, *Environmental Engineering Science*, 19 (6) (2002) 441.
- [42] L.D. Nghiem, A.I. Schäfer and M. Elimelech, Removal of natural hormones by nanofiltration membranes: measurement, modelling and mechanisms, *Environmental Science & Technology*, 38 (2004) 1888.
- [43] A.I. Schäfer, L.D. Nghiem and T.D. Waite, Removal of the natural hormone estrone from aqueous solutions using nanofiltration and reverse osmosis, *Environmental Science & Technology*, 37 (2003) 182.
- [44] Y. Yoon, P. Westerhoff, J. Yoon and S.A. Snyder, Removal of  $17\beta$ -estradiol and fluoranthene by nanofiltration and ultrafiltration, *Journal of Environmental Engineering*, 130 (12) (2004) 1460.
- [45] K. Kimura, G. Amy, J.E. Drewes and Y. Watanabe, Adsorption of hydrophobic compounds onto NF/RO membranes – an artifact leading to overestimation of rejection, *Journal of Membrane Science*, 221 (2003) 89.
- [46] J. Schaep, C. Vandecasteele, A. Wahab Mohammad and W.R. Bowen. Modelling the retention of ionic components for different nanofiltration membranes. *Separation and Purification Technology*, 22-23 (2001) 169.

[47] D. Vezzani and S. Bandini. Donnan equilibrium and dielectric exclusion for characterization of nanofiltration membranes. *Desalination*, 149 (1-3) (2002) 477.

[48] A. Wahab Mohammad and M. Sobri Takriff. Predicting flux and rejection of multicomponent salts mixture in nanofiltration membranes. *Desalination*, 157 (1-3) (2003) 105.

# **Chapter 2:**

## **Rejection of uncharged organic solutes**

**(Influence of steric and solute-membrane (hydrophobic) interactions)**

Parts of this chapter were based on:

A.R.D. Verliefde, E.R. Cornelissen, S.G.J. Heijman, G.L. Amy, B. Van der Bruggen and J.C. van Dijk, The influence of hydrophobic interactions on the rejection of uncharged solutes by nanofiltration/reverse osmosis, to be submitted to Water Research.

A.R.D. Verliefde, E.M.V. Hoek, E.R. Cornelissen, S.G.J. Heijman, G.L. Amy, B. Van der Bruggen and J.C. van Dijk, A predictive model for the rejection of uncharged solutes by nanofiltration/reverse osmosis – incorporation of solute-membrane (hydrophobic) interactions, in preparation for Environmental Science & Technology.

## 1. Introduction

As mentioned in the introductory chapter, NF and RO are complex processes and rejection properties of organic solutes are not only dependent on process conditions, but also on physical-chemical aspects of the solutes and the membrane material. Because of the wide variety of organic pollutants involved (and the discovery of even more pollutants), experimental determination of rejection behaviour for each separate pollutant would be too tedious and time-consuming. Therefore, a great advancement in the field would be made if methods could be developed that provide an a priori screening of the rejection behaviour of pollutants, based on their molecular properties/molecular structure and on characteristic performance data of the membrane.

This chapter will present two different modelling approaches for the rejection of uncharged solutes with NF/RO membranes. The first modelling approach will be more empirical, and will be based on a log-normal model for the pore size distribution of the membranes. The second modelling approach will be a more fundamental transport model. It will offer a mathematical description of the solute-membrane interactions that influence rejection. Both models will also be validated.

The first model will be a simple tool to provide the user with a quick idea of the removal of an uncharged organic solute, based on the knowledge of a few key solute physico-chemical properties. Even though the model is fast and easy, it will not give an exact value for solute rejection. Therefore, a second, more fundamental model is also developed.

## **2. Model construction for uncharged solutes**

For uncharged organic solutes, the literature mentions two main solute-membrane interactions that may influence solute rejection: a steric hindrance ( $\sim$  sieving) effect between large solutes and the membrane matrix, and hydrophobic (Van der Waals) interactions between hydrophobic solutes and hydrophobic membrane surfaces [1-9].

Steric hindrance is mainly determined by the size of the solute and the size of the membranes pores: solutes larger than the membrane pores (or with a molar mass above the MWCO) are well rejected; solutes smaller than the membrane pores (or with a molar mass lower than the MWCO) can permeate through the membrane more easily. This typically leads to an S-shaped curve when rejection is plotted as a function of the solute molar mass or the solute size.

For hydrophobic solutes with hydrophobic membranes, hydrophobic-hydrophobic (Van der Waals) interactions between the solutes and the membranes may have an additional influence on the rejection, in addition to steric hindrance. Experiments have shown [10] that hydrophilic molecules are better rejected compared to hydrophobic molecules of similar size. This is explained by the hydrophobic-hydrophobic interactions between membrane and solute: hydrophobic solutes can partition into the membrane matrix more easily, and consequently diffuse to the permeate side. Hydrophobic solutes are thus transported to the permeate side of the membrane more easily, explaining the lower rejection values. Moreover, hydrophobic solutes also adsorb more onto hydrophobic membranes and into the membrane pores. This adsorption can affect solute rejection: several studies have shown that adsorption of hydrophobic compounds onto hydrophobic membranes can lead to a

temporary overestimation of the observed rejection [11-13]. To obtain an accurate evaluation of membrane performance, saturation of the membrane with the compound of interest must be accomplished: initial rejection values of hydrophobic compounds can be high due to adsorption, but rejection generally decreases to a steady-state value when saturation of the membrane is reached. After saturation of the membranes is complete, the lower rejection for hydrophobic solutes compared with hydrophilic solutes is observed, which is due to the higher partitioning of the hydrophobic solutes, as mentioned above. To make sure adsorption equilibrium is reached in the experiments, and rejection values obtained are not biased, the time necessary to reach this adsorption equilibrium will be tested in this chapter.

The hydrophobicity of organic molecules is often expressed as the logarithm of the octanol-water partition coefficient,  $\log K_{ow}$ . Molecules with  $\log K_{ow} > 2$  are generally referred to as hydrophobic. The hydrophobicity of NF/RO membranes is usually characterized by the contact angle ( $\theta$ ) with a water droplet on the membrane surface. Studies have shown that membranes with larger contact angles can adsorb more mass per unit area of organic compounds than membranes with smaller contact angles, and hydrophobic molecules are more adsorbed than hydrophilic molecules [12].

Even though plenty of literature data exist that explain the lower observed rejection values of hydrophobic solutes by increased solute-membrane affinity, there is no approach that is able to quantify this effect or that is able to distinguish the contributions of steric and hydrophobic interactions to rejection.

This study will investigate whether  $\log K_{ow}$  and contact angle values are valuable parameters to estimate the magnitude of the hydrophobic-hydrophobic (Van der Waals) interactions between solute and membrane, and the effect of these



interactions on solute rejection. Also, an alternative approach will be formulated, which will consider solute transport through membranes as a function of solute-membrane affinity, expressed as the free energy of interaction between solute and membrane. This calculated solute-membrane affinity will be incorporated in a thermodynamic convection-diffusion transport equation, which allows making a clear distinction between steric and hydrophobic-hydrophobic effects determining uncharged organic solute rejection.

## 2.1. Log-normal model for uncharged organic solutes as a function of solute hydrophobicity

A simplified modelling approach to yield a quick screening of the solute-membrane interactions that influence solute rejection will first be derived and evaluated. The aim is to develop a modelling tool which allows a quick estimation/prediction of solute rejection, based on the knowledge of selected, readily available solute and membrane parameters.

The model is based on the approach by Van der Bruggen et al. (2000) [14], who used the assumption of a log-normal pore size distribution to model the reflection coefficient of uncharged organic molecules. In theory, the reflection coefficient of a solute is the rejection of this solute at infinite flux or pressure. For the experimental results used to validate the model, it is assumed that the obtained rejection values (which are determined at 10% recovery), are approximately equal to the reflection coefficient.

The rejection values in this chapter will thus be modelled using a similar log-normal pore size distribution model. The rejection of a solute is dependent on the distribution

of the pore size of the membrane, compared to the size of the solute. This results in the following equation:

$$R(r^*) = \int_0^{r^*} \frac{1}{s_p \cdot \sqrt{2\pi}} \cdot \frac{1}{r} \cdot \exp\left(-\frac{(\ln(r) - \ln(\bar{r}))^2}{2 \cdot s_p^2}\right) dr \quad (2.1)$$

Where  $r$  is the solute radius,  $R(r^*)$  is the rejection of a solute with radius  $r^*$ ,  $\bar{r}$  is the mean pore size of the membrane and  $s_p$  is the standard deviation of the pore size distribution.

This model was later adapted by Van der Bruggen et al. (2002) [15] to replace solute size and pore size by solute molar mass and membrane molecular weight cut-off. This results in the following equation for the rejection of organic solutes as a function of their molar mass:

$$R(MW^*) = \int_0^{MW^*} \frac{1}{s_{MW} \sqrt{2\pi}} \frac{1}{MW} \exp\left[-\frac{(\ln(MW) - \ln(MWCO) + 0.56s_{MW})^2}{2s_{MW}^2}\right] dMW \quad (2.2)$$

Where  $MW$  is the solute molar mass,  $R(MW^*)$  is the rejection of a solute with molar mass  $MW^*$ ,  $MWCO$  is the membrane molecular weight cut-off and  $s_{MW}$  is the standard deviation on this molecular weight cut-off.

Integration of Equation (2.2) leads to a typical S-shaped curve of the rejection as a function of the solute molar mass: solutes with a molar mass under the  $MWCO$  of the membrane are not efficiently rejected by the membrane, whereas solutes with a molar mass larger than the  $MWCO$  are efficiently removed.

The modelling approach as followed by Van der Bruggen et al. [15] thus only takes steric hindrance effects between the solutes and the membrane polymeric matrix into account. This approach could work well for solutes without any affinity for the membrane surface, but it does not account for the influence of solute-membrane hydrophobic interactions. Therefore, the model is adapted in a simple manner in this

chapter, to incorporate the effects of hydrophobic interactions on the rejection. Instead of fitting a single rejection curve for all solutes with a given membrane (based on Equation (2.2)), different rejection curves are constructed for solutes with different hydrophobicity and thus different hydrophobic interactions with the membrane. Since the most straightforward way of describing organic solute hydrophobicity is by using  $\log K_{ow}$ , the organic solutes are divided into three different categories of  $\log K_{ow}$ -values ( $\log K_{ow} < 1$  ;  $1 < \log K_{ow} < 3$  ;  $3 < \log K_{ow}$ ) and a different rejection curve is modelled for every category. Solute with increasing molar mass are chosen in the different categories of  $\log K_{ow}$ -values, so the influence of hydrophobic interactions and size exclusion on the rejection can be studied simultaneously. This allows for investigation of the influence of hydrophobic interactions and size on the rejection by the shape of the curve and the location of the modelled MWCO for every category of hydrophobicity. Solute with  $\log K_{ow} < 1$  are referred to as hydrophilic in this chapter, solute with  $3 < \log K_{ow}$  are referred to as hydrophobic and solute with  $1 < \log K_{ow} < 3$  are referred to as transphilic.

The aim of this model is a simple quantification of the influence of hydrophobicity on rejection of uncharged organic molecules, as a function of readily available solute and membrane parameters.

## 2.2. Advanced transport model for uncharged organic solutes

In addition to the log-normal model, some other earlier modelling attempts for organic solute rejection are reported in the literature. Most models for uncharged organic solutes are based on solution-diffusion mechanisms, which are valid for reverse osmosis [16] but may not be entirely correct for nanofiltration or low-pressure reverse

osmosis membranes, because of the additional convective transport of organic molecules through the membranes. Therefore, the modelling approach followed here will be derived, based on the well-known Spiegler-Kedem equation for steady-state transport in pressure-driven membrane processes (which incorporates both convection and diffusion) [17,18]:

$$J_s = J_v \cdot C_p = -D_p \cdot \frac{dc}{dx} + J_v \cdot K_c \cdot c \quad (2.3)$$

Where  $J_s$  and  $J_v$  are respectively the solute and solvent flux,  $C_p$  is the solute bulk permeate concentration,  $D_p (=K_d \cdot D_\infty)$  is the diffusion coefficient of the solute in the membrane,  $D_\infty$  is the solute diffusion coefficient in water,  $c$  and  $x$  are respectively the solute concentration and the axial position within the membrane and  $K_c$  and  $K_d$  are respectively the convective and diffusive transport hindrance factors.

### 2.2.1. Development of the model

Equation (2.3) can be integrated with the following boundary conditions [19-21]:

$$\text{at } x=0 \text{ (within the membrane at the feed side): } c(x=0) = c_f = K \cdot C_f \quad (2.4)$$

$$\text{at } x=\Delta x \text{ (within the membrane at the permeate side): } c(x=\Delta x) = c_p = K \cdot C_p \quad (2.5)$$

where  $\Delta x$  is the membrane thickness,  $c_f$  and  $c_p$  are the solute concentrations in the membrane matrix at the feed and permeate side, respectively,  $C_f$  and  $C_p$  are the solute feed and permeate concentrations in the bulk, respectively, and  $K$  is the solute partitioning coefficient in the membrane polymeric matrix.

The integration with the boundary conditions yields the following equation:

$$\frac{C_p}{C_f} = \frac{K \cdot K_c}{1 - ((1 - K \cdot K_c) \cdot \exp(-Pe))} \quad (2.6)$$

Where  $Pe = J_v \cdot K_c \cdot \Delta x / \varepsilon \cdot D_p$  is the Peclet-number and  $\varepsilon$  is the porosity of the membrane.

If the rejection of a solute is determined as  $R=1-(C_p/C_f)$ , Equation (2.6) can be rewritten as:

$$R = 1 - \frac{K \cdot K_c}{1 - \left( (1 - K \cdot K_c) \cdot \exp\left(\frac{J_v \cdot K_c \cdot \Delta x}{K_d \cdot \varepsilon \cdot D_\infty}\right) \right)} \quad (2.7)$$

Equation (2.7) describes the rejection of a solute as a function of the solvent flux and contains 4 unknown model parameters: the partitioning coefficient  $K$ , the steric hindrance factors  $K_c$  and  $K_d$  and the ratio membrane thickness/membrane porosity  $\Delta x/\varepsilon$ . The diffusion coefficients  $D_\infty$  of different organic solutes are generally known from literature, or can be determined experimentally or estimated using known correlations (e.g. the Wilke-Chang correlation).

Equation (2.7) is used as the basis for the advanced transport model, but is also the basis of traditional size exclusion based convection-diffusion models. The only difference between the two models is in the determination of the partition coefficient  $K$ .

The goal is to develop a thermodynamic model with parameters which are easy to determine and have an actual physical meaning.

### 2.2.2. Calculation of hindrance parameters $K_c$ and $K_d$

If a fully developed parabolic flow velocity profile (Hagen-Poiseuille velocity profile) is assumed for the flow within the membrane pores, the hindrance factors for convection and diffusion can be calculated as follows [19]:

$$K_c = (2 - (1 - \lambda)^2) (1 + 0.054\lambda - 0.988\lambda^2 + 0.441\lambda^3) \quad (2.8)$$

$$K_d = 1 - 2.3\lambda + 1.154\lambda^2 + 0.224\lambda^3 \quad (2.9)$$

with  $\lambda = r_s/r_p$  being the ratio of the solute radius to the hypothetical “pore radius”. In this study, it will be assumed that NF/RO membranes contain “voids”, which can be regarded as actual pores and can be represented by a mean average pore size  $r_p$ . The hindrance factors for convection and diffusion are thus only determined by steric hindrance between the solute and the membrane matrix.

### 2.2.3. Determination of the partition coefficient $K$

In fact, the partition coefficient  $K$  relates the solute concentration outside the membrane pores, to the solute concentration inside the membrane pores. The partition coefficient  $K$  can be written as [22]:

$$K = 2 \int_0^{1-\lambda} g(\rho) \rho d\rho \quad (2.10)$$

where  $\rho$  is the dimensionless position in the pore ( $\rho=r/r_p$ ) (with  $r$  the radial position in the pore),  $\lambda=r_s/r_p$  the ratio between solute and pore size and  $g(\rho)$  the radial distribution function.

In the traditional size exclusion approach for organic solute rejection,  $g(\rho)=0$  and the partition coefficient  $K$  is equal to  $(1-\lambda)^2$ . In the traditional size exclusion approach,  $K$  is thus independent of solute-membrane interactions.

For the new advanced transport model,  $K$  will be determined from steady-state thermodynamics and will thus be dependent on solute-membrane affinity.

It may be assumed that the radial concentration profile is governed by the Boltzmann equation [22]:

$$g(\rho) = \exp\left(-\frac{\Delta G_i}{k \cdot T}\right) \quad (2.11)$$

where  $k$  is the Boltzmann constant,  $T$  is the absolute temperature (in K) and  $\Delta G_i$  is the free-energy difference associated with the differences in interactions of the solute

in the water phase and the membrane phase (the interaction energy between solute and membrane in the water phase).

After substitution and integration, Equation (2.10) then becomes (since  $\Delta G_i$  is constant):

$$K = (1 - \lambda)^2 \exp\left(-\frac{\Delta G_i}{k \cdot T}\right) \quad (2.12)$$

Thus, the partitioning of a solute from the water phase to the membrane phase (membrane pores) is dependent on both size exclusion effects (expressed as the factor  $(1-\lambda)^2$ ) and on solute-membrane affinity (expressed as  $\Delta G_i$ , the free energy of interaction between a solute and the membrane in the water phase).

In the literature, another definition for the partition coefficient  $K$  can also be found, which unites the size exclusion and the solute-membrane affinity into one term [23,24]:

$$K = \exp\left(\frac{-\Delta G}{k \cdot T}\right) \quad (2.13)$$

where  $k$  is again the Boltzmann constant and  $T$  is the temperature. Here,  $\Delta G$  is equal to the total the free-energy change associated with the transfer of the solute of interest from the bulk fluid to the membrane phase.  $\Delta G$  can further be split into two terms [23,25]:

$$\Delta G = \Delta G_i + v\Pi \quad (2.14)$$

The term  $\Delta G_i$  again reflects the solute membrane affinity. The second term  $v.\Pi$  contains the molecular volume  $v$  of the solute and the pressure  $\Pi$ , exerted by the rigid polymeric matrix of the membrane on the solute molecules. It can be regarded as the steric hindrance, superposed on the free-energy of interaction-change  $\Delta G_i$ ,

when the solute moves from the water phase to the membrane phase. It can be assumed that this second term  $v \cdot \Pi$  will be pressure/flux dependent, since Kimura et al. (2003) [12], demonstrated that adsorption onto and partitioning into membranes depend on pressure (and  $\Delta G_i$  is independent of pressure).

In a way,  $\Delta G_i$  can be considered as the quantification of the hydrophobic interactions occurring between the solute and the membrane. If  $\Delta G_i$  is negative (e.g. for a hydrophobic solute), transfer of the solute to the membrane will be facilitated. This will result in a lower rejection than expected, purely based on size exclusion effects. However, if  $\Delta G_i$  is positive, there will be resistance against partitioning of the solute into the membrane phase, resulting in a higher rejection than expected, based on size exclusion effects. The traditional size exclusion model will only be valid for solutes for which  $\Delta G_i=0$ .

$\Delta G_i$  is equal to the free energy of interaction between two different entities, S' (the solute) and S'' (the membrane) in a liquid L (in this case water),  $\Delta G_{S'L S''}$ . This free energy can be related to the interfacial tensions between the two different entities and the water phase, using the well-known Dupré equation [26]:

$$\Delta G_i = A \cdot \Delta G_{S'L S''} = \gamma_{S'S''} - \gamma_{S'L} - \gamma_{S''L} \quad (2.15)$$

where  $\gamma_{S'S''}$  is the interfacial tension between the solute S' and the membrane S'',  $\gamma_{S'L}$  is the interfacial tension between the liquid solvent L (in this case water (W)) and the solute S',  $\gamma_{S''L}$  is the interfacial tension between the membrane and the liquid solvent L and A is the contact area between a molecule S' and the membrane S''.



Each interfacial tension can be determined from the surface tensions of the different components of the interface. The surface tension of liquids, solids and gasses consists of an apolar and polar part and can be written (e.g. for a liquid L) as:

$$\gamma_L = \gamma_L^{LW} + \gamma_L^{AB} = \gamma_L^{LW} + \sqrt{\gamma_L^+ \gamma_L^-} \quad (2.16)$$

where  $\gamma_L^{LW}$  is the apolar (Lipshitz-Van der Waals) part and  $\gamma_L^{AB}$  is the polar part of the surface tension.  $\gamma_L^+$  and  $\gamma_L^-$  describe the electron-acceptor and the electron-donor aspects of the surface tension.

The following expression relates surface tension parameters to the interfacial tension between different components and describes the polar and apolar interactions determining the interfacial tension (e.g. for the solid-liquid interfacial tension):

$$\gamma_{SL} = \left( \sqrt{\gamma_S^{LW}} - \sqrt{\gamma_L^{LW}} \right)^2 + 2 \left( \sqrt{\gamma_S^+ \gamma_S^-} + \sqrt{\gamma_L^+ \gamma_L^-} - \sqrt{\gamma_S^+ \gamma_L^-} + \sqrt{\gamma_S^- \gamma_L^+} \right) \quad (2.17)$$

where  $\gamma_S^{LW}$  and  $\gamma_L^{LW}$  describe the apolar (Lipshitz-Van der Waals) parts of the solute and solvent surface tension, respectively, and  $\gamma_S^+, \gamma_S^-, \gamma_L^+, \gamma_L^-$  describe the electron-acceptor and electron donor aspects of the polar part of the solute and solvent surface tension, respectively.

Substituting Equation (2.17) in Equation (2.15) for the solute (S'), the membrane (S'') and the solvent (L) gives:

$$\Delta G_i = A \cdot \Delta G_{S'LS''} = 2 \left[ \begin{aligned} & \sqrt{\gamma_{S'}^{LW} \gamma_L^{LW}} + \sqrt{\gamma_{S''}^{LW} \gamma_L^{LW}} - \sqrt{\gamma_{S'}^{LW} \gamma_{S''}^{LW}} - \gamma_L^{LW} + \sqrt{\gamma_L^+} \left( \sqrt{\gamma_{S'}^-} + \sqrt{\gamma_{S''}^-} - \sqrt{\gamma_L^-} \right) \\ & + \sqrt{\gamma_L^-} \left( \sqrt{\gamma_{S'}^+} + \sqrt{\gamma_{S''}^+} - \sqrt{\gamma_L^+} \right) - \sqrt{\gamma_{S'}^+ \gamma_{S''}^-} - \sqrt{\gamma_{S'}^- \gamma_{S''}^+} \end{aligned} \right] \quad (2.18)$$

This equation contains 9 variables,  $\gamma_L^{LW}, \gamma_L^+, \gamma_L^-, \gamma_{S'}^{LW}, \gamma_{S'}^+, \gamma_{S'}^-, \gamma_{S''}^{LW}, \gamma_{S''}^+, \gamma_{S''}^-$ . In the case of water as a solvent, the values for  $\gamma_W^{LW}, \gamma_W^+$  and  $\gamma_W^-$  are known from literature.

Also for several other liquids, the values of  $\gamma_L^{LW}$ ,  $\gamma_L^+$  and  $\gamma_L^-$  can be found in the literature [27].

The surface tension parameters for the membrane can be determined through contact angle measurements via the Young-Dupré equation [26]:

$$(1 + \cos \theta) \cdot \gamma_L = 2 \left( \sqrt{\gamma_{S''}^{LW} \gamma_L^{LW}} + \sqrt{\gamma_{S''}^+ \gamma_L^-} + \sqrt{\gamma_{S''}^- \gamma_L^+} \right) \quad (2.19)$$

where  $\theta$  is the contact angle formed between a droplet of liquid L and the membrane surface. By performing contact angle measurements on the membrane surface, 3 times with 3 different liquids L with known properties for  $\gamma_L^{LW}$ ,  $\gamma_L^+$  and  $\gamma_L^-$ , the membrane surface tension parameters  $\gamma_{S''}^{LW}$ ,  $\gamma_{S''}^+$  and  $\gamma_{S''}^-$  can be determined by using Equation (2.19) and solving the set of equations.

The parameters  $\gamma_{S'}^{LW}$ ,  $\gamma_{S'}^+$  and  $\gamma_{S'}^-$  for the solutes S' can be determined using a similar approach as for the determination of the surface tension parameters for the membrane. By measuring the contact angle of one liquid with unknown parameters with 3 different membrane surfaces with known (and different)  $\gamma_{S''}^{LW}$ ,  $\gamma_{S''}^+$  and  $\gamma_{S''}^-$  values, the parameters  $\gamma_{S'}^{LW}$ ,  $\gamma_{S'}^+$  and  $\gamma_{S'}^-$  of the liquid can be determined by using Equation (2.19) 3 times and solving the set of 3 equations. Alternatively, for some liquids, the surface thermodynamic parameters are already known from the literature [27].

If the solute of interest is a solid, the following relationship between the aqueous solubility and surface tension parameters is valid [28]:

$$2 \cdot \gamma_{S'W} \cdot S_c = 2 \cdot \left( \left( \sqrt{\gamma_{S'}^{LW}} - \sqrt{\gamma_W^{LW}} \right)^2 + 2 \left( \sqrt{\gamma_{S'}^+ \gamma_{S'}^-} + \sqrt{\gamma_W^+ \gamma_W^-} - \sqrt{\gamma_{S'}^+ \gamma_W^-} + \sqrt{\gamma_{S'}^- \gamma_W^+} \right) \right) \cdot S_c = -k \cdot T \cdot \ln s \quad (2.20)$$

where  $S_c$  is the contactable surface area between two solute molecules  $S'$ ,  $k$  is the Boltzmann constant,  $T$  is the absolute temperature and  $s$  is the aqueous solubility of solute  $S'$  (expressed in mole fractions). By determining the solubility of solute  $S'$  at 3 different temperatures  $T$ ,  $\gamma_{S'}^{LW}$ ,  $\gamma_{S'}^+$  and  $\gamma_{S'}^-$  can be determined using Equation (2.20). The difficulty in using Equation (2.20) is the determination of the contactable surface area  $S_c$  between two molecules  $S'$ .  $S_c$  may be determined by calculating the molecular dimensions of the solute. This was already shown by Docoslis et al. (2000) [29].

However, this approach will not be followed in this chapter and only the surface thermodynamic properties of liquid solutes will be determined.

Once all the thermodynamic properties  $\gamma_L^{LW}$ ,  $\gamma_L^+$ ,  $\gamma_L^-$ ,  $\gamma_{S'}^{LW}$ ,  $\gamma_{S'}^+$ ,  $\gamma_{S'}^-$ ,  $\gamma_{S''}^{LW}$ ,  $\gamma_{S''}^+$  and  $\gamma_{S''}^-$  are determined, they can be introduced into Equation (2.18) to determine  $\Delta G_i$ .

Once  $\Delta G_i$  is known, it can be filled into Equations (2.12) and (2.14).

If Equation (2.12) is used as the expression for the partition coefficient  $K$ , then Equation (2.7) for the solute rejection is solely dependent on the unknown parameters  $\lambda$  and  $\Delta x/\varepsilon$ . By fitting experimentally obtained rejection data as a function of permeate flux for a single solute to Equation (2.7), the values of the parameters  $\Delta x/\varepsilon$  and  $\lambda$  (and thus  $r_p$ ) can be determined. This characterizes the membrane completely and turns Equation (2.7) into a predictive model for other solutes, if their solute size and interaction energy  $\Delta G_i$  with the membrane are known.

If the other Equation (2.13) for the partition coefficient is used, the size dependent factor  $v \cdot \Pi$  as a function of permeate flux remains an unknown variable. By fitting  $K$  to the experimentally obtained rejection data as a function of permeate flux for different solutes,  $v \cdot \Pi$  can be determined as a function of solute size and permeate flux. This

approach is not predictive, but allows to model rejection as a function of pressure/flux, and it gives more information on the pressure/flux dependency, but also on the solute size dependency of  $\nu_{II}$ .

### **3. Materials and methods**

#### **3.1. Equipment and filtration protocol**

A schematic diagram of the bench-scale membrane system used in the membrane filtration experiments can be found in Figure 2.1. The feed solution is delivered to a pressure vessel, accommodating a single 4040-membrane element, by a multi-impellor centrifugal pump (Grundfos CRE-3). The pump is capable of providing pressures of up to 25 bar at a flow rate of 3 m<sup>3</sup>/h. The feed water is fed from a 600 L stainless steel vessel. An immersed stainless-steel coil with cooling liquid fed from a cooling system (Tamson TLC 10B) is used to maintain a constant feed water temperature.

Permeate, concentrate and feed flow are monitored by rotameters (Heinrichs messgeräte). Applied transmembrane pressure is regulated using a needle valve in the concentrate stream, with transmembrane pressure measured with a precision manometer (Wika fein-druckmessgerät). All test unit parts in contact with the solution are made of stainless steel to minimize adsorption of the investigated organic compounds.

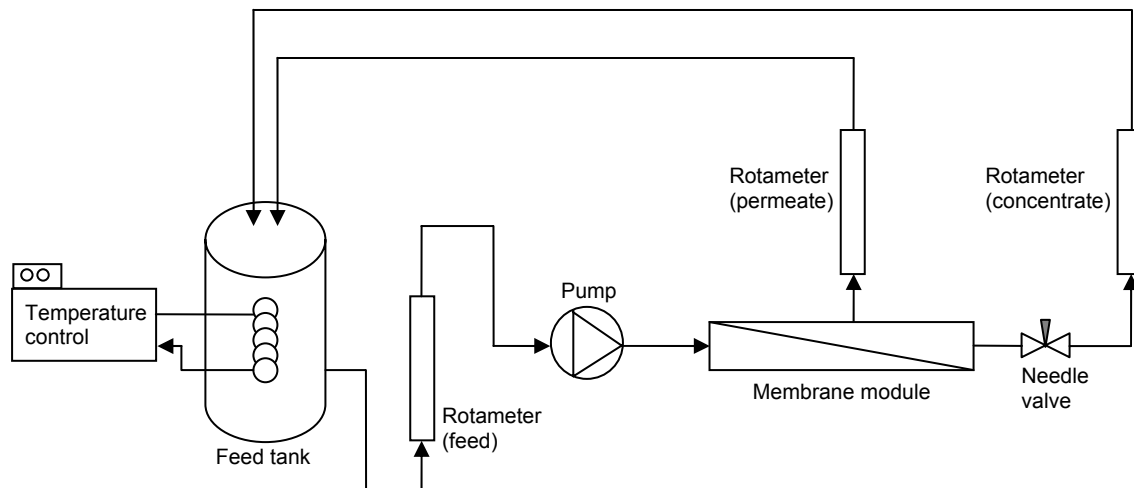


Figure 2.1 – Membrane filtration set-up for rejection experiments

Membrane filtration experiments were carried out at a constant cross-flow velocity of 0.2 m/s, corresponding to a feed flow of 1500 l/h (which is representative for full-scale installations) and a concentration polarization factor of 1.02. For the log-normal model, experiments were carried out at a constant recovery of 10%. For the advanced transport model, feed pressure was varied, and rejection was measured as a function of permeate flux.

Feed water temperature was set to  $20 \pm 1^\circ\text{C}$ . All experiments were carried out in a recycle mode with a single batch of water, with both permeate and concentrate recycled back into the feed reservoir.

Figure 2.2 shows a picture of the set-up.

Since adsorption of solutes onto the membrane surface, and sorption into the inner membrane structure, may influence measured rejection values, an accurate evaluation of the rejection of a given solute is not possible until saturation of the membrane with the solute of interest is accomplished [12]. Therefore, this study will also investigate how long it takes before adsorption equilibrium is reached on 4-inch

spiral wound modules. Afterwards, all rejection experiments will be carried out for this time period, to ensure that steady state rejection values are obtained.



Figure 2.2 – Membrane filtration set-up for rejection experiments (in blue: membrane module)

### 3.2. Membranes

The membranes used in this study were commercially available nanofiltration membranes: Trisep TS-80 TSF (Trisep Corp., Goleta CA, USA), Desal HL (GE Osmonics, Fairfield CT, USA), Koch TFC-XR (Koch Membrane Systems Inc., Wilmington MA, USA) and Dow-Filmtec BW-30 (Dow-Filmtec, Minneapolis MN, USA).

All membranes are polyamide thin film composite membranes. Before use, all membranes were rinsed with tap water for two hours to remove preservation liquids present in the membrane. Afterwards, the membranes were characterized for pure water permeability with Milli-Q water and for  $\text{MgSO}_4$  or NaCl rejection with a 500 ppm

MgSO<sub>4</sub> or NaCl solution in Milli-Q water. The membrane properties are summarized in Table 2.1.

	MWCO (g/mol)	Pure water permeability (m/(s.bar))	% Salt rejection	Contact angle (°)	ζ-potential (mV)
DESAL HL (NF)	150-300	$2.0 \times 10^{-6}$	98% (MgSO <sub>4</sub> )	41 ± 2	-11
Trisep TS-80 TSF (NF)	175	$1.2 \times 10^{-6}$	99% (MgSO <sub>4</sub> )	48 ± 2	-20 to -25
Dow BW-30 (RO)	n.d.	$6.7 \times 10^{-7}$	99,5% (NaCl)	53 ± 3	-20
Koch TFC-XR (RO)	n.d.	$5.2 \times 10^{-7}$	> 99,7% (NaCl)	40 ± 3	-22

Table 2.1 – Membrane properties for selected membranes for organic solutes rejection experiments

The molecular weight cut-off (MWCO) values were provided by the membrane manufacturers. The membrane ζ-potentials were determined in a 10mM KCl-solution using commercially available equipment (SurPASS, Anton Paar, Graz, Austria). Membranes with different membrane properties were chosen in order to assess the influence of membrane properties on rejection. For the rejection experiments, single elements (4040-membrane modules) were used.

### 3.3. Solutes for adsorption experiment

Since adsorption of solutes onto membranes can influence measured rejection values and an accurate evaluation of the rejection of a given solute cannot be accurately determined until saturation of the membrane with the solute of interest is accomplished [12], the time to reach saturation of a 4-inch membrane module was investigated. This was carried out by spiking different pesticides onto a Trisep TS80 membrane, and analysing the time necessary for the feed concentrations to equilibrate (if solute adsorption is occurring, the feed concentrations will decrease if

filtration is carried out in a recycle mode (concentrate and permeate recycled to the feed reservoir)).

The different pesticides were spiked in Milli-Q water, in concentrations of 4 to 5 µg/l.

Table 2.2 summarizes the physico-chemical properties of these pesticides.

	MW (g/mol)	log K <sub>ow</sub> (-)	Henry's law constant (atm.m <sup>3</sup> /mol)
atrazine	215.69	2.61	2.36 x 10 <sup>-9</sup>
simazine	201.66	2.18	9.42 x 10 <sup>-10</sup>
diuron	233.10	2.68	5.04 x 10 <sup>-10</sup>
metamitron	202.22	0.83	9.53 x 10 <sup>-13</sup>

Table 2.2 – Physico-chemical properties of selected pesticides used for adsorption experiment on Trisep TS-80

The pesticides were analysed by gas chromatography, coupled with mass spectrometry. It is assumed that, when adsorption equilibrium is reached for solutes in these low concentrations, adsorption equilibrium will also have been reached for solutes at higher concentrations, since the driving force for adsorption is higher when feed concentration is higher.

### 3.4. Solutes for rejection experiments

The solutes used for the rejection experiments were mainly selected based on their different physico-chemical properties.

For the log-normal model as a function of solute hydrophobicity, model solutes were chosen, based on their hydrophobicity (expressed as log K<sub>ow</sub>) and divided into three categories, i.e. hydrophilic (log K<sub>ow</sub><1), hydrophobic (3<log K<sub>ow</sub>) and transphilic (1<log K<sub>ow</sub><3) solutes. For each category, solutes of increasing molar mass were



chosen, to allow measurement of a sigmoidal rejection curve for each category of hydrophobicity.

For the advanced transport model, 4 different model solutes with different size and hydrophobicity ( $\log K_{ow}$ ) were chosen. All the solutes were liquids, to be able to determine the surface tension parameters used in the model.

All the solutes and their physico-chemical parameters are summarized in Table 2.3.

The solute radii were determined in two ways. The first way is by using the definition of the Stokes radius:

$$r_s = \frac{k \cdot T}{6\pi\eta D_\infty} \quad (2.21)$$

where  $k$  is again the Boltzmann constant,  $T$  is the absolute temperature,  $\eta$  is the solvent viscosity and  $D_\infty$  is the solute diffusion coefficient in water.

The second way of determining the solute radii is using a molecular modelling program (Hyperchem, Hypercube Inc., Gainesville FL, USA). The exact protocol to determine the average solute radius using this molecular modelling software was described before by Van der Bruggen et al. (2000) [14].

The solute diffusion coefficients were determined using the equation developed by Hayduk and Laurie (1974) [30]:

$$D_\infty = \frac{13.26 \times 10^{-5}}{\eta^{1.4} \times V_a^{0.589}} \quad (2.22)$$

where  $\eta$  is the solvent viscosity and  $V_a$  is the Le Bas molecular volume (also calculated using molecular modelling software).

		MW (g/mol)	log K <sub>ow</sub> (-)	diff.coeff. (m <sup>2</sup> /s)	solute diameter (nm)	Stokes radius (nm)	measured on TS80	measured on HL
<b>log-normal model</b>								
<b>log K<sub>ow</sub>&lt;1</b>	ethanol	46	-0.31	n.d.	0.28	n.d.	X	X
	NDMA	74	-0.57	n.d.	0.31	n.d.	X	X
	2-methoxyethanol	76	-0.32	n.d.	0.36	n.d.	X	X
	2-ethoxyethanol	90	-0.77	n.d.	0.42	n.d.	X	X
	glycerol	92	-1.76	n.d.	0.38	n.d.	X	X
	MTBE	88	0.94	n.d.	0.36	n.d.	X	X
	glucose	180	-3.24	n.d.	0.40	n.d.	X	X
	sucrose	342	-3.7	n.d.	0.58	n.d.	X	X
<b>1&lt;log K<sub>ow</sub> &lt; 3</b>	2-(1H)-quinoline	145	1.26	n.d.	0.47	n.d.	X	X
	methacetin	165	1.03	n.d.	0.56	n.d.	X	X
	monomethylphthalate	180	1.13	n.d.	0.52	n.d.	X	X
	dimethylphthalate	194	1.6	n.d.	0.51	n.d.	X	X
	N-acetyl-L-tyrosine	223	1.32	n.d.	0.63	n.d.	X	X
	atropine	289	1.83	n.d.	0.65	n.d.	X	X
<b>3 &lt; log K<sub>ow</sub></b>	2-methylisoborneol	168	3.31	n.d.	0.45	n.d.		X
	N-nitrosodiphenylamine	198	3.13	n.d.	0.60	n.d.	X	
	4-nonylphenol	220	5.76	n.d.	0.83	n.d.		X
	bisphenol-A	228	3.32	n.d.	0.63	n.d.	X	X
	linuron	249	3.2	n.d.	0.60	n.d.	X	
	estrone	270	3.13	n.d.	0.65	n.d.	X	X
	lindane	291	3.72	n.d.	0.48	n.d.	X	X
<b>advanced transport model</b>								
	2-ethoxyethanol	90	-0.77	1.1 x 10 <sup>-9</sup>	0.42	0.23	X	X
	glycerol	92	-1.76	9.3 x 10 <sup>-10</sup>	0.38	0.19	X	X
	diethylphthalate (DEP)	222	2.42	6.1 x 10 <sup>-10</sup>	0.6	0.35	X	X
	dibutylphthalate (DBP)	278	4.5	5.1 x 10 <sup>-10</sup>	0.73	0.42	X	X

Table 2.3 - Physico-chemical characteristics for selected organic solutes (n.d.: not determined; X indicates solute rejection has been determined on selected membrane)

All solutes were spiked separately in Milli-Q water and measured by analyzing the non-purgeable organic carbon (NPOC ~ total organic carbon (TOC)) -content of feed and permeate. The limit of detection for the NPOC-analysis is 0.2 mg/l. Therefore, all solutes were spiked in concentrations of 10 mg carbon/l, in order to be able to measure at least 98% rejection (which corresponds to a permeate concentration of 0.2 mg/l).

### 3.5. Determination of surface tension components

The surface tension components  $\gamma_{S''}^{LW}$ ,  $\gamma_{S''}^{+}$  and  $\gamma_{S''}^{-}$  of the membranes were determined by performing contact angle measurements on the membrane surfaces and solving the set of three equations using the following three liquids: Milli-Q water, diiodomethane and glycerol (using Equation (2.19)). The surface tension parameters  $\gamma_L^{LW}$ ,  $\gamma_L^{+}$ ,  $\gamma_L^{-}$  of Milli-Q, diiodomethane and glycerol are given in Table 2.4 [31].

	$\gamma^L$	$\gamma^{LW}$	$\gamma^{+}$	$\gamma^{-}$
milli-Q water	72.8	21.8	25.5	25.5
glycerol	64	34	3.92	57.4
diiodomethane	50.8	50.8	0	0

Table 2.4 – Surface tension components of liquids used for contact angle measurements at 20°C (in mJ/m<sup>2</sup>)

After the surface tension components of the two different membranes were determined, the surface tension components of a piece of glass were also determined in a similar way.

The surface tension components  $\gamma_{S'}^{LW}$ ,  $\gamma_{S'}^+$  and  $\gamma_{S'}^-$  for the three liquid solutes used for the validation of the advanced transport model were determined by performing contact angle measurements on three different solid surfaces: the two membranes and the glass. Afterwards, the set of three equations (using Equation (2.19)) was solved for each solute.

All contact angles were measured using commercial contact angle measuring equipment (Krüss DSA10 goniometer, Krüss GmbH, Hamburg, Germany) equipped with commercial contact angle calculation software (Drop Shape Analysis, Krüss GmbH). For the determination of all contact angles, the average was taken of at least 20 different measurements on different locations of the membrane and glass samples.

#### **4. Results and discussion**

In order to determine the influence of solute-membrane hydrophobic interactions, the two models derived before were used to fit experimentally obtained rejection data. Afterwards, the fitted model parameters were analysed in more detail to reveal the contributions of both steric and hydrophobic interactions to uncharged organic solute rejection. However, first, the time necessary to reach adsorption equilibrium has to be determined.

#### 4.1. Membrane adsorption equilibration

Figure 2.3 shows the feed concentrations of the selected pesticides over time.

It can be assumed that the decrease of feed concentration of the pesticides is due to adsorption onto/partitioning into the membrane. Volatilization of the pesticides is ruled out, since the Henry's law coefficients of the pesticides are low. Adsorption of pesticides onto the experimental apparatus (e.g. reservoir, connections, etc.) was ruled out since most parts of the set-up in contact with the solution are made out of stainless steel to minimize adsorption.

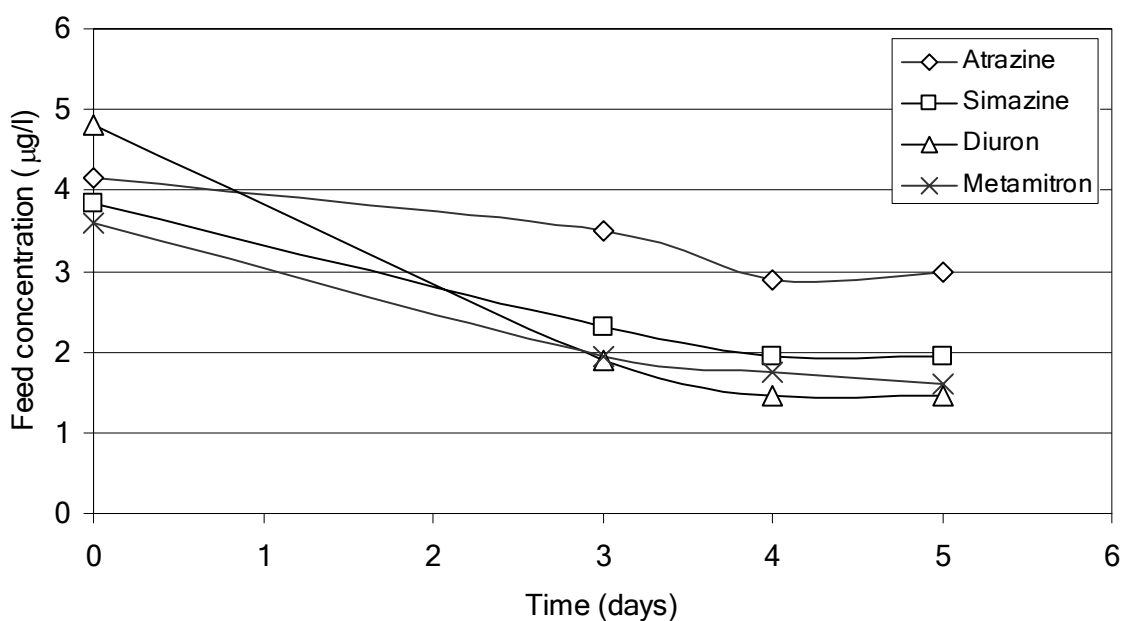


Figure 2.3 – Decrease of feed concentration of selected pesticides in time during filtration run with Trisep TS-80 membrane

From Figure 2.3 it is apparent that a period of 3 to 4 days is needed to reach saturation of the membrane with the solutes.

Therefore, all rejection experiments with organic solutes in this study are carried out for 4 days, in order to avoid the transient regime that is due to the influence of adsorption and to ensure that steady state rejection values are obtained. It is hereby assumed that adsorption behaviour of the other organic solutes is similar to the adsorption behaviour of pesticides.

Especially for solutes spiked in higher concentrations, adsorption equilibrium should be reached faster than the 4 day period. Even at these higher concentrations, however, rejection experiments are still carried out for 4 days, to make sure the same protocol is followed for all rejection experiments.

#### 4.2. Log-normal model as a function of solute hydrophobicity

In Figures 2.4 and 2.5, the data points represent the measured rejection values for the solutes in Table 2.3 with the Trisep TS80 and Desal HL nanofiltration membranes.

It can be observed from the figures that rejection values for the solutes with both membranes generally increase with increasing molar mass for the different categories of  $\log K_{ow}$ -values. At molar masses above 200 g/mol, most organic solutes are very well rejected (>90%) by the membranes. The membranes thus offer an effective barrier for most organic pollutants with a molar mass over 200 g/mol.

Upon comparison of rejection values in the different categories of hydrophobicity, it becomes clear that for both membranes, rejection values are significantly lower for transphilic ( $1 < \log K_{ow} < 3$ ) and hydrophobic compounds ( $\log K_{ow} > 3$ ) compared to hydrophilic compounds of similar molar mass. This has also been observed before in the literature [1-9].

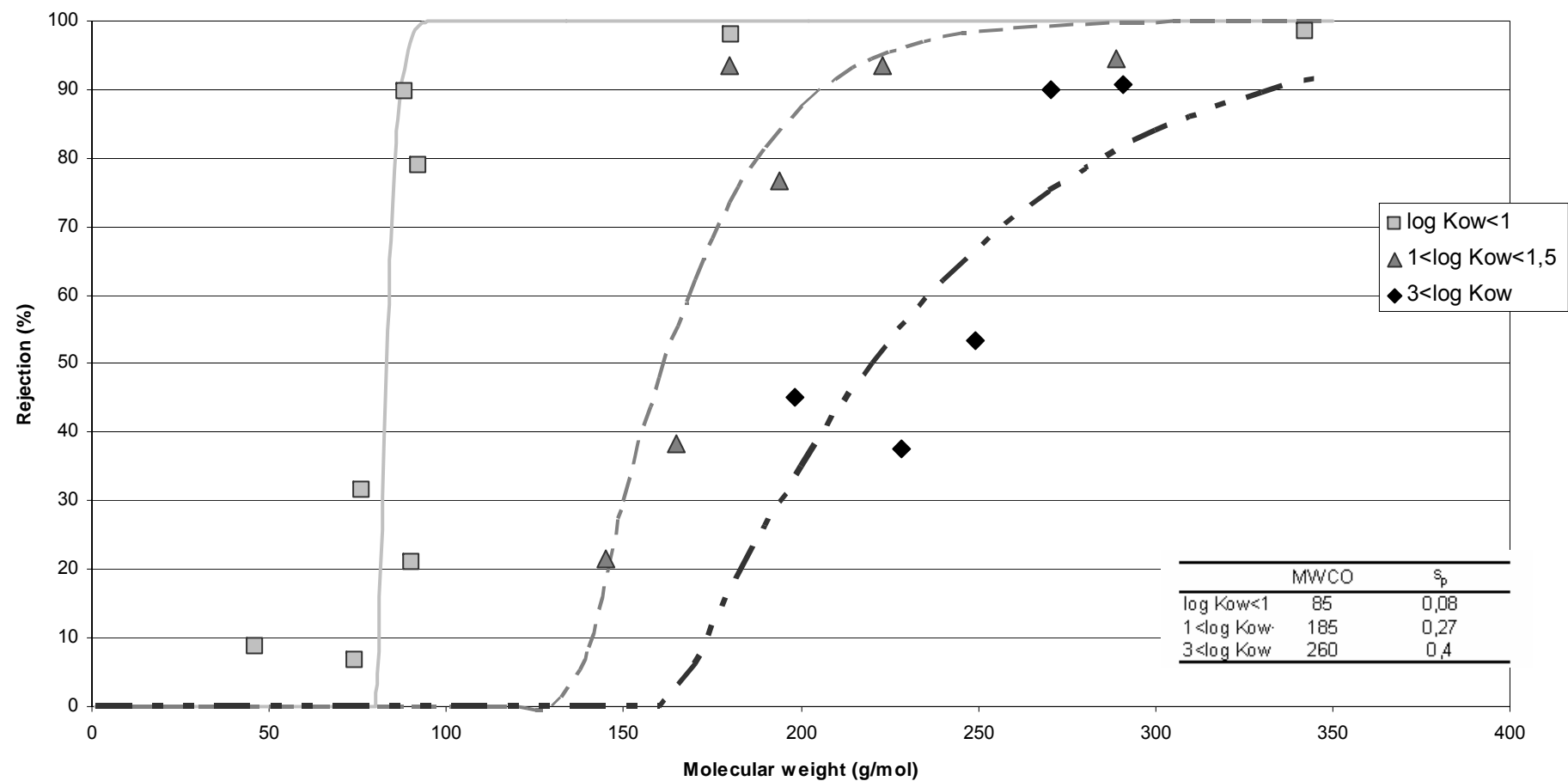


Figure 2.4 – Rejection of selected organic solutes of different hydrophobicity as a function of molar mass for Trisep TS80

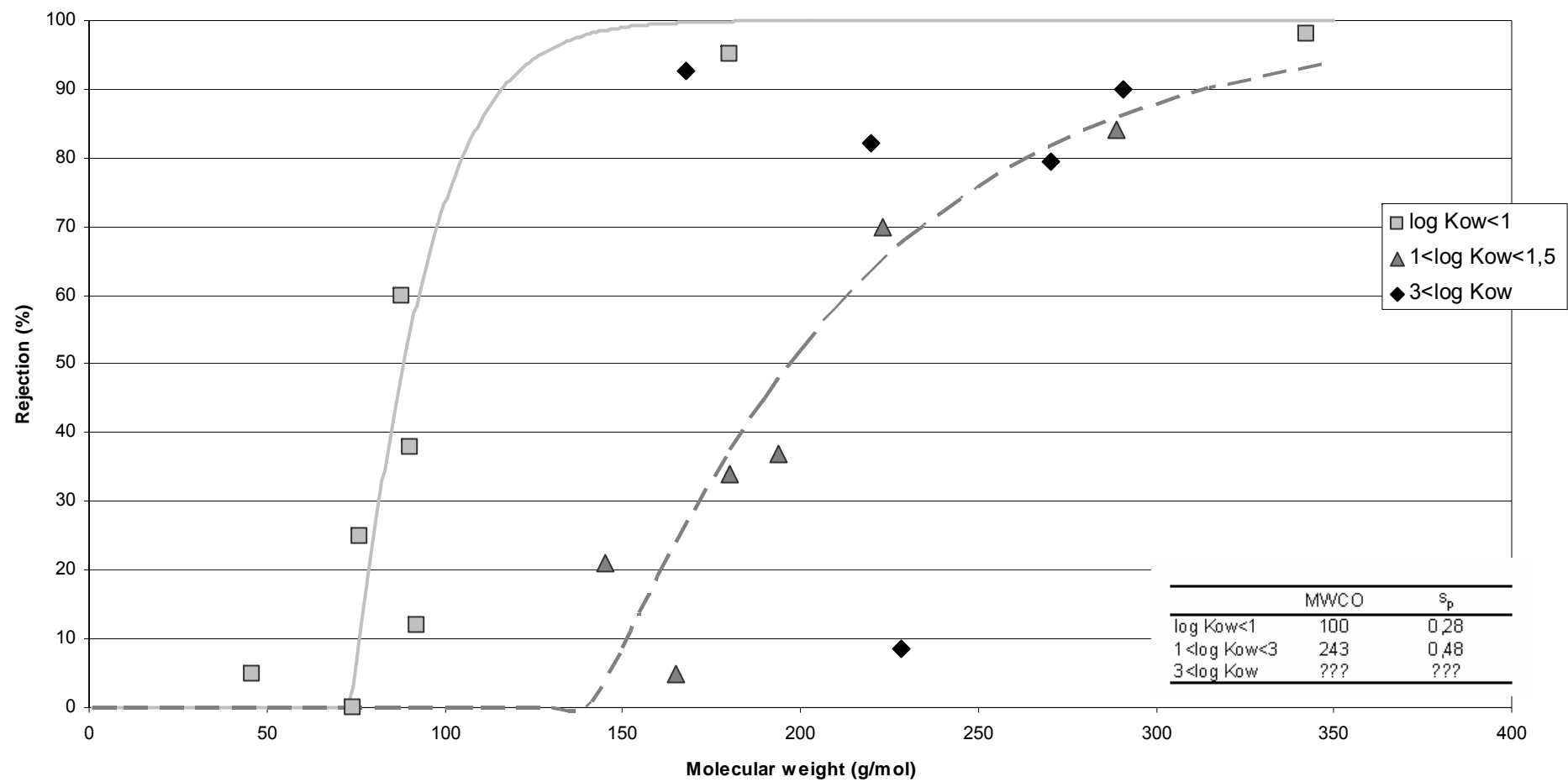


Figure 2.5 – Rejection of selected organic solutes of different hydrophobicity as a function of molar mass for Desal HL



Hydrophilic molecules ( $\log K_{ow} < 1$ ) with low molar mass ( $MW < 150$ ) are removed to a much higher extent by the membranes than the transphilic and hydrophobic molecules, which demonstrate low rejections up to higher molar mass values (e.g., approximately 250 g/mol for the Trisep TS80 membrane).

The curves in Figures 2.4 and 2.5 represent the modelled rejection curves, modelled as described in Equation (2.2). The values of the fitting parameters for the rejection curves are summarized in the inlay. For each curve representing solutes of different hydrophobicity, two fitting parameters, namely the molecular weight cut-off and the standard deviation on this cut-off are determined. The fitted MWCO-values reflect the molar masses at which rejection for solutes of a certain category of hydrophobicity reaches 90% (and can thus be compared to the MWCO-value given by the manufacturer), whereas the values for the standard deviation reflect the shape of the curves (a small standard deviation corresponds to a sharp increase in rejection, a larger standard deviation corresponds to a more gradual increase of the rejection).

The results clearly indicate that the hydrophobicity of solutes has a large effect on the rejection. It is apparent that for the Trisep TS80 membrane, the sigmoidal rejection curves are located at much higher molar mass values for the hydrophobic solutes, indicating that more hydrophobic solutes have lower rejection compared to hydrophilic solutes (which is in agreement with the literature). The rejection curve for the transphilic solutes is located in between the two extremes. Also for the Trisep TS 80, it can be seen that the shape of the rejection curve is changing for solutes of different hydrophobicity. For hydrophilic solutes, a sharp increase in rejection is observed, around a molar mass value of about 90 g/mol. For hydrophobic solutes on the other hand, the transition from low to high rejection is less pronounced. This can be explained by the difference in solute-membrane interactions: for hydrophilic

solutes, it is assumed that no hydrophobic/adsorptive interactions occur and steric hindrance is the only rejection mechanism. Therefore, it was hypothesized that the rejection curve for hydrophilic solutes represents the actual pore size distribution of the membrane.

For hydrophobic solutes, hydrophobic/adsorptive interactions with the membrane surface influence the rejection (hydrophobic interactions result in a lower rejection (i.e. an increased solute mass transfer)). As can be seen from the shape of the rejection curve, the influence of the hydrophobic interactions on the rejection is larger for larger solutes (i.e. the decrease in rejection is larger for larger solutes). The latter trend is logical: if steric hindrance would be the only rejection mechanism, all hydrophobic solutes with a molar mass above the molecular weight cut-off (which is 200 g/mol for this membrane) would have a similar, high rejection value.

For the Desal HL membrane, the same trends can be seen for the hydrophilic and transphilic solutes. For the hydrophobic solutes however, the correlation is less clear. This indicates that solute hydrophobicity, expressed as  $\log K_{ow}$ , is not always the most suitable parameter to describe solute-membrane affinity and a more advanced transport model is necessary. Moreover, the categories are just a rough division between hydrophilic, transphilic and hydrophobic solutes. Especially for hydrophobic solutes the solute-membrane affinity effect may be more critical than expressed by these categories.

When comparing the fitting parameters, it becomes apparent that Desal HL has a higher MWCO than Trisep TS80 for the hydrophilic and transphilic solutes. This is probably due to a larger pore size of the Desal HL membrane (which is also shown by the higher pure water permeability).

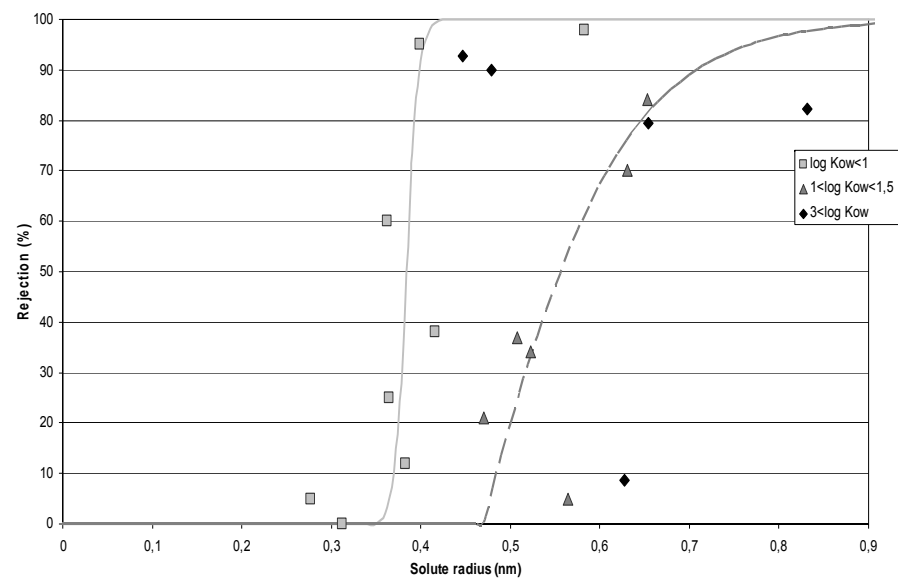
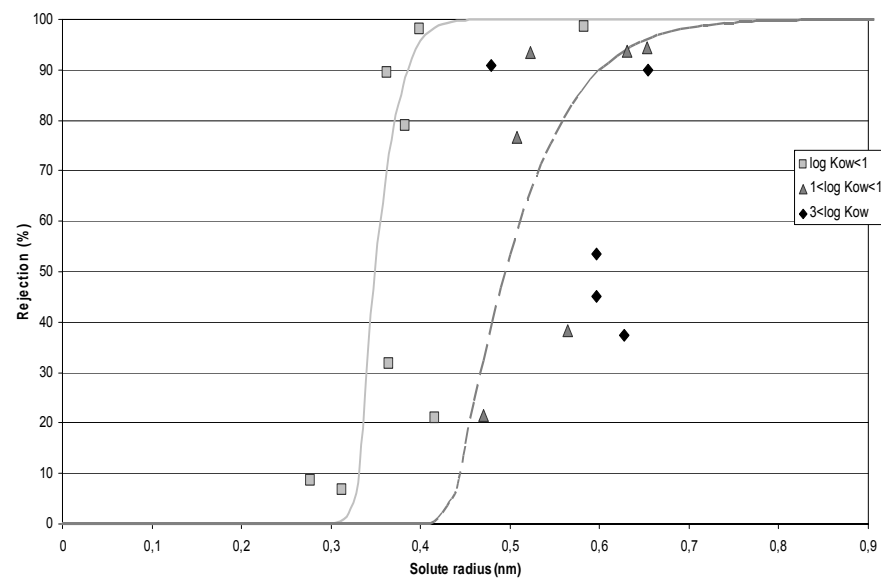


Figure 2.6 – Rejection of selected organic solutes of different hydrophobicity as a function of solute size for Trisep TS80 (left) and Desal HL (right)

The same results can also be plotted as a function of solute size, instead of solute molar mass. Figure 2.6 summarizes the results for both Trisep TS80 and Desal HL. It is obvious that the same trends can be seen as when the rejection is plotted as a function of molar mass. Rejection is lower for hydrophobic and transphilic solutes, and the rejection curves are less steep compared to the hydrophilic solutes. It is again apparent that the correlation is less clear for hydrophobic solutes, indicating again that  $\log K_{ow}$  is not always the most suitable parameter to describe the extent of the hydrophobic-hydrophobic interactions

For unknown uncharged compounds, the modelling approach followed here allows for semi-quantitative prediction of rejection by knowledge of two readily available parameters: molar mass and  $\log K_{ow}$ . Of course this prediction would only be valid for these two types of membranes since the difference between rejection curves for hydrophilic and hydrophobic solutes for these membrane are known from the experiments. To solve this drawback, a method needs to be developed to yield a quick screening of the shift in molecular weight cut-off (i.e. the fitted MWCO values) and the change of the shape (i.e. the fitted standard deviation) of the curves for different membranes. This in turn should be related to readily available knowledge about the membranes. Since contact angle and theoretical molecular weight cut-off or pure water permeability are readily available parameters, the fitted molecular weight-cut off and standard deviation values in the inlays in Figures 2.4 and 2.5 should be related to the contact angle and molecular weight cut-off (or pure water permeability) for different membranes.

One example of the latter approach is shown in Figure 2.7. The rejection curve for the hydrophilic solutes in Table 2.3 (indicating the actual cut-off of the membranes, since it is assumed that no solute-membrane interactions are occurring), was

measured for two other membranes (Dow-Filmtec BW-30 and Koch TFC-XR, data not shown here) and again the MWCO was fitted.

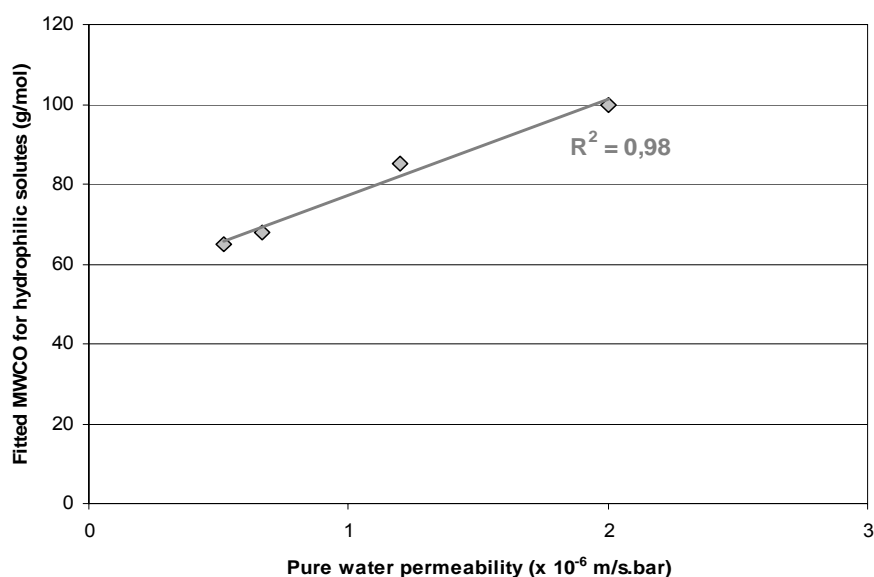


Figure 2.7 – Relationship between fitted MWCO for hydrophilic solutes and pure water permeability for selected membranes

Figure 2.7 shows the relationship between the fitted MWCO for hydrophilic solutes and the pure water permeability of all four membranes measured (the two nanofiltration membranes, Trisep TS80 and Desal HL; and the two reverse osmosis membranes Dow BW-30 and Koch TFC-XR). A clear correlation is observed, indicating that the size exclusion effect for organic solutes is closely related to membrane pure water permeability.

#### 4.3. Advanced transport model for uncharged solutes

As was indicated in the previous paragraph, solute hydrophobicity, expressed as log  $K_{ow}$ , may not be the best parameter to describe solute-membrane affinity. Therefore,

an advanced transport model was developed, in which solute-membrane affinity is derived from contact angle measurements.

The advanced transport model will be used in this section to model the rejection of four organic solutes as a function of water flux (or feed pressure). The model will be compared to the conventional convection-diffusion rejection model, solely based on size exclusion effects. Rejection models, solely based on steric effects, generally lead to an overestimation of the rejection values of solutes that interact with the membrane surface [32].

The goal of the advanced transport model is to reduce this overestimation by incorporating solute-membrane interactions into the model. The model will result in better insight into the contributions of steric vs. hydrophobic interactions to solute rejection.

#### 4.3.1. Determination of solute-membrane affinity parameter $\Delta G_i$

The different surface tension parameters  $\gamma_{S''}^{LW}$ ,  $\gamma_{S''}^+$  and  $\gamma_{S''}^-$  of the membranes, determined by the contact angle measurements with the three liquids diiodomethane, Milli-Q water and glycerol, are shown in Table 2.5. The same table also shows the surface tension parameters of the glass plate used.

	$\gamma^{LW}$	$\gamma^+$	$\gamma^-$
Trisep TS 80	40.8	0	37.0
Desal HL	34.8	0.8	37.0
glass	27.7	4.2	50.0

Table 2.5 – Surface tension components of the membranes as determined by contact angle measurements (at 20°C, in mJ/m<sup>2</sup>)

Trisep TS80 has the highest contribution of the apolar part  $\gamma_{S''}^{LW}$  of the surface tension, indicating that it is probably the most hydrophobic (as could already be expected based on the higher contact angle with water (compared to the Desal HL membrane)).

The surface tension parameters of the three different solutes, 2-ethoxyethanol, diethylphthalate and dibutylphthalate, were determined by performing contact angle measurements with the three liquid solutes on the two different membranes and on the glass. For glycerol, the surface tension parameters were already known from the literature (see also Table 2.4).

With the obtained values for all surface tension components, the solute-membrane affinities  $\Delta G_i$  in aqueous solution were determined using Equation (2.18). The contact area  $A$  between a solute molecule and the membrane is determined from the solute diameter as [22]:

$$A = \frac{\pi \cdot r_s^2}{2} \quad (2.23)$$

The Stokes-radii of the solutes will be used from here on in the calculations. The different calculated values of  $\Delta G_i$  are summarized in Table 2.6. A positive value of  $\Delta G_i$  indicates that repulsive Van der Waals forces exist between solute and membrane and no spontaneous transfer of the solute from the water phase to the membrane phase will occur. Therefore, rejection will be higher than could be expected based on purely steric hindrance. A negative value of  $\Delta G_i$  indicates solute-membrane affinity (Van der Waals attraction) and easier transfer of the solute from the water phase to the membrane phase. At more negative  $\Delta G_i$ , the solute-membrane affinity will be higher and rejection lower than expected, based on size exclusion.

$\Delta G_i$ ( $\times 10^{-21}$ J)	
<b>Trisep TS-80</b>	
glycerol	5.3
2-ethoxyethanol	-9.4
diethylphthalate (DEP)	-16.8
dibutylphthalate (DBP)	-96.3
<b>Desal HL</b>	
glycerol	4.6
2-ethoxyethanol	-7.3
diethylphthalate (DEP)	-12.7
dibutylphthalate (DBP)	-57.7

Table 2.6 – Calculated values of solute-membrane interaction energies  $\Delta G_i$  (in J) for the different solutes on the different membranes.

As can be seen from Table 2.6,  $\Delta G_i$  is smaller (more negative) for the Trisep TS80 membrane, indicating more affinity of the organic solutes for the Trisep TS80 than for the Desal HL membrane. This could be expected based on the contact angle measurements of both membranes with water: the Desal HL has a smaller contact angle with water and is thus more hydrophilic.

#### 4.3.2. Characterisation of the membrane pore size

For glycerol, the free energy of interaction with the membrane ( $\Delta G_i$ ) is larger than 0 for both the Trisep TS80 and the Desal HL membrane, indicating that no spontaneous partitioning of glycerol due to solute-membrane affinity will occur. In contrast to glycerol, 2-ethoxyethanol shows significant affinity for the membrane surface, as can be seen from the negative values of  $\Delta G_i$  in Table 2.6. This presence of solute-membrane interactions for 2-ethoxyethanol is surprising, since according to its  $\log K_{ow}$ , it should be hydrophilic, like glycerol. This again confirms the conclusion



that  $\log K_{ow}$  is not the most suitable parameter to describe solute-membrane affinity (and thus hydrophobic-hydrophobic interactions).

Experimentally obtained rejection values for glycerol and 2-ethoxyethanol are plotted as a function of solvent flux for the Trisep TS80 and Desal HL membranes in Figures 2.8 and 2.9 (squares).

The full-lines in the figures represent the rejection curves, modelled with the advanced transport model, using Equation (2.12) for the partition coefficient  $K$ . With  $\Delta G_i$  known from Paragraph 4.3.1, the only unknown variables in the model for each membrane are  $r_p$  and  $\Delta x/\varepsilon$ .

The rejection curves for glycerol and 2-ethoxyethanol on both membranes were thus fitted by the parameters  $r_p$  (the average membrane pore size) and the ratio of membrane thickness over membrane porosity  $\Delta x/\varepsilon$ , using an optimisation procedure (Solver, Excel<sup>®</sup>).

The values of the average pore radii  $r_p$  obtained with glycerol for the Trisep TS80 and the Desal HL membrane are 0.36 nm and 0.43 nm, respectively. With the same value of  $\Delta x/\varepsilon$ , the values of the average pore radii obtained with 2-ethoxyethanol are 0.36 nm and 0.42 nm on the Trisep TS80 and Desal HL membranes, respectively. It is obvious that the values for the pore radii obtained with the different solutes glycerol and 2-ethoxyethanol are very close, even though the interaction energies with the membrane are completely different. Moreover, the modelled rejection values seem to fit/predict the experimentally obtained rejection values quite well. This demonstrates the applicability of the advanced transport model.

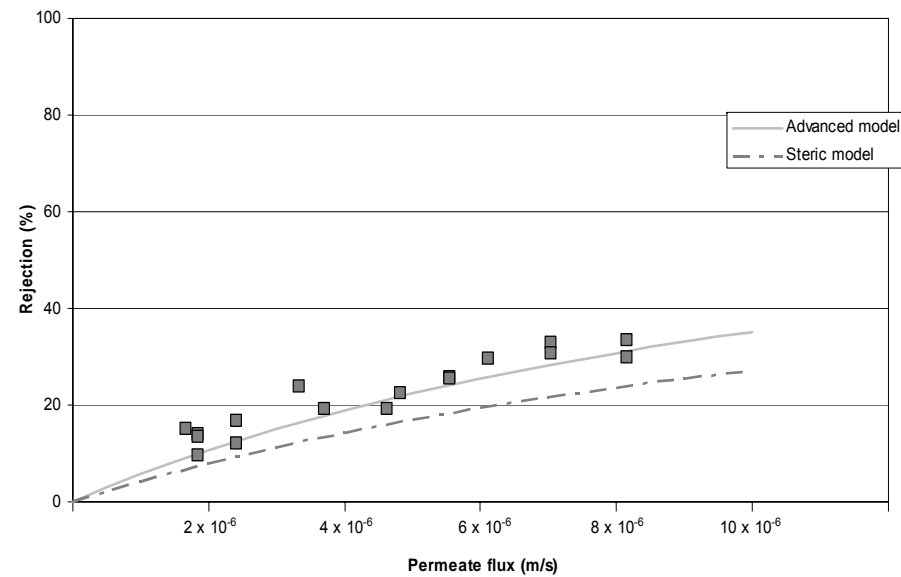
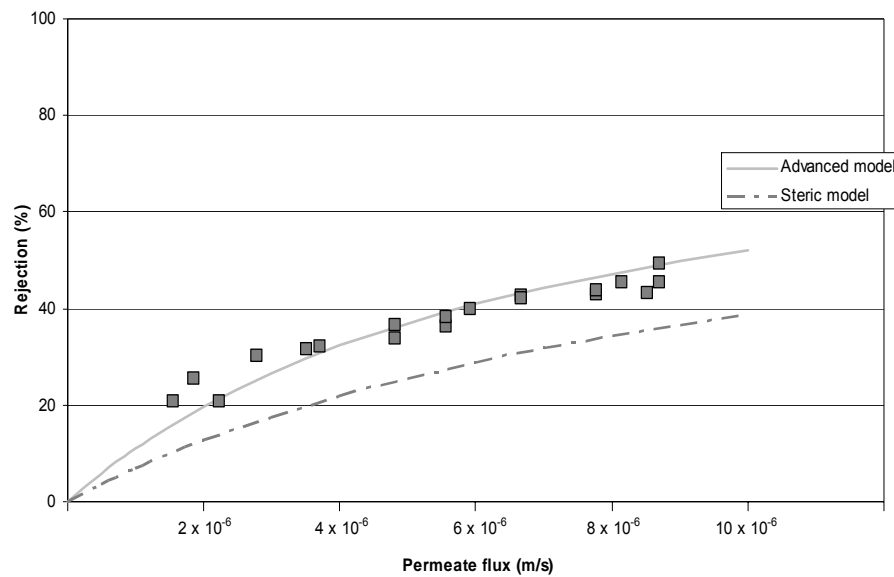


Figure 2.8 – Rejection values and models for glycerol las a function of permeate flux on Trisep TS80 (left) and Desal HL (right) membranes

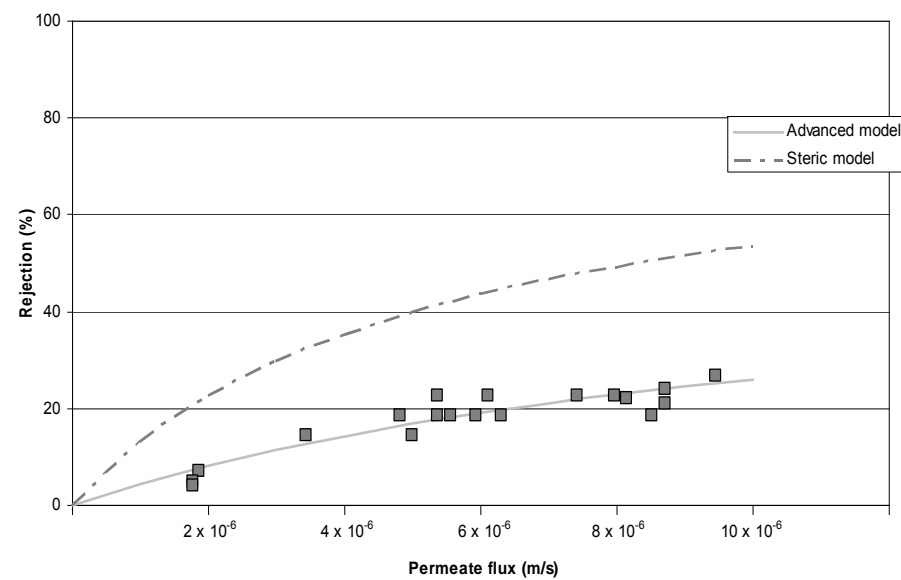
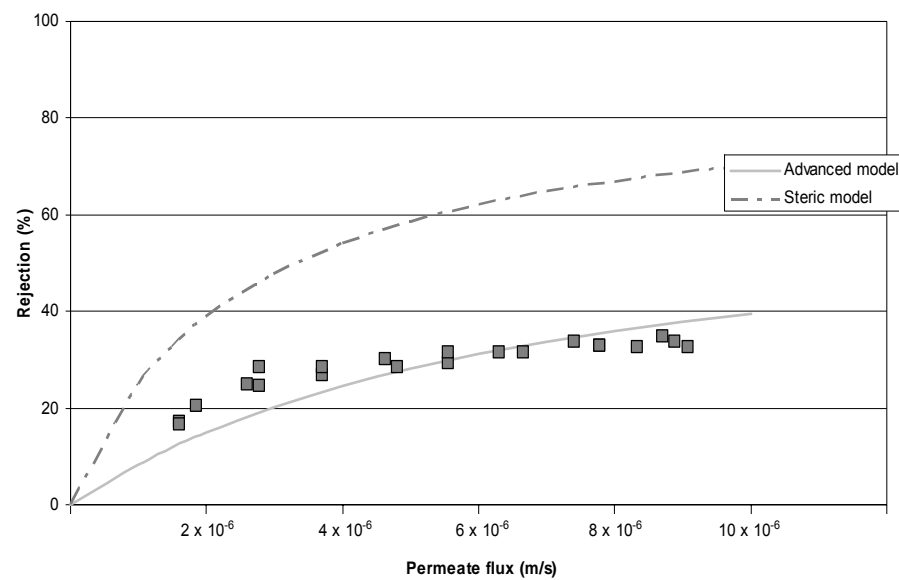


Figure 2.9 – Rejection values and models for 2-ethoxyethanol as a function of permeate flux on Trisep TS80 (left) and Desal HL (right) membranes

The values of the average pore radii  $r_p$  for the Trisep TS80 and the Desal HL membrane are 0.36 nm and 0.43 nm, respectively. The Trisep TS80 thus has a smaller pore size than the Desal HL, which could already be expected based on the lower pure water permeability and the lower fitted MWCO for hydrophilic solutes, as discussed in Paragraph 4.2. Steric hindrance between the solutes and the membranes will thus be larger for the Trisep TS80 as was also already clear from Paragraph 4.2.

The obtained values of  $r_p$  and  $\Delta x/\varepsilon$  can now be used as parameters in the simple steric hindrance model, using  $K=(1-\lambda)^2$  as partition coefficient. The results for the steric hindrance model are represented as the dashed lines in Figures 2.8 and 2.9. From the figures, it is apparent that the rejection values of glycerol are underestimated on both membranes, and the rejection values of 2-ethoxyethanol are overestimated on both membranes, when using the traditional steric hindrance transport model. This could be expected, since 2-ethoxyethanol showed significant membrane affinity, leading to an increased partitioning and a facilitated transport of the solute through the membrane, resulting in lower observed rejections than could be expected, based purely on size exclusion effects. For glycerol,  $\Delta G_i$ , the interaction energy with the membrane, is higher than 0, indicating that glycerol will not spontaneously partition into the membrane phase, and energy input is necessary for the solute to enter the membrane phase. Therefore, the rejection of glycerol is higher than could be expected, based purely on size exclusion effects.

#### 4.3.3. Rejection prediction

With the values of  $r_p$  and  $\Delta x/\varepsilon$  determined from the previous paragraph, the advanced transport model, using the partition coefficient  $K$  from Equation (2.12), can now be used as a predictive model for the rejection of other organic solutes on the Trisep TS80 and Desal HL membrane, given that the solute-membrane interaction energy  $\Delta G_i$  is known. The rejection values of the two solutes diethylphthalate and dibutylphthalate as a function of feed pressure are shown in Figures 2.10 and 2.11 for the Trisep TS80 and Desal HL membranes (squares). For both solutes, rejection was modelled using both the traditional steric rejection model and the advanced rejection model accounting for hydrophobic interactions. Both model curves were calculated, using the membrane parameters  $r_p$  and  $\Delta x/\varepsilon$  as determined above. As can be seen from the figures, the steric model significantly overpredicts the rejection values for the solutes that show affinity for the membrane surface. The advanced transport model, however, quite accurately predicts the experimental rejection values. The advanced transport model thus offers good opportunities for rejection modelling and prediction.

#### 4.3.4. Influence of steric and hydrophobic interactions on rejection as a function of permeate flux

As can be seen from Figures 2.8 to 2.11, the advanced transport model, using the partition coefficient  $K = (1 - \lambda)^2 \exp\left(-\frac{\Delta G_i}{k \cdot T}\right)$  offers good opportunities to model and predict the rejections of uncharged organic solutes with polymeric membranes. It has to be noted, however, that the partition coefficient as determined above, is constant

as a function of permeate flux, and thus not always predicts rejection values at low permeate fluxes correctly (see Figures 2.10 and 2.11).

Therefore, the following definition of the partition coefficient  $K = \exp\left(\frac{-(\Delta G_i + v\Pi)}{k \cdot T}\right)$

is introduced into the model in this paragraph. The partition coefficient thus becomes a function of both the solute-membrane affinity, and a pressure dependent size exclusion term,  $v\Pi$ .

By introducing the pressure/flux dependent term  $v\Pi$ , the model loses its predictive capabilities and can now only be used as a fitting tool. A closer fit to the experimentally obtained rejection values can be obtained, however.

In this Paragraph, the previously obtained values of  $r_p$  and  $\Delta x/\varepsilon$  will be used in Equation (2.7), but the value of the partition coefficient  $K$  will be fit to the rejection values, to obtain the closest fit between the rejection data and the model.

Figures 2.12 to 2.15 show the closest fit possible of the model to the rejection data for all solutes on the two membranes. The fitted values of the partition coefficient  $K$  used in the advanced transport model are given in Table 2.7 (for both membranes).

Closer analysis of the values of  $K$  can give more information on the separate contribution of solute-membrane affinity and steric effects on the rejection of the organic solutes and show how rejection is dependent on feed pressure/permeate flux. With the fitted values of  $K$  and the calculated values for  $\Delta G_i$ ,  $v\Pi$  can be calculated. The calculated values of  $v\Pi$  are shown in Table 2.7. A comparison of the values of  $\Delta G_i$  and  $v\Pi$  clearly shows the contribution of hydrophobic vs. steric interactions on the partitioning of the solutes in the membranes.

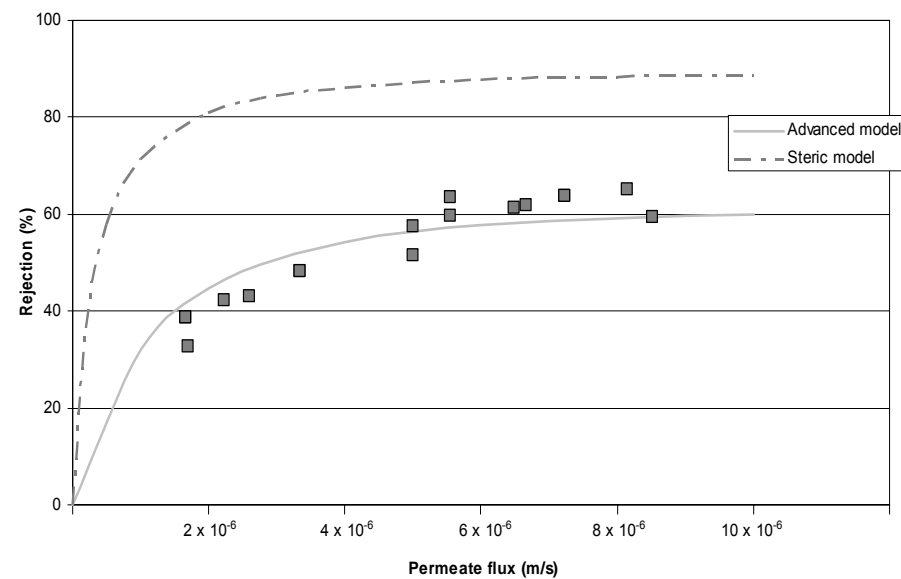
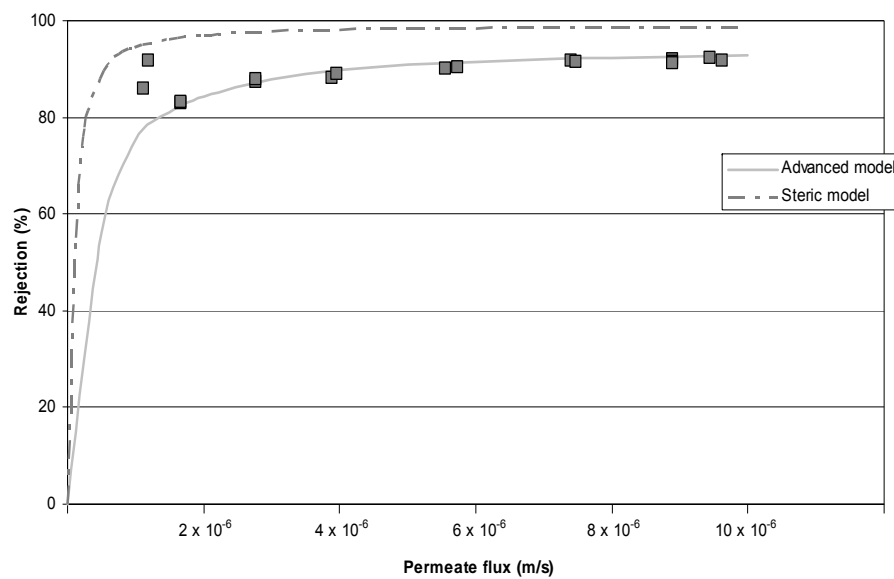


Figure 2.10 – Rejection values and models for diethylphthalate as a function of permeate flux on Trisep TS80 (left) and Desal HL (right) membranes

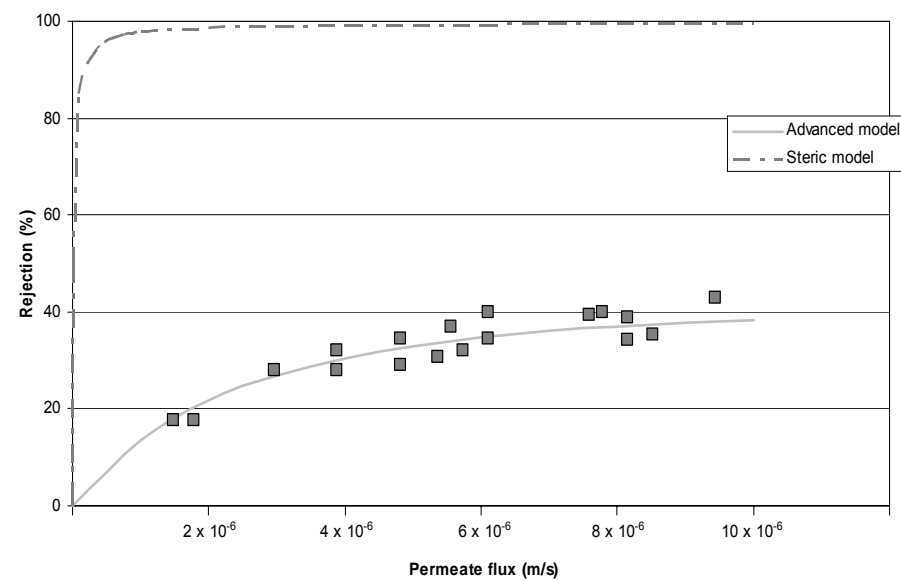
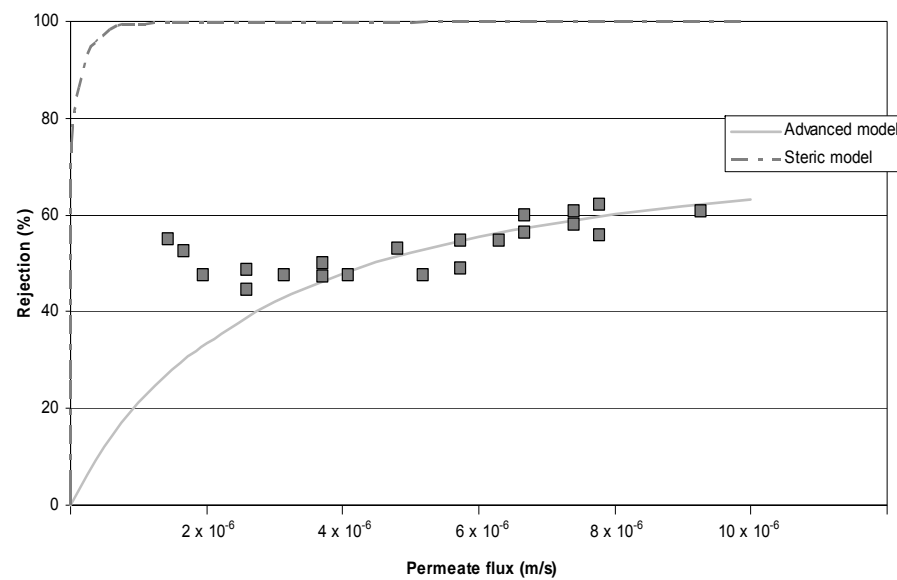


Figure 2.11 – Rejection values and models for dibutylphthalate as a function of permeate flux on Trisep TS80 (left) and Desal HL (right) membrane



It is obvious that for all solutes on both membranes:  $|\Delta G_i| < |\nu \cdot \Pi|$ . The influence of steric hindrance effects thus still seems to prevail in determining partitioning (which is also, since membrane filtration is still a sieving process), but it is apparent that the influence of solute-membrane affinity can definitely not be neglected.

Glycerol is the smallest of the 4 solutes, and the free energy of steric interaction ( $\nu \cdot \Pi$ ) is the smallest of all solutes for both membranes. This indicates that steric partitioning of glycerol is easier than for the other solutes, i.e., steric hindrance is the smallest. However, no partitioning of glycerol due to solute-membrane affinity will occur spontaneously (since  $\Delta G_i > 0$ ). 2-ethoxyethanol is slightly larger than glycerol, which immediately becomes clear in the value of  $\nu \cdot \Pi$ : the free steric energy to overcome for 2-ethoxyethanol to partition into the membrane is larger than for glycerol, indicating that more steric hindrance is occurring.

For diethylphthalate (DEP) and dibutylphthalate (DBP), the values of  $\Delta G_i$  become increasingly negative, indicating that both solutes show significant membrane affinity. The affinity is largest for DBP (which incidentally also has the highest  $\log K_{ow}$ ). DBP is also larger than DEP, which is translated into a larger (more positive) value for  $\nu \cdot \Pi$ : the steric hindrance to overcome for DBP to partition into the membrane is considerably larger than for DEP, 2-ethoxyethanol or glycerol.

The free energy of steric interaction ( $\nu \cdot \Pi$ ) thus follows the same trend as the solute size: a larger solute size results in a more positive free energy of steric interaction (and thus in a larger energy to overcome for the solute to partition into the membrane).

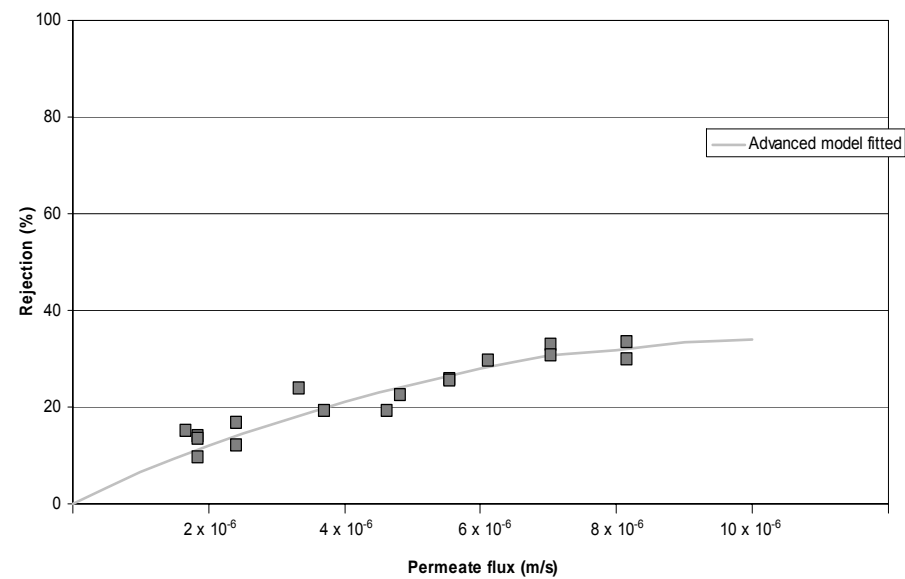
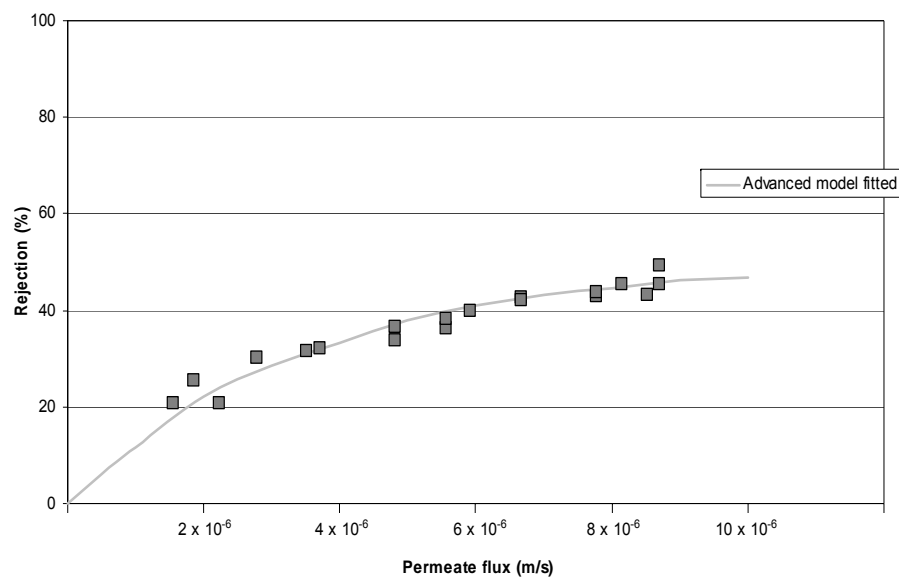


Figure 2.12 – Rejection values and closest fit with advanced model for glycerol as a function of permeate flux on Trisep TS80 (left) and Desal HL (right) membrane

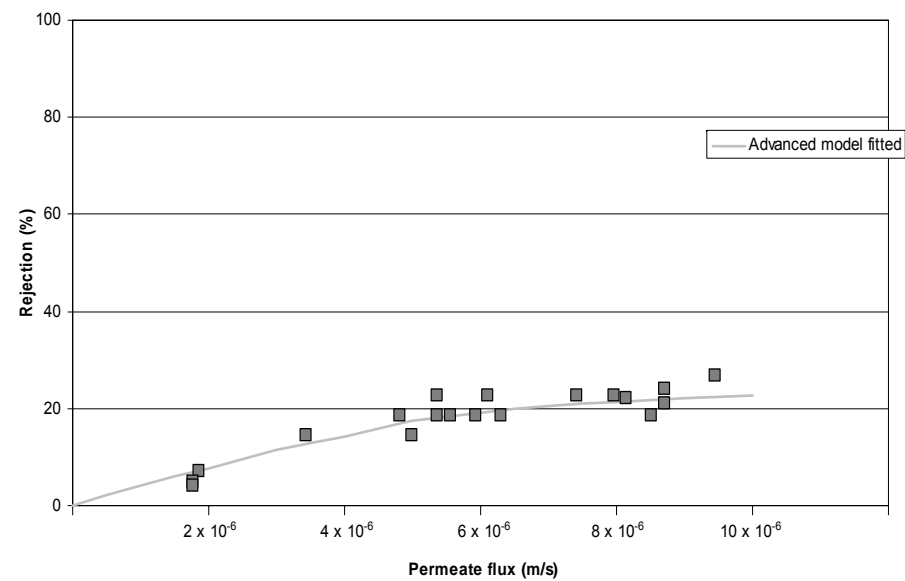
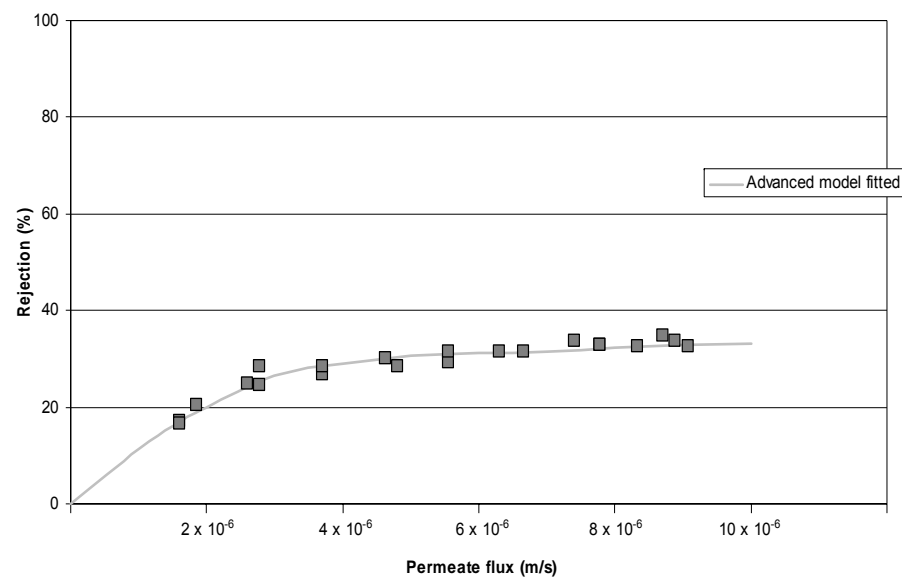


Figure 2.13 – Rejection values and closest fit with advanced model for 2-ethoxyethanol as a function of permeate flux on Trisep TS80 (left) and Desal HL (right) membrane

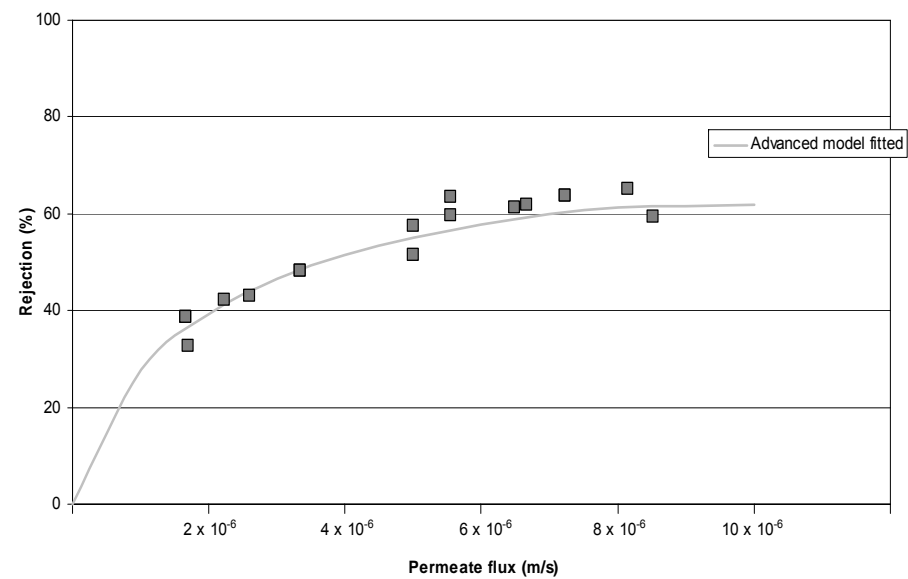
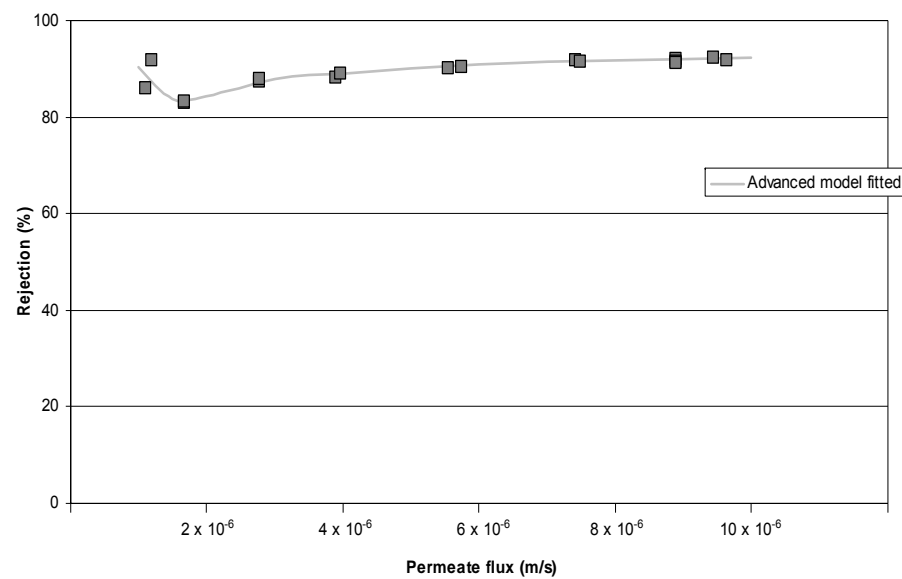


Figure 2.14 – Rejection values and closest fit with advanced model for diethylphthalate as a function of permeate flux on Trisep TS80 (left) and Desal HL (right) membrane

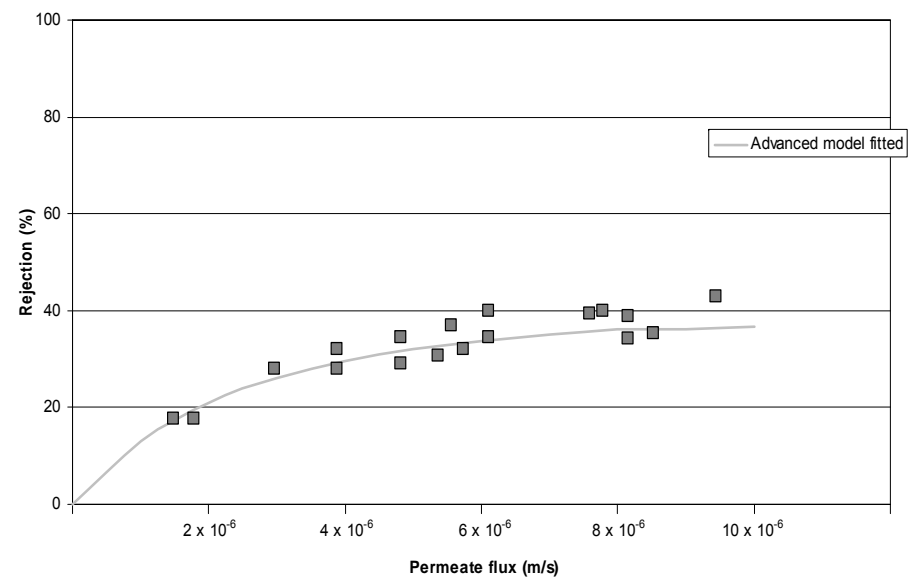
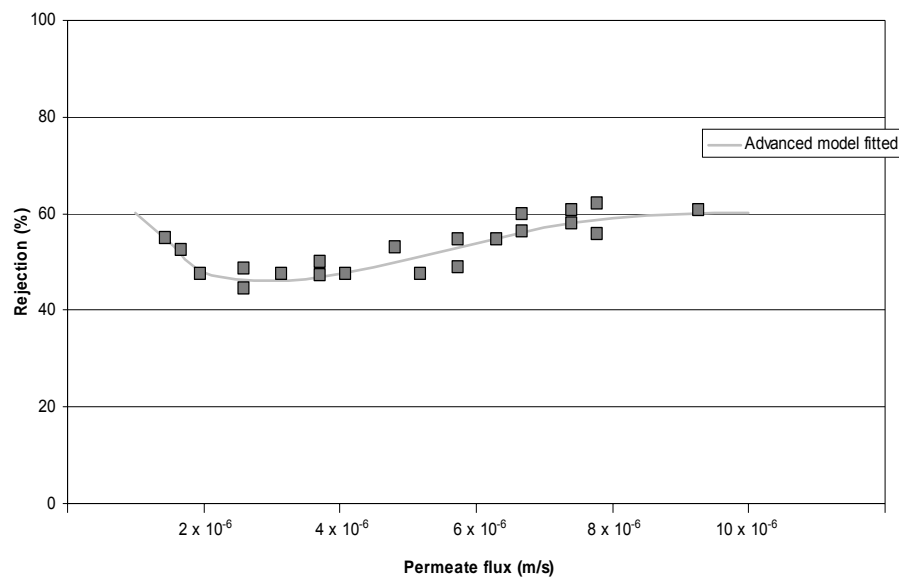


Figure 2.15 – Rejection values and closest fit with advanced model for dibutylphthalate as a function of permeate flux on Trisep TS80 (left) and Desal HL (right) membrane

The values of  $\nu \cdot \Pi$  for all solutes are smaller for the Desal HL membrane than for the Trisep TS80 membrane due to the larger average pore size of the Desal HL: a larger pore size results in less steric hindrance, and thus a smaller  $\nu \cdot \Pi$ . The relationship of  $\nu \cdot \Pi$  with  $\lambda$  is thus clear.

Unexpectedly, it is apparent that for all solutes with both membranes,  $\nu \cdot \Pi$  becomes smaller with increasing feed pressure (or increasing water flux). Thus, the pressure exerted by the elastic polymer matrix on the different solutes, decreases with increasing water flux. This could be due to two effects: one effect is called the “suction effect” [33]: at higher water fluxes, the water has a preferential flow through the pores and “sucks” dissolved molecules through these membrane pores due to the high preferential flow. Another effect could be an increase of the pore size with increasing feed pressure: due to the elasticity of the pores, the pores expand with higher feed flows through the pores, thus increasing the average pore size of the membrane.

The higher partitioning of organic solutes into the membranes with increasing feed pressure is in agreement with previous observations made by Kimura et al. (2003) [12], who indicated an increased adsorption of hydrophobic solutes onto hydrophobic membranes with increasing feed pressure.

	$J_v$ ( $\times 10^{-6}$ m/s)	glycerol		2-ethoxyethanol		diethylphthalate		dibutylphthalate	
		K (-)	$v.\Pi$ ( $\times 10^{-21}$ J)	K (-)	$v.\Pi$ ( $\times 10^{-21}$ J)	K (-)	$v.\Pi$ ( $\times 10^{-21}$ J)	K (-)	$v.\Pi$ ( $\times 10^{-21}$ J)
<b>Trisep TS-80</b>	1.0	0.14	6.34	0.27	8.85	0.02	22.7	0.065	35.8
	2.0	0.13	6.34	0.27	8.85	0.06	18.2	0.18	31.7
	3.0	0.14	6.64	0.27	8.85	0.06	18.2	0.25	30.3
	4.0	0.14	6.49	0.29	8.57	0.065	17.9	0.285	29.8
	5.0	0.14	6.34	0.31	8.30	0.065	17.9	0.295	29.7
	6.0	0.15	6.34	0.33	8.04	0.065	17.9	0.295	29.7
	7.0	0.15	6.20	0.35	7.81	0.065	17.9	0.29	29.7
	8.0	0.16	6.06	0.36	7.69	0.065	17.9	0.292	29.7
	9.0	0.16	5.88	0.37	7.58	0.065	17.9	0.30	29.6
	10.0	0.17	5.75	0.38	7.47	0.065	17.9	0.31	29.5
<b>Desal HL</b>	1.0	0.2	5.10	0.41	6.35	0.34	9.51	0.58	21.2
	2.0	0.2	5.10	0.41	6.35	0.34	9.51	0.58	21.2
	3.0	0.2	5.10	0.40	6.45	0.33	9.63	0.58	21.2
	4.0	0.2	5.10	0.40	6.45	0.32	9.75	0.58	21.2
	5.0	0.2	5.10	0.39	6.55	0.31	9.88	0.58	21.2
	6.0	0.2	5.10	0.40	6.45	0.30	10.0	0.58	21.2
	7.0	0.2	5.10	0.405	6.4	0.29	10.2	0.58	21.2
	8.0	0.21	4.90	0.415	6.30	0.285	10.2	0.58	21.2
	9.0	0.215	4.81	0.42	6.25	0.285	10.2	0.585	21.2
	10.0	0.225	4.63	0.43	6.16	0.285	10.2	0.585	21.2

Table 2.7 – Fitted values for partition coefficient K and calculated values for steric hindrance energies  $v.\Pi$  as a function of permeate flux/feed pressure

This study showed that the advanced transport model gives a good indication of the effect of solute-membrane hydrophobic interactions on the rejection of uncharged organic solutes and can even serve as a predictive tool for the rejection of organic solutes with NF/RO.

The disadvantage for the advanced transport model is, for the moment, that calculation of the solute-membrane affinity is relatively easy for liquid solutes, but cumbersome for solid solutes.

## **5. Conclusions**

Two different models were constructed in this chapter to assess the influence of hydrophobic interactions (solute-membrane affinity) on the rejection of uncharged organic solutes.

Using a log-normal pore distribution model, different rejection curves for solutes of different hydrophobicity (expressed as  $\log K_{ow}$ ) were modelled based on experimental rejection values for organic solutes obtained with two different membranes (Trisep TS80 and Desal HL). Rejection of hydrophilic solutes ( $\log K_{ow} < 1$ ) appeared to be mainly (only) determined by steric interactions with the membrane, whereas for hydrophobic solutes ( $\log K_{ow} > 3$ ) solute-membrane affinity resulted in lower rejection values than could be expected purely based on steric interactions.

The modelled MWCO for hydrophilic solutes was located at lower molar mass values and a sharp increase in rejection at molar mass values above the MWCO was observed, whereas for hydrophobic solutes, the MWCO was located at higher molar mass values and a more gradual increase in rejection was found. Construction of a



rejection curve for hydrophobic solutes was more difficult and more scattering of experimental data points around the modelled curve was seen, indicating that  $\log K_{ow}$  may not be the most suitable parameter to describe solute-membrane interactions.

The second model used a novel approach in organic solute rejection, by introducing a solute-membrane affinity-dependent partition coefficient in the traditional Spiegler-Kedem transport equation. The partition coefficient consists of a term describing solute-membrane affinity and a term describing steric hindrance. The solute-membrane affinity could be determined by contact angle measurements and solving a set of Young-Dupré equations. Solute-membrane affinity appeared to be more significant for the most hydrophobic membrane, but did not always show a good correlation with the  $\log K_{ow}$  of the solutes.

Depending on the definition of the partition coefficient, the term describing steric hindrance was regarded as flux dependent or flux independent. The use of a flux independent partition coefficient turns the advanced transport model into a predictive model (incorporating solute-membrane affinity) for the rejection of uncharged organic solutes. The transport model was able to predict rejection values quite well. Based on the membrane pore size, determined from the advanced transport model, the purely steric model gave underpredictions for the rejection of solutes for which repulsive Van der Waals forces between solute and membrane were present (no spontaneous transfer of the solute from the water to the membrane phase). For solutes that showed membrane affinity (spontaneous transfer of the solute to the membrane phase is occurring), the purely steric model gave overpredictions of the rejection. This demonstrates that solute-membrane affinity is an important factor in rejection of uncharged organic solutes.

If the flux dependent partition coefficient is used, the model loses its predictive capacity, but the influences of steric hindrance and solute-membrane affinity on rejection can be compared in more detail. If the model is fit to the experimental rejection data with the partition coefficient  $K$ , the influence of steric hindrance on organic solute partitioning in the membrane can be calculated from  $K$  and the calculated solute-membrane affinity. As could be expected, the steric hindrance seemed to increase for larger solutes, and also increased with decreasing membrane pore size, indicating the model is physically correct. The steric hindrance also seemed to decrease with increasing feed pressure, indicating more partitioning of solutes at higher feed pressures. This is in agreement with observations from the literature.

## References

- [1] K.O. Agenson, J.I. Oh and T. Urase, Retention of a wide variety of organic pollutants by different nanofiltration/reverse osmosis membranes: controlling parameters of process, *Journal of Membrane Science*, 225 (2003) 91.
- [2] K. Kimura, G. Amy, J.E. Drewes, T. Heberer, T.U. Kim and Watanabe Y., Rejection of organic micropollutants (disinfection by-products, endocrine disrupting compounds, and pharmaceutically active compounds) by NF/RO membranes, *Journal of Membrane Science*, 227 (2003) 113.
- [3] Y. Kiso, T. Kon, T. Kitao and K. Nishimura, Rejection properties of alkyl phthalates with nanofiltration membranes, *Journal of Membrane Science*, 182 (2001) 205.
- [4] Y. Kiso, Y. Sugiura, T. Kitao and K. Nishimura, Effects of hydrophobicity and molecular size on rejection of aromatic pesticides with nanofiltration membranes, *Journal of Membrane Science*, 192 (2001) 1.
- [5] L.D. Nghiem and A.I. Schäfer, Adsorption and transport of trace contaminant estrone in NF/RO membranes, *Environmental Engineering Science*, 19 (6) (2002) 441.
- [6] L.D. Nghiem, A.I. Schäfer and M. Elimelech, Removal of natural hormones by nanofiltration membranes: measurement, modelling and mechanisms, *Environmental Science & Technology*, 38 (2004) 1888.
- [7] A.I. Schäfer, L.D. Nghiem and T.D. Waite, Removal of the natural hormone estrone from aqueous solutions using nanofiltration and reverse osmosis, *Environmental Science & Technology*, 37 (2003) 182.
- [8] Y. Yoon, P. Westerhoff, J. Yoon and S.A. Snyder, Removal of 17 $\beta$ -estradiol and fluoranthene by nanofiltration and ultrafiltration, *Journal of Environmental Engineering*, 130 (12) (2004) 1460.
- [9] Y. Yoon, P. Westerhoff, S.A. Snyder and E.C. Wert, Nanofiltration and ultrafiltration of endocrine disrupting compounds, pharmaceuticals and personal care products, *Journal of Membrane Science*, 270 (2006) 88.
- [10] L. Braeken, R. Ramaekers, Y. Zhang, G. Maes, B. Van der Bruggen and C. Vandecasteele, Influence of hydrophobicity on retention in nanofiltration of aqueous solutions containing organic compounds, *Journal of Membrane Science*, 252 (2005) 195.

- [11] T.U. Kim, G. Amy and J.E. Drewes, Rejection of trace organic compounds by high-pressure membranes, *Water Science & Technology*, 51 (6-7) (2005) 335.
- [12] K. Kimura, G. Amy, J.E. Drewes and Y. Watanabe, Adsorption of hydrophobic compounds onto NF/RO membranes – an artifact leading to overestimation of rejection, *Journal of Membrane Science*, 221 (2003) 89.
- [13] K. Kimura, S. Toshima, G. Amy and Y. Watanabe, Rejection of neutral endocrine disrupting compounds (EDCs) and pharmaceutical active compounds (PhACs) by RO membranes, *Journal of Membrane Science*, 245 (2004) 71.
- [14] B. Van der Bruggen, J. Schaep, D. Wilms and C. Vandecasteele, A comparison of models to describe the maximal retention of organic molecules in nanofiltration, *Separation Science and Technology*, 35 (2) (2000) 169.
- [15] B. Van der Bruggen and C. Vandecasteele, Modelling of the retention of uncharged molecules with nanofiltration, *Water Research*, 36 (5) (2002) 1360.
- [16] E.R. Cornelissen, J. Verdouw, A.J. Gijsbertsen-Abrahamse and J.A.M.H. Hofman, A nanofiltration retention model for trace contaminants in drinking water sources, *Desalination*, 178 (1-3) (2005) 179.
- [17] W.M. Deen, Hindered transport of large molecules in liquid-filled pores, *AIChE Journal*, 33 (9) (1987), 1409.
- [18] K.S. Spiegler and O. Kedem, Thermodynamics of hyperfiltration (reverse osmosis): criteria for efficient membranes. *Desalination*, 1 (1966) 311.
- [19] W.R. Bowen, A.W. Mohammad and N. Hilal, Characterisation of nanofiltration membranes for predictive purposes – use of salts, uncharged solutes and atomic force microscopy, *Journal of Membrane Science*, 126 (1997) 91.
- [20] W.R. Bowen, J.S. Welfoot and P.M. Williams, Linearized transport model for nanofiltration: development and assessment, *AIChE Journal*, 48 (2002) 760.
- [21] A.W. Mohammad and N. Ali, Understanding the steric and charge contributions in NF membranes using increasing MWCO polyamide membranes, *Desalination*, 147 (2002) 205.
- [22] S. Bhattacharjee, A. Sharma and P.K. Bhattacharya, Estimation and influence of long range solute. Membrane interactions in ultrafiltration, *Industrial & Engineering Chemistry Research*, 35 (1996) 3108.

- [23] A. Ben-David, Y. Oren and V. Freger, Thermodynamic factors in partitioning and rejection of organic compounds by polyamide composite membranes, *Environmental Science and Technology*, 40 (2006) 7023.
- [24] R.H. Perry and D.W. Green, *Perry's Chemical Engineer's Handbook*, 7th ed., McGraw-Hill, New York, 1997.
- [25] T.L. Hill, *An introduction to statistical thermodynamics*, Addison-Wesley, Reading, 1960.
- [26] C.J. van Oss, Development and applications of the interfacial tension between water and organic or biological surfaces, *Colloids and Surfaces B: Biointerfaces*, 54 (2007) 2.
- [27] J.J. Jasper, The Surface Tension of Pure Liquid Compounds, *Journal of Physical Chemistry Reference Data*, 1 (1972) 841.
- [28] C.J. van Oss and R.F. Giese, Role of the properties and structure of liquid water in colloidal and interfacial systems, *Journal of Dispersion Science and Technology*, 25 (2004) 631.
- [29] A. Docoslis, R.F. Giese and C.J. van Oss, Influence of the water–air interface on the apparent surface tension of aqueous solutions of hydrophilic solutes, *Colloids and Surfaces B: Biointerfaces*, 19 (2) (2000) 147.
- [30] W. Hayduk and H. Laurie, Prediction of diffusion-coefficient for non-electrolytes in dilute aqueous solutions, *AIChE Journal*, 20 (1974) 611.
- [31] C.J. van Oss, *Interfacial forces in aqueous media*, 2<sup>nd</sup> ed., CRC Press, London, 2006.
- [32] L.D. Nghiem, A.I. Schäfer and M. Elimelech, Removal of natural hormones by nanofiltration membranes: measurement, modelling, and mechanisms, *Environmental Science and Technology*, 38 (2004) 1888.
- [33] V. Geraldes and M.D. Afonso, Prediction of the concentration polarization in the nanofiltration/reverse osmosis of dilute multi-ionic solutions, *Journal of Membrane Science*, 300 (1-2) (2007) 20.



# **Chapter 3:**

## **Rejection of charged organic solutes**

**(Influence of electrostatic interactions)**

Parts of this chapter were based on:

A.R.D. Verliefde, E.R. Cornelissen, S.G.J. Heijman, J.Q.J.C. Verberk, G.L. Amy, B. Van der Bruggen and J.C. van Dijk, The role of electrostatic interactions on the rejection of organic solutes in aqueous solutions with nanofiltration, *Journal of Membrane Science*, (2008) in press, doi:10.1016/j.memsci.2008.05.022

## 1. Introduction

In the previous chapter, models for the rejection of uncharged organic solutes with NF/RO were developed and validated. It seemed that rejection of the uncharged organic solutes with NF/RO was mostly attributed to steric hindrance and hydrophobic effects between the solutes and the membrane polymeric matrix. Steric hindrance or size exclusion is basically a sieving mechanism: solutes with a size larger than the pore size of the membranes are efficiently removed, whereas smaller solutes may pass through the membrane [1-4]. Hydrophobic interactions between solutes and membranes may influence this steric hindrance: hydrophobic solutes can adsorb onto, and partition into, a hydrophobic membrane surface more easily, facilitating diffusion through the membrane, often resulting in lower rejections for hydrophobic solutes than may be expected purely based on size exclusion effects [5-9].

Most studies on the rejection mechanisms of organic micropollutants with NF/RO membranes have historically focused on neutral solutes, and especially on pesticides [1,2,10-21].

However, most NF/RO membranes are negatively charged at neutral pH due to the dissociation of acidic functional groups on the membrane surface. Therefore, electrostatic interactions between charged organic solutes and the charged membrane surface can also play a role in the rejection of organic micropollutants. Most studies on electrostatic interactions have reported an increase in rejection of negatively charged organic solutes due to electrostatic repulsion between the negatively charged membrane and the negatively charged organic solute [7,22-25]. This high rejection, however, is dependent on feed water pH, since both membrane



surface charge and organic solute charge vary according to pH (through the dissociation of the functional groups as a function of the  $pK_a$ ) [24]. Apart from feed water pH, membrane surface charge is also dependent on other feed water parameters, such as the presence of divalent cations (which appear to “shield” and thus reduce the effective membrane surface charge [24,26]), but also on the amount and nature of natural organic matter (NOM) in the feed water. Some studies have reported an increased, others a decreased negative membrane surface charge due to the deposition of natural organic matter [27-28].

Several numerical models have been suggested to explain the electrostatic effects on the rejection of inorganic ions [29-31]. These models always account for the Donnan exclusion effect: if the co-ion of a certain salt (the ion with a charge similar to the membrane surface charge) can not pass the membrane due to electrostatic repulsion, then the counter-ion is also rejected in order to counteract the potential difference that would arise between the different sides of the membrane if the counter-ion would not be rejected.

This study will investigate whether the Donnan exclusion mechanism also plays a role in the rejection of organic solutes bearing a charge opposite to the membrane surface charge. Most previous studies have focused, as mentioned before, only on effects of electrostatic repulsion between the membrane and organic ions carrying a similar charge.

This chapter will mechanistically investigate the effect of charge, but also of other organic solute parameters such as size and hydrophobicity on the rejection of these organic solutes with charged high pressure membranes. Firstly, the rejection of different organic acids with increasing molar mass will be determined. Since most

organic acids are negatively charged at neutral pH, this approach will help to study the effects of solute size and electrostatic repulsion on rejection. Secondly, the rejection of neutral, negatively charged, and positively charged pharmaceuticals with a wide range of physico-chemical properties will be determined. The effects of charge interactions, but also of other solute properties on the rejection will be determined. Furthermore, the effects of feed water chemistry (pH, NOM content, ionic strength (presence/absence of divalent cations) and pharmaceutical concentration) on the rejection of the pharmaceuticals will be investigated for different membranes (in order to incorporate the effect of membrane properties on rejection). Finally, a simplified tool to model the effect of electrostatic interactions on the rejection of both positively and negatively charged organic solutes will be presented and validated with experimental data.

## **2. Materials and methods**

### **2.1. Equipment and filtration protocol**

The schematic diagram of the bench-scale membrane system used in the membrane filtration experiments was already described in Paragraph 3.1 in Chapter 2.

Membrane filtration experiments were again carried out at a constant cross-flow velocity of 0.2 m/s (corresponding to a feed flow of 1500 l/h and a concentration polarization factor of 1.07) and at a constant recovery of 10%. The cross-flow velocity of 0.2 m/s corresponds to cross-flow velocities used in full-scale nanofiltration plants. Feed water temperature was set to  $20 \pm 1^\circ\text{C}$ . All experiments were carried out in a

recycle mode with a single batch of water, with both permeate and concentrate recycled back into the feed reservoir.

Since adsorption of solutes onto the membrane surface, and sorption into the inner membrane structure, may influence measured rejection values, an accurate evaluation of the rejection of a given solute is not possible until saturation of the membrane with the solute of interest is accomplished [32]. Therefore, all rejection experiments were carried out for 4 days, which was shown in Paragraph 4.1 in Chapter 2 to be adequate to accomplish saturation and ensure that steady state rejection values are obtained.

## 2.2. Membranes

Two commercially available nanofiltration membranes with different membrane properties (to be able to also assess the influence of membrane properties on rejection) were used in this study: Trisep TS80 TSF (Trisep Corp., Goleta CA, USA) and Desal HL (GE Osmonics, Fairfield CT, USA). Both membranes are thin film composite membranes with a cross-linked aromatic polyamide top layer. Before use, all membranes were rinsed with tap water for two hours to remove preservation liquids present in the membrane. Afterwards, the membranes were characterized for pure water permeability with Milli-Q water and for  $\text{MgSO}_4$  rejection with a 500 ppm  $\text{MgSO}_4$  solution in Milli-Q water.

Membrane	MWCO (g/mol)	Contact angle (°)	Pure water permeability (m/(s.bar))	% MgSO <sub>4</sub> -rejection
Trisep TS80	200	48 ± 2	1.2 × 10 <sup>-6</sup>	99%
Desal HL	150-300	43 ± 3	2.0 × 10 <sup>-6</sup>	98%

Table 3.1 – Membrane properties for selected membranes used in rejection experiments with charged solutes

Membrane properties are summarized in Table 3.1 and Figure 3.1. The molecular weight cut-off (MWCO) values were provided by the membrane manufacturers. The contact angles were determined with Milli-Q water using the sessile drop method. The membrane zeta potentials were calculated from measured streaming potential data in a background solution containing 10 mM KCl using commercially available equipment (SurPASS, Anton Paar, Graz, Austria).

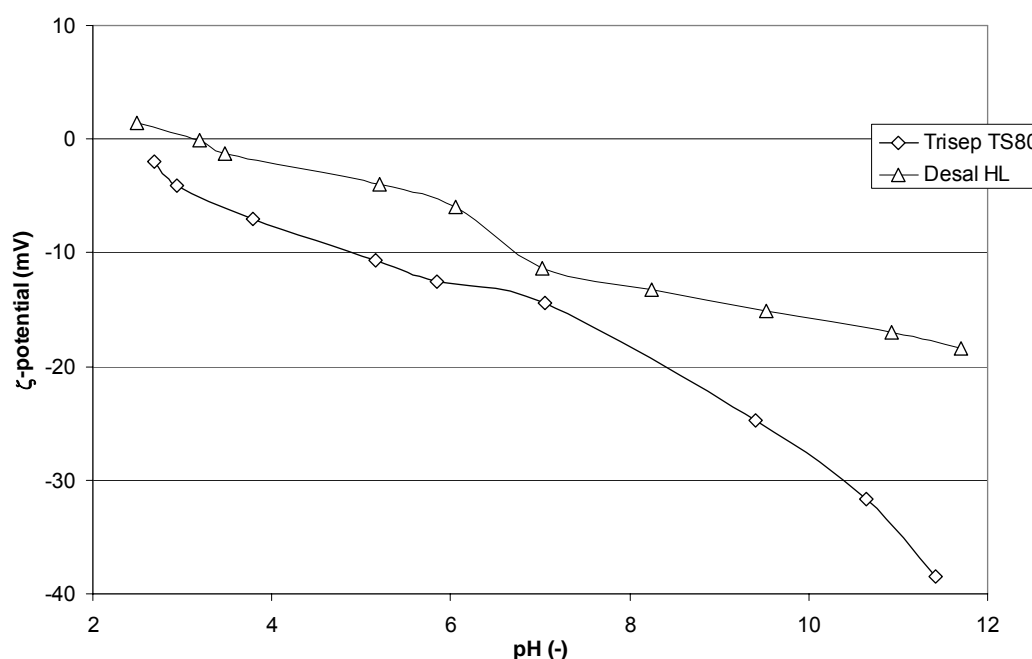


Figure 3.1 –  $\zeta$ -potential of selected membranes as a function of feed water pH (background solution: 10 mM KCl)

## 2.3. Solutes and analyses

Rejection experiments were carried out with different types of solutes in order to encompass a wide range of solute physico-chemical properties and gain a better understanding of the rejection mechanisms. Rejection experiments were first carried out with different organic acids. Organic acids are always neutral or negatively charged and the effective charge depends on the feed water pH and the  $pK_a$  of the acids. Secondly, rejection experiments were carried out with selected pharmaceutically active compounds. Neutral, as well as negatively charged, but also positively charged pharmaceuticals were chosen. In a final step, rejection values of the organic solutes tetraethylenepentamine and 1,3,5-benzenetricarboxylic (a polyprotic base and acid, respectively) were determined. The obtained rejection values for these last two solutes were used to validate the accuracy of a proposed model for the influence of charge interactions on the rejection.

### 2.3.1. *Organic acids*

The organic acids used in the rejection experiments are listed in Table 3.2 and were mainly selected for their different physico-chemical properties (especially their increasing molar mass). The  $pK_a$ -values of all solutes are quite similar, so in terms of electrostatic interactions, no large differences between the solutes are expected. However, the different molar masses of the solutes allow for observation of size exclusion effects for charged solutes.

All organic acids were obtained from Acros Organics (Geel, Belgium) and were all at least reagent grade.

		MW (g/mol)	log K <sub>ow</sub> (-)	pK <sub>a</sub> (-)	Charge at pH 7	log D <sub>(pH 7)</sub> (-)
<b>Organic acids</b>	formic acid	46.0	-0.54	3.75	-	-3.79
	acetic acid	60.1	-0.17	4.76	-	-2.41
	glycolic acid	76.1	-1.11	3.83	-	-4.28
	lactic acid	90.1	-0.72	3.86	-	-3.86
	malonic acid	104.1	-0.81	2.85	-	-4.96
	benzoic acid	122.1	1.87	4.19	-	-0.94
<b>Pharmaceuticals</b>	terbutaline	225.3	0.90	8.86	+	- 0.97
	salbutamol	239.3	0.64	9.27	+	- 1.63
	pindolol	248.3	1.75	9.26	+	- 0.52
	propranolol	259.4	3.48	9.58	+	0.90
	atenolol	266.3	0.16	9.43	+	- 2.27
	metoprolol	267.4	1.88	9.49	+	- 0.61
	sotalol	272.4	0.24	9.44	+	- 2.20
	clenbuterol	277.2	2.00	9.29	+	- 0.29
	phenazon	188.2	0.38	n.a.	neutral	n.a.
	aminopyrine	231.3	1.00	n.a.	neutral	n.a.
	carbamazepine	236.3	2.45	n.a.	neutral	n.a.
	cyclophosphamide	261.1	0.63	n.a.	neutral	n.a.
	pentoxifylline	278.3	0.29	n.a.	neutral	n.a.
	ibuprofen	206.3	3.97	4.47	-	1.44
	clofibric acid	214.7	2.57	3.35	-	- 1.08
	fenoprofen	242.3	3.90	4.21	-	1.11
	gemfibrozil	250.3	4.77	4.45	-	2.22
	ketoprofen	254.3	3.12	4.29	-	0.41
	diclofenac	296.2	4.51	4.08	-	1.59
	bezafibrate	361.8	4.25	3.44	-	0.69
<b>Model solutes</b>	tetraethylenepentamine	189.3	-3.16	different pK <sub>a</sub> 's	- - -	n.d.
	1,3,5-benzenetricarboxylic acid	210.1	1.64	different pK <sub>a</sub> 's	+ + / + + +	n.d.

Table 3.2 – Physico-chemical characteristics of selected organic solutes for rejection experiments (n.a.: not applicable; n.d.: not determined)

All organic acids were spiked separately in Milli-Q water and measured by analyzing the non-purgeable organic carbon (NPOC ~ total organic carbon (TOC)) -content of feed and permeate. The limit of detection for the NPOC-analysis is 0.2 mg/l.

Therefore, all solutes were spiked in concentrations of 10 mg carbon/l, in order to be able to measure at least 98% rejection (which corresponds to a permeate concentration of 0.2 mg/l).

### 2.3.2. Pharmaceuticals

The pharmaceuticals used for spiking were also mainly selected for their wide range of different physico-chemical properties. Pharmaceuticals with a molar mass close to the MWCO of the membranes, but with different hydrophobicities (expressed as  $\log K_{ow}$ , the logarithm of the octanol-water partitioning coefficient) and especially with different charge characteristics were chosen to assess the influence of hydrophobic interactions and charge on rejection. Table 3.2 summarizes their physico-chemical properties. For ionizable solutes, the hydrophobicity is dependent on the percentage of uncharged versus charged species, and thus it is pH dependent. Therefore, an apparent partitioning coefficient at a given pH is calculated for the ionizable solutes. The pH dependent octanol-water distribution coefficient,  $D$ , is the ratio of the equilibrium concentrations of all species (unionized *and* ionized) of a molecule in octanol to the same species in the water phase. The logarithm of the distribution coefficient can be calculated from the  $pK_a$  and  $\log K_{ow}$  of the solute [33]:

$$\log D_{(pH)} = \log K_{ow} - \log (1+10^{(pH-pK_a)}) \quad (3.1)$$

for acids, and

$$\log D_{(pH)} = \log K_{ow} - \log (1+10^{(pK_a-pH)}) \quad (3.2)$$

for bases, respectively. Calculated log D values for a pH of 7.0 are also summarized in Table 3.2.

All pharmaceuticals were obtained from Sigma-Aldrich (St Louis MO, USA), except phenazon, ibuprofen, aminopyrine, carbamazepine and cyclophosphamide, which were obtained from Acros Organics (Geel, Belgium). All chemicals were at least reagent grade.

High performance liquid chromatography with tandem mass spectrometric detection was used to determine concentrations of all pharmaceuticals. A solid phase extraction at pH 3 was performed using styrene divinylbenzene (SDB) material. The limit of quantitation (LOQ) was 10 ng/l for all pharmaceuticals. More information about the analytical procedures was published by Sacher et al. (2001) [34].

The pharmaceuticals were spiked in concentrations of 2 µg/l, to be able to accurately measure 99% rejection (which corresponds to a permeate concentration of 20 ng/l, well above the LOQ of 10 ng/l).

However, in order to rule out influences of feed concentrations of pharmaceuticals on rejection and make sure results could be compared to other studies at higher or lower feed concentrations, rejection experiments were repeated for the Desal HL membrane, with higher feed concentrations. These higher concentrations will later be used in experiments on the combination of NF with granular activated carbon (GAC).

The low and high feed concentrations for all pharmaceuticals are shown in Table 3.3.

All pharmaceuticals were spiked simultaneously as a cocktail. The cocktail was prepared as a concentrated stock solution of 10 l of the selected feed water. To prevent co-solvent effects and possible problems with biological growth in the system, no methanol was used to facilitate dissolution of the pharmaceuticals. The desired volume of the stock solution was then added to the feed tank.



	$C_{\text{feed low}} (\mu\text{g/l})$	$C_{\text{feed high}} (\mu\text{g/l})$
terbutaline	2	40
salbutamol	2	3
pindolol	2	50
propranolol	2	100
atenolol	2	50
metoprolol	2	80
sotalol	2	2.5
clenbuterol	2	2.5
phenazone	2	100
aminopyrine	2	100
carbamazepine	2	25
cyclophosphamide	2	100
pentoxifylline	2	100
ibuprofen	2	30
clofibric acid	2	100
fenoprofen	2	100
gemfibrozil	2	100
ketoprofen	2	50
diclofenac	2	5
bezafibrate	2	50

Table 3.3 – High and low feed concentrations for pharmaceuticals used in rejection experiments

### 2.3.3. Model validation solutes

The solutes tetraethylenepentamine and 1,3,5-benzenetricarboxylic acid were chosen as solutes for the validation of a model to predict the influence of electrostatic interactions on the rejection (the model is presented later). The reason for choosing these solutes is that their speciation is a function of the feed water pH (Figure 3.2). Both solutes occur as different species with different ion valences, making them particularly appropriate for modelling purposes.

Both solutes were obtained in reagent grade from Acros Organics (Geel, Belgium). Similar to the organic acids, tetraethylenepentamine and 1,3,5-benzenetricarboxylic acid were also spiked separately in a concentration of 10 mg carbon/l in Milli-Q water and measured by analyzing the NPOC content of feed and permeate.

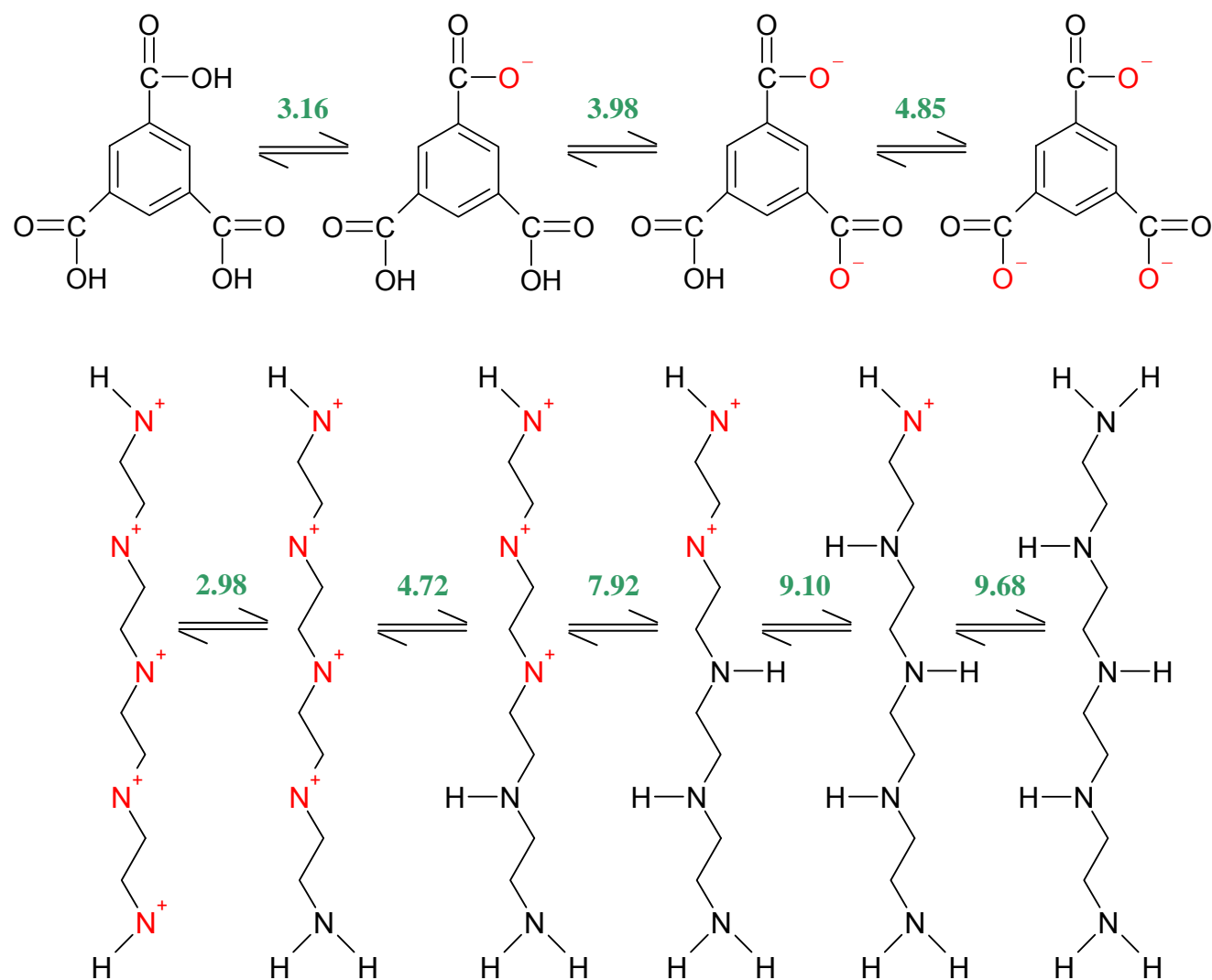


Figure 3.2 – Speciation of 1,3,5-benzenetricarboxylic acid (top) and tetraethylenepentamine (bottom) as a function of feed water pH

Samples of feed and permeate streams of the membrane filtration unit were analyzed for organic solutes to obtain rejection values as follows:

$$R_i = 1 - \frac{c_{p,i}}{c_{b,i}} \quad (3.3)$$

where  $i$  is the solute of interest, and  $R_i$ ,  $c_{p,i}$  and  $c_{b,i}$  are, respectively, the rejection, the permeate concentration and the feed concentration of the solute.

Duplicate samples of all streams were taken to minimize the statistical variance of the results. All samples were shipped to the laboratory for analysis within 24 hours. Blank samples were sent along as control.

## 2.4. Feed water types

The influence of feed water chemistry on the rejection of organic solutes was studied by using different feed water types with varying NOM content, pH and ionic strength (the presence of divalent cations). Moreover, the rejection of some selected organic solutes in urine was also studied.

The first water type used was Milli-Q water with 5 mM of sodium chloride (NaCl, Sigma-Aldrich) added as background electrolyte. To test the effect of the presence of divalent cations, calcium chloride ( $\text{CaCl}_2$ , Sigma-Aldrich) was later added at concentrations of 5 or 10 mM  $\text{Ca}^{2+}$ . These three Milli-Q water types were used to determine the rejection of the organic acids, the pharmaceuticals and the solutes tetraethylenepentamine and 1,3,5-benzenetricarboxylic acid.

The second water type used was surface water sampled from the intake of the Weesperkarspel treatment plant in Amsterdam, the Netherlands (operated by drinking water company Waternet). The pre-treatment consists of coagulation-flocculation and sedimentation, followed by passage in a reservoir with a residence

time of about 100 days. After settling in the reservoir, the water is passed through rapid sand filters and pumped to the treatment plant. Some general water quality parameters of the Weesperkarspel water at the intake of the water treatment plant are summarized in Table 3.4. This water type was used to determine the effect of the presence of NOM on the rejection of the pharmaceuticals. Additionally, the effect of feed water pH on the rejection of pharmaceuticals was tested with this water type. The pH of the water was adjusted by adding hydrochloric acid (HCl) or sodium hydroxide (NaOH) (both from Sigma-Aldrich).

The third and final feed water type used was fresh urine, collected from co-workers at Kiwa Water Research, Nieuwegein, the Netherlands. The composition of the urine is also given in Table 3.4. From the table, it is apparent that the urine is extremely high in both dissolved organic carbon (DOC) content and ionic strength. The rejection in fresh urine was determined for four selected pharmaceuticals from Table 3.2: metoprolol, phenazon, carbamazepine and bezafibrate.

Weesperkarspel	
pH (-)	7.5
Dissolved Organic Carbon (DOC) (mg/l)	6.0
Conductivity ( $\mu\text{S}/\text{cm}$ )	530
$\text{Ca}^{2+}$ (mg/l)	88
$\text{Mg}^{2+}$ (mg/l)	6.8
$\text{SiO}_2$ (mg/l)	12
$\text{K}^+$ (mg/l)	3.1
$\text{Na}^+$ (mg/l)	25

Table 3.4 – Water quality parameters for Weesperkarspel surface water used for rejection experiments

### 3. Results and discussion

#### 3.1. Rejection of organic acids as a function of pH

The rejection values of the organic acids in Table 3.2 with the Trisep membrane are shown in Figure 3.3. The rejection of all the acids in Milli-Q water at pH 8 is above 93%. This high rejection is due to electrostatic repulsion between the negatively charged membrane and the completely dissociated organic acids (Figure 3.4) [24]. The rejection of the acids at pH 8 also increases with increasing molar mass of the acids, except for the rejection of benzoic acid, which is slightly lower than the rejection of malonic and lactic acid, in spite of its higher molar mass. This lower rejection is probably caused by the smaller spacial configuration of the phenyl-group of benzoic acid, in comparison to the linear carbon backbones of lactic and malonic acid. A lower rejection for phenylic organic solutes has been observed previously by other authors as well [35-36].

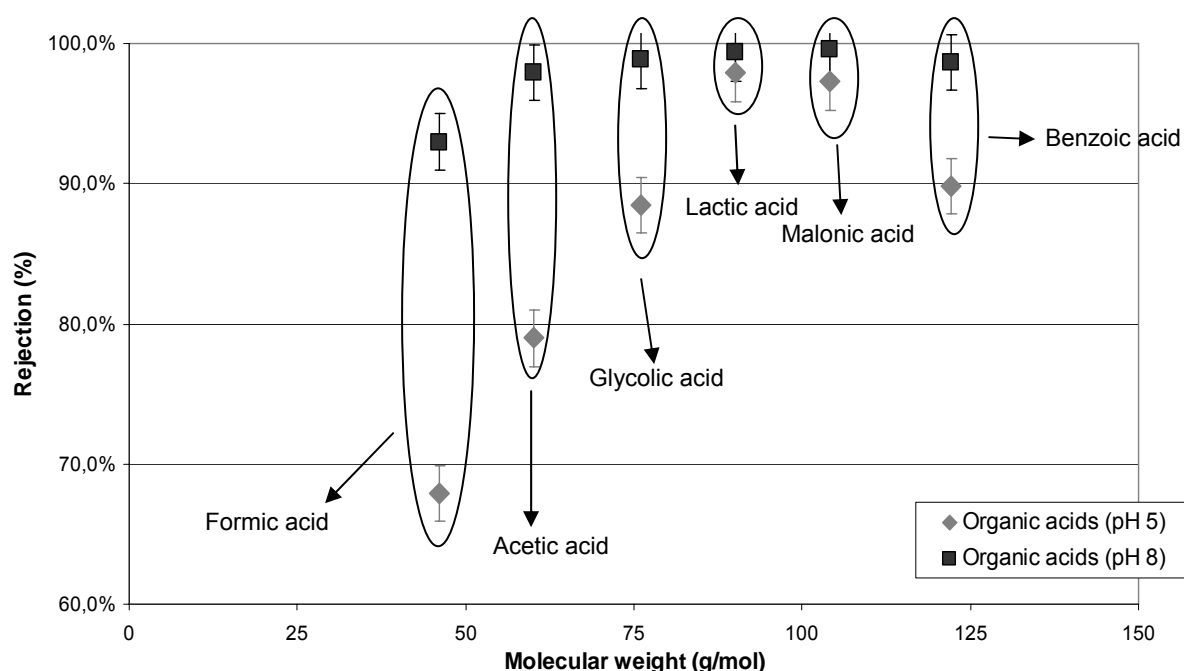


Figure 3.3 – Rejection of organic acids with Trisep TS80 in Milli-Q as a function of solute molar mass and feed water pH

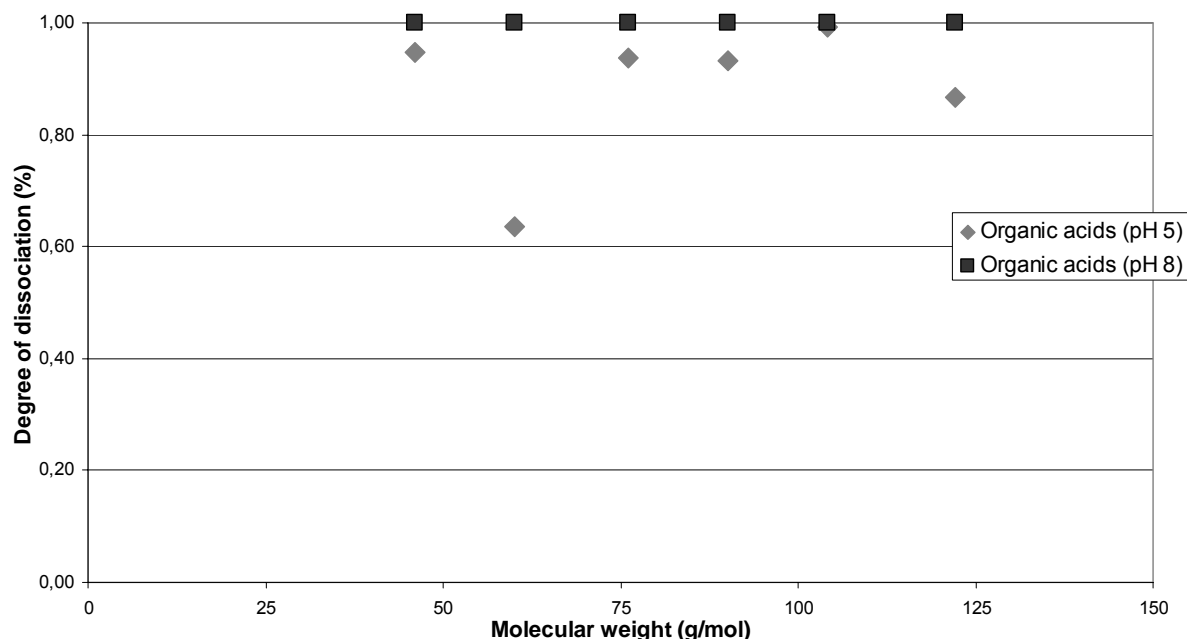


Figure 3.4 – Degree of dissociation of organic acids as a function of molar mass and feed water pH

At pH 8, all acids are completely dissociated and thus rejection is independent of the degree of dissociation. At pH 5, however, dissociation is incomplete (except for malonic acid), and rejection of all organic acids is lower than at pH 8.

Rejection of formic acid decreases the most (25%) at pH 5, compared to pH 8, even though the decrease in dissociation degree is not the largest (<10%). The rejection of acetic acid, for example, varies only 20%, even though the variation in dissociation degree is 40%. This shows that rejection of organic acids is not only determined by charge interactions, but steric interactions also play a major role.

This also explains, just as for pH 8, the lower rejection of benzoic acid, compared to lactic and malonic acid. However, the degree of dissociation may also have an effect at this pH, since the degree of dissociation of benzoic acid is lower than for lactic and malonic acid.

For malonic acid, the dissociation degree is still 100% at pH 5, but rejection does decrease compared to the rejection at pH 8. This is mainly due to the lower membrane surface charge at pH 5 (Figure 3.1).

### 3.2. Rejection of pharmaceuticals as a function of pH in surface water

Even though data in this study and literature data are univocal on the rejection of negatively charged organic solutes (such as organic acids and the negatively charged pharmaceutical ibuprofen) [7, 22-25], very few rejection data for positively charged organic solutes are mentioned in the literature.

The rejection values of the selected pharmaceuticals (negatively charged, neutral, but also positively charged) from Table 3.2 in surface water from the Weesperkarspel treatment plant in Amsterdam at pH 6.5 – 7 are shown in Figure 3.5 for both Trisep TS80 and Desal HL membranes.

Rejection values of all pharmaceuticals are relatively high ( $\geq 75\%$ ) for both membranes. Rejections on the Trisep membrane are slightly higher, probably due to the larger pore size of the Desal membrane (demonstrated by its larger MWCO). It can clearly be observed that the rejection values for positively charged pharmaceuticals are lower than the rejection values for neutral pharmaceuticals, which are in turn lower than the rejection values for negatively charged pharmaceuticals. This can be explained by electrostatic interactions between the solutes and the membrane surface: for negatively charged solutes, charge repulsion exists between the solutes and the negatively charged membrane surface. For neutral solutes, no charge interactions with the membrane surface exist, but for positively charged solutes, the charges promote charge attraction.

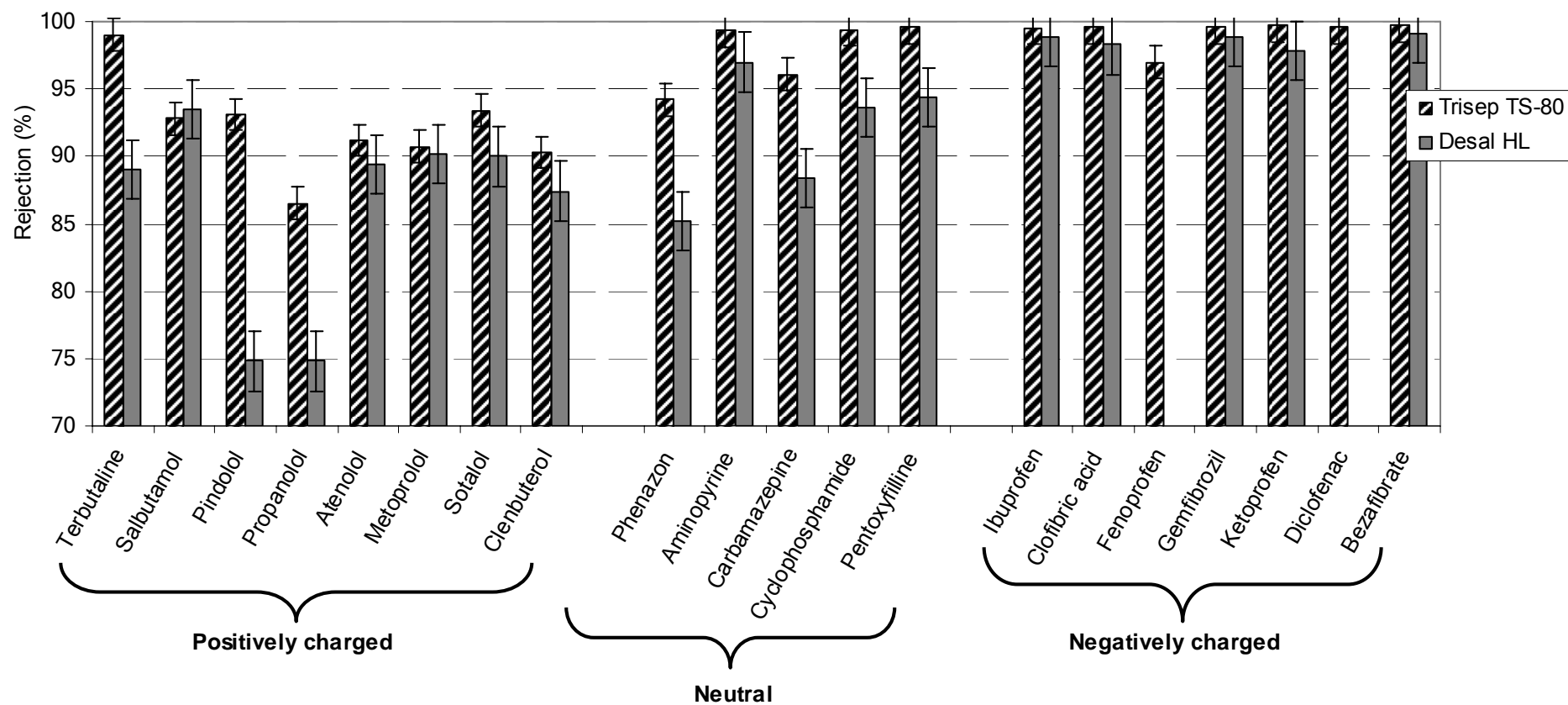


Figure 3.5 – Rejection of selected pharmaceuticals in Weesperkarspel surface water at pH 7 with Trisep TS 80 and Desal HL



This charge attraction causes an increased concentration of positively charged solutes at the membrane surface compared to the bulk solution (solute are attracted towards the oppositely charged membrane), which results in lower observed rejection values. For negatively charged solutes, the opposite holds: the charge repulsion results in a lower concentration of negatively charged solutes at the membrane surface, and thus a higher rejection. This concept may be called “charge concentration polarisation”. Proof for this “charge concentration polarisation” concept is provided when observing the rejection values of all pharmaceuticals as a function of feed water pH in Figures 3.6 to 3.8 for both the Desal HL and the Trisep TS80 membrane. At a feed water pH around 3, the Desal membrane is positively charged and the Trisep membrane is practically uncharged (Figure 3.1). It is apparent that at this pH, the rejection of the positively charged solutes increases dramatically, compared to the rejection at pH 7. For the Desal membrane, this is probably due to electrostatic repulsion between the positively charged solutes and the positively charged membrane. At pH 7, all pharmaceuticals in Figure 3.6 are also positively charged, but both membranes become negatively charged. Therefore, the electrostatic repulsion for the Desal membrane changes into electrostatic attraction, thus leading to an increased concentration of positively charged solutes at the membrane surface, finally resulting in a lower rejection at pH 7. For the Trisep membrane however, there are no electrostatic interactions at lower pH, but at pH 7, the membrane becomes negatively charged and the charge attraction with the positively charged solutes causes a decrease in the rejection.

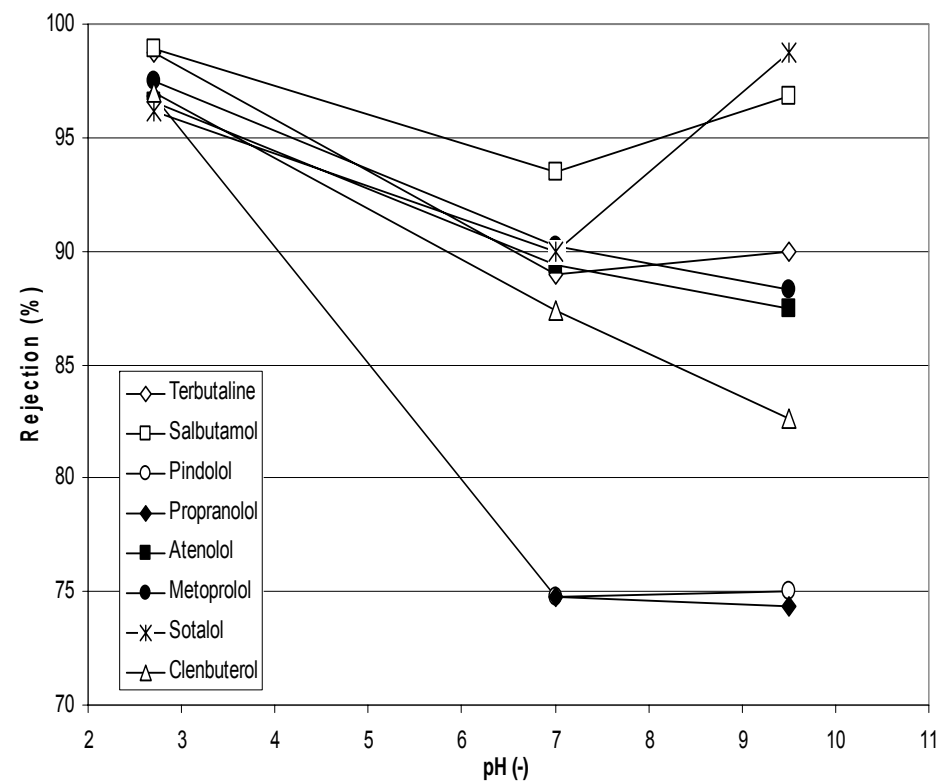
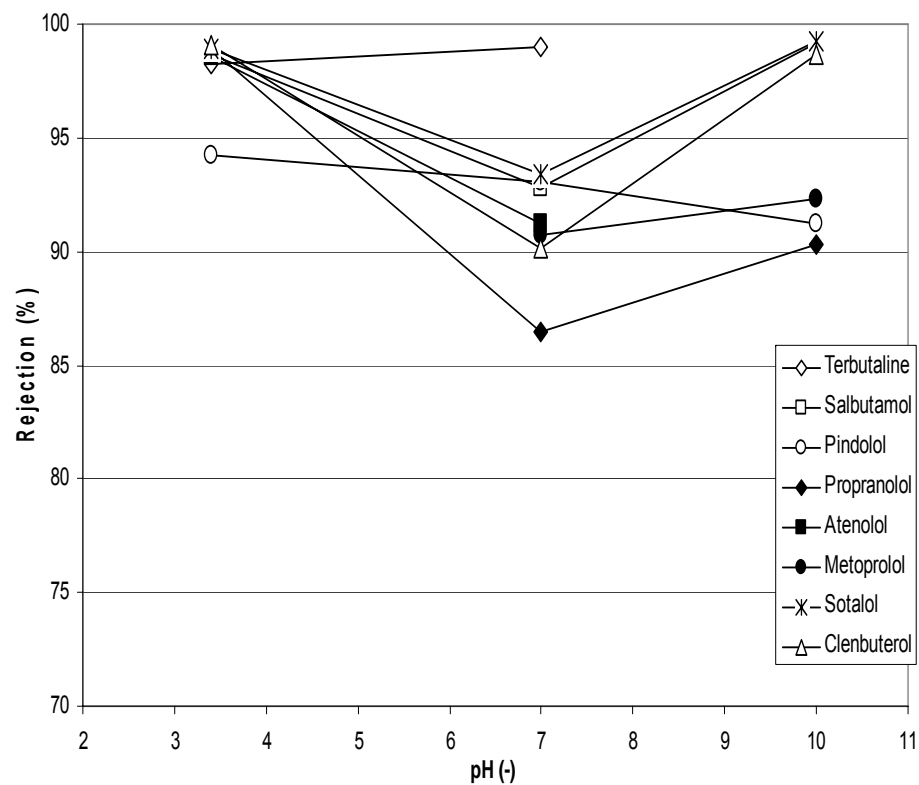


Figure 3.6 – Rejection of positively charged (basic) pharmaceuticals as a function of feed water pH with Trisep TS80 (left) and Desal HL (right)

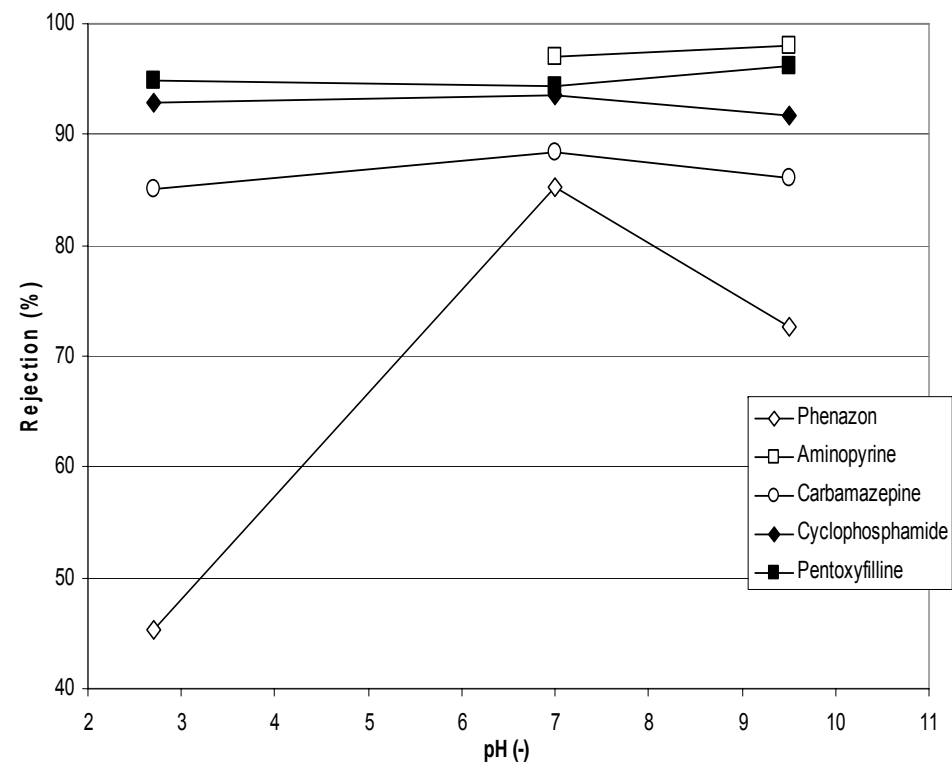
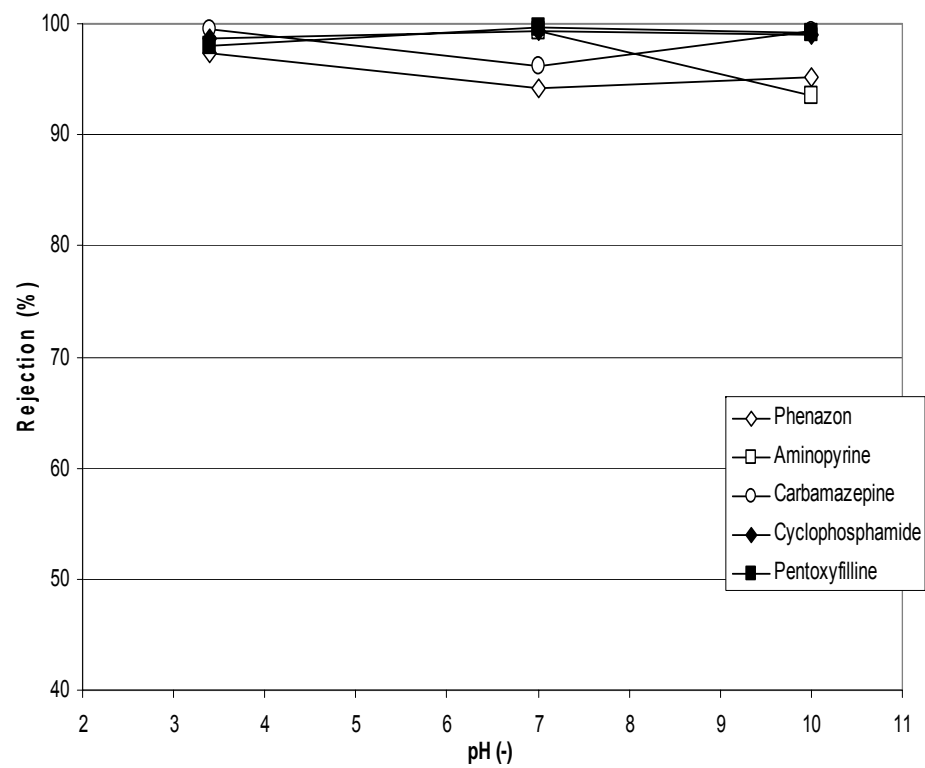


Figure 3.7 – Rejection of neutral pharmaceuticals as a function of feed water pH with Trisep TS80 (left) and Desal HL (right)

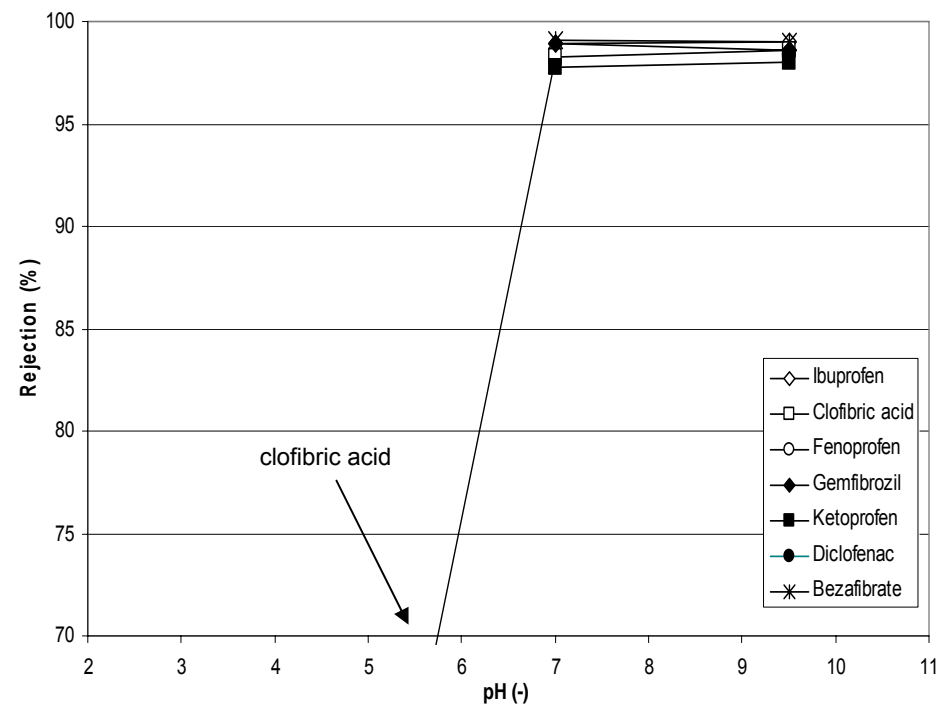
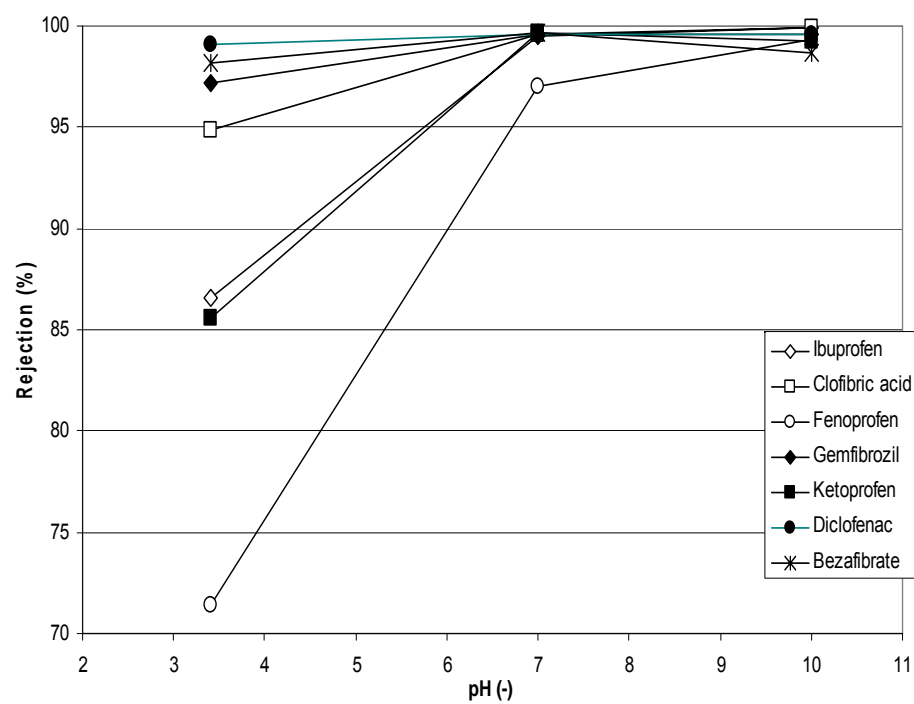


Figure 3.8 – Rejection of negatively charged (acidic) pharmaceuticals as a function of feed water pH with Trisep TS80 (left) and Desal HL (right)

More proof that the lower rejection of positively charged pharmaceuticals at pH 7 is not only due to the absence of an electrostatic repulsion, but that the electrostatic attraction causes an additional decrease in rejection, is given by the fact that the rejection of almost all basic pharmaceuticals increases again when the pH increases from 7 to 10. At a pH of 10, the membrane is more negatively charged than at pH 7, but most basic pharmaceuticals are neutral instead of positively charged at this pH. Therefore, no electrostatic interactions between membrane and solutes should be occurring at pH 10, but still the rejection is higher than at pH 7. This proves that the lower rejection of positively charged solutes compared to uncharged solutes is caused by charge attraction between the opposite charges of the solutes and the membrane surface.

Thus, in contrast to the rejection of inorganic solutes, it is not the combination of electrostatic repulsion and the Donnan exclusion mechanism that determines the rejection of organic solutes with polymeric membranes. The main reason why the Donnan exclusion mechanism does not play a role here, is that the size of the counterions (of the pharmaceuticals) is much smaller than the actual size of the pharmaceuticals themselves (the counterions in this case are mainly  $H^+$  and  $OH^-$  ions). This is an essential difference with the exclusion mechanisms for inorganic ions often described in literature (for inorganic ions, the sizes of co- and counterion are often comparable) .

For the Desal HL, the rejection values of the basic pharmaceuticals at higher pH increase less than for the Trisep TS80 membrane. This is probably due to the slightly lower pH of the experiments with the Desal HL membrane: at this slightly lower pH, some of the basic pharmaceuticals are still slightly positively charged.

For neutral solutes, the pH has almost no effect on rejection (Figure 3.7): all rejection values are relatively constant within the whole pH-range tested. Only the rejection of the smallest neutral pharmaceutical (phenazon) with the Desal HL membrane changes noticeably. This could be due to changes in the pore size of the membrane with varying pH. Several authors [37,38] mention the effect of pH on pore size: at lower pH values, the permeability of most membranes (also the Desal HL) is higher, which is due to the absence of electrostatic repulsion between the active groups on the membrane surface: at higher pH, the electrostatic repulsion between these groups causes the membranes to swell, which causes the pores or the vacant spaces in the surface layer to shrink. Thus, at lower pH, the membrane pores are larger, causing less steric hindrance and thus a lower rejection. This is only apparent for the smallest solute (phenazon) with the Desal HL membrane, since phenazon is probably close to the MWCO of the membrane and a small change in pore size may lead to large changes in rejection. The Trisep TS80 membrane is more dense (the pores are smaller), so this effect does not play a role.

For the negatively charged (acidic) pharmaceuticals, the rejection trends obtained are in close agreement with the organic acid results and observations made in the literature [7, 22-25]. Rejection values for all acidic pharmaceuticals at neutral and high pH (pH 7 and 10) are high, due to electrostatic repulsion between the negatively charged solutes and the negatively charged membrane surface. Even though the membrane surface charge is lower at pH 7 (Figure 3.1) compared with pH 10, the surface charge is apparently still sufficiently high to maintain electrostatic repulsion and cause the high observed rejection values. Only the rejection value of fenopufen with the Trisep TS80 decreases slightly.

At lower pH (pH 3), the membranes become neutral (or even positively charged), and the dissociated, negatively charged (acidic) pharmaceuticals regain their proton and become neutral. Therefore, no electrostatic repulsion exists anymore and the rejection of the solutes is only determined by steric hindrance and hydrophobic interactions between the solute and the membrane. The effect of steric hindrance on the rejection is difficult to determine, since the rejections of both fenoprofen and ketoprofen on the Trisep TS80 membrane at pH 3 are lower than the rejection of the smaller ibuprofen. Moreover, rejection of clofibric acid is also high, even though the solute is quite small. This shows that the steric hindrance effect is not always the decisive parameter that determines rejection, and electrostatic effects and especially hydrophobic effects also play a role for these acidic pharmaceuticals.

Hydrophobic interactions may explain, for example, why the rejection values of the undissociated (neutral) acidic pharmaceuticals at pH 3 in Figure 3.8 are lower than the rejection values for the deprotonated (neutral) basic pharmaceuticals at pH 10 in Figure 3.6, even though all solutes are similar in size and no charge interactions are present (Table 3.2). As can be seen from Table 3.2, the hydrophobicity ( $\log K_{ow}$ ) of the acidic pharmaceuticals is considerably higher than the hydrophobicity of the basic pharmaceuticals. Therefore, more adsorption is likely to occur, the acidic pharmaceuticals in neutral state will partition more easily into the membrane and therefore, their rejection will be lower [9,32]. Proof for the presence of these hydrophobic interactions is most obvious for the acidic pharmaceuticals with the Desal HL membrane: in Figure 3.8, it is apparent that the rejection values of most acidic pharmaceuticals at pH 3 can not even be determined. This is due to the low feed concentration: since experiments are carried out in recycle mode, adsorption of solutes onto the membrane surface leads to a depletion of these solutes in the feed

water. After 4 days of recycling, the feed concentration of the acids at low pH for the Desal HL membrane was below the detection limit, due to adsorption.

Figure 3.9 plots the rejection of the charged solutes as a function of their pH-dependent hydrophobicity ( $\log D$ ) for the Trisep TS80 membrane. The rejection of the positively charged (basic) pharmaceuticals is clearly dependent on the hydrophobicity, at least for the higher pH values (pH 7 and 10). At pH 7 and 10, no electrostatic repulsion (only attraction) is present and the solutes can freely approach the membrane surface and engage in hydrophobic interactions, which lead to lower rejections for hydrophobic solutes. This is clearly shown by the correlations between  $\log D$  and rejection in Figure 3.9 and helps explain the low observed rejections for pindolol and propranolol in Figure 3.6. For the basic pharmaceuticals, the hydrophobicity of the solutes and thus the extent of hydrophobic interactions seems to have a larger effect on rejection than the solute size (and thus steric hindrance): the rejection values of the deprotonated basic pharmaceuticals at pH 10 do not follow the order of increasing solute size: rejection values of, for example, pindolol and metoprolol are lower than the rejection values of the smaller solute salbutamol. Both pindolol and metoprolol are more hydrophobic than salbutamol.

At pH 3, electrostatic repulsion exists between the positively charged membrane and the protonated (and thus also positively charged) basic pharmaceuticals. At this pH, no clear correlation is seen between the hydrophobicity and the rejection anymore, possibly because solutes can not approach the membrane surface due to electrostatic repulsion and can not engage in hydrophobic interactions. However, it also has to be noted that the  $\log D$ -values of the basic pharmaceuticals at pH 3 are very low ( $\log D < -2$ ) and under these conditions, the pharmaceuticals are less hydrophobic.



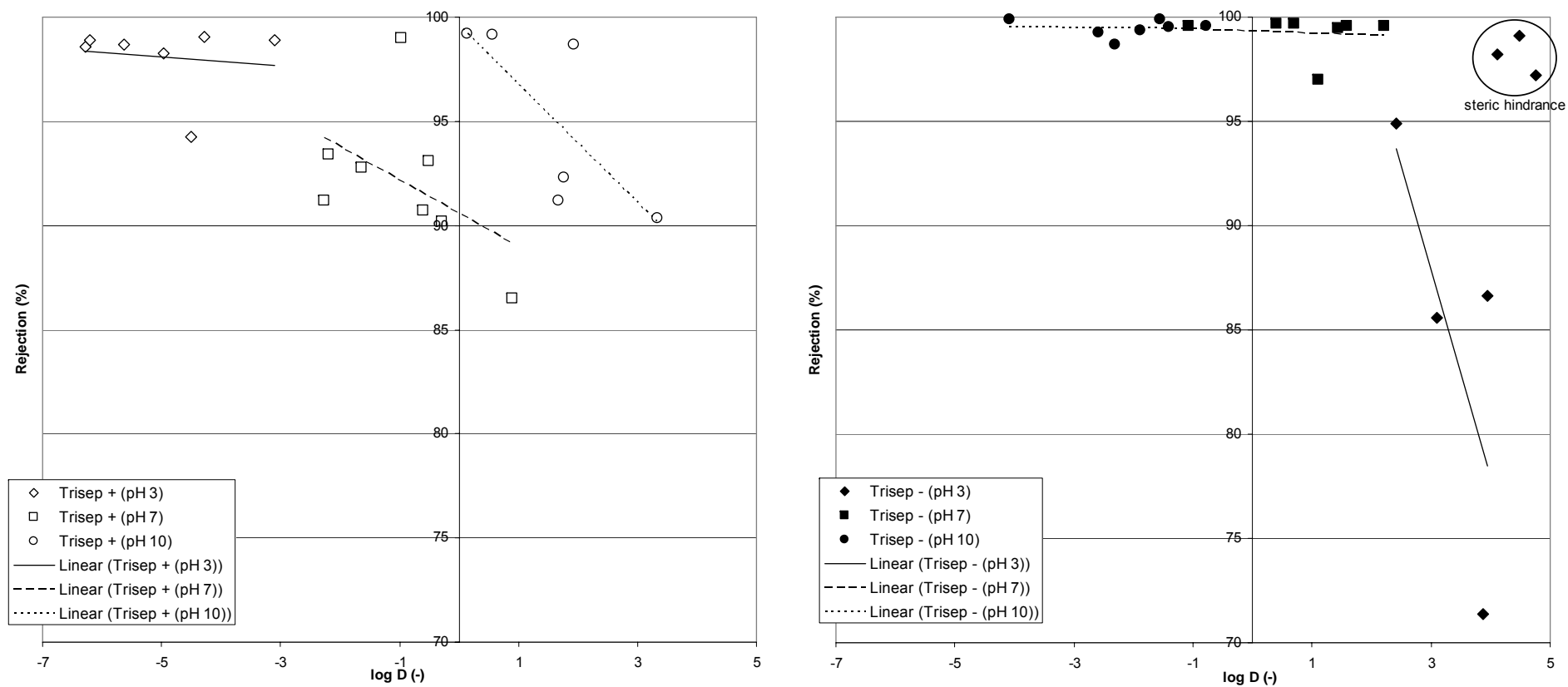


Figure 3.9 – Rejection of basic (left) and acidic (right) pharmaceuticals at different pH as a function of solute hydrophobicity with Trisep TS80

Nghiem and Coleman [39] showed that the extremely hydrophobic solute triclosan could still engage in hydrophobic interactions with the membrane surface, even though electrostatic repulsion was present.

For the acidic pharmaceuticals, the correlation between  $\log D$  and rejection is not so clear, since steric hindrance effects also play a role. At higher pH values (pH 7 and 10), electrostatic repulsion exists between the negatively charged solutes and the negatively charged membrane, and no hydrophobic interactions occur. Therefore, no correlation between solute hydrophobicity and rejection is observed. At pH 3, the acidic pharmaceuticals regain their proton and become neutral. At this pH, a decrease in rejection with increasing hydrophobicity is observed when selected data are abstracted, corresponding to the large solutes diclofenac, bezafibrate and gemfibrozil. Rejection values of these solutes remain high in the neutral state, because the solutes are substantially larger than the membrane pore size. However, rejections are lower than expected, purely based on their size (rejections < 100%). For the smaller acidic pharmaceuticals at low pH, a clear decrease in rejection with increasing hydrophobicity is noticeable.

The relationship between solute hydrophobicity and rejection for neutral solutes was already shown in Chapter 2. The rejection values for the neutral solutes are shown as a function of solute hydrophobicity in Figure 3.10. The rejection value of phenazone is omitted in the figure because its molar mass is below the molecular weight cut-off of the membrane and hydrophobic interactions mainly influence the rejection of solutes with a molar mass larger than the molecular weight cut-off [6]. Also here, it can be observed that neutral solutes can approach and interact with the membrane surface and therefore a decrease in rejection with increasing hydrophobicity is seen.

Since rejection values of the neutral pharmaceuticals only change marginally as a function of pH, these conclusions remain valid at different pH values.

It must be stressed, however, that the correlation between solute hydrophobicity and rejection is not always very accurate, which was already apparent from Chapter 2.

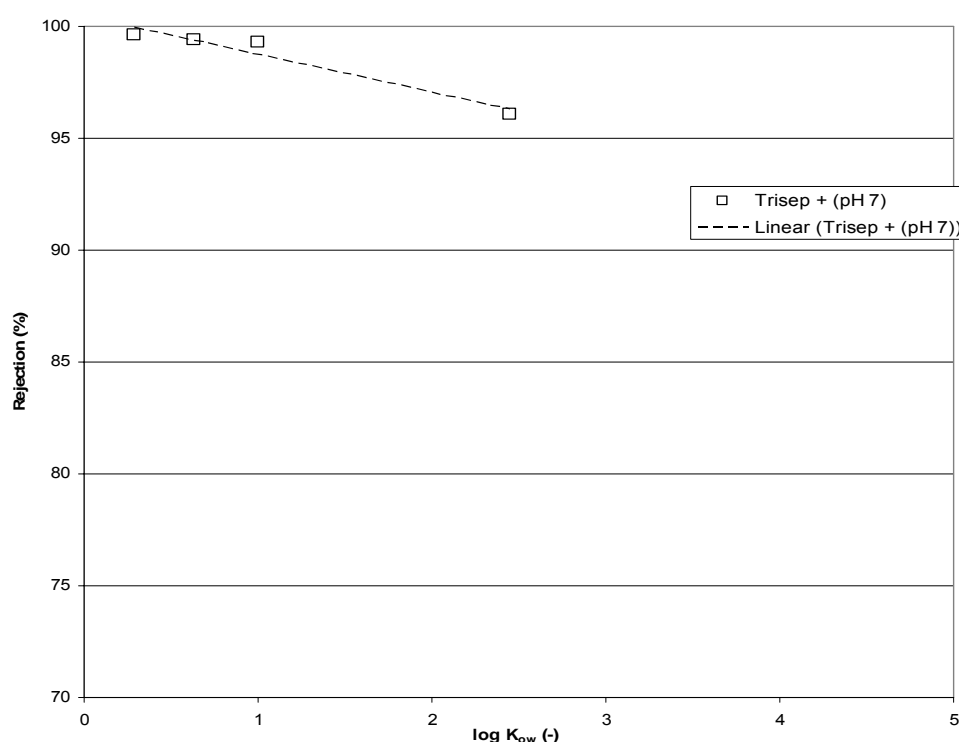


Figure 3.10 – Rejection of neutral pharmaceuticals as a function of solute hydrophobicity with Trisep TS80

### 3.3. Influence of feed water composition on rejection of pharmaceuticals

#### 3.3.1. Influence of natural organic matter on pharmaceutical rejection

The rejection values of charged and uncharged pharmaceuticals in Weesperkarspel surface water were shown previously for both the Desal and the Trisep membranes. Figures 3.11 and 3.12 compare the rejection data for the Weesperkarspel water at pH 7 to the rejection data for the selected pharmaceuticals in Milli-Q water with 5 mM NaCl added as background electrolyte at pH 7, for both tTrisep TS80 and Desal HL.

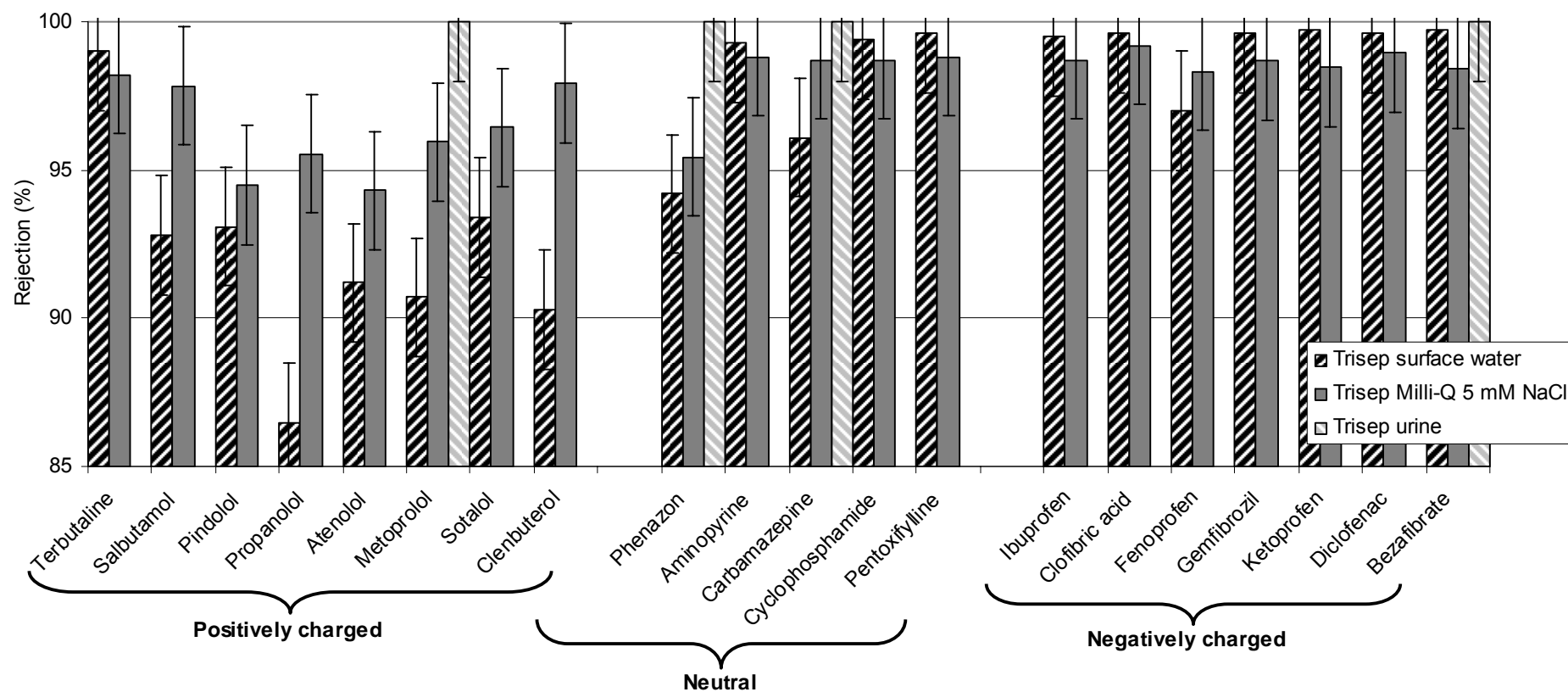


Figure 3.11 – Rejection of selected pharmaceuticals in different feed water types at pH 7 with Trisep TS80

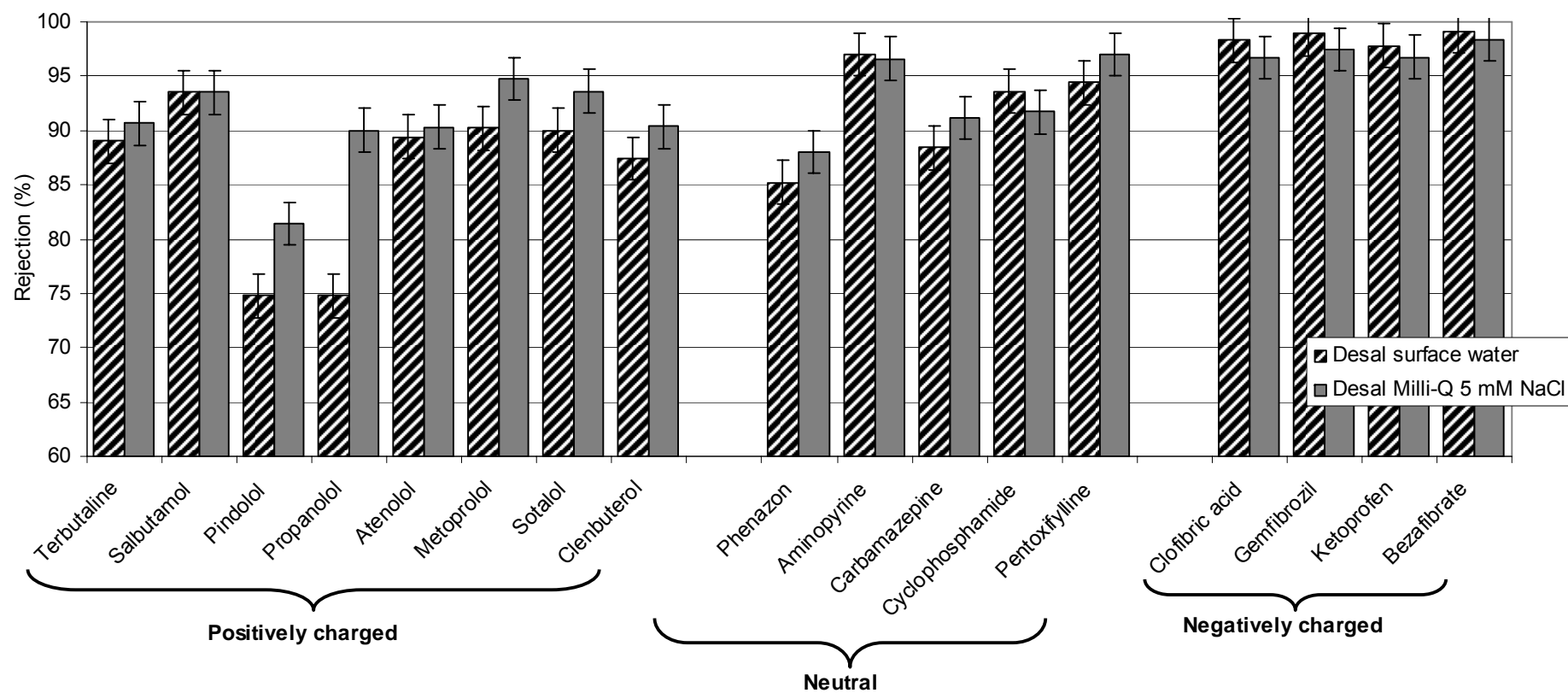


Figure 3.12 – Rejection of selected pharmaceuticals in different feed water types at pH 7 with Desal HL

The total ionic strengths of both the Milli-Q and the surface water are comparable: the conductivity of the Weesperkarspel-water is 530  $\mu\text{S}/\text{cm}$ , whereas the conductivity of the Milli-Q with 5 mM NaCl is about 570  $\mu\text{S}/\text{cm}$ . The largest difference between the two water types is the presence of 6 mg/l of natural organic matter in the surface water. In Figure 3.11, the rejection values for 4 selected pharmaceuticals (metoprolol, phenazon, carbamazepine and bezafibrate) with the Trisep TS80 membrane in fresh urine are also shown.

It is apparent that rejection values of the differently charged pharmaceuticals follow the same trends in the Milli-Q water as in the surface water: highest rejection for the negatively charged, lowest rejection for the positively charged and an intermediate rejection for the neutral pharmaceuticals. Moreover, differences in rejection values between the Milli-Q and the surface water seem to be quite small in comparison with the experimental error associated with the rejection data. However, a few trends are noticeable: the rejection of positively charged solutes seems to be slightly higher for the Milli-Q water compared with the rejection of the positively charged solutes in the surface water, for both membranes. The rejection of negatively charged solutes, on the other hand, seems to be slightly lower in the Milli-Q water compared with the surface water. For neutral solutes, no real trends can be observed. Rejection of different neutral solutes seems to change in opposite directions for the Desal HL and the Trisep TS80 membranes.

The higher rejection of positively charged solutes and the lower rejection of negatively charged solutes in the Milli-Q water could possibly be explained by a decrease in the membrane surface charge in Milli-Q compared with the surface water: the deposition of negatively charged NOM molecules on the membrane

surface could possibly lead to an increased negative surface charge of the membranes in surface water [28].

For the 4 selected pharmaceuticals spiked in fresh urine with the Trisep TS80 membrane the rejection seems to be significantly higher compared to the other two feed water types. Higher rejection values in fresh urine were also observed by Pronk et al. (2006) [23], who attributed this to complexation of the pharmaceuticals with oxalic, uric and amino acids in the urine. In contrast, complexation of positively charged pharmaceuticals with negatively charged humic acid molecules in surface water does not seem to occur in the surface water (since rejection values of the positively charged pharmaceuticals in the surface water are lower compared with Milli-Q, as mentioned before).

### *3.3.2. Influence of feed water ionic strength on pharmaceutical rejection*

Several literature studies [24,27,39] have reported the effect of feed water ionic strength on the membrane surface charge and thus the rejection of organic and inorganic ions. Especially divalent ions, such as  $\text{Ca}^{2+}$ , seem to reduce the thickness of the electric double layer at the membrane surface and shield the membrane surface charge.

This shielding of the membrane charge generally leads to a decrease in electrostatic interactions with charged species. It was reported that this results in a decrease of rejection of negatively charged ions for negatively charged membrane surfaces, due to the absence of electrostatic repulsion [24,27]. It is interesting to check whether the shielding of the membrane charge will also result in a decrease of electrostatic attraction, and thus an increase of the rejection of oppositely charged ions.

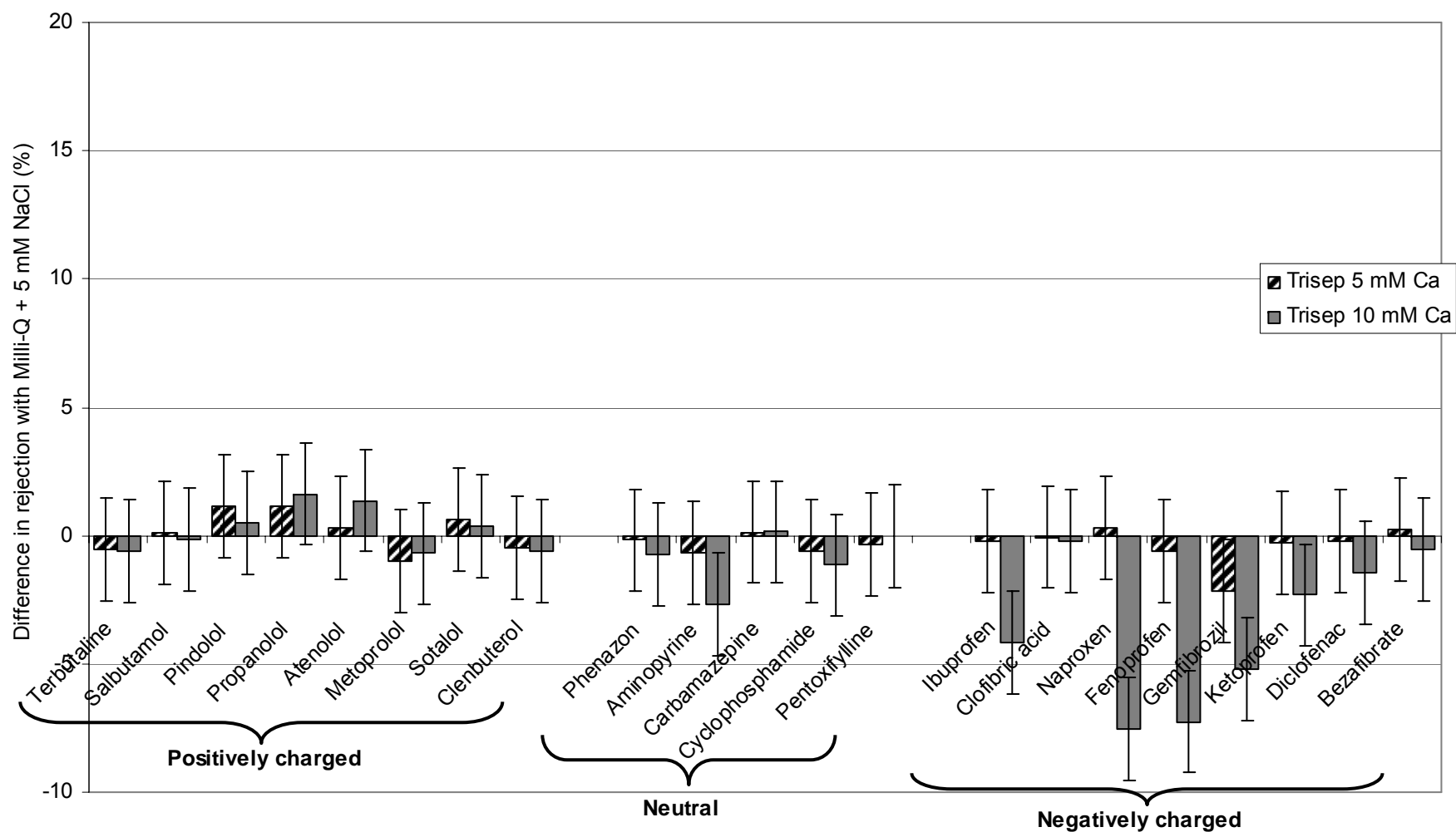


Figure 3.13 – Rejection of selected pharmaceuticals as a function of  $\text{Ca}^{2+}$  concentration at pH 7 with Trisep TS80



The influence of the addition of  $\text{Ca}^{2+}$  (added as  $\text{CaCl}_2$ ) on the rejection of the pharmaceuticals is shown in Figures 3.13 and 3.14 for the Trisep and Desal membranes. Rejection values are shown as the difference in rejection compared to the rejection in Milli-Q with 5 mM NaCl as background electrolyte (Figures 3.11 and 3.12). A positive difference corresponds to an increase, a negative difference corresponds to a decrease in rejection compared to the rejection in Milli-Q + 5 mM NaCl.

The influence of  $\text{Ca}^{2+}$  addition on the rejection of pharmaceuticals is quite small for the Trisep membrane (all rejection differences < 7.5 %). For the positively charged and neutral solutes, no effect is noticeable. For the negatively charged solutes, a small decrease in rejection is noticeable, which is probably due to smaller electrostatic repulsion, caused by charge shielding of the membrane charged and the negative solute charge by the  $\text{Ca}^{2+}$ -ions.

Just as for the Trisep membrane, no (significant) effect on the rejection of the uncharged pharmaceuticals with the Desal membrane is observed, except perhaps for the smallest solute phenazon. The large difference for phenazon is probably due to an experimental error, since the rejection increases with the addition of 5 mM of  $\text{Ca}^{2+}$  and decreases upon the addition of 10 mM of  $\text{Ca}^{2+}$ , so no clear conclusions can be drawn. For the negatively charged solutes, the decrease in rejection is not very significant, only the rejection of fenoprofen changes drastically. For the positively charged solutes, however, a significant increase in the rejection is seen upon the addition of 10 mM  $\text{Ca}^{2+}$ . This increase in rejection for positively charged solutes was not observed for the Trisep membrane.

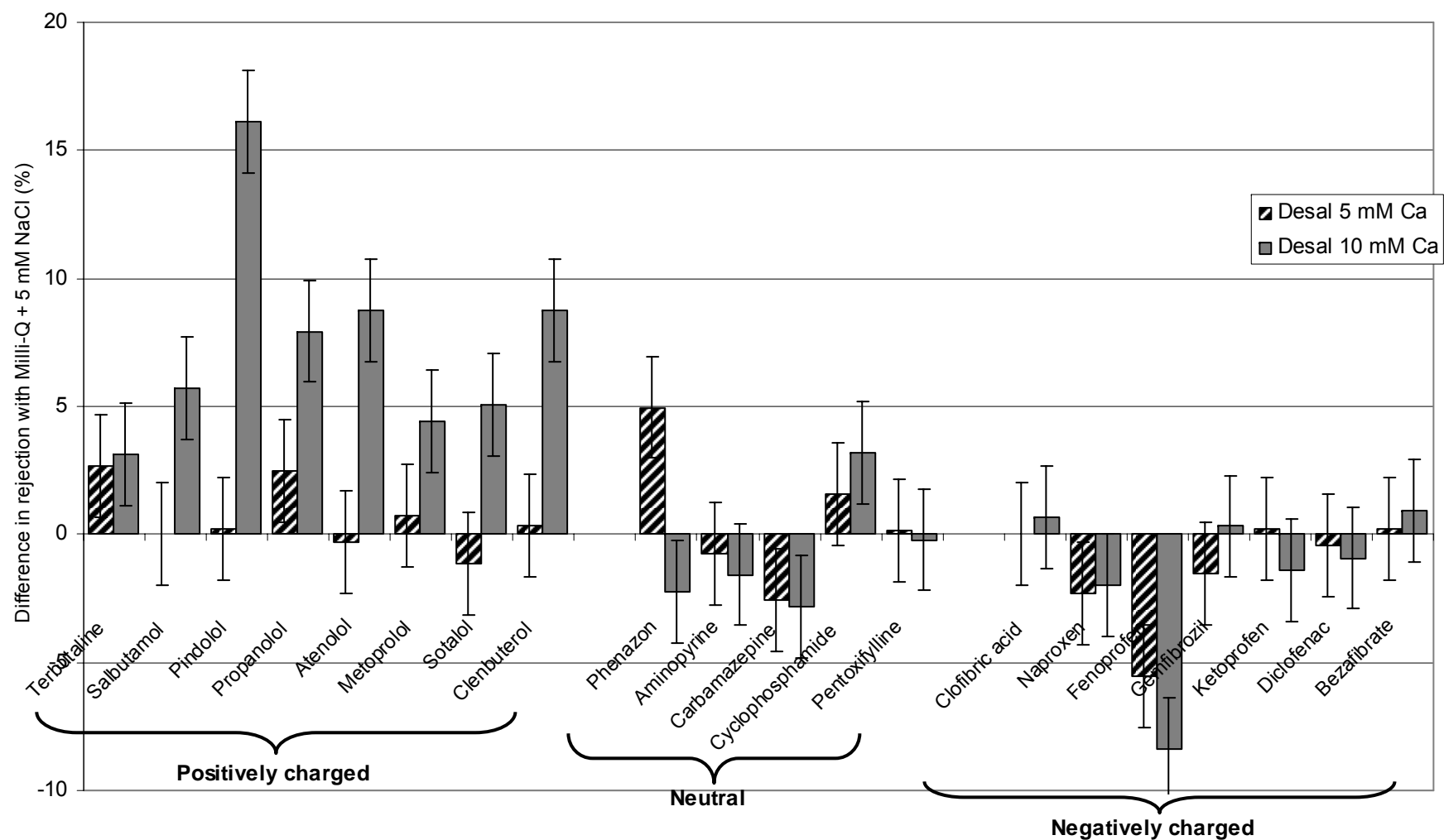


Figure 3.14 – Rejection of selected pharmaceuticals as a function of  $\text{Ca}^{2+}$  concentration at pH 7 with Desal HL

One possible explanation for this might be the lower surface charge of the Desal membrane, compared to the Trisep. Due to the adsorption of  $\text{Ca}^{2+}$ -ions, it might be possible that the negative membrane charges become completely depleted, and the membrane assumes a small positive charge, resulting in increased rejection values for positively charged solutes due to electrostatic repulsion. Since the Trisep membrane is more negatively charged, this depletion will not occur. However, it is nevertheless obvious that the addition of  $\text{Ca}^{2+}$ -ions does cause a shielding of the surface charge for the Desal membrane, since the rejection of negatively charged solutes decreases, and the rejection of positively charged solutes increases due to the absence of electrostatic repulsion and attraction. For the Trisep membrane, which has smaller pores, the shielding effect and the influence on rejection are less obvious than for the Desal membrane. This is in agreement with Boussahel et al. (2002) [40], who observed that inorganic ions have a greater effect on the rejection of organic solutes in the case of wide-pore membranes.

It is important to keep this effect of ionic strength on rejection in mind for future modelling attempts for the rejection of charged organic solutes in full-scale installations: in installations operating at 80% recovery, the total ionic strength of the feed water may be up to five times higher in the final stages of the installation. At these high ionic strengths (especially in the case of membranes with wider pores), the rejection of charged organic solutes may deviate largely from the rejection in the first stages of the installation.

### *3.3.3. Influence of pharmaceutical feed concentration on rejection of pharmaceuticals*

Since, in a full-scale installation, the feed concentration of the solutes is continuously increasing with increasing recovery throughout the stages of the installation, the influence of this feed concentration on the rejection has to be studied, to incorporate this influence in further full-scale modelling attempts.

Therefore, the nanofiltration experiments with Weesperkarspel water at pH 7 were repeated with the Desal HL membrane, but this time with higher feed water concentrations (see Table 3.3). These higher feed water concentrations will later also be used in Chapter 6 of this thesis, where two different treatment steps will be combined, and it will be necessary to determine 99% rejection for the pharmaceuticals in both treatment steps (higher feed concentrations are then required, because of the LOQ of the pharmaceutical analysis).

Van der Bruggen et al. (1998) [13] and Zhang et al. (2004) [17] already demonstrated that rejection of neutral solutes is independent of concentration for the low concentration range used herein. Therefore, the influence of feed concentration on the rejection was only studied for negatively and positively charged solutes here. Rejection values for the high feed concentrations on the Desal HL membrane in Weesperkarspel water are compared with the rejection values for the low feed concentrations in Figure 3.15. It is readily apparent that rejection values for positively charged pharmaceuticals are slightly higher for higher feed concentrations. This can possibly be explained by shielding effects: the higher feed pharmaceutical concentrations lead to a partial shielding of the negative membrane surface charge by positively charged pharmaceuticals. Due to this shielding effect, attractions between the membrane and the positively charged pharmaceuticals are lower, leading to a smaller “charge concentration polarisation”.

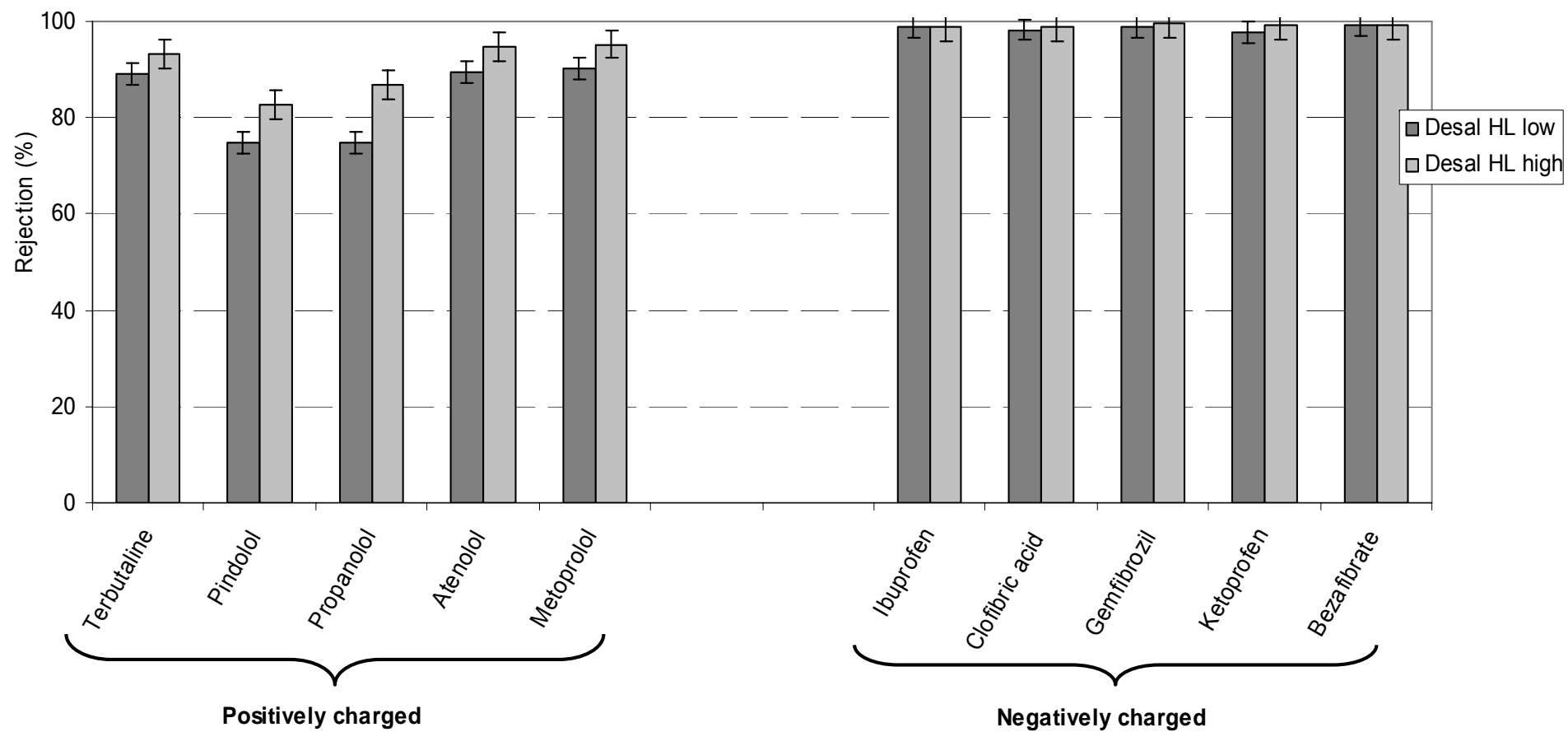


Figure 3.15 – Influence of feed concentration on rejection of selected positively and negatively charged pharmaceuticals in Weesperkarspel water at pH 7 with Desal HL

A smaller charge concentration polarisation means lower concentrations at the membrane surface and thus higher observed rejections (this corresponds to a compression of the electric double layer of the membrane). It has to be mentioned that the increase in rejection is relatively small for a 20- to 50-fold increase in feed concentration. Therefore, in full-scale installations, where concentration usually only increases up to a factor of maximum 5 at 80% recovery, this effect should be negligible.

For negatively charged pharmaceuticals, the shielding effect appears to be less obvious: rejection values are almost equal to those observed at low feed concentrations. Apparently, the shielding effect is too small to influence repulsive forces between the negatively charged membrane and negatively charged solutes. It might be assumed that the shielding effect will become more important at very high feed concentrations. However, again, in full-scale installations, where concentration usually only increases up to a factor of maximum 5 at 80% recovery, this effect should also be negligible

### 3.4. Simplified modelling of charged organic solute rejection

The “charge concentration polarisation” concept can be used as a basis for simplified modelling of the rejection of charged organic solutes. In this paragraph, the charge concentration polarisation is calculated theoretically, but is also experimentally determined by comparing the rejection of solutes in the absence of charge interactions with the rejection in the presence of charge interactions.

Figure 3.16 summarizes the rejection values of the solutes 1,3,5-benzenetricarboxylic acid and tetraethylenepentamine for the Trisep TS-80 membrane at pH 2.5 and pH 7 and 10 in Milli-Q water with 5 mM NaCl as background electrolyte.

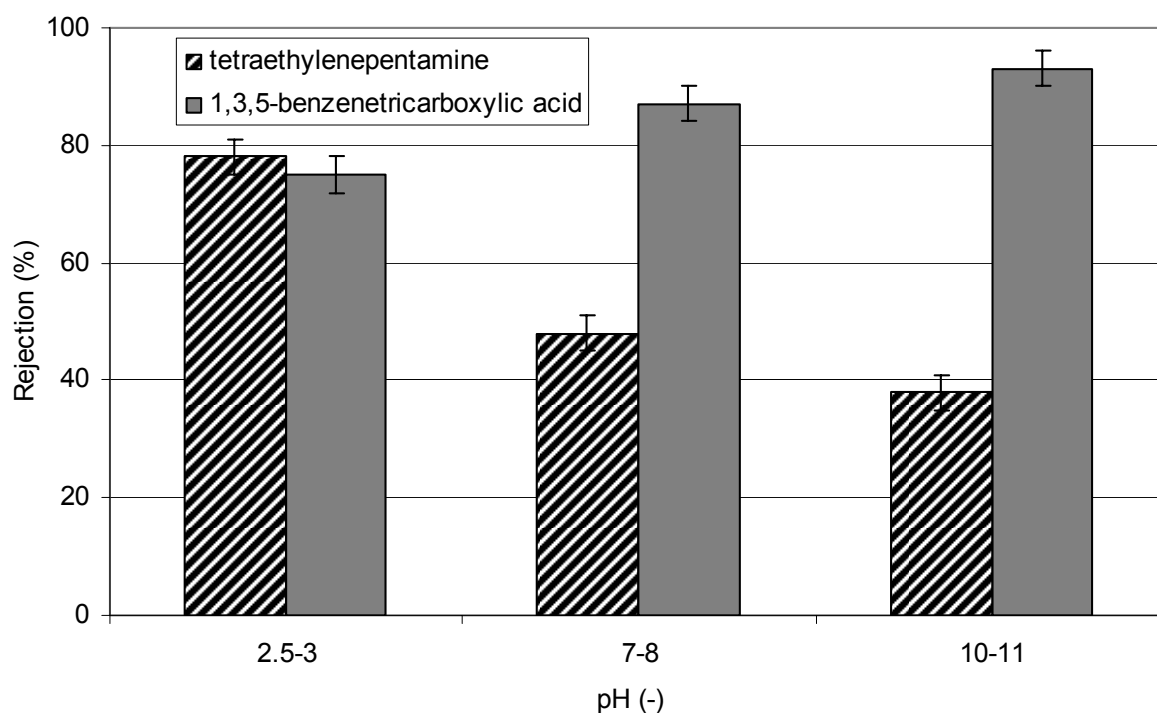


Figure 3.16 – Rejection values of 1,3,5-benzenetricarboxylic acid and tetraethylenepentamine in Milli-Q as a function of feed water pH with Trisep TS80

At pH 2.5, the Trisep membrane is uncharged (or has a very low surface charge). Therefore, the rejection values of both solutes at this pH will be regarded as the rejection values in the absence of electrostatic interactions. The only concentration polarisation that influences the rejection of the solutes at this pH, is the hydrodynamic concentration polarisation. Since the hydrodynamic concentration polarisation is quite low in spiral wound membranes ( $\beta \sim 1.07$  at a cross-flow velocity of 0.2 m/s), it is assumed to be equal to 1 in this simplified modeling approach. Thus, the rejection of the solutes at low pH can be calculated as follows:

$$R_{uncharged} = 1 - \frac{c_p}{c_b} \approx 1 - \frac{c_p}{c_m} \quad (3.4)$$

where  $R$  is the rejection and  $c_p$ ,  $c_b$  and  $c_m$  are respectively the solute concentration in the permeate, the bulk and at the membrane surface. The second and third term of Equation (3.4) are assumed to be equal by the assumption that the hydrodynamic concentration polarisation is equal to 1.

At higher pH values, the membrane assumes a negative surface charge and charge interactions will affect the rejection of the solutes. Therefore, the rejection differs from the rejection at low pH. For the positively charged tetraethylenepentamine, the rejection decreases because the concentration of the solutes at the membrane surface increases due to charge attraction (charge concentration polarisation  $> 1$ ). For the negatively charged 1,3,5-benzenetricarboxylic acid, the rejection increases because the concentration of the solutes at the membrane surface decreases due to charge repulsion (charge concentration polarisation  $< 1$ ).

Concentration profiles of charged solutes in the vicinity of a charged surface can be calculated using the Gouy-Chapman and DLVO-theories for colloidal solutes and extrapolating these theories to charged solutes approaching flat surfaces. This leads to the following Boltzmann distribution for charged organic solutes approaching the membrane surface:

$$\beta_{charge} = \frac{c_m}{c_b} = \exp\left(\frac{-Z_m \cdot V \cdot F}{RT}\right) \quad (3.5)$$

where  $\beta_{charge}$  is the charge concentration polarisation,  $Z_m$  is the organic ion valence,  $V$  is the membrane potential (in mV),  $F$  is Faraday's constant,  $R$  is the universal gas constant,  $T$  is the temperature (in K) and  $c_m$  and  $c_b$  are the charged solute concentrations at the membrane surface and in the bulk fluid, respectively. This is



schematically represented in Figure 3.17. Again, abstraction of the hydrodynamic concentration polarisation is made in the figure.

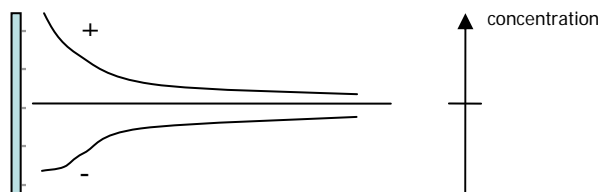


Figure 3.17 - Concentration profiles for positively (+), negatively (-) and uncharged (0) solutes in the vicinity of a negatively charged membrane surface

For the charged solutes, the rejection can be calculated as follows:

$$R_{charge} = 1 - \frac{c_p}{c_b} \approx 1 - \beta_{charge} \frac{c_p}{c_m} = 1 - \beta_{charge} (1 - R_{uncharged}) \quad (3.6)$$

With  $c_p/c_m$  substituted by  $(1 - R_{uncharged})$  according to Equation (3.4). Thus, if  $R_{uncharged}$  is known, and  $\beta_{charge}$  can be calculated according to Equation (3.5), the theoretical rejection of a charged solute can be predicted. As a first approach, the membrane zeta-potential is used instead of the membrane potential in the calculation of Equation (3.5).

The calculated rejection values for both solutes are compared to the measured rejection values in Table 3.5. The ion valence for both solutes can be determined from Figure 3.2. The membrane zeta-potential can be determined from Figure 3.1, and is equal to  $-14 \pm 4$  mV at pH 7 and to approximately  $-27 \pm 4$  mV at pH 10. It is apparent that the predicted theoretical rejection values are in quite close agreement with the experimentally determined rejection values.

	Ion valence	$\zeta$ -potential (mV)	Experimental rejection (%)	Theoretical rejection (%)
<b>Tetraethylenepentamine</b>				
pH 2.5	+ 4	0	$78 \pm 3$	/
pH 8	+ 2 to + 3	$- 14 \pm 3$	$48 \pm 3$	$43 \pm 7$
pH 10	+ 1	$- 27 \pm 3$	$38 \pm 3$	$36 \pm 7$
<b>1,3,5-benzenetricarboxylic acid</b>				
pH 2.5	0 to - 1	0	$75 \pm 3$	/
pH 8	- 3	$- 14 \pm 3$	$87 \pm 3$	$95 \pm 4$
pH 10	- 3	$- 27 \pm 3$	$93 \pm 3$	$98 \pm 3$

Table 3.5 – Experimental and calculated rejection values for tetraethylenepentamine and 1,3,5-benzenetricarboxylic acid with Trisep TS80 in Milli-Q

The inaccuracy of the predictions is slightly larger than for the experimentally determined rejections. For the positively charged solutes, the rejection is slightly underestimated, whereas for the negatively charged solutes, it is slightly overestimated. The reason for this is the experimental error made during the determination of the  $\zeta$ -potential. The  $\zeta$ -potential determination from streaming potential-measurements is not always accurate, since for instance, it does not take the effects of surface conductance into account. Moreover, the  $\zeta$ -potential does not always accurately represent the real membrane potential that is needed for the calculations in Equation (3.5). Therefore, better methods to describe the membrane potential need to be developed to predict the rejection of charged organic solutes more accurately.

In a first approach, however, this model can be used as a simplified tool to predict the effect of charge interactions on the rejection of organic solutes. The rejection of positively or negatively charged solutes can be modelled, based on known rejection values of uncharged solutes: if the rejection of an uncharged solute with comparable physico-chemical properties (i.e. similar size and hydrophobicity) is known, the

rejection of the charged solute can be predicted by using the calculated charge concentration polarisation.

Of course, the rejection of such an uncharged solute has to be known. Therefore, it would be ideal if this charge concentration polarisation model could be combined with a transport model for uncharged organic solutes. Several studies have already addressed this transport for uncharged solutes [3,6, 41-42].

#### **4. Conclusions**

High rejection values of organic acids with NF at pH 8 seem to be mainly dependent on charge repulsion between the organic acids and the negatively charged membranes. However, some steric effects also seem to play a role, since the rejection of benzoic acid, a phenylic organic acid, was lower than expected. At pH 5, less electrostatic repulsion takes place since the dissociation of the acids is lower and also the membrane surface charge is lower. At this lower pH, rejection of the organic acids is largely determined by steric hindrance effects, but electrostatic effects are still present. Rejection of positively charged pharmaceuticals is lower than the rejection of neutral pharmaceuticals, which is in turn lower than the rejection of negatively charged pharmaceuticals. Charge attraction leads to an increased concentration of positively charged solutes at the negatively charged membrane surface, charge repulsion to a decrease in concentration of negatively charged solutes at the negatively charged membrane surface. This concept is called “charge concentration polarisation” and shows good potential as a simplified modelling tool to predict the rejection of charged solutes, based on the rejection of uncharged solutes

with similar physico-chemical characteristics. The presence of natural organic matter in surface water leads to an increase in the rejection of negatively charged pharmaceuticals and a decrease in the rejection of positively charged pharmaceuticals, probably due to an increased negative surface charge. The addition of  $\text{Ca}^{2+}$  leads to a shielding of the membrane surface charge, which resulted in increased rejection values for positively charged solutes and decreased rejection values for negatively charged solutes. For the neutral pharmaceuticals, neither  $\text{Ca}^{2+}$  addition, nor the presence of NOM influenced the rejection.

Rejection values of pharmaceuticals in fresh urine increased compared to the rejection in other water types, probably due to complexation of the pharmaceuticals with organic acids in the urine.

The influence of solute feed concentrations was only noticeable for the positively charged pharmaceuticals: a small increase in rejection at higher feed concentrations is seen. This is probably also due to shielding of the membrane charge. However, it is not expected that this phenomenon will play a role in normal operation. For neutral and negatively charged organic solutes, no influence of the feed concentration on rejection is seen or expected.

## References

- [1] S.-S. Chen, J.S. Taylor, L.A. Mulford and C.D. Norris. Influences of molecular weight, molecular size, flux, and recovery for aromatic pesticide removal by nanofiltration membranes. *Desalination*, 160 (2004) 103.
- [2] J.A.M.H. Hofman, E.F. Beerendonk, H.C. Folmer and J.C. Kruithof. Removal of pesticides and other micropollutants with cellulose-acetate, polyamide and ultra-low pressure reverse osmosis membranes. *Desalination*, 113 (1997) 209.
- [3] B. Van der Bruggen and C. Vandecasteele. Modelling of the retention of uncharged molecules with nanofiltration. *Water Research*, 36 (2002) 1360.
- [4] B. Van der Bruggen, J. Schaep, D. Wilms and C. Vandecasteele. Influence of molecular size, polarity and charge on the retention of organic molecules by nanofiltration. *Journal of Membrane Science*, 156 (1999) 29.
- [5] L.D. Nghiem and A.I. Schäfer. Adsorption and transport of trace contaminant estrone in NF/RO membranes. *Environmental Engineering Science*, 19 (6) (2002) 441.
- [6] L.D. Nghiem, A.I. Schäfer and M. Elimelech. Removal of natural hormones by nanofiltration membranes: measurement, modeling, and mechanisms. *Environmental Science and Technology*, 38 (2004) 1888.
- [7] Y. Yoon, P. Westerhoff, S.A. Snyder and E.C. Wert. Nanofiltration and ultrafiltration of endocrine disrupting compounds, pharmaceuticals and personal care products. *Journal of Membrane Science*, 270 (2006) 88.
- [8] K. Kimura, S. Toshima, G. Amy and Y. Watanabe. Rejection of neutral endocrine disrupting compounds (EDCs) and pharmaceutical active compounds (PhACs) by RO membranes. *Journal of Membrane Science*, 245 (2004) 71.
- [9] L. Braeken, R. Ramaekers, Y. Zhang, G. Maes, B. Van der Bruggen and C. Vandecasteele. Influence of hydrophobicity on retention in nanofiltration of aqueous solutions containing organic compounds. *Journal of Membrane Science*, 252 (2005) 195.
- [10] Y. Kiso, A. Mizuno, R.A. Adawiah binti Othman, Y.-J. Jung, A. Kumano and A. Arijji, Rejection properties of pesticides with a hollow fiber NF membrane (HNF-1). *Desalination*, 143 (2002) 147.

- [11] K. Kosutic, L. Furac, L. Sipos and B. Kunst. Removal of arsenic and pesticides from drinking water by nanofiltration. *Separation and Purification Technology*, 42 (2005) 137.
- [12] P. Berg, G. Hagmeyer and R. Gimbel. Removal of pesticides and other micropollutants by nanofiltration. *Desalination*, 113 (1997) 205.
- [13] B. Van der Bruggen, J. Schaep, W. Maes, D. Wilms and C. Vandecasteele. Nanofiltration as a treatment method for the removal of pesticides from ground waters. *Desalination*, 117 (1998) 139.
- [14] K.M. Agbekodo, B. Legube and S. Dard. Atrazine and simazine removal mechanisms by nanofiltration: influence of natural organic matter concentration. *Water Research*, 30 (11) (1996) 2535.
- [15] Y. Zhang, C. Causserand, P. Aimar and J.P. Cravedi. Removal of bisphenol A by a nanofiltration membrane in view of drinking water production. *Water Research*, 40 (2006) 3793.
- [16] C. Causserand, P. Aimar, J.P. Cravedi and E. Singlande. Dichloroaniline retention by nanofiltration membranes. *Water Research*, 39 (2005) 1594.
- [17] Y. Zhang, B. Van der Bruggen, G.X. Chen, L. Braeken and C. Vandecasteele. Removal of pesticides by nanofiltration: effect of the water matrix. *Separation and Purification Technology*, 38 (2004) 163.
- [18] K. Majewska-Nowak, M. Kabsch-Korbutowicz and M. Dodz. Effects of natural organic matter on atrazine rejection by pressure driven membrane processes. *Desalination*, 145 (2002) 281.
- [19] Y.J. Jung, Y. Kiso, R.A. Adawih binti Othman, A. Ikeda, K. Nishimura, K.-S. Min, A. Kumano and A. Arijji. Rejection properties of aromatic pesticides with a hollow-fiber NF membrane. *Desalination*, 180 (2005) 63.
- [20] E.C. Devitt, F. Ducellier, P. Cote and M.R. Wiesner. Effects of natural organic matter and the raw water matrix on the rejection of atrazine by pressure-driven membranes. *Water Research*, 32 (9) (1998) 2563.
- [21] K.V. Plakas, A.J. Karabelas, T. Wintgens and T. Melin. A study of selected herbicides retention by nanofiltration membranes – The role of organic fouling. *Journal of Membrane Science*, 284 (2006) 291.
- [22] L.D. Nghiem, A.I. Schäfer and M. Elimelech. Role of electrostatic interactions in the retention of pharmaceutically active contaminants by a loose nanofiltration membrane. *Journal of Membrane Science*, 286 (2006) 52.

- [23] W. Pronk, H. Palmquist, M. Biebow and M. Boller. Nanofiltration for the separation of pharmaceuticals from nutrients in source-separated urine. *Water Research*, 40 (2006) 1405.
- [24] C. Bellona and J.E. Drewes. The role of membrane surface charge and solute physico-chemical properties in the rejection of organic acids by NF membranes. *Journal of Membrane Science*, 249 (2005) 227.
- [25] K. Kimura, G. Amy, J.E. Drewes, T. Heberer, T.-U. Kim and Y. Watanabe. Rejection of organic micropollutants (disinfection by-products, endocrine disrupting compounds and pharmaceutically active compounds) by NF/RO membranes. *Journal of Membrane Science*, 227 (2003) 113.
- [26] Y. Yoon, G. Amy, J. Cho, N. Her and J. Pellegrino. Transport of perchlorate ( $\text{ClO}_4^-$ ) through NF and UF membranes. *Desalination*, 147 (2002) 11.
- [27] L.D. Nghiem and S. Hawkes. Effects of membrane fouling on the nanofiltration of pharmaceutically active compounds (PhACs): Mechanisms and role of membrane pore size. *Separation and Purification Technology*, 57 (2007) 182.
- [28] P. Xu, J.E. Drewes, T.-U. Kim, C. Bellona and G. Amy. Effect of membrane fouling on transport of organic contaminants in NF/RO membrane applications. *Journal of Membrane Science*, 279 (1-2) (2006) 165.
- [29] J. Schaep, C. Vandecasteele, A. Wahab Mohammad and W.R. Bowen. Modelling the retention of ionic components for different nanofiltration membranes. *Separation and Purification Technology*, 22-23 (2001) 169.
- [30] D. Vezzani and S. Bandini. Donnan equilibrium and dielectric exclusion for characterization of nanofiltration membranes. *Desalination*, 149 (1-3) (2002) 477.
- [31] A. Wahab Mohammad and M. Sobri Takriff. Predicting flux and rejection of multicomponent salts mixture in nanofiltration membranes. *Desalination*, 157 (1-3) (2003) 105.
- [32] K. Kimura, G. Amy, J. Drewes and Y. Watanabe. Adsorption of hydrophobic compounds onto NF/RO membranes: an artifact leading to overestimation of rejection. *Journal of Membrane Science*, 221 (2003) 89.
- [33] I.V. Tetko and P. Bruneau. Application of ALOGPS to predict 1-octanol/water distribution coefficients, log P, and log D, of AstraZeneca in-house database. *Journal of Pharmaceutical Sciences*, 93 (12) (2004) 3103.

- [34] F. Sacher, F.T. Lange, H.-J. Brauch and I. Blankenhorn. Pharmaceuticals in groundwaters: analytical methods and results of a monitoring program in Baden-Württemberg, Germany. *Journal of Chromatography A*, 938 (2001) 199.
- [35] Y. Kiso, Y. Nishimura, T. Kitao and K. Nishimura. Rejection properties of non-phenylic pesticides with nanofiltration membranes. *Journal of Membrane Science*, 171 (2000) 229.
- [36] Y. Kiso, Y. Sugiura, T. Kitao and K. Nishimura. Effects of hydrophobicity and molecular size on rejection of aromatic pesticides with nanofiltration membranes. *Journal of Membrane Science*, 192 (2001) 1.
- [37] E.S. Tarleton and R.J. Wakeman. Understanding flux decline in crossflow microfiltration: Part I – Effects of particle and pore size. *Chemical Engineering Research and Design*, 71a (1993) 399.
- [38] A.E. Childress and M. Elimelech. Relating nanofiltration membrane performance to membrane charge (electrokinetic) characteristics. *Environmental Science & Technology*, 34 (2000) 3710.
- [39] L.D. Nghiem and P.J. Coleman. NF/RO filtration of the hydrophobic ionogenic compound triclosan: transport mechanisms and the influence of membrane fouling. *Separation and Purification Technology*, in press (2008), doi:10.1016/j.seppur.2008.03.027.
- [40] R. Boussahel, A. Montiel and M. Baudu. Effects of organic and inorganic matter on pesticide rejection by nanofiltration. *Desalination*, 145 (2002) 109.
- [41] T.-U. Kim, J.E. Drewes, R.S. Summers and G.L. Amy. Solute transport model for trace organic neutral and charged compounds through nanofiltration and reverse osmosis membranes. *Water Research*, 41 (17) (2007) 3977.
- [42] V. Yangali-Quintanilla, T.-U. Kim, M. Kennedy and G. Amy. Prediction of RO/NF membrane rejections of PhACs and organic compounds: a statistical analysis. *Drinking Water Engineering and Science*, 1 (1) (2008) 21.





# **Chapter 4:**

## **Rejection in full-scale plants**

Parts of this chapter were based on:

A.R.D. Verliefde, E.R. Cornelissen, S.G.J. Heijman, G.L. Amy, B. Van der Bruggen and J.C. van Dijk,  
Construction and validation of a predictive model for the rejection of trace organic pollutants in full-scale  
nanofiltration/reverse osmosis installations, to be submitted to Journal of Membrane Science.

## 1. Introduction

The previous chapters have investigated removal mechanisms for organic micropollutants with NF and RO membranes. Removal of organic micropollutants seems to be mainly dependent on three different solute-membrane interactions: steric hindrance between the solute and the membrane phase, hydrophobic interactions between solute and membrane, and electrostatic interactions between charged solutes and the charged membrane surface. Different models were constructed that were able to predict rejection values for charged and uncharged solute on single membrane elements. However, rejection values of organic micropollutants in full-scale membrane installations usually differ from observations made on laboratory-scale units [1]. Especially for large membrane filtration installations, operating at high feed water recovery, organic micropollutant rejection may be significantly lower than rejection values obtained on single membrane elements. This is partly due to the internal increase in solute concentration with increasing feed water recovery in the installation, but also to the flux dependency of the rejection (rejection is lower at lower permeate fluxes, and not all membrane elements in full-scale installations operate at the same flux). Up to this date, no conclusive model has yet been constructed that is able to predict rejections of organic micropollutants in full-scale NF/RO plants.

A general model for the rejection of charged and uncharged organic solutes in full-scale installations will be presented in this chapter. This model will be validated by comparing modelled rejection values to experimentally obtained rejection values for 19 pharmaceutically active compounds, 8 pesticides and 7 organic acids on a 2:1

pilot scale membrane filtration plant. The pilot installation is operated for five different runs with two different membrane types on three different types of feed water, at feed water recoveries ranging from 75 to 90%.

## 2. Model development

In order to model rejection in full-scale plants, a mathematical model is necessary to describe mass transfer through membranes. In the previous chapters, different models for uncharged and charged organic solutes were derived.

In this chapter, these transport models will be used and translated to full-scale plants.

### 2.1. Transport model for uncharged organic solutes

The transport model for uncharged solutes was derived in Chapter 2 and is based on a combination of convective and diffusive transport through the membranes. Diffusion-based rejection models [2] usually only yield good results for rather dense RO membranes; for more open NF membranes, convection has to be taken into account.

The basic transport equation used in the model is:

$$J_s = J_v \cdot C_p = -K_d D_\infty \frac{dc}{dx} + J_v \cdot K_c \cdot c \quad (4.1)$$

Where  $J_s$  and  $J_v$  are the solute and solvent fluxes, respectively,  $D_\infty$  is the solute diffusion coefficient in water,  $K_s$  and  $K_c$  are the hindrance coefficients for diffusive and convective transport,  $C_p$  is the bulk permeate concentration and  $c$  and  $x$  are the solute concentration and axial distance within the membrane.

After integration with the boundary conditions (2.4) and (2.5), this yields the following equation for uncharged organic solute rejection:

$$R = 1 - \frac{K \cdot K_c}{1 - \left( (1 - K \cdot K_c) \cdot \exp\left(-\frac{J_v \cdot K_c \cdot \Delta x}{K_d \cdot D_\infty}\right) \right)} \quad (4.2)$$

Where K is the solute partitioning coefficient in the membrane phase. K relates the solute concentration outside the membrane to the concentration in the membrane pores.

As mentioned in Chapter 2, the partition coefficient K can be defined in different ways.

In a purely steric model (steric hindrance between solute and membrane is regarded as the only rejection mechanism), the partition coefficient K is equal to  $(1-\lambda)^2$ , with  $\lambda = r_s/r_p$ , the ratio of solute over pore size.

In practical NF/RO applications, however, steric hindrance is not the only rejection mechanism. Solute-membrane affinity has to be taken into account, since it affects partitioning and thus also determines the partition coefficient. A more correct definition of the partition coefficient K is:

$$K = (1 - \lambda)^2 \cdot \exp\left(-\frac{\Delta G_i}{k \cdot T}\right) \quad (4.3)$$

(see Chapter 2) where  $\Delta G_i$  represents the free energy associated with differences in interactions of the solute in the water and the membrane phase. If  $\Delta G_i > 0$ , the solute will not partition into the membrane phase spontaneously, since repulsive Van der Waals interactions exist between solute and membrane. Therefore, partitioning will be hindered beyond steric partitioning and rejection will be higher than could be expected, based on solely size exclusion effects. If  $\Delta G_i < 0$ , the solute shows affinity for the membrane (attractive Van der Waals forces) and will partition into the

membrane more easily, resulting in a larger partition coefficient (and thus a lower rejection) than expected, purely based on size exclusion effects.

The parameter  $\Delta G_i$  can easily be determined for liquid solutes. For solids, however, determination of  $\Delta G_i$  is more difficult. Therefore, this chapter will not deal with the determination of  $\Delta G_i$ , but will use the simple (steric) definition of the partition coefficient. The predicted rejection, using the partition coefficient determined with the steric model, will be compared with a fitted rejection, where  $K$  is used as a fitting parameter. Comparison of the calculated (steric) value for  $K$  with the fitted value for  $K$  for each solute, will give information on the solute-membrane affinity (the value of  $\Delta G_i$ ) for each solute.

## 2.2. Transport model for charged organic solutes

As was shown in Chapter 3, the effect of charge interactions on rejection can be modelled. This means that rejection values of charged organic solutes can be modelled, based on known rejection values of uncharged solutes: if the rejection of an uncharged solute with comparable physico-chemical properties (i.e. similar size and hydrophobicity) is known, the rejection of the charged solute can be predicted by using the calculated “charge concentration polarisation”.

This charge concentration polarisation was defined in Paragraph 3.4 in Chapter 3 as:

$$\beta_{charge} = \frac{c_m}{c_f} = \exp\left(\frac{-Z_m \cdot V \cdot F}{R \cdot T}\right) \quad (4.4)$$

where  $\beta_{charge}$  is the charge concentration polarisation,  $Z_m$  is the organic ion valence,  $V$  is the membrane potential (in mV),  $F$  is Faraday’s constant,  $R$  is the universal gas

constant,  $T$  is the temperature (in K) and  $c_m$  and  $c_f$  are the charged solute concentrations at the membrane surface and in the bulk fluid, respectively.

As a first approach, the membrane zeta-potential is used instead of the membrane potential in the calculation of Equation (4.4).

For charged solutes, the rejection can then be calculated as follows:

$$R_{charged} = 1 - \frac{c_p}{c_f} \approx 1 - \beta_{charged} \frac{c_p}{c_m} = 1 - \beta_{charged} (1 - R_{uncharged}) \quad (4.5)$$

Of course, the substitution of  $c_p/c_m$  by  $(1 - R_{uncharged})$  can only be made if the hydrodynamic concentration polarisation is assumed to be equal to one. Otherwise,

$c_p/c_m$  has to be substituted by  $\frac{(1 - R_{uncharged})}{\beta}$ , where  $\beta$  is the hydrodynamic

concentration polarisation.

Thus, to calculate the rejection of a charged solute, the rejection of an uncharged solute with similar physico-chemical properties (size and hydrophobicity) has to be known.

In this chapter, the rejection values for the charged organic solutes will be determined using Equation (4.5), with the rejection values for the uncharged solutes modelled with Equation (4.2).

### 2.3. Upscaling to full-scale plants

The equations derived above for the rejection values of uncharged and charged solutes are only valid for single membrane elements.

For these single membrane elements, following mass-balances and definitions can be written:

$$Q_f = Q_p + Q_c \quad (4.6)$$

$$Q_f C_f = Q_p C_p + Q_c C_c \quad (4.7)$$

$$S = \frac{Q_p}{Q_f} \quad (4.8)$$

$$R = 1 - \frac{C_p}{C_f} \quad (4.9)$$

where  $Q_f$ ,  $Q_p$  and  $Q_c$  are the feed, permeate and concentrate flow,  $C_f$ ,  $C_p$  and  $C_c$  are the bulk feed, permeate and concentrate solute concentrations,  $S$  is the feed water recovery over the element and  $R$  is the solute rejection over the element.

To describe solute rejection in a multi-stage membrane array, the solute rejection values on the single membrane elements have to be combined with mass-balances throughout the system: in multi-stage membrane arrays, the feed concentration of membrane element  $i$  is equal to the concentrate concentration of element  $i-1$ .

The total rejection of a solute in a multi-stage membrane array can then be described by the following equation:

$$R_{tot} = 1 - \frac{\sum_{i=1}^n \left[ J_{v,i} \cdot (1 - R_i) \prod_{j=0}^{i-1} \frac{1 - S_j (1 - R_j)}{1 - S_j} \right]}{\sum_{i=1}^n J_{v,i}} \quad (4.10)$$

Where the subscripts  $i$  and  $j$  denote the stage/membrane number in the full-scale array. The total rejection in a multi-stage membrane array is thus a function of the solute rejection, feed water recovery and permeate flow of the single membrane elements.

Since the values of single element permeate fluxes  $J_{v,i}$  and recoveries  $S_i$  can easily be determined by the user in a full-scale plant, the only unknown parameter to predict the total rejection of an organic solute for a full-scale plant, is the rejection value  $R_i$  of



the solute on each single membrane element. To determine these rejection values  $R_i$ , Equations (4.2) and (4.5) can be used.

#### 2.4. Incorporation of hydrodynamic concentration polarisation

The models constructed above make abstraction of the hydrodynamic concentration polarisation. This hydrodynamic concentration polarisation can easily be incorporated. The hydrodynamic concentration polarisation arises as the flow of dissolved solutes towards the membrane surface and the (partial) rejection of these solutes result in a concentration build-up at the membrane surface. The convective flow of solutes towards the membrane surface, and the smaller flow of solutes through the membrane, are counterbalanced by a diffusive flow of solutes, back to the bulk feed solution. In steady-state systems, the equilibrium between these phenomena, is a function of, amongst others, the flow conditions in the vicinity of the membrane surface.

The hydrodynamic concentration polarisation is defined by the film theory [3] as follows:

$$\beta = \frac{C_m - C_p}{C_b - C_p} \approx \frac{C_m}{C_f} = \exp\left(\frac{J_v}{k}\right) \quad (4.11)$$

where  $\beta$  is the hydrodynamic concentration polarisation factor,  $C_m$ ,  $C_b$  and  $C_p$  are the solute concentrations at the membrane surface, in the bulk of the feed and in the permeate, respectively, and  $k$  is the mass transfer coefficient. The mass transfer coefficient  $k$  can be determined from empirical correlations, e.g. the Shock and Miquel-correlation [4]:

$$Sh = \frac{k.d_h}{D_\infty} = 0.065 \cdot Re^{0.875} Sc^{0.25} \quad (4.12)$$

where Sh is the Sherwood number,  $d_h$  is the hydraulic diameter, Re is the Reynolds number ( $= \frac{\rho \cdot v \cdot d}{\eta}$ ) and Sc is the Schmidt number ( $= \frac{\nu}{D_\infty}$ ).

The mass transfer coefficient  $k$  and, consequently, the hydrodynamic concentration polarisation  $\beta$ , are thus a function of the flow conditions in the membrane element (as expressed by the Reynolds number Re), the nature of the feed solution (as expressed by the Schmidt number Sc) and the geometry of the system (as expressed by the hydraulic diameter  $d_h$ ).

In the transport model for uncharged solutes, the hydrodynamic concentration polarisation factor  $\beta$  has to be incorporated in the boundary condition (2.4):

$$c(x=0) = c_f = K \cdot C_m = K \cdot \beta \cdot C_b \quad (4.13)$$

Thus, Equation (4.2) becomes:

$$R = 1 - \frac{\beta \cdot K \cdot K_c}{1 - \left( (1 - K \cdot K_c) \cdot \exp\left(-\frac{J_v \cdot K_c \cdot \Delta x}{K_d \cdot D_\infty}\right) \right)} \quad (4.14)$$

And for charged solutes, this can be translated to:

$$R = 1 - \frac{\beta_{charge} \cdot \beta \cdot K \cdot K_c}{1 - \left( (1 - K \cdot K_c) \cdot \exp\left(-\frac{J_v \cdot K_c \cdot \Delta x}{K_d \cdot D_\infty}\right) \right)} \quad (4.15)$$

## 2.5. Determination of model parameters

### 2.5.1. Transport model for uncharged solutes

In order to be able to solve Equation (4.14), the values of the model parameters  $K$ ,  $K_c$ ,  $K_d$ ,  $D_\infty$  and  $\Delta x/\varepsilon$  need to be determined.

The hindrance factors  $K_c$  and  $K_d$  are only dependent on the factor  $\lambda=r_s/r_p$ , and can be calculated as shown in Paragraph 2.2 in Chapter 2. The solute radii  $r_s$  can be calculated using molecular modelling software (see Chapter 2) or by using the definition for the Stokes radius (Equation (2.21)). In this chapter, the Stokes radius will be used.

The solute diffusion coefficients  $D_\infty$  were determined using the equation developed by Hayduk and Laurie (1974) [5] (see also Chapter 2).

The values of the membrane pore size  $r_p$  and the factor  $\Delta x/\varepsilon$  were already determined in Chapter 2 for both the Trisep TS80 and the Desal HL membrane used in this study.

The only unknown variable remaining is thus the partition coefficient  $K$ . It was shown before (Chapter 2) that this partition coefficient can theoretically be determined.

However, this process is cumbersome and time-consuming for solid solutes.

Therefore, in this study, where the goal is to test the applicability of the proposed full-scale rejection model, the values of  $K$  will be determined in 2 simple ways:

firstly, by using the simple steric definition of  $K=(1-\lambda)^2$ . This approach will result in an overestimation of the rejection if the solute shows affinity for the membrane. On the other hand, it will result in an underestimation of the rejection if the solute experiences repulsive Van der Waals interactions with the membrane surface.

In the second approach, the partition coefficient  $K$  will be determined by fitting the model to experimentally obtained rejection data of the solute on single membrane elements. By comparing the fitted  $K$  to the  $K$  determined with the steric model, information can be obtained on the type of Van der Waals interactions (repulsive or attractive) of the solute with the membrane surface.

### *2.5.2. Transport model for charged solutes*

The only unknown variable in Equations (4.4) and (4.15) for the rejection of charged organic solutes is the membrane potential  $V$ . As in Chapter 3, the membrane zeta potential  $\zeta$  will be used as an approximation for the membrane potential.

Since the zeta-potential is highly dependent on ionic strength, the zeta-potential will be determined in different solutions containing different concentrations of background electrolyte, to mimic the effect of increasing salt concentrations with increasing feed water recovery in pilot- and full-scale membrane filtration installations.

### *2.5.3. Full-scale model*

Finally, in order to solve Equation (4.10) for the rejection of an organic solute on a full-scale or pilot-scale membrane filtration plant, the values of the permeate fluxes and feed water recoveries for the different elements in the installation need to be known. Even though it was possible in the pilot plant used in this study to measure most of these fluxes, full-scale installations usually do not offer this option. Therefore, fluxes need to be determined theoretically. Fortunately, most membrane manufacturers offer projection programs, which allow the user to calculate pressures and fluxes of single membrane elements if the lay-out of the plant and the composition of the feed water are known. In this study, the commercial software packages Troi<sup>®</sup> (by the Trisep Corporation) and Winflows<sup>®</sup> (by GE-Osmonics) were used. Fluxes and pressures calculated with this software corresponded well to the experimentally measured values.

### 3. Materials and methods

#### 3.1. Equipment and filtration protocol

##### 3.1.1. *Single membrane element set-up*

The single membrane element set-up was used to fit the model parameter  $K$  for the transport model for uncharged solutes by determining solute rejection as a function of permeate flux. Afterwards, these values for  $K$  were compared with the values obtained, using the simple steric model to calculate  $K$ . The set-up was described before in Chapter 2.

Membrane filtration experiments were carried out with single 4-inch spiral wound membrane elements at a constant cross-flow velocity of 0.2 m/s (corresponding to a feed flow of 1500 l/h and a concentration polarization factor of 1.07). Feed water temperature was maintained at  $13 \pm 1^\circ$  (which corresponds to the feed water temperature used in the pilot installation on both water types), using an immersed stainless-steel coil with cooling liquid fed from a cooling system (Tamson TLC 10B).

All experiments were carried out in a recycle mode with a single batch of water, with both permeate and concentrate recycled back into the feed reservoir.

All rejection experiments were carried out for 4 days (as in the previous chapters), to make sure that the membranes were saturated with the organic solutes used, and to make sure that steady state rejection values are obtained.

##### 3.1.2. *Nanofiltration pilot plant*

The nanofiltration pilot plant consists of a stacking of 18 spiral wound 4-inch membrane elements in a 2-stage membrane array. The first stage consist of 2 parallel pressure vessels, each containing 6 membrane elements. The second stage consists of a single pressure vessel, also containing 6 membrane elements.

A schematic diagram of the installation is shown in Figure 4.1 and a picture of the installation in Figure 4.2.

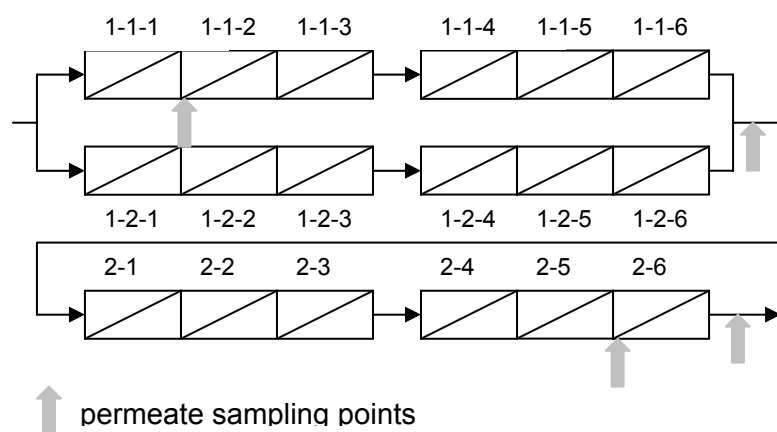


Figure 4.1 – Schematic diagram of pilot NF installation with membrane coding

The feed solution is delivered to the installation, by a multi-impellor centrifugal pump (Grundfos CRN-5). The pump is capable of providing pressures of up to 25 bar at a flow rate of 8 m<sup>3</sup>/h. Permeate flows of the first membrane elements of the first stage, of the complete first stage, of the complete second stage and of the last element in the second stage, as well as concentrate and feed flow are monitored by precision flow meters (Endress&Hauser).



Figure 4.2 – Picture of the NF pilot installation

Applied pressure and feed water recovery over the installation are regulated using two needle valves in the feed and concentrate stream. All test unit parts in contact with the feed solution are made of stainless steel to minimize adsorption of the organic compounds used. Pressure measurements are possible inbetween all membrane elements and in the feed and concentrate stream to measure transmembrane pressure for each element separately. A precision manometer (Cerabar S, Endress&Hauser) was used for pressure measurements.

The installation was loaded with two different membrane types, during five different runs on two different types of source water.

Membrane filtration experiments were also carried out at a constant cross-flow velocity of 0.2 m/s (corresponding for the pilot installation to a feed flow of 3000 l/h (1500 l/h for each parallel pressure vessel)). During the first two runs, Trisep TS80 membranes were placed inside the installation and the installation was fed with

ground water. Feed water recovery of the installation was set to 75% during the first run and to 87% in the second run.

For the last three runs, Desal HL membranes were placed inside the installation and the installation was fed with tap water from the city of Nieuwegein in the Netherlands. Feed water recovery was set to 75% and 82.5% during the third and fourth run, respectively. For the last run, feed water recovery was set to 90%, after multivalent scaling ions were removed from the feed water using a cationic ion exchange resin. All experiments were carried out in a single pass (once-through) mode, except for the last run at 90% recovery.

As well as for the single element set-up, experiments were carried out for 4 days to accomplish saturation of the membrane with the organic compounds used and ensure that steady state rejection values were obtained.

Anti-scalant (4AQUA OSM92, AquaCare, 's Hertogenbosch, the Netherlands) was dosed to prevent precipitation of sparingly soluble salts (scaling).

### 3.2. Membranes

The same commercially available nanofiltration membrane as in Chapters 2 and 3 were used in this study: Trisep TS80 TSF (Trisep Corp., Goleta CA, USA) and Desal HL (GE Osmonics, Fairfield CT, USA).

Before use, all membranes were rinsed with tap water for two hours to remove preservation liquids. Afterwards, the membranes were characterized for pure water permeability with Milli-Q water and for  $\text{MgSO}_4$  rejection with a 500 ppm  $\text{MgSO}_4$  solution in Milli-Q water. The properties of the membranes are summarized in Table 4.1.



	Trisep TS80	Desal HL
MWCO (g/mol)	175	150-300
Contact angle (°)	48 ± 2	41 ± 2
Pure water permeability (m/(s.bar))	1.2 × 10 <sup>-6</sup>	2.0 × 10 <sup>-6</sup>
% MgSO <sub>4</sub> -rejection	99%	98%
ζ-potential in 5 mM NaCl (mV)	-19 ± 2	-14 ± 2
ζ-potential in 5 mM NaCl + 5 mM CaCl <sub>2</sub>	-14 ± 2	-10 ± 2
ζ-potential in 5 mM NaCl + 10 mM CaCl <sub>2</sub>	n.d.	-7 ± 2

Table 4.1 – Membrane properties for Trisep TS80 and Desal HL membrane used in rejection experiments (n.d.: not determined)

The molecular weight cut-off (MWCO) values were provided by the membrane manufacturers. The contact angles were determined with Milli-Q water using the sessile drop method. The membrane zeta potentials were measured at the pH of the feed water in different background solutions using commercially available equipment (SurPASS, Anton Paar, Graz, Austria). Zeta potential values were determined in solutions containing 5 mM NaCl; 5 mM NaCl and 5 mM CaCl<sub>2</sub>; and 5 mM NaCl and 10 mM CaCl<sub>2</sub> as background electrolyte, respectively. The dependency of the zeta potential on the feed water ionic strength was determined to incorporate the effect of increasing salt concentrations with increasing feed water recovery in the pilot plant.

### 3.3. Organic solutes and analysis

Rejection experiments were carried out with a variety of organic solutes: the same organic acids and pharmaceuticals as in Chapter 3 were used, and selected pesticides were also spiked during the rejection experiments (solutes were again chosen for their physico-chemical parameters). The organic acids were spiked at a

feed water pH of 8, but also at pH 5. It was shown in Chapter 3 that the organic acids are dissociated (and thus negatively charged) at pH 8, but they regain their proton and become neutral at pH 5. Choosing these two operating conditions allows to determine the effect of electrostatic interactions on the rejection of organic acids on pilot scale equipment.

The cocktail of neutral, as well as negatively and positively charged pharmaceuticals was also spiked again to gain more insight in the effects of electrostatic interactions on rejection. The pharmaceutical properties encompass an as wide as possible range of solute-membrane interactions (size, charge and hydrophobic interactions).

The selected pesticides were also chosen with a wide range of solute physico-chemical properties.

The physico-chemical properties of all solutes are shown in Table 4.2.

		MW (g/mol)	log K <sub>ow</sub> (-)	pK <sub>a</sub> (-)	Charge at pH 8	log D <sub>(pH 8)</sub> (-)	Diff. coeff. (x 10 <sup>-10</sup> m <sup>2</sup> /s)	r <sub>s</sub> (nm)	r <sub>s</sub> Stokes (nm)
<b>Organic acids</b>	formic acid	46.0	-0.54	3.75	-	-4.79	14.70	0.15	0.15
	acetic acid	60.1	-0.17	4.76	-	-3.41	11.40	0.16	0.19
	glycolic acid	76.1	-1.11	3.83	-	-5.28	11.30	0.20	0.19
	lactic acid	90.1	-0.72	3.86	-	-4.86	9.66	0.22	0.22
	malonic acid	104.1	-0.81	2.85	-	-5.96	9.67	0.22	0.22
	benzoic acid	122.1	1.87	4.19	-	-1.94	7.95	0.27	0.27
	phenylacetic acid	136.1	1.41	4.31	-	-2.28	8.21	0.31	0.26
<b>Pharmaceuticals</b>	terbutaline	225.3	0.90	8.86	+	- 0.97	5.34	0.41	0.40
	salbutamol	239.3	0.64	9.27	+	- 1.63	5.25	0.43	0.41
	pindolol	248.3	1.75	9.26	+	- 0.52	5.17	0.48	0.42
	propranolol	259.4	3.48	9.58	+	0.90	4.91	0.48	0.44
	atenolol	266.3	0.16	9.43	+	- 2.27	4.93	0.52	0.44
	metoprolol	267.4	1.88	9.49	+	- 0.61	4.66	0.56	0.46
	sotalol	272.4	0.24	9.44	+	- 2.20	5.13	0.43	0.42
	clenbuterol	277.2	2.00	9.29	+	- 0.29	5.10	0.48	0.42
	phenazon	188.2	0.38	n.a.	neutral	n.a.	6.06	0.35	0.35
	aminopyrine	231.3	1.00	n.a.	neutral	n.a.	5.30	0.40	0.41
	carbamazepine	236.3	2.45	n.a.	neutral	n.a.	5.97	0.40	0.36
	cyclophosphamide	261.1	0.63	n.a.	neutral	n.a.	5.62	0.35	0.38
	pentoxifylline	278.3	0.29	n.a.	neutral	n.a.	4.50	0.46	0.48
	ibuprofen	206.3	3.97	4.47	-	1.44	5.27	0.37	0.41
	clofibric acid	214.7	2.57	3.35	-	- 1.08	5.83	0.33	0.37
	naproxen	242.2	3.9	4.15	-	0.05	5.44	0.40	0.39
	fenoprofen	242.3	3.90	4.21	-	1.11	5.24	0.39	0.41
	gemfibrozil	250.3	4.77	4.45	-	2.22	4.81	0.44	0.45
	ketoprofen	254.3	3.12	4.29	-	0.41	5.11	0.41	0.42
	diclofenac	296.2	4.51	4.08	-	1.59	5.21	0.37	0.41
	bezafibrate	361.8	4.25	3.44	-	0.69	4.25	0.56	0.51

<b>Pesticides</b>	carbendazim	191.2	1.52	n.a.	neutral	n.a.	7.02	0.38	0.31
	metamitron	202.2	0.83	n.a.	neutral	n.a.	5.70	0.34	0.38
	metribuzin	214.3	1.70	n.a.	neutral	n.a.	5.32	0.36	0.40
	atrazin	215.7	2.61	n.a.	neutral	n.a.	5.61	0.37	0.38
	diuron	233.1	2.68	n.a.	neutral	n.a.	6.01	0.38	0.36
	pirimicarb	238.3	1.70	n.a.	neutral	n.a.	5.23	0.42	0.41
	dimethenamid	275.8	2.15	n.a.	neutrat	n.a.	4.99	0.36	0.43

Table 4.2 – Physico-chemical characteristics of selected organic solutes (n.a.: not applicable;  $r_s$ : solute radius, calculated via molecular modelling software;  $r_s$  Stokes: Stokes radius)

All pharmaceuticals and pesticides were obtained from Sigma-Aldrich (St Louis MO, USA), except phenazon, ibuprofen, aminopyrine, carbamazepine and cyclophosphamide, which were obtained from Acros Organics (Geel, Belgium). All organic acids were obtained from Acros Organics (Geel, Belgium). All chemicals were at least reagent grade.

High performance liquid chromatography with tandem mass spectrometric detection and gas chromatograph with mass spectrometric detection were used to determine concentrations of all pharmaceuticals and pesticides, respectively. A solid phase extraction at pH 3 was performed using styrene divinylbenzene (SDB) material. The limit of quantitation (LOQ) was 10 ng/l for all pharmaceuticals and pesticides. More information about the analytical procedures for the pharmaceuticals and pesticides was published by Sacher et al. (2001) and van Hoof et al. (2001) [6,7].

The pharmaceuticals and pesticides were spiked in concentrations of 2 µg/l, to be able to accurately measure 99% rejection (which corresponds to a permeate concentration of 20 ng/l, well above the LOQ of 10 ng/l).

All pharmaceuticals and pesticides were spiked simultaneously as a cocktail. The cocktail was prepared as a concentrated stock solution of 10 l within the selected feed water. To prevent co-solvent effects and possible problems with biological growth in the system, no methanol was used to facilitate dissolution of the pharmaceuticals and pesticides. The desired volume of the stock solution was added to the feed tank for the single element testing. For the pilot scale testing, the desired concentration of pharmaceuticals and pesticides was obtained by dosing the cocktail continuously into the feed stream from the concentrated stock solution.

The organic acids were all spiked separately in Milli-Q water and measured by analysing the non-purgeable organic carbon (NPOC ~ total organic carbon (TOC)) -

content of feed and permeate. The limit of detection for the NPOC-analysis is 0.2 mg/l. Therefore, all solutes were spiked in concentrations of 10 mg carbon/l, in order to be able to measure at least 98% rejection (which corresponds to a permeate concentration of 0.2 mg/l). Since the background organic carbon content of the feed water can not be neglected, blank measurements were taken at all sampling points and the values obtained were subtracted from the measured concentrations during the rejection experiments, to obtain the concentration of the organic acids.

### 3.4. Feed water types

Three different feed water types were used in the experiments. The first water type was ground water from the pumping station Spannenburg (the Netherlands), operated by the Dutch drinking water company Vitens. The feed water for the NF experiments was pretreated with ultrafiltration (X-Flow UFC-M5 membranes). The organic content of the water is quite high. Halfway during the second rejection run at 87% recovery, the pH of the feed water was changed to pH 5, to be able to measure the rejection of two organic acids (formic and acetic acid) in neutral regime (at higher pH, the organic acids are dissociated and thus negatively charged). The pH of the feed water was lowered by continuously dosing concentrated  $\text{H}_2\text{SO}_4$  (98%, Sigma-Aldrich) to the feed stream.

The second water type was tap water from the city of Nieuwegein in the Netherlands. The water was extracted as anaerobic groundwater and subsequently treated with aeration and rapid sand filtration. The organic content of the water is quite low.

	ground water (Spannenburg)	tap water (Nieuwegein)	tap water + cationic ion exchange
pH (-)	7.6	7.9	7.9
Dissolved Organic Carbon (DOC) (mg/l)	7.6	1.9	1.9
Conductivity ( $\mu\text{S}/\text{cm}$ )	500	395	450
Turbidity (FTE)	0.1	0.35	0.23
$\text{Ca}^{2+}$ (mg/l)	32	68	12
$\text{Mg}^{2+}$ (mg/l)	9.8	5.4	2.1
$\text{K}^{+}$ (mg/l)	2.2	3.1	3.1
$\text{Na}^{+}$ (mg/l)	74	25	95
Fe	< 0.1	0.1	< 0.1
$\text{Cl}^{-}$ (mg/l)	30	9.1	9.1
$\text{SO}_4^{2-}$ (mg/l)	< 1	< 1	< 1

Table 4.3 – Water quality parameters of selected feed water types for rejection experiments

The third water type was the same tap water from the city of Nieuwegein, but treated with a cationic ion exchange resin (Amberlite IRC86 (Rohm & Haas, Philadelphia PA, USA)). This treatment removes all the divalent ions, that may cause scaling in the nanofiltration unit, from the feed water, by exchanging them for  $\text{Na}^{+}$  ions.

Some general water quality parameters of all feed waters are summarized in Table 4.3. Table 4.4 summarizes which solutes have been spiked during each rejection run.

## 4. Results and discussion

### 4.1. Operation of the pilot-plant

The pilot plant was operated during five different runs on three types of feed water, with two membranes at 75% (2x); 82.5%; 87% and 90% recovery.

		measured on Trisep TS80 (Spannenburg)		measured on Desal HL (Nieuwegein)	
		RUN 1 (75%)	RUN 2 (87%)	RUN 3 & 4 (75%&82.5%)	RUN 5 (90%)
<b>Organic acids</b>	formic acid		X		
	acetic acid		X		
	glycolic acid		X		
	lactic acid		X		
	malonic acid		X		
	benzoic acid		X		
	phenylacetic acid		X		
	formic acid pH 5		X		
	acetic acid pH 5		X		
<b>Pharmaceuticals</b>	terbutaline			X	X
	salbutamol			X	X
	pindolol			X	X
	propranolol			X	X
	atenolol			X	X
	metoprolol			X	X
	sotalol				X
	clenbuterol				X
	phenazon			X	X
	aminopyrine			X	X
	carbamazepine			X	X
	cyclophosphamide			X	X
	pentoxifylline			X	X
	ibuprofen			X	X
	clofibrilic acid			X	X
	naproxen			X	X
	fenoprofen			X	X
	gemfibrozil			X	X
	ketoprofen			X	X
	diclofenac			X	X
	bezafibrate			X	X
<b>Pesticides</b>	carbendazim			X	X
	metamitron	X		X	X
	metribuzin			X	X
	atrazin			X	X
	diuron	X			
	pirimicarb			X	X
	dimethenamid			X	X

Table 4.4 – Spiked solutes during different filtration runs with different membranes and feed water types



Figure 4.3 shows the normalized permeate flows of the complete first and second stage of the installation and of the first and last membrane element, together with feed and concentrate flow during a 10 day run at 75% recovery on tap water from the city Nieuwegein. Also the normalized feed pressure and normalized salt passage during the filtration run are shown. It is apparent that the installation was operating quite smoothly during the whole filtration run. No organic/particulate membrane fouling was expected, due to the origin of the source water (tap water), guaranteeing a low organic content and a small load of particles/colloids. Furthermore, no scaling and biological fouling were expected because of the dosing of anti-scalant and the short duration of the experiment.

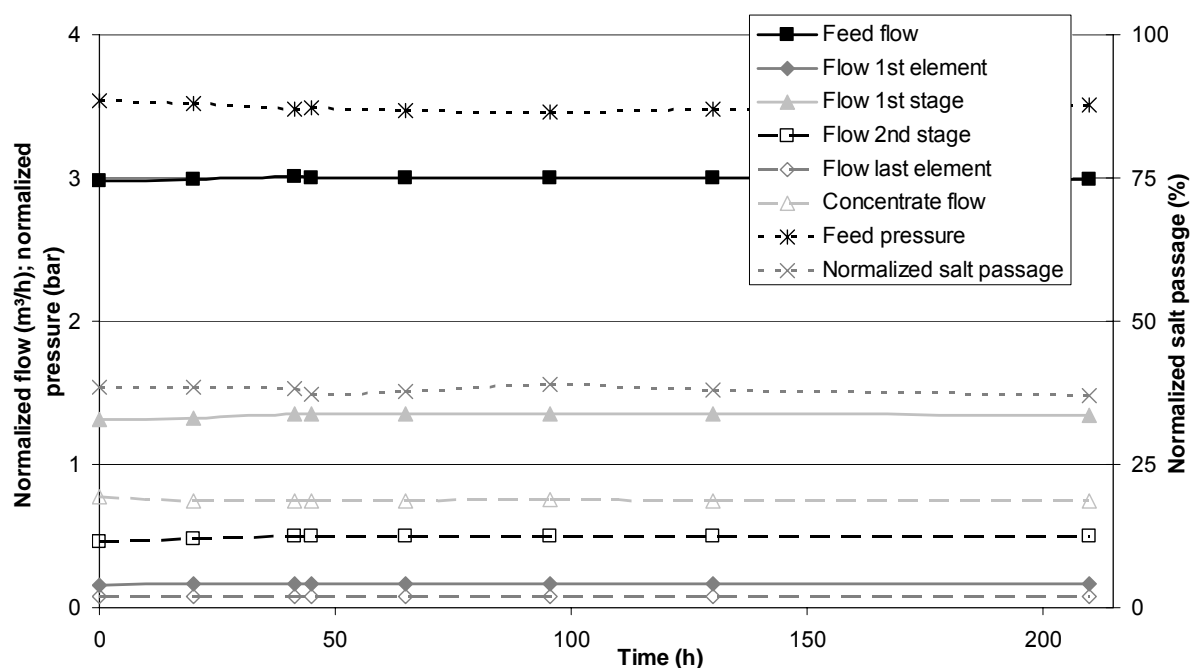


Figure 4.3 – Operational parameters of the NF pilot installation during a 10 day run at 75% recovery

Figure 4.4 shows the normalized permeate flows and concentrate and feed flow, together with normalized feed pressure and salt passage for the 5-day run at 90% recovery.

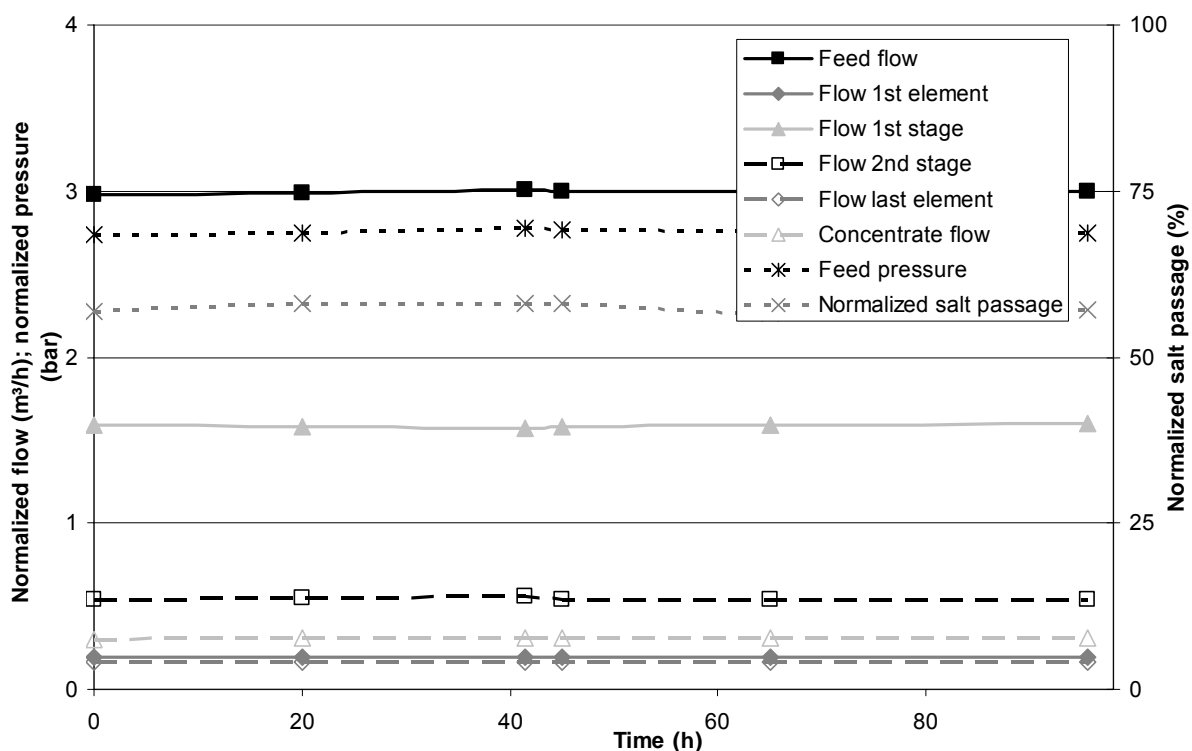


Figure 4.4 – Operational parameters of the NF pilot installation during a 4 day run at 90% recovery

The feed pressure is lower in the 90%, even though the permeate flows are higher. This is due to the higher feed water temperature in the 90% recovery experiment. The experiment was carried out in recycle mode, and feed water temperature was kept constant at  $20 \pm 2$  °C.

As for the run at 75% recovery, no significant fouling was observed in the 90% recovery run. For all other experiments, similar observations were made. It can thus be concluded that in none of the rejection experiments, the experimental rejection values obtained were influenced/biased by fouling of the membrane surface.

#### 4.2. Rejection values on single membrane elements

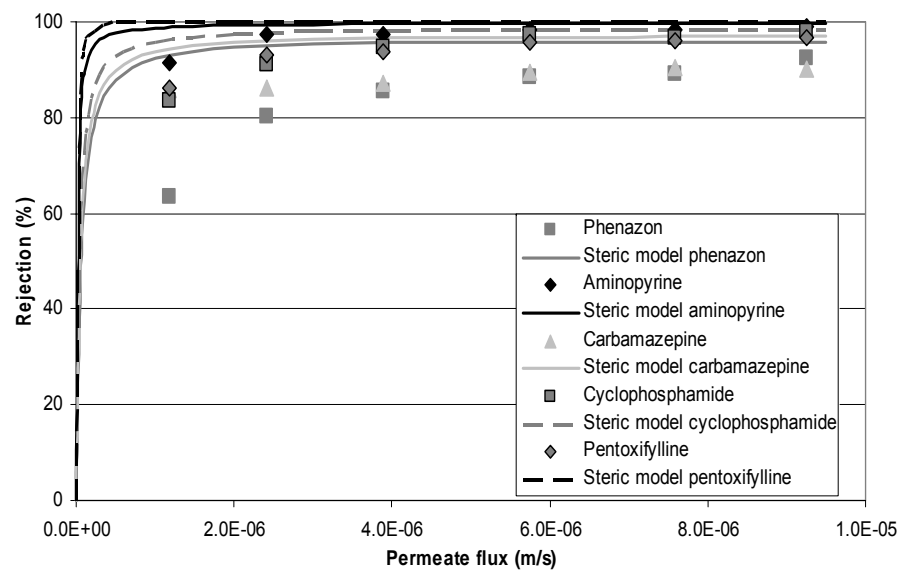
The rejection values of all neutral solutes in Table 4.2 were determined as a function of feed pressure (and thus permeate flux) on single Trisep TS80 and Desal HL membrane elements.

For neutral organic solutes, the rejection as a function of the permeate flux can be modelled using Equation (4.14) if all the parameters  $K_c$ ,  $K_d$ ,  $K$  and  $\Delta x/\varepsilon$  are known. The hindrance parameters  $K_d$  and  $K_c$  can be determined using Equations (2.8) and (2.9). The parameter  $\Delta x/\varepsilon$  is known for both membranes from Chapter 2.

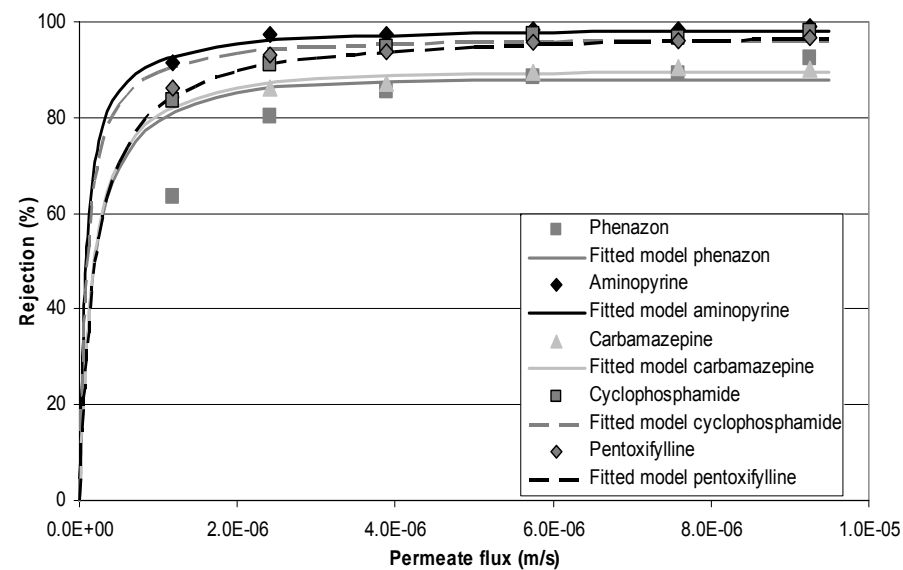
Since the goal of this chapter is mainly the validation of the full-scale rejection model, the partition coefficient  $K$  will not be determined in a rigorous, theoretical manner, but will be determined in two simple ways, as mentioned before: by using the simplified “steric” definition for  $K$  ( $= (1-\lambda)^2$ ), and by estimating  $K$  by fitting the experimentally obtained rejection values on the single membrane element to the model (Equation (4.14)). With these obtained  $K$  values, the full-scale model can then be constructed.

The solid points in Figures 4.5 (a) and 4.5 (b) represent the experimentally determined data for the neutral pharmaceuticals on the Desal HL membrane in tap water. The solid lines in Figure 4.5 (a) represent the modelled rejections as a function of permeate flux, using the simple steric definition of the partition coefficient  $K$ . The solid lines in Figure 4.5 (b) represent the same modelled rejections, obtained by fitting the partition coefficient  $K$  to the experimental rejections. Only a single value of  $K$  is fitted (thus  $K$  will be considered constant as a function of permeate flux here), to simplify comparison between the “steric”  $K$  and the fitted  $K$ .

The rejection model using the fitted values of  $K$  appears to fit the experimental data quite well. Use of the steric model results in a overestimation of rejection for all neutral pharmaceuticals.

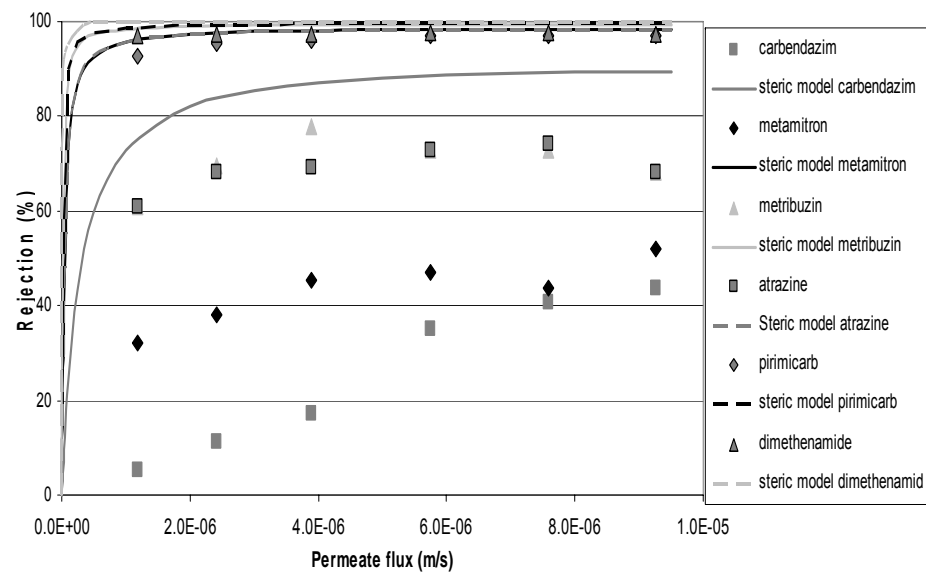


(a)

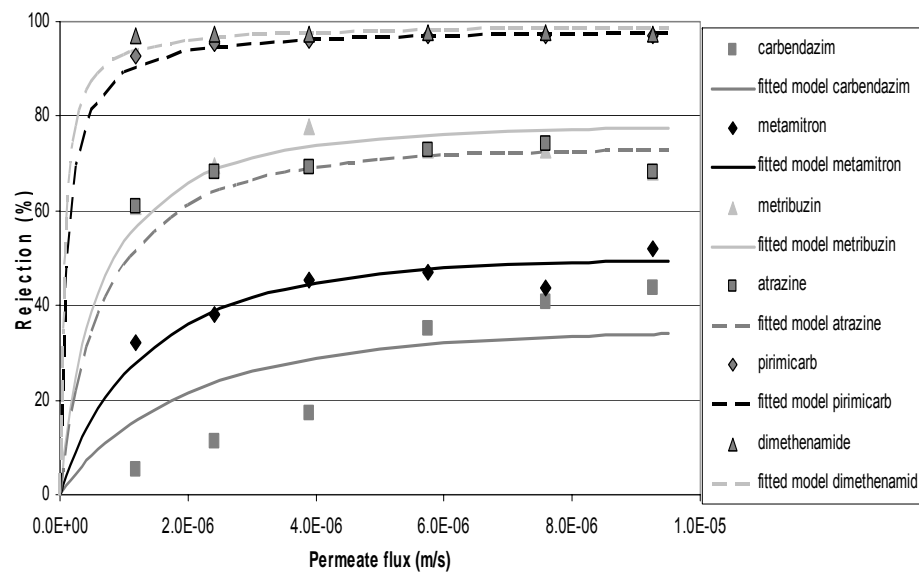


(b)

Figure 4.5 - Experimental and modelled rejection values for neutral pharmaceuticals as a function of permeate flux on single Desal HL membrane element (left: steric model, right: fitted model)



(a)



(b)

Figure 4.6 - Experimental and modelled rejection values for neutral pesticides as a function of permeate flux on single Desal HL membrane element (left: steric model, right: fitted model)

A similar approach is followed for the rejection of the neutral pesticides on the Desal HL membrane. These results are shown in Figures 4.6 (a) and 4.6 (b). The fitted model appears to give better results, compared to the steric model, for the pesticides as well.

The rejection values of the pesticides follow the exact same trend as the molar mass (and thus the size) of the molecules: the higher the molar mass, the higher the rejection. The rejection values of the pesticides metribuzin and atrazine are almost identical, and so are their molar masses.

For the neutral pharmaceuticals, the trend is less clear. Phenazon is the smallest solute, and rejection is also the lowest. For the other solutes however, the rejection does not really follow the trends of increasing molar mass. This is probably caused by the high molar masses of these solutes: except for phenazon, the molar masses of the pharmaceuticals are probably above the molecular weight cut-off of the membrane, explaining the high rejections. In spite of its high molar mass, the neutral pharmaceutical carbamazepine is less efficiently removed compared to other neutral pharmaceuticals of similar (or lower) molar mass. This is caused by the higher hydrophobicity (as expressed by the higher log  $K_{ow}$ -value) of carbamazepine (and thus to the larger solute-membrane affinity and increased partitioning).

For all neutral solutes on both membranes, (including the organic acids formic and acetic acid at pH 5), the values of the fitted partition coefficient  $K$  are compared to the values of the partition coefficient  $K$ , calculated from  $K=(1-\lambda)^2$  in Table 4.5.

It is apparent that the use of the steric definition for  $K$  leads to a lower value than the fitted value for  $K$  and thus to an overestimation of rejection for all neutral pharmaceuticals and pesticides. For the uncharged organic acids, the use of the

steric value for K leads to a higher value than the fitted value for K and thus an underestimation of rejection.

In conclusion, the steric values for K do not succeed very well in predicting the rejection of the neutral solutes. This indicates that solute-membrane Van der Waals interactions can not be neglected in the rejection of organic solutes on polymeric membranes. Solute-membrane interactions are repulsive for the uncharged organic acids used here (higher rejection than predicted by steric effects only); solute-membrane interactions are attractive for the neutral pharmaceuticals and pesticides (lower rejections than predicted by steric effects only).

The fitted values for K thus appear to yield better results for modelling purposes. Therefore, the fitted values for K will further be used as model parameters in the calculation of the rejection of charged solutes, since they allow a more accurate evaluation of the rejection.

Values for partition coefficient K			
		Steric model	Fitted from bench-scale results
<b>Pharmaceuticals</b>	phenazon	0.035	0.1
	aminopyrine	0.002	0.015
	carbamazepine	0.027	0.09
	cyclophosphamide	0.014	0.035
	pentoxifylline	0	0.028
<b>Pesticides</b>	carbendazim	0.078	0.5
	metamitron	0.014	0.45
	metribuzin	0.005	0.21
	atrazin	0.014	0.24
	pirimicarb	0.002	0.02
	dimethenamid	0	0.009
<b>Organic acids (pH 5)</b>	formic acid	0.35	0.15
	acetic acid	0.22	0.18

Table 4.5 – Values for partition coefficient for neutral organic solutes

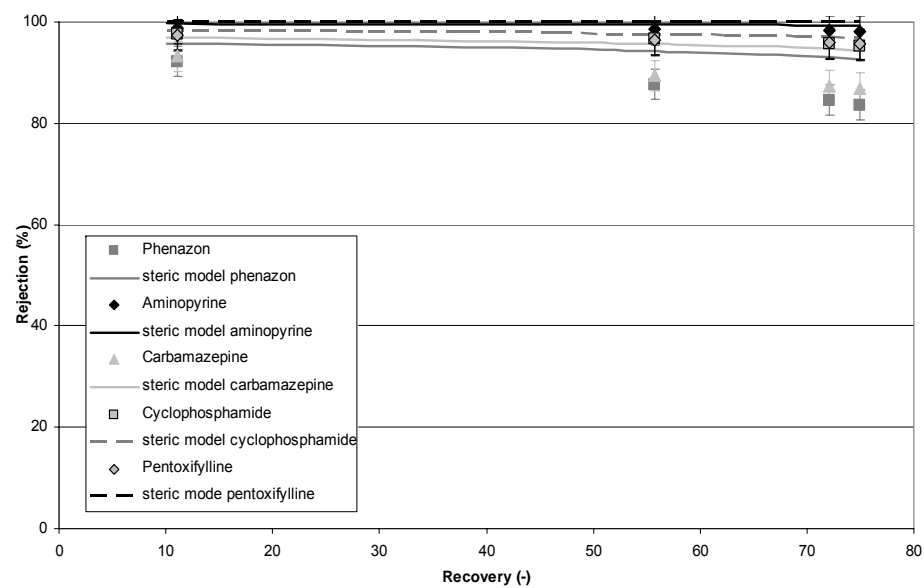
#### 4.3. Rejection values and model results at higher recoveries in the pilot installation

The rejection values for the neutral pharmaceuticals during the 75% recovery run on tap water from the city Nieuwegein are shown as a function of feed water recovery in Figure 4.7.

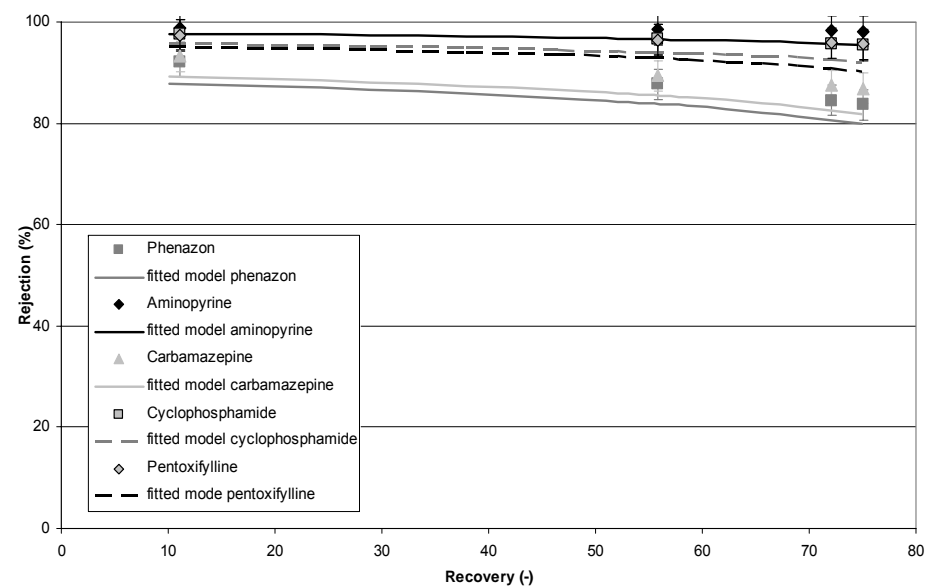
The data points show the experimentally obtained rejection values. The rejection value at 10% recovery was obtained by analysing the separate permeate of the first membrane element. The rejection value at 50% recovery was obtained by analysing the permeate of the complete first stage of the installation. The rejection value at 70% was obtained by analysing the collective permeate of all membrane elements but the last one. And finally, the rejection value at 75% was obtained by analysing the collective permeate of the complete pilot-scale installation. The concentrate of the installation was sampled as well, and the concentrate concentration was used as a check to see whether mass-balances were correct and no adsorption was indeed occurring after the 4 days of equilibrating. No large discrepancies were found in the mass balances.

It can be seen that the rejection of the organic solutes in the pilot-scale installation is decreasing with increasing recovery. This is partly due to the internal increase of solute concentration in the higher stages of the installation with increasing permeate production, and also to the lower rejections of the last membrane elements in each stage (as shown in Figures 4.5 and 4.6, rejection decreases with decreasing permeate flux).





(a)



(b)

Figure 4.7 – Experimental and modelled rejection values for neutral pharmaceuticals on pilot scale NF installation, as a function of feed water recovery for filtration run at 75% recovery (left: steric model; right: fitted model)

The curves in Figure 4.7 (a) represent the modelled rejection curves for the neutral pharmaceuticals, using Equation (4.10) and replacing the unknown values of  $R_i$  by the values obtained using Equation (4.14) and the steric values of  $K$ . The curves in Figure 4.7 (b) represent the same modelled curves, but using the fitted values of  $K$  (from the single element experiments). The permeate fluxes  $J_i$  and recoveries  $S_i$  of the separate membrane elements were determined using the commercially available projection software (Winflows, GE Osmonics). As mentioned before, the projected fluxes and pressures over the membrane elements correspond very well to the measured fluxes and pressures in the installation.

As can be seen from Figure 4.7, the calculated rejection with the fitted values for  $K$  appear to model the experimentally obtained rejection values quite well (within an accuracy range of  $\pm 5\%$ ), hereby proving the applicability of the full-scale rejection model. Again, the use of the steric value for the partition coefficient  $K$  appears to result in an overprediction of the rejection, since solute-membrane affinity is not taken into account.

The experimentally obtained and the modelled rejection values during the rejection run at 75% recovery with the Nieuwegein tap water for the positively charged pharmaceuticals from Table 4.2 are shown in Figure 4.8. The modelled values were calculated using Equation (4.15). The fitted values of  $K$  for uncharged solutes with similar physico-chemical properties (size and hydrophobicity) were used, and the charge concentration polarisation  $\beta_{\text{charge}}$  was used to determine the rejection of the charged pharmaceuticals. The fitted values for  $K$  were used, instead of the values for  $K$  using the steric model, since the fitted values of  $K$  correspond to the experimental rejection values better. The membrane zeta-potential, which is used in the calculation

of  $\beta_{\text{charge}}$  at pH 8 is given in Table 4.1 at different ionic strengths of the electrolyte. Since the salt concentration in the pilot plant is increasing from the first to the last stage, the dependency of the zeta-potential on the ionic strength has to be incorporated. A linear decrease of the zeta-potential with increasing salt concentration in the installation is assumed.

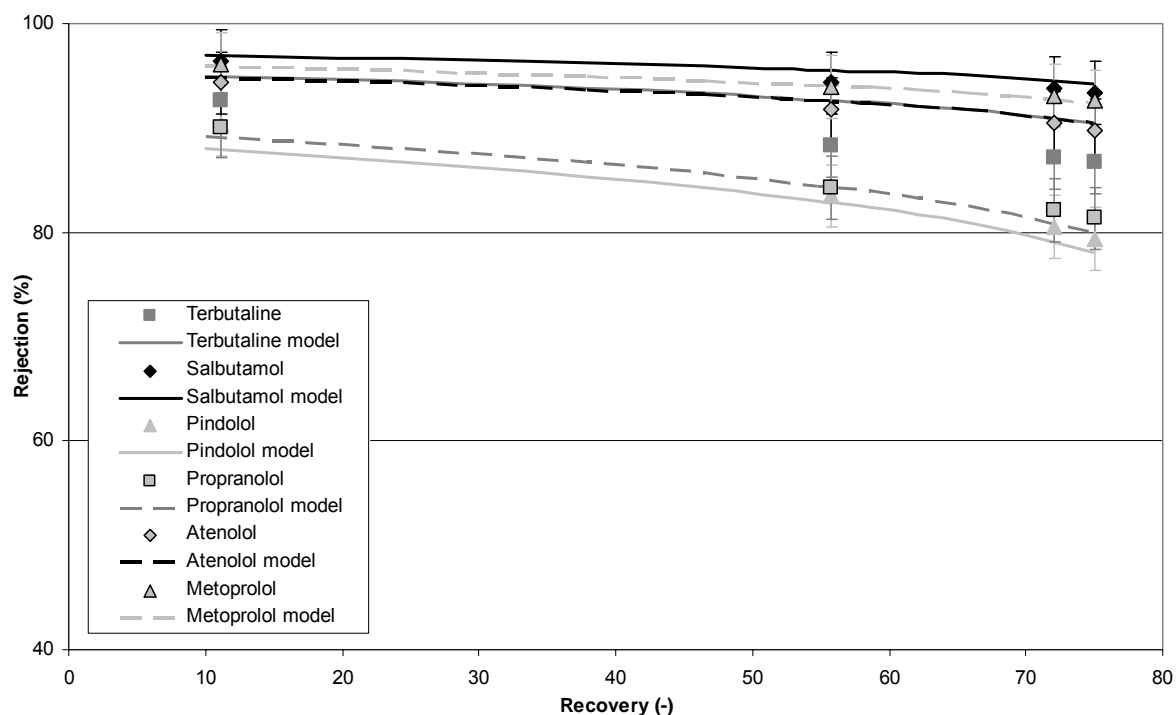


Figure 4.8 – Experimental and modelled rejection values for positively charged pharmaceuticals on pilot scale NF installation, as a function of feed water recovery for filtration run at 75% recovery

A necessity for the calculation of the rejection of the charged solutes is that an uncharged solute with similar physico-chemical properties has to be available.

As an example: the rejection values of the solute salbutamol were calculated based on values of the partition coefficient  $K$ , obtained for the neutral pharmaceutical aminopyrine. For atenolol, the values of  $K$  obtained for cyclophosphamide were used.

For the positively charged pharmaceuticals, the predicted rejection values also correspond well to the experimentally obtained rejection values, once again providing proof for the applicability of the model.

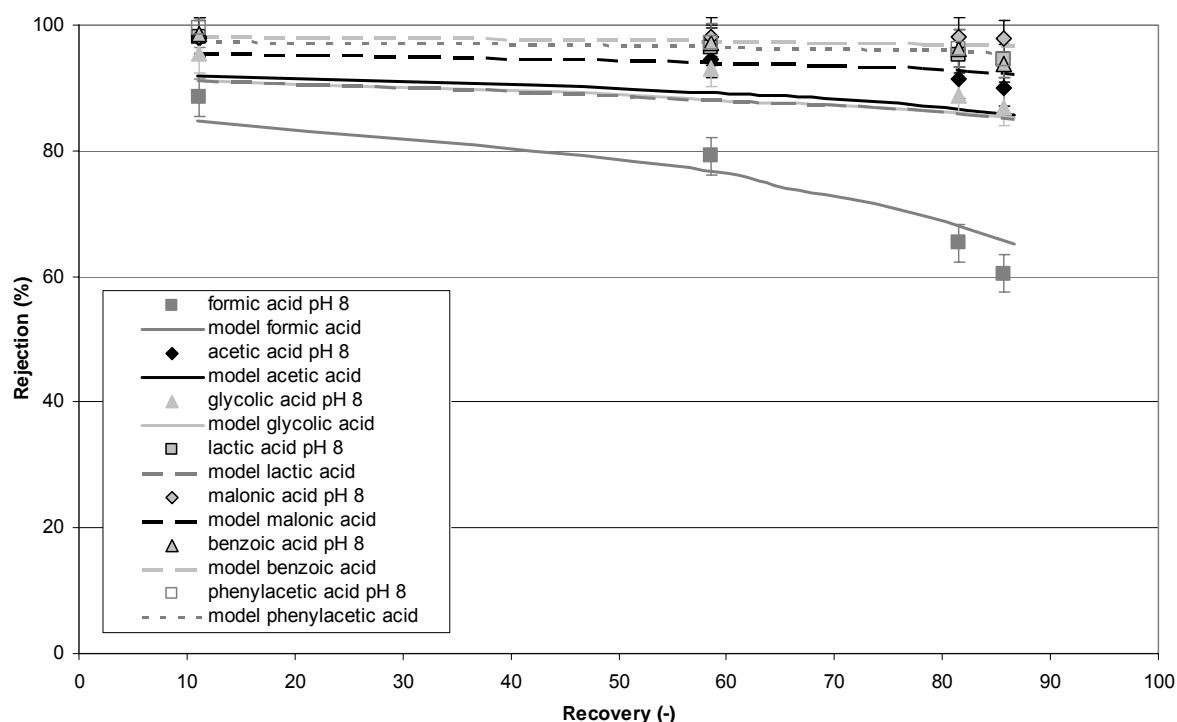


Figure 4.9 – Experimental and modelled rejection values for negatively charged organic acids on pilot scale NF installation at pH 8, as a function of feed water recovery for filtration run at 87% recovery

The experimental and modelled rejection values for the organic acids at pH 8 are shown in Figure 4.9. Again, the model results appear to correspond to the experimentally obtained values quite well.

All experimentally obtained rejection values for the selected neutral organic solutes during the five runs are summarized in Table 4.6 and compared to the modelled rejection values (rejection values for the steric model are given, as well as the rejection values calculated using the fitted value for K).

Total rejection values for pilot plant in tap water (Nieuwegein) (± 3 %)										
		75% recovery			82.5% recovery			90% recovery		
		Experi- mental	Steric model	Fitted model	Experi- mental	Steric model	Fitted model	Experi- mental	Steric model	Fitted model
Pharmaceuticals	phenazon	82	93	80	73	92	78	48	91	75
	aminopyrine	98	99	95	97	99	95	94	99	95
	carbamazepine	84	94	82	82	94	80	64	93	78
	cyclophosphamide	95	97	92	94	97	92	84	96	90
	pentoxifylline	96	100	90	92	100	90	85	100	89
Pesticides	carbendazim	20	80	18	15	78	16	13	76	13
	metamitron	30	97	31	36	97	28	22	96	24
	metribuzin	73	99	56	68	99	54	57	98	50
	atrazin	68	97	56	50	97	53	34	96	49
	pirimicarb	97	99	94	95	99	94	89	99	93
	dimethenamid	98	100	97	97	100	96	95	100	96
Total rejection values for pilot plant in groundwater (Spannenburg) (± 3 %)										
		75% recovery			87% recovery					
		Experimental	Steric model	Fitted model		Experimental	Steric model	Fitted model		
Organic acids	formic acid pH 5	/				4	11	3		
	acetic acid pH 5	/				12	17	13		
Pesticides	metamitron	67	100	79		/				
	diuron	62	100	71		/				

Table 4.6 - Experimental and modelled rejection values for selected neutral organic solutes on pilot scale NF installation, with different feed water types and recovery

Total rejection values for pilot plant in tap water (Nieuwegein) ( $\pm 3\%$ )							
		75% recovery		82.5% recovery		90% recovery	
		Experimental	Model	Experimental	Model	Experimental	Model
<b>Pharmaceuticals</b>	Terbutaline	87	91	86	90	78	88
	Salbutamol	93	94	n.d.	94	86	93
	Pindolol	79	78	75	73	32	62
	<i>positively charged</i> Propanolol	81	80	76	75	55	62
	Atenolol	90	90	85	90	75	84
	Metoprolol	93	92	88	93	78	84
	Sotalol	/		/		88	84
	Clenbuterol	/		/		71	81
<i>negatively charged</i>	Ibuprofen	98	88	97	88	84	85
	Clofibric acid	98	88	97	88	95	96
	Naproxen	97	89	94	89	92	86
	Fenoprofen	97	97	91	97	87	86
	Gemfibrozil	98	96	99	96	98	95
	Ketoprofen	96	96	96	96	95	95
	Diclofenac	98	98	98	98	94	97
	Bezafibrate	99	98	99	98	97	97

Table 4.7 - Experimental and modelled rejection values for selected charged pharmaceuticals on pilot scale NF installation, with Desal HL membrane in tap water at different feed water recoveries

Table 4.7 summarizes the experimental and modelled rejection values of the charged pharmaceuticals during the different filtration runs.

All experimental rejection values in Tables 4.6 and 4.7 are taken as the average of the rejection values obtained using the permeate concentration and the concentrate concentration. As mentioned before, no significant discrepancies between the two values could be observed.

For some charged pharmaceuticals, it is apparent from Table 4.7 that rejection is slightly under- or overpredicted. This is probably due to the dissociation of the organic acids and pharmaceuticals as a function of feed water pH. Not all pharmaceuticals and organic acids are completely dissociated at the feed water pH, thus explaining slight variations in rejection. Also, the use of the membrane zeta-potential as an approximation of the real membrane potential may cause slight discrepancies between the modelled and experimental results.

In general, it can be concluded that the modelled (predicted) rejection values for the pilot (full) scale installation, using the steric model, are not always in agreement with the experimentally obtained rejection values. The steric model results in an underprediction of rejection for the pharmaceuticals and pesticides, because the influence of solute-membrane affinity (attractive Van der Waals interactions) is not taken into account. For organic acids, the use of the steric model leads to an overprediction of the rejection. Apparently, solute-membrane Van der Waals interactions are repulsive for organic acids. This could be expected from the log D-values of the organic acids, which are significantly lower (i.e. the organic solutes are more hydrophilic) than for the pharmaceuticals and pesticides.

The full-scale rejection model, using the fitted value for the partition coefficient  $K$ , however, provides predicted full-scale rejection values for uncharged organic solutes which are in good correspondence with experimentally obtained rejection values.

For the charged organic solutes, incorporation of the calculated “charge concentration polarisation” factor yields satisfactory results.

The proposed full-scale model thus proves to be a valuable tool in the design of full-scale plants for removal of organic micropollutants.

## **5. Conclusions**

A model to predict rejection values of organic micropollutants in full-scale nanofiltration/reverse osmosis membrane plants has been presented.

A convection-diffusion transport model was used to describe uncharged organic solute transport through the membranes. For charged organic solutes, the influence of charge interaction was added to the model as an extra “charge” concentration polarisation. Also the influence of the hydrodynamic concentration polarisation was added to the model.

Modelled rejection values were compared to experimentally obtained rejection values for a mixture of 19 pharmaceuticals, 8 pesticides and 7 organic acids on a pilot plant operated during five different runs at different feed water recoveries (ranging from 75% to 90%) with different types of feed water, using two different membranes.

Even though the partition coefficient in the convection-diffusion model could be calculated theoretically, a more simple approach was followed here. The partition



coefficient was first calculated theoretically, and was then also determined by fitting the model to experimentally obtained rejection values on single membrane elements. Both values for the partition coefficient were compared to each other. For organic acids, the steric partition coefficient was higher than the fitted partition coefficient, indicating that rejection was underestimated, because repulsive solute-membrane Van der Waals interactions were not taken into account in the steric model. For the pharmaceuticals and pesticides, the opposite was true: rejection was overestimated by the steric model, because solute-membrane attractive Van der Waals interactions were not taken into account.

With the fitted value for the partition coefficient, the rejection of the neutral pesticides, organic acids and pharmaceuticals on the pilot plant at higher recovery could be modelled quite accurately.

For the charged pharmaceuticals and organic acids, rejection values were predicted, based on the calculated rejection values of the uncharged pharmaceuticals, organic acids and pesticides and using the “charge concentration polarisation” concept.

The predicted rejection values for the charged solutes also appeared to correspond to the experimentally obtained rejection values quite well.

## References

- [1] C. Bellona and J.E. Drewes, Viability of a low-pressure nanofilter in treating recycled water for water reuse applications: A pilot-scale study, *Water Research*, 41 (17) (2007) 3948.
- [2] J.S. Taylor, J.A.M.H. Hofman, S.J. Duranceau, J.C. Kruithof and J.C. Schippers, Simplified modelling of diffusion-controlled membrane systems, *Journal Water Supply: Research & Technology - Aqua*, 43(5) (1994) 238.
- [3] I. Sutzkover, D. Hasson and R. Semiat, Simple technique for measuring the concentration polarisation level in a reverse osmosis system, *Desalination*, 131 (2000) 117.
- [4] G. Schock and A. Miquel, Mass transfer and pressure loss in spiral wound modules, *Desalination*, 64 (1987) 339.
- [5] W. Hayduk and H. Laurie, Prediction of diffusion-coefficient for non-electrolytes in dilute aqueous solutions, *AIChE Journal*, 20 (1974) 611.
- [6] F. Sacher, F.T. Lange, H.-J. Brauch and I. Blankenhorn. Pharmaceuticals in groundwaters: analytical methods and results of a monitoring program in Baden-Württemberg, Germany, *Journal of Chromatography A*, 938 (2001) 199.
- [7] F. van Hoof, P. van Wiele, A. Bruchet, I. Schmitz, I. Bobeldiji, F. Sacher, F. Ventura, I. Marti, M.H. Marecos Do Monte and M. Sa Da Costa, Multiresidue determination of pesticides in drinking and related water by gas chromatography/mass spectrometry after solid-phase extraction: Interlaboratory study, *Journal of AOAC International*, 84 (5) (2001) 1420.

# **Chapter 5: Influence of membrane fouling**

Parts of this chapter were based on:

A.R.D. Verliefde, E.R. Cornelissen, S.G.J. Heijman, G.L. Amy, I. Petrinic, T. Luxbacher, B. Van der Bruggen, and J.C. van Dijk, The influence of colloidal and organic fouling on the removal of trace organic pollutants with nanofiltration, to be submitted to Journal of Membrane Science.

## 1. Introduction

In full-scale applications of NF/RO membranes, deterioration of membrane performance due to membrane fouling, is still a major challenge. Membrane fouling can be: i) microbial in origin (biofouling); ii) a consequence of the accumulation of natural organic matter (NOM) on the membrane surface (organic fouling); iii) due to the accumulation of small colloidal particles in the feed water on the membrane surface (colloidal/particulate fouling); or iv) the result of inorganic depositions on the membrane surface when the solubility product of sparingly soluble salts is exceeded (scaling). Numerous studies on membrane fouling have been conducted [1-18], since the deposition of foulant material on the membrane surface can lead to serious operational problems, such as flux decline or an increase in pressure drop over the membrane installation.

Deposition of a foulant layer on the NF/RO membrane surface also alters the membrane surface properties [19]. In the previous chapters, it was shown that these membrane surface properties influence the solute-membrane interactions (such as steric hindrance, hydrophobic interactions and charge interactions) that determine the rejection of organic micropollutants.

Therefore, as a result of membrane fouling, the solute-membrane interactions that determine organic micropollutant rejection will also be affected, and thus the rejection of the organic micropollutants may change. Some studies have investigated the influence of NF/RO membrane fouling by secondary waste water treatment effluent organic matter or landfill leachate organic matter on the rejection of organic micropollutants [19-21]. Other studies have used artificial water types, containing only humic acids or model colloidal particles [22,23]. Conclusions from these studies are

not always useful for the operation of NF/RO membranes for organic micropollutant removal in natural surface water, because of the heterogeneous character of both natural particles and organic matter. Therefore, this chapter investigates the effect of membrane fouling on the rejection of organic micropollutants in surface water applications.

An extensive pretreatment is normally used to remove foulant material in order to prevent severe fouling of membrane elements in full-scale NF/RO plants. This study will address both the influence of feed water pretreatment on membrane fouling, as well as the effects of fouling on rejection of organic micropollutants, by studying three different surface water types: surface water, surface water pretreated with a fluidized anionic ion exchange resin (FIX) (to remove negatively charged natural organic matter components) and surface water pretreated with ultrafiltration (UF) (to removed colloidal particles). In this way, it will be concluded whether pretreatment of surface water has an effect on membrane performance.

It is expected that water pretreated with a fluidized anionic ion exchange would contain mostly colloidal particles, since the dominant fraction of natural organic matter (NOM acids) is expected to be removed by the ion exchange resin, but the colloidal particles would still pass the resin column, since it is operated in a fluidized mode [24]. The literature [23] mentions a decreased rejection of organic micropollutants due to colloidal deposits on the membrane surface.

Water pretreated with ultrafiltration would, most likely, only contain NOM molecules and almost no colloidal particles (in some cases, a small fraction of the particulate NOM may also be removed). Different studies have reported different effects of NOM-deposits on the membrane surface, influencing trace organics rejection.

Increased concentrations have been reported, due to an enhanced steric hindrance by the NOM cake layer formed on the membrane surface [22]. However, lower rejections of several pharmaceuticals after NOM fouling have also been reported [19,20].

The untreated surface water contains both colloidal particles and NOM-molecules and it is difficult to predict the effect of the synergy between the two on membrane fouling and rejection.

Most previous studies on the influence of membrane fouling on rejection of trace organics have only focused on the rejection of neutral and negatively charged trace organic solutes [19-23,25,26]. This study will also investigate the rejection of selected positively charged organic solutes. It was shown in Chapter 3 that rejection of positively charged organic solutes with negatively charged membranes can be substantially lower than the rejections of neutral and negatively charged solutes and the Donnan exclusion mechanism does not play a role in rejection of charged organic solutes. Thus, it is interesting to investigate whether rejection values with fouled membranes differ significantly from rejection values using virgin (clean) membranes. This study will be mainly conducted on a small, laboratory scale set-up with 140cm<sup>2</sup>, flat sheet membrane specimens. These small-scale filtration units are not always representative for practical applications. At the end of this chapter, some discussion will be added on the consequences of using this small-scale set-up and a comparison will be made with fouling on 4-inch spiral wound membrane elements.

## **2. Materials & methods**

## 2.1. Equipment and filtration protocol

A schematic diagram of the small lab-scale membrane system used in the membrane filtration experiments is shown in Figure 5.1.

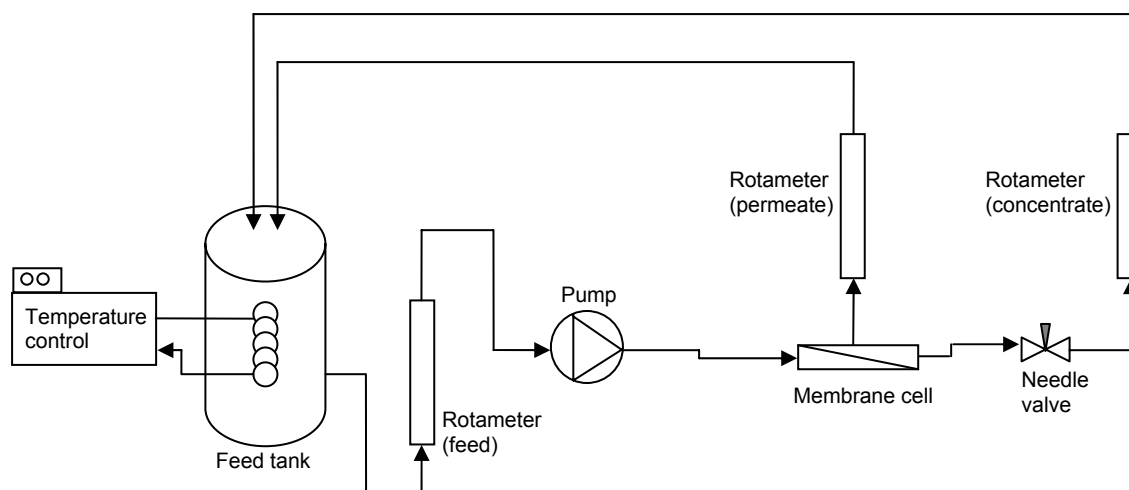


Figure 5.1 – Nanofiltration set-up for rejection experiments with selected membranes

The feed solution is delivered to a flat sheet cross-flow membrane cell (Sepa CF II, GE Osmonics, Fairfield CT, USA (Figure 5.2)) with an active membrane area of 140 cm<sup>2</sup>, by a gear pump (Verder Liquiflo). The feed water is fed from an 80 L stainless steel vessel, cooled by an immersed stainless-steel coil fed from a cooling system (Tamson TLC 10B). Permeate, concentrate and feed flow are monitored by rotameters (Heinrichs messgeräte). Applied transmembrane pressure is regulated using a needle valve in the concentrate stream, with transmembrane pressure measured with a precision manometer (Endress & Hauser, Cerabar). All test unit parts in contact with the solution are made of stainless steel to minimize adsorption of the organic compounds used.



Figure 5.2 – Sepa CF II cross-flow membrane cell for fouling/rejection experiments

Membrane filtration experiments were carried out at a constant cross-flow velocity of 0.2 m/s (corresponding to a feed flow of  $\pm 60$  l/h) and at a constant feed pressure of 15 bar for the fouling runs, and 5 bar for the rejection experiments. The cross-flow velocity of 0.2 m/s corresponds to a typical value used in NF/RO spiral wound membrane elements in full-scale plants. Feed water temperature was set to  $20 \pm 1^\circ\text{C}$ . All experiments were carried out in recycle mode with a single batch of water, with both permeate and concentrate recycled back into the feed reservoir.

In order to make a relative comparison between the rejection experiments with virgin and fouled membranes, the filtration protocol schematically depicted in Figure 5.3 is followed.



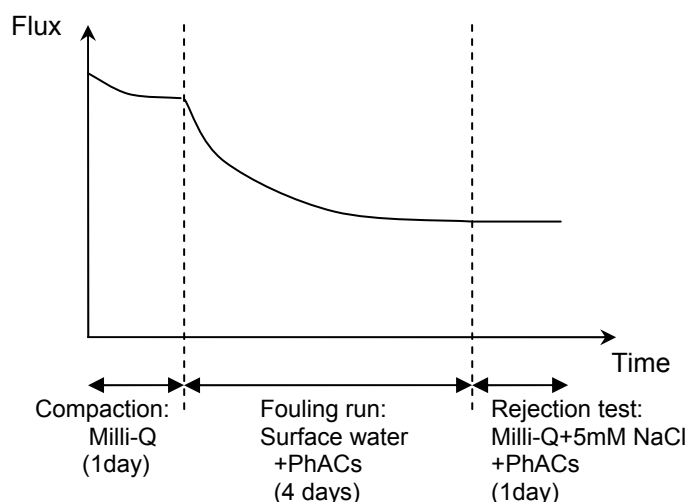


Figure 5.3 – Filtration protocol for fouling/rejection experiments with selected membranes

In a first step, before the start of the fouling experiments, each membrane is flushed with Milli-Q water for 24h at a feed pressure of 15 bar, to remove remaining preservatives and to ensure compaction of the membranes. In the second step, the membranes are fouled with one of the three water matrices for a period of 4 days at a fixed feed pressure of 15 bar. The decline in permeate flux is monitored during this 4 day period, in order to compare the extent of membrane fouling between the different experiments. In the third and final step a rejection test with pharmaceuticals is carried out. Milli-Q water with a background electrolyte (5 mM of NaCl) is added to the feed tank, and the pharmaceuticals are also added. After 24 hours of permeation at 5 bar (with permeate and concentrate recycled to the feed tank), the rejection of the pharmaceuticals is determined. The rejection step is limited in time, to prevent alteration of the fouling layer on the membrane by the Milli-Q, but has to be long enough to allow for equilibration of flux and rejection. The rejection experiments are carried out with Milli-Q, in order to be able to compare the influence of the different fouling types on the membrane surface, without having to incorporate the effect of the different water matrices.

As was shown before in Paragraph 4.1 of Chapter 2, adsorption of solutes onto the membrane surface, and sorption into the inner membrane structure, may influence measured rejection values, an accurate evaluation of the rejection of a given solute is not possible until saturation of the membrane with the solute of interest is accomplished [27]. In the same paragraph, it was shown that an equilibration period of 4 days should be adequate to accomplish saturation and ensure that steady state rejection values are obtained. Therefore, the pharmaceuticals are already added during the fouling stage (but no rejections are measured during this stage) to ensure that the final rejection values measured are not biased by an incomplete adsorption/saturation. For very hydrophobic pharmaceuticals, adsorption onto NOM molecules may occur, but it is expected that this will not prevent saturation of the membrane surface with the pharmaceuticals.

## 2.2. Membranes and characterisation

The membranes used in this study were the same commercially available nanofiltration membranes used in the previous chapters: Trisep TS80 TSF (Trisep Corp., Goleta CA, USA) and Desal HL (GE Osmonics, Fairfield CT, USA). Both membranes are thin film composite membranes with a cross-linked aromatic polyamide top layer. Before use, all membrane specimens were rinsed with tap water for two hours to remove preservatives present in the membrane. Afterwards, the membranes were characterized for pure water permeability with Milli-Q water and for  $\text{MgSO}_4$  rejection with a 500 ppm  $\text{MgSO}_4$  solution in Milli-Q water. Virgin membrane properties are summarized in Table 2.1 (Chapter 2).

The molecular weight cut-off (MWCO) values were provided by the membrane manufacturers. Two membranes with different membrane properties were chosen, in order to assess the influence of membrane properties on rejection. Flat sheet membrane specimens with an active membrane area of 140 cm<sup>2</sup> were used for the rejection experiments.

Membrane zeta-potentials were determined in a background solution containing 10 mM KCl using commercially available streaming potential/current equipment (SurPASS, Anton Paar, Graz, Austria). Membrane hydrophobicity was characterised by sessile drop contact angle measurements with Milli-Q water, using commercial contact angle measuring equipment and drop shape analysis software (Krüss, Hamburg, Germany). In order to minimise any interference of surface morphology on the contact angle, at least 15 different measurements at 3 different positions on each membrane sample were performed and the average of the measurements was taken. Membrane samples were dried during 24h in a dessicator before measuring contact angles.

Scanning electron microscopy (SEM, JSM 5600LV, JEOL Ltd., Tokyo, Japan) was used to examine the morphology of the different membrane surfaces before and after fouling.

Elemental composition of the membrane surface was determined using X-ray photoelectron spectroscopy (XPS) measurements (Quantera XPS, Physical Electronics, Chanhassen, MN, USA). XPS was chosen as characterisation method since XPS measures only a few nm into the sample and is thus able of determining the actual chemical composition of the membrane surface, whereas methods such as FTIR measure over the whole membrane thickness, making characterisation of only the membrane surface or only the fouling layer more difficult.

Adenosine triphosphate (ATP) measurements were carried out to assess biological activity on the membrane surface. Fouled membrane samples were placed in a fixed volume of Milli-Q and sonicated to remove the fouling layer from the membrane surface. After sonication, the ATP levels in the Milli-Q phase were measured. The method to determine ATP levels has already been described by Magic-Knezev and van der Kooij [28].

### 2.3. Pharmaceuticals & analysis

The same pharmaceuticals were spiked as in Chapters 3 and 4. The pharmaceuticals were mainly selected for their different physico-chemical properties. Table 3.2 summarizes the physico-chemical properties of the selected pharmaceutically active compounds and more info on their analysis can be found in Chapter 3, Paragraph 2.3.

All pharmaceuticals were spiked in concentrations of 2 µg/l, in order to be able to accurately measure 99% rejection (which corresponds to a permeate concentration of 20 ng/l, well above the LOQ). Samples of feed and permeate streams of the NF installations were analyzed for pharmaceuticals in order to obtain rejection values according to the following equation:

$$R_i = 1 - (c_{p,i} / c_{f,i}) \quad (5.1)$$

where  $i$  is the solute of interest, and  $R_i$ ,  $c_{p,i}$  and  $c_{f,i}$  are, respectively, the rejection, the permeate concentration and the feed concentration of the solute. Duplicate samples of all streams were taken to minimize statistical variance of the results. All samples were shipped to the laboratory for analysis within 24 h. Blank samples were sent along as control.

## 2.4. Feed water pretreatment and characterisation

The fouling experiments were carried out with surface water from the Lek river in Nieuwegein, the Netherlands. The water was used: i) untreated (direct nanofiltration of surface water); ii) after a fluidized anionic ion exchange pretreatment and iii) after an ultrafiltration pretreatment. The NF experiments were carried out in recirculation mode, with batches of 80L of the different feed water types.

A strong base macroporous Type I anion exchange resin (Purolite A860S, The Purolite Company, Bala Cynwyd (PA), USA) was used in the fluidized anionic ion exchange column. The resin beads are composed of positively charged quaternary ammonium on a macroporous polyacrylic support, crosslinked with divinylbenzene. The positive groups are countered by chloride ions that provide the anionic exchange capacity. The resin was regenerated using a 10% concentrated NaCl-solution. The column was fed with untreated Lek river water. A short empty bed contact time (EBCT) of about 3 minutes was used. The column was operated in a fluidized mode: an upward feed water velocity of 15 m/h was applied, which is higher than the settling speed of suspended solids and colloidal particles, but lower than the settling speed of the ion exchange resin [24]. As a consequence, suspended solids and particles can move through the column freely, while the ion exchange resin remains in the column. Negatively charged organic matter from the feed water is captured by the ion exchange resin and exchanged for chloride ions in the feed water.

For the ultrafiltration pretreatment, an X-flow UFC-M5 ultrafiltration module with a membrane surface of 125 cm<sup>2</sup> was operated at a constant flux of 120 l/(m<sup>2</sup>.h). The membrane consists of a polyethersulfone and polyvinylpyrrolidone mixture and has a molecular weight cut-off of approximately 100 kDa (~ 0.03 µm). The membrane was

backwashed every 15 minutes to prevent too high of an increase of transmembrane pressure. The UF pretreatment was carried out using untreated Lek river water. Feed water characterisation was performed using different techniques: LC-OCD (Liquid Chromatography – Organic Carbon Detection) measurements were applied to study the composition of the NOM in the different surface waters. Pasteurised water samples are filtered through a 0.45 mm filter to separate the total organic carbon (TOC) into particulate organic carbon (POC) and dissolved organic carbon (DOC). The DOC is then separated into different groups by chromatography and analysed with organic carbon detection, based on a *Gräntzel* gravity-flow thin-film reactor [29]. Furthermore, SUVA (specific UV-A) of the total DOC, which provides insight into the aromaticity of the DOC, was calculated from the DOC concentration and the measured UV-A absorbance at 254nm. LC-OCD measurements were carried out at DOC Labor (Karlsruhe, Germany).

The particle size distributions and the zeta potentials of the colloids and particles in the untreated Lek water and the FIX pretreated water were determined using Mastersizer 2000 equipment (Malvern Instruments, Worcestershire, UK). Zetasizer equipment (Malvern Instruments) was used for the smaller particles in the UF pretreated water.

The concentrations of all cations in the different feed waters were determined using inductively coupled plasma - mass spectrometry (ICP-MS). Sulphate, nitrate and chloride anions were measured using ion chromatography.

### **3. Results and discussion**

#### **3.1. Effect of pretreatment on surface water characteristics**

The characteristics of the different treated and untreated water types are given in Table 5.1.

	Lek water	Lek + FIX	Lek + UF
pH (-)	7.7 – 8	7.9	8.2
Conductivity ( $\mu\text{S}/\text{cm}$ )	645	665	636
Turbidity (NFU)	30	29	0.07
TOC (mg/l)	3.4	1.1	3.2
DOC (mg/l)	3.1	1.0	3.1
POC (mg/l)	0.3	0.1	0.1
SUVA ( $\text{l}/\text{mg}\cdot\text{m}$ )	3.23	1.82	3.03
Na (mg/l)	41	65	43
Mg (mg/l)	10	10	11
Al (mg/l)	0.05	0.01	0.03
Si (mg/l)	2.8	1.6	3.0
K (mg/l)	4.1	4.2	4.3
Ca (mg/l)	66	64	70
Fe (mg/l)	0.6	0.4	0.3
Sr (mg/l)	0.4	0.4	0.5
Ba (mg/l)	0.06	0.07	0.06
$\text{Cl}^-$ (mg/l)	50	101	47
$\text{SO}_4^{2-}$ (mg/l)	30	2.2	28

Table 5.1 – Water quality parameters of selected feed waters for fouling and rejection experiments

The untreated surface water is moderate in natural organic matter content (expressed as TOC) and high in turbidity. It is apparent that the different pretreatment steps significantly alter the composition of the untreated water. The ultrafiltration step removes 95% of the turbidity (in NTU), while the organic carbon content remains relatively constant (only a small decrease is observed, and the decrease is mainly due to a decrease in particulate organic matter (POC)). The largest part of the suspended solids and colloids are thus removed in the UF step, while most of the dissolved NOM is not.

The fluidized anionic ion exchange (FIX) removes about 70% of the organic carbon (NOM) from the untreated Lek river water, while the total turbidity remains almost constant. The FIX thus removes most of the negatively charged NOM, but suspended solids and colloids (and also the neutral NOM-molecules) can freely pass the column. The operation of the FIX is based on the exchange of negatively charged molecules in the feed water for chloride ions on the ion exchange resin. The removal of negatively charged NOM is limited by the competitive removal of negatively charged inorganic ions. Especially sulphate ( $\text{SO}_4^{2-}$ ) ions are also removed to a large extent. Table 5.1 shows a significant increase in  $\text{Cl}^-$  after the ion exchange, indicating actual ion exchange. However, also the concentration of  $\text{Na}^+$  is increasing after FIX pretreatment. This is probably due to the incomplete washing of the resin after regeneration. The increase in  $\text{Na}^+$  is about 24 mg/l, which means about 26 mg/l of the increase in  $\text{Cl}^-$  concentration is originating from the washing of the resin. The rest of the decrease in  $\text{Cl}^-$  concentration originates from the removal of NOM and  $\text{SO}_4^{2-}$ . Table 5.1 shows a decrease in SUVA of the Lek water after FIX pretreatment, which reflects removal of humic and fulvic acids.

Since it is expected that the colloidal particles and the natural organic matter in the feed waters will contribute to membrane fouling, the particle size distribution and the organic composition of the different water types were investigated. The particle size distributions and LC/OCD diagrams are shown in more detail in Table 5.2 and Figure 5.4, respectively.

Lek + UF	/	< 0.2	/	-7.7	0.07
Particle size distribution					
	$d_{0.1} (\mu\text{m})$	$d_{0.5} (\mu\text{m})$	$d_{0.9} (\mu\text{m})$	$\zeta$ -potential (mV)	Turbidity (NTU)
Lek water	2.9	14.5	49.3	-13.5	30
Lek + FIX	4.2	13.9	36.4	-13.3	29



Table 5.2 – Particle size distribution and zeta-potential of the particles in the different feed waters

The Lek water is a surface water with moderate TOC, containing low amounts of biogenic organic matter (biopolymers, neutrals and acids). The humics are of pedogenic origin, meaning they are leached into the water from the soil. The total organic carbon content of the UF permeate is almost equal to the untreated Lek water, both in concentration but also in composition. A slightly lower concentration of biopolymers is present after UF treatment, probably due to the adsorption of polysaccharides on the UF membrane surface or rejection by the membrane (polysaccharides are often mentioned as important foulants in UF applications).

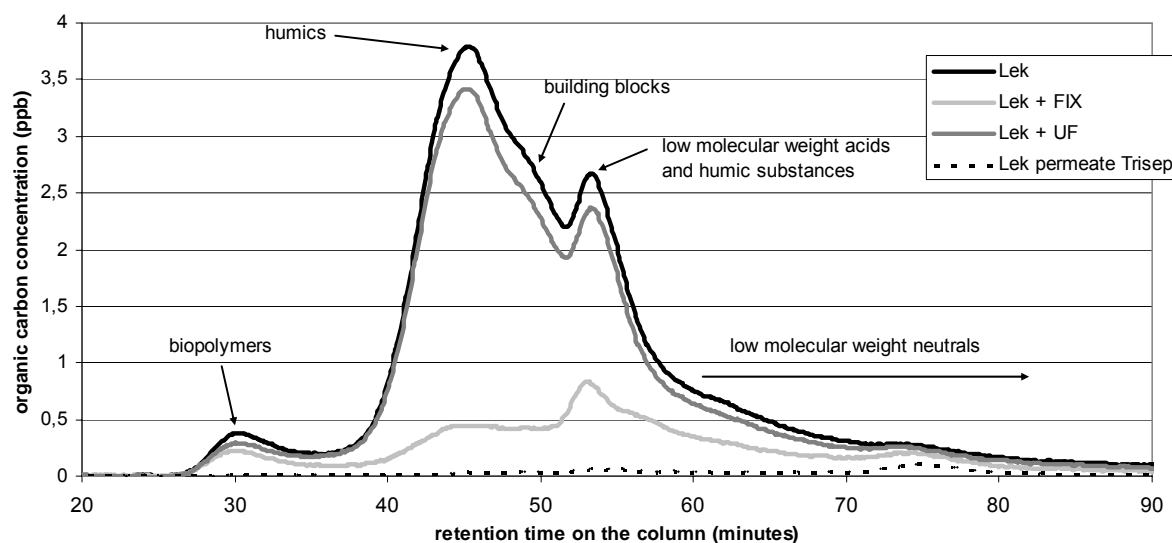


Figure 5.4 – LC/OCD diagramma for the different feed waters for the fouling experiments

Compared to the untreated Lek water, a strong decrease in organic carbon content can be seen after FIX treatment. The more polar humic substances and building blocks show the greatest reduction in concentration compared to the Lek water.

Uncharged biopolymers and neutrals are less efficiently removed, due to the absence of an ion exchange mechanism.

From the particle size distribution of the untreated Lek water in Table 5.2, it can be seen that the mean size of the particles is around 14  $\mu\text{m}$ . This is comparable to the distribution of the particles in the effluent of the FIX column. It can be concluded that most colloidal particles are not removed during FIX pretreatment, since the turbidities of the Lek water and the effluent of the FIX are also comparable. Another conclusion is that most particles are not organic in origin, since the TOC of the effluent of the FIX is 70% lower than for the untreated surface water. The only effect of the FIX on the particle size distribution is a narrowing of the distribution: the particles are more concentrated in the middle region. The difference is very small, however.

It is also apparent from Table 5.2 that the particle distribution of the UF permeate is altered: the average particle diameter is smaller than 0.2  $\mu\text{m}$ . The pore size of the UF membrane is around 0.03  $\mu\text{m}$ , so it can be expected that no larger particles will be present in the UF effluent. Also the total concentration of particles is significantly lower in the UF permeate, compared to the untreated surface water. (which is illustrated by the low turbidity and the decrease in particulate organic matter (POC) compared to the other two water types, as seen in Table 5.1).

Table 5.2 also shows the zeta-potential of the colloidal particles. Even though the colloidal particles are negatively charged, they are not removed by the anionic ion exchange resin. This is probably due to size exclusion effects: the 14  $\mu\text{m}$  particles can not diffuse into the porous resin beads and do not have the same high surface area available for adsorption as the NOM molecules.

It can be concluded that the UF membrane removes most of the particles from the Lek water (relatively large particles are completely removed), but does not remove

the dissolved natural organic matter, thus, the UF permeate mainly consists of dissolved organic matter. The FIX pretreatment of the Lek water, on the other hand, removes a large percentage of the dissolved natural organic matter, but does not remove the (in)organic colloids and particles. Therefore, the FIX effluent consists mainly of colloidal particles. The untreated Lek water contains a mixture of dissolved natural organic matter and particles.

### 3.2. Effect of fouling on membrane performance

#### 3.2.1. Effect of fouling on permeate flux

The observed flux decline at constant pressure as a function of time, which reflects fouling, is shown for the different water types and the different membranes in Figure 5.5. The flux values during the 24-hour compaction run prior to filtration are not shown.

$$norm.fluxdecline(t) = \frac{\frac{J(t)}{TMP(t)}}{\frac{J_0}{TMP_0}} = e^{U \left( \frac{1}{T(t)} - \frac{1}{T_0} \right)} \cdot \frac{A_m \cdot \left( \frac{P_f(t) + P_c(t)}{2} - P_p(t) \right)}{Q_{p,0}} \cdot \frac{Q_p(t)}{A_m \cdot \left( \frac{P_{f,0} + P_{c,0}}{2} - P_{p,0} \right)} \quad (5.2)$$

where:

- $J(t)$ ,  $J_0$ : permeate fluxes at time  $t$  and at the start of the experiment, respectively [m/(s.bar)]
- $TMP(t)$ ,  $TMP_0$ : applied transmembrane pressure at time  $t$  and at the start of the experiment, respectively [bar]
- $U$ : membrane dependent temperature correction factor for the flux [1/K]

- $T(t)$ ,  $T_0$ : temperature at time  $t$  and at the start of the experiment, respectively [K]
- $Q_p(t)$ ,  $Q_{p,0}$ : permeate flow at time  $t$  and at the start of the experiment, respectively [ $\text{m}^3/\text{s}$ ]
- $P_f(t)$ ,  $P_c(t)$ ,  $P_p(t)$ ,  $P_{f,0}$ ,  $P_{c,0}$ ,  $P_{p,0}$ : feed, concentrate and permeate pressure at time  $t$  and at the start of the experiment, respectively [bar]
- $A_m$ : active membrane area [ $\text{m}^2$ ]

No significant flux decline can be observed for both membranes when they are filtrated with Milli-Q water. This is due to the 24-hour compaction period, prior to the 4-day filtration run.

It can be assumed that the flux declines observed in this study are mainly due to the deposition of natural organic matter and colloidal particles on the membrane surface. Considering the feed water composition and the low feed water recovery used in the filtration experiments, no scaling is expected to occur. Also biological fouling is not expected to have played a role in the observed flux declines, since ATP measurements showed negligible biological activity on all membranes (less than 400 pg ATP/ $\text{cm}^2$ , which should not result in biofouling [30]) and the experiments were only carried out for a short period of 4 days (too short for a biofilm to develop).

For the different surface water types, a substantial flux decline is observed during the 4-day fouling run. This flux decline is due to the deposition of foulant material on the membrane surface (and in the membrane pores).

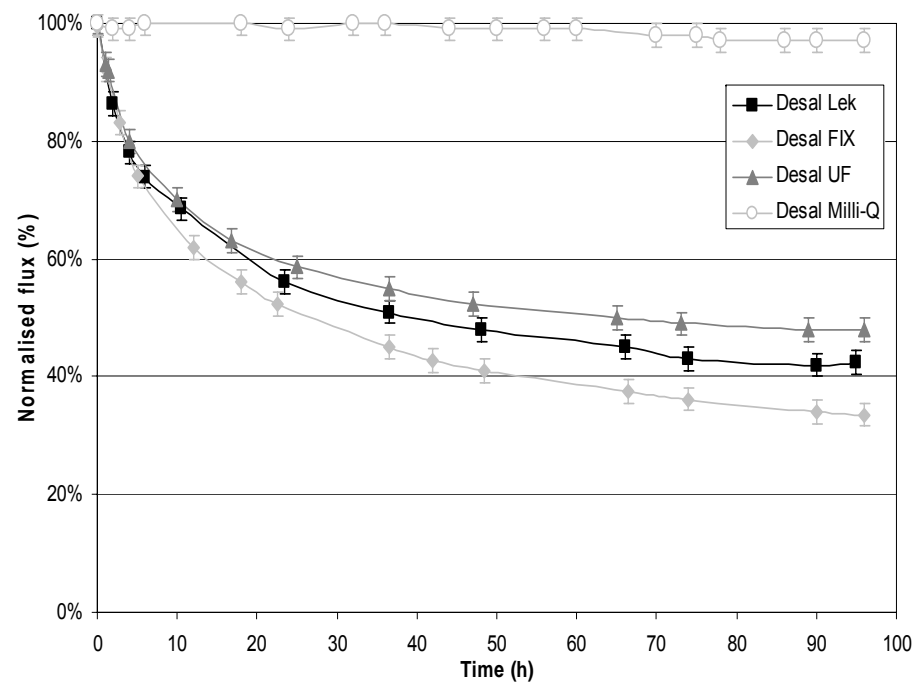
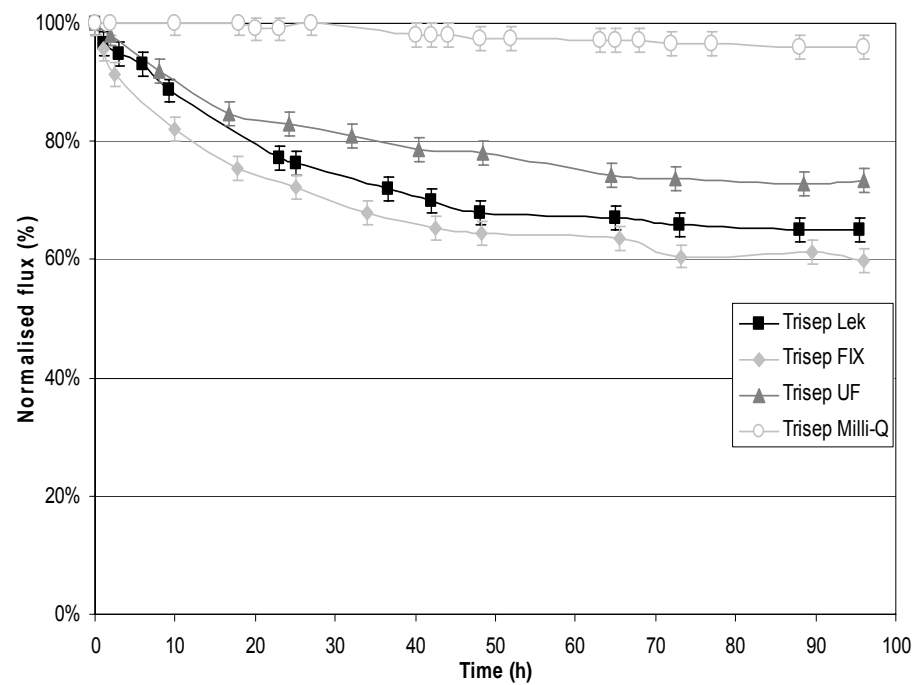


Figure 5.5 – Normalised flux for different membranes with different feed water types as a function of time

For the Desal HL membrane, the largest flux decline was observed for the Lek river water, pretreated with the fluidized anionic ion exchange (Lek FIX). The flux decreases steeply at the start of the filtration run, and reaches an equilibrium value at a normalized flux of around 37% after about 65 hours of filtration. The flux decline observed with the UF pretreated Lek water (Lek UF) is the lowest for the Desal HL. The flux decrease is more gradually, but still after 4 days of filtration, the flux also decreased with more than 50%. The flux decline curve for the untreated river water (Lek) is located in between the two other curves. This is not in agreement with observations made by Li and Elimelech [2] and Lee et al. [5], who stated that the combination of colloidal and natural organic matter fouling (as is expected with the untreated Lek water) leads to a more substantial flux decline.

The explanation for this is the removal of negatively charged NOM molecules by the FIX column: in untreated Lek water, the majority of the NOM molecules is negatively charged, and there is repulsion of this NOM by the negatively charged membrane. Moreover, negatively charged NOM will not adsorb onto the negatively charged colloidal particles and will not form stabilized colloid-NOM complexes.

In the FIX effluent, most of the negatively charged NOM is removed, and the remaining NOM is more hydrophobic and will adsorb more readily onto the surface of the colloids and the membrane. This results in the formation of a more stable cake-layer of colloids, coated with NOM, on the membrane surface.

The same trend is observed for the Trisep TS80: the flux decline with the FIX pretreated Lek water is the most severe (almost 50%), and the flux declines for the Lek UF and the Lek water are lower. Also here, no flux decline with Milli-Q is observed.

It is also clearly noticeable that the flux declines on the Trisep TS80 membrane are lower than for the Desal HL membrane. According to the membrane manufacturer, the Trisep TS80 is especially engineered for its low fouling characteristics. Moreover, it has a higher negative surface charge than the Desal HL, making it less susceptible to adsorption of negatively charged colloids or negatively charged natural organic matter molecules on the membrane surface.

### 3.2.2. Effect of fouling on salt rejection

The influence of membrane fouling on the evolution of the salt rejection (expressed as conductivity) is shown in Figure 5.6 for both membranes.

The permeate conductivity at the start appears to be the lowest for the FIX effluent. This is probably caused by the high chloride concentration of the water (from the ion exchange mechanism) and the relatively low chloride rejection of both membranes. For both membranes it also appears that the rejection of salts decreases with increasing fouling for the FIX effluent. A decrease of salt rejection has been observed before [23,31-33], where it was explained by the presence of a layer of colloids on the membrane surface, that can lead to a hindered back-diffusion of salts away from the membrane surface, and thus an increased concentration of salts at the membrane surface (referred to as cake-enhanced concentration polarisation). The decrease in rejection follows the same trends as the flux decline.

For the UF permeate, rejection of salts appears to increase slightly for both membranes. This could be explained by the formation of some sort of “active layer” on the membrane surface by the foulant material. This phenomenon has been described in the literature for artificial water types containing NOM [22].

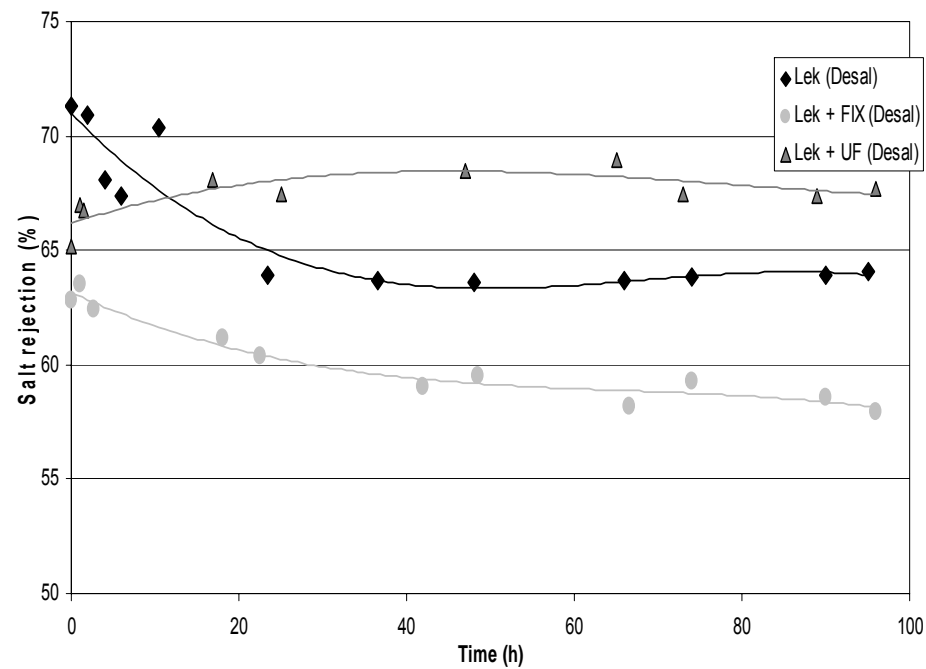
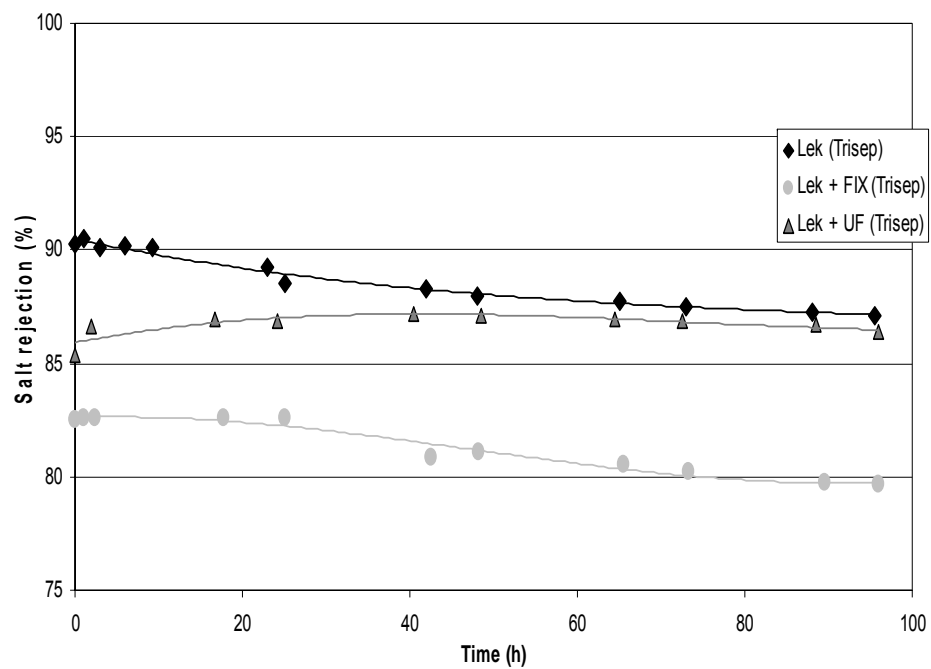


Figure 5.6 – Rejection of salts (expressed as  $1 - \frac{cond_{perm}}{cond_{feed}}$ ) for different membranes with different feed water types as a function of time



The larger increase in salt rejection for the Desal HL membrane is probably due to the larger pore size of the Desal HL: pores of the Desal HL membrane may become blocked with small NOM-molecules (this occurs to a lesser extent, for the Trisep TS80 membrane with the smaller pores), leaving these pores unavailable for solute transport, resulting in increased rejection.

For untreated Lek water, a combination of both effects seems to determine salt rejection. At the start, rejection is high due to the formation of an active layer on the membrane surface, but it gradually declines due to the build-up of a cake-enhanced concentration polarisation as the membrane becomes fouled with the combination of NOM and colloids.

### 3.3. Characteristics of the fouled membranes

#### 3.3.1. XPS measurements

The elemental compositions of the top layers (1-10 nm) of all membranes are given in Table 5.3. The clean Desal HL and Trisep TS80 membranes are quite different in composition: the Trisep TS80 membrane contains more carbon in the top layer, explaining the slightly higher contact angle (the Trisep TS80 membrane is more hydrophobic). The nitrogen (N) content of both membranes is quite comparable, but the clean Desal HL membrane contains considerably more oxygen (O). Relating nitrogen (N) and oxygen (O) concentrations to surface charge is not possible, since not all nitrogen and oxygen are present as free amine groups or carboxylic acid groups, but can be bound as amide or carbonyl groups.

	Relative composition (%)				
	C	N	O	S	Cl
Trisep clean	70.9	9.1	18.4	0.9	0.8
Trisep Lek	49.1	5.6	44.7	2.0	0.2
Trisep FIX	55.4	5.6	37.4	1.4	0.2
Trisep UF	65.6	5.4	28.7	0.2	0.2
Desal clean	62.8	8.8	26.2	2.0	0.2
Desal Lek	43.9	5.3	50.0	0.5	0.3
Desal FIX	54.7	7.6	37.0	0.5	0.3
Desal UF	65.4	6.7	27.5	0.3	0.05

Table 5.3 – Composition of the top layer of the clean and fouled membranes, as determined by XPS

After fouling, the composition of the top layers of both membranes changes significantly: the composition of the top layer of the membrane becomes shielded by the foulant layer. It is apparent from Table 5.3 that this foulant layer is quite consistent: the compositions of the different fouling layers on both membranes are almost identical (e.g., when comparing Trisep FIX with Desal FIX and Trisep UF with Desal UF). For both membranes, the UF fouled membranes are the closest in composition to the clean membranes, maybe indicating that fouling is the least severe for the UF fouled membranes. This would also explain the lower flux declines for the UF fouled membranes.

### 3.3.2. Zeta-potential data

Figure 5.7 shows the zeta-potential data as determined from streaming current measurements using commercially available equipment (Anton Paar, Graz, Austria). The clean Trisep TS80 membrane has a significantly higher negative surface charge than the clean Desal HL membrane.

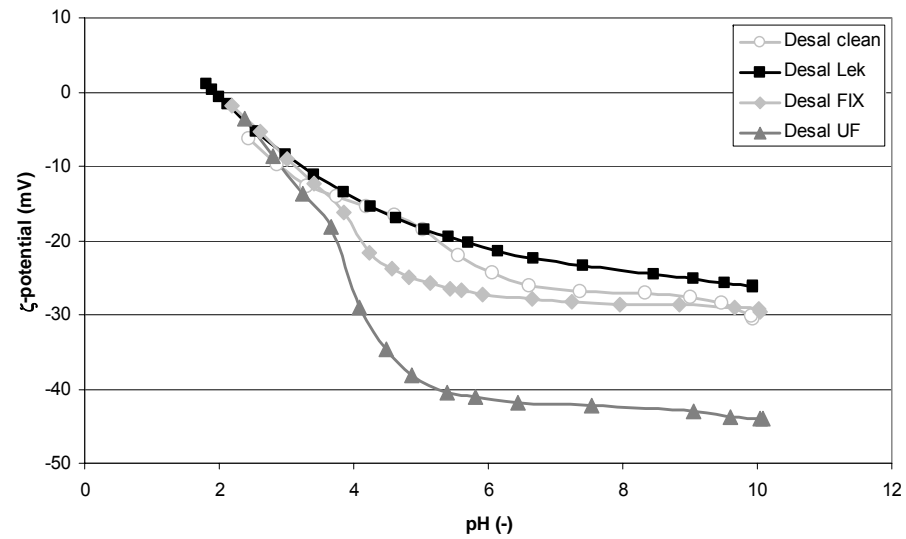
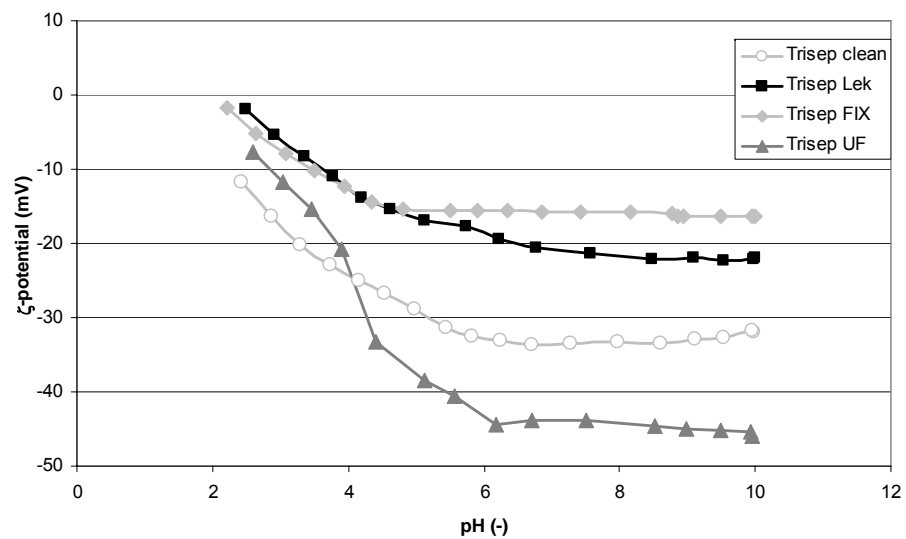


Figure 5.7 – Measured  $\zeta$ -potential data for different (fouled) membranes as a function of pH

However, after the membranes have been fouled, the difference between the Trisep TS80 and Desal HL membranes is less pronounced. It is apparent that the UF fouled Desal HL and the UF fouled Trisep TS80 have a comparable surface charge, which indicates that the surface charge is mainly determined by the foulant deposits. The surface charge of both membranes after UF fouling is significantly more negative than the surface charge of the clean membranes. This is probably due to the fact that the foulant layer after UF pretreatment consists mainly of natural organic matter fouling (especially humic acids), which is mostly negatively charged (since the NOM-molecules often contain many carboxylic acid functional groups).

Also the Lek fouled Trisep TS80 and Desal HL membranes are quite comparable to each other in surface charge. This charge is less negative than the clean membrane surface charge for both membranes. This might be attributed to the less negative zeta-potential of the colloidal particles which are present in the untreated water (Table 5.2), and which counteract the increase in surface charge caused by the deposit of highly negative NOM-molecules.

The zeta-potentials of the membranes after FIX fouling are quite different (for the Desal HL, as well as the Trisep TS80). It was, however, visually observed for the Desal HL membrane, that the FIX fouling layer of the membrane sample used for zeta-potential determination was damaged, and the underlying membrane was exposed. Therefore, for the Desal HL membrane, the zeta-potential of the FIX fouled membrane might reflect a combination of both foulant layer and membrane zeta-potential. To that respect, it can be expected that if the surface were undamaged, the zeta-potential might have been closer to that of the FIX fouled Trisep TS80 membrane. For this membrane, the zeta-potential is comparable to the zeta-potential

of the particles contained in the water, thus proving that the fouling layer on the FIX fouled membrane is mainly caused by colloids and particles.

### 3.3.3. Scanning electron microscopy images

The fouling layers on the fouled Desal HL membranes, visualised by SEM, are shown in Figure 5.8. The colloidal deposits on the FIX fouled membranes can be clearly observed in Figure 5.8 (c). The size of these colloids corresponds to the mean diameter of the colloids, as shown in Table 5.2. The fouling layer on the UF fouled membrane appears to be very smooth, which is typical for NOM fouling [22]. It can be observed that the UF fouled membrane in Figure 5.8 (d) is quite comparable to the unfouled membrane, indicating again that fouling is the least pronounced after UF pretreatment. For the membrane fouled with untreated Lek water, a combination of the two fouling mechanisms can be observed. The fouling layer is smoother than for the particle fouled FIX membrane, but rougher and more brittle than for the NOM fouled membrane (after UF pretreatment). The inclusion of some particles within the NOM cake-layer can clearly be seen for the Lek fouled membrane.

### 3.3.4. Contact angle measurements

The contact angle values are summarized in Table 5.4. The values of the contact angles were not only determined for the virgin membranes, but also for the membranes, compacted with Milli-Q water. The contact angle of both the Desal HL and the Trisep TS80 membrane decreases noticeably after compaction, which is in agreement with the decrease in flux during compaction.

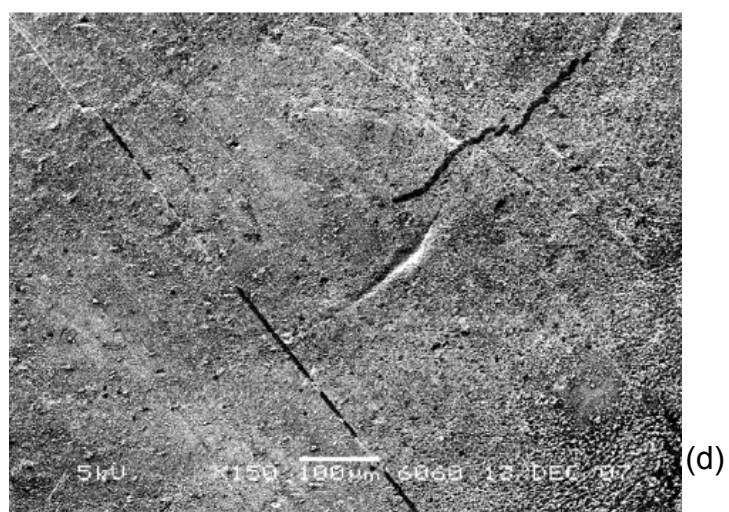
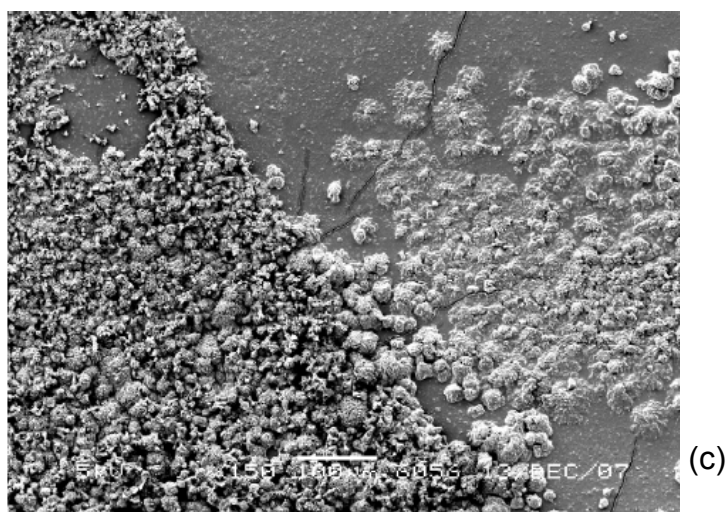
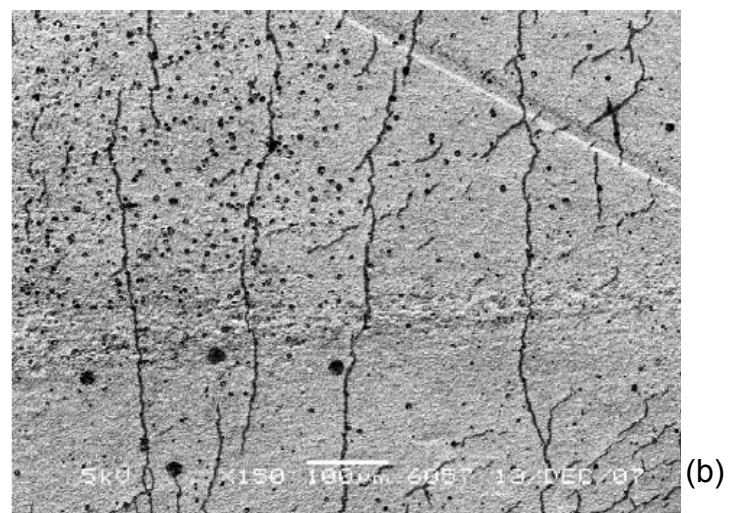
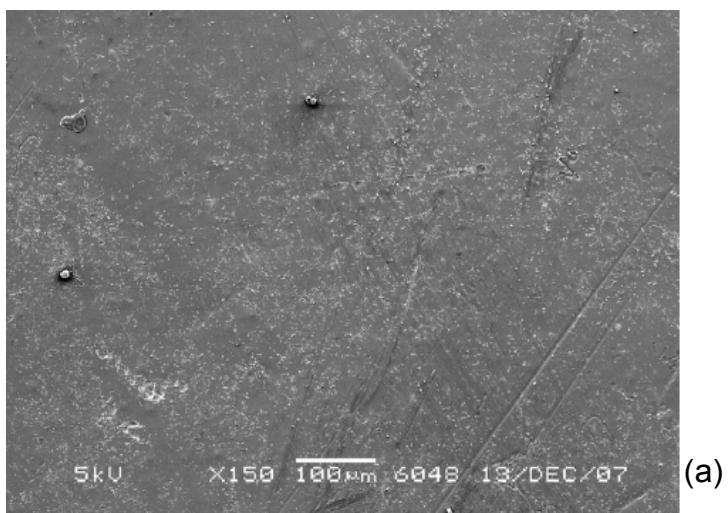


Figure 5.8 - SEM-images of clean and fouled Desal membranes (a: Desal clean; b: Desal Lek; c: Desal FIX; d: Desal UF)

	contact angle ( $\pm 2^\circ$ )
Trisep virgin	48
Trisep Milli-Q compacted	80
Trisep Lek	77
Trisep FIX	78
Trisep UF	74
Desal virgin	43
Desal Milli-Q compacted	63
Desal Lek	76
Desal FIX	80
Desal UF	76

Table 5.4 – Contact angles of the different membranes, determined with Milli-Q water

The decrease in contact angle is smaller for the Desal HL membrane, probably partly because the membrane was initially more hydrophilic, but also because the membrane has a larger pore size, and is thus less susceptible to compaction.

However, also the removal of surfactants during the first flushing of the membrane may have influenced this large difference in contact angle. To the best of our knowledge, no literature data are available on contact angles of compacted membranes, making comparison with the results of this study difficult.

For both membranes, the filtration of different surface water types leads to an increase of the contact angle compared with the virgin membranes, indicating membranes become more hydrophobic. However, when comparing the contact angles of the fouled membranes with those of the compacted membranes, the increase in contact angle is less pronounced. For the Desal HL membrane, the fouled membranes are still more hydrophobic than the compacted membrane, but for the Trisep TS80 membrane, this increase in hydrophobicity was not observed. The fouled Trisep TS80 membranes are at least as hydrophilic as the compacted membrane, or perhaps even more hydrophilic.

### 3.4. Rejection of pharmaceutically active compounds

The rejection values of the selected pharmaceuticals were first determined with a clean membrane Trisep TS80 and a clean Desal HL membrane.

Afterwards, rejection values with the fouled membranes were determined.

#### 3.4.1. Rejection with “virgin” membranes

The rejection values of the pharmaceuticals with the clean membranes are shown in Figure 5.9. Rejection values of all pharmaceuticals are relatively high ( $\geq 70\%$ ) for both membranes. Rejections with the Trisep TS80 are slightly higher, probably due to the larger pore size of the Desal HL (reflected by its larger MWCO).

It can be observed for both membranes that the rejection values for positively charged pharmaceuticals are lower than the rejection values for neutral pharmaceuticals, which are in turn lower than the rejection values for negatively charged pharmaceuticals. This was explained in Chapter 3 by electrostatic interactions between the solutes and the membrane surface.

It is interesting to observe that rejection values obtained with the small-scale flat sheet membrane cell in this study (Sepa CF II, GE Osmonics), are lower compared to the rejection values obtained on 4-inch spiral wound membrane modules in Chapter 3. This is probably due to hydrodynamic conditions in the Sepa cell. The length/width ratio of the cell is probably too small for a steady-state velocity profile to develop over the cell, resulting in a decreased mass-transfer and a higher hydrodynamic concentration polarisation compared with 4-inch spiral wound modules.



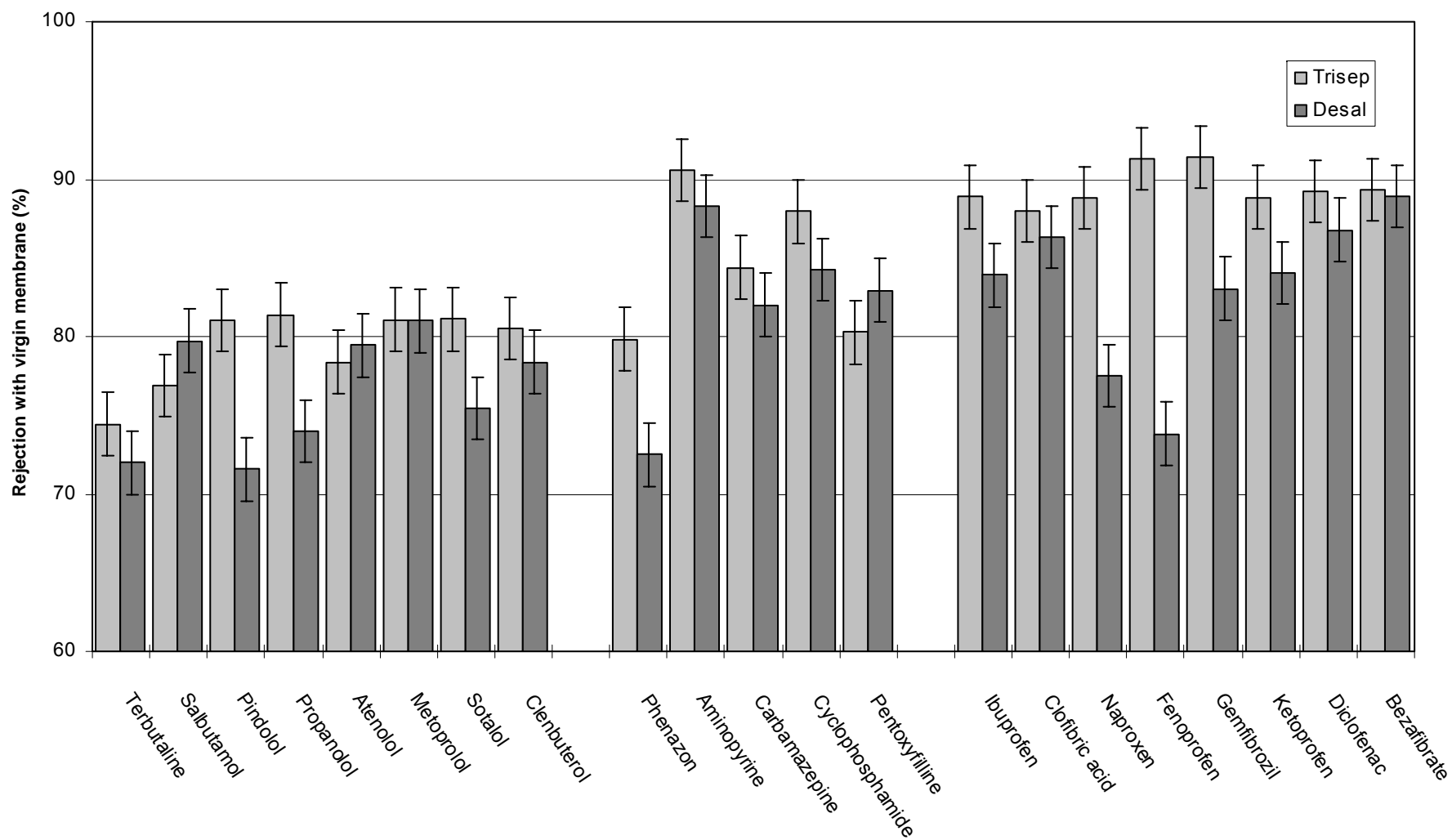


Figure 5.9 – Rejection values of selected pharmaceuticals on clean Trisep TS80 and Desal HL membrane

### 3.4.2. Rejection with fouled membranes

Figures 5.10 and 5.11 show the rejection values of the spiked pharmaceuticals with the different fouled Trisep TS80 and Desal HL membranes. The rejection values are plotted as the absolute difference in rejection between the fouled membranes and the clean membranes (filtrated with Milli-Q for 4 days). A positive value for the difference in rejection corresponds to an increase in rejection compared with the rejection value on the clean membrane, a negative value corresponds to a decrease in rejection compared with the clean membrane. The rejection values on the clean membranes were shown in Figure 5.9.

For the Desal HL membrane it is apparent that the rejection of positively charged solutes decreases significantly. Rejection values decrease up to 43% with the Desal HL membrane filtered with FIX effluent. Rejection values for the neutral solutes remain approximately constant for all the water types: a small increase or decrease in rejection for certain solutes can be observed but no clear trends can be seen. The only exception is the hydrophobic solute carbamazepine, for which rejection decreases about 10% for all the fouled Desal HL membranes. For almost all negatively charged solutes, rejection appears to increase with all fouled Desal HL membranes.

When comparing the influence of the different types of membrane fouling on the Desal HL membrane, however, major differences can be observed. The greatest variation in rejection is observed with the FIX pretreated Lek water. For the untreated Lek water and the water pretreated with ultrafiltration, the differences in rejection are smaller and quite comparable.

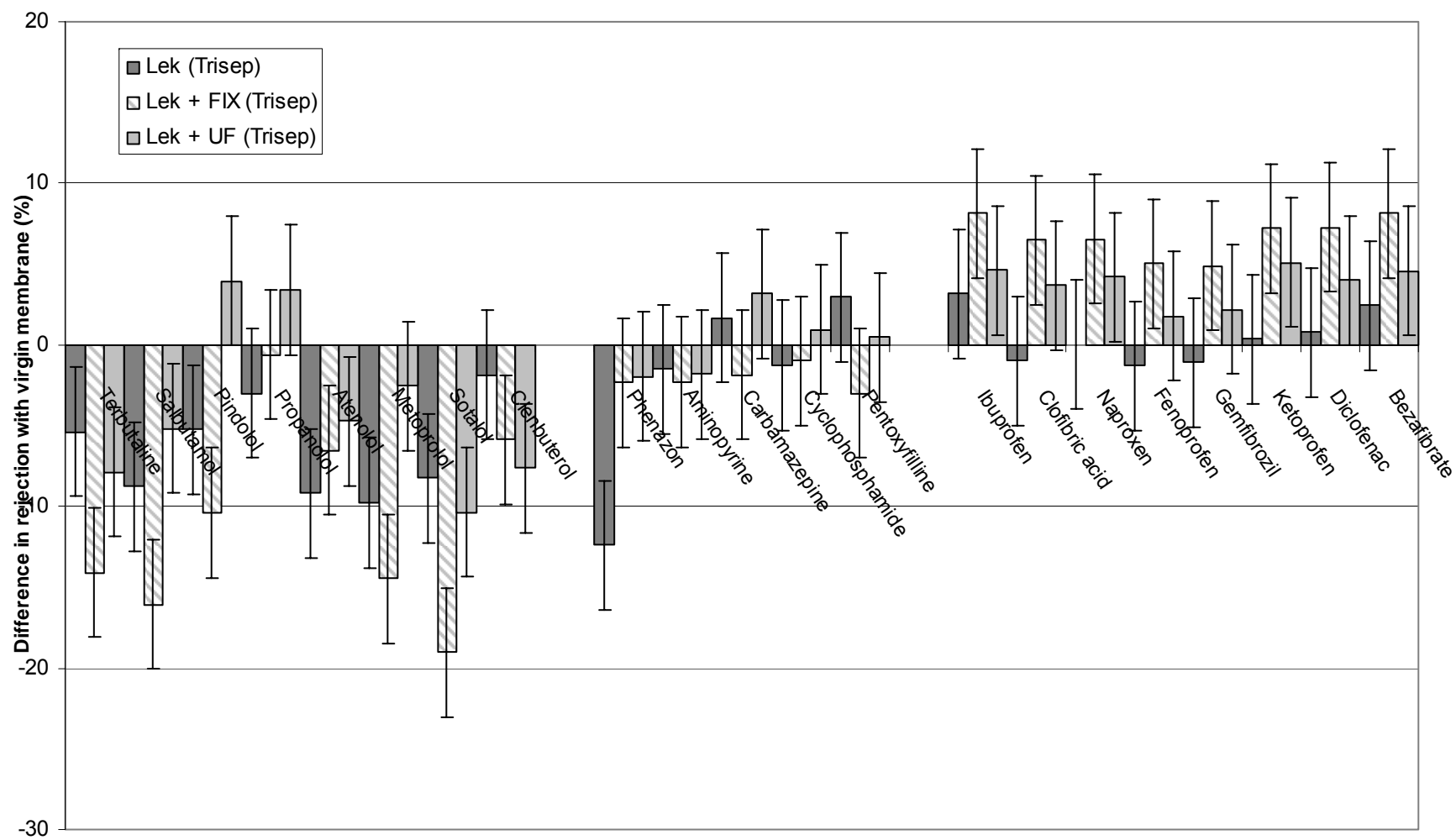


Figure 5.10 – Difference in rejection for different fouled Trisep TS80 membranes in comparison with a clean Trisep TS80 membrane

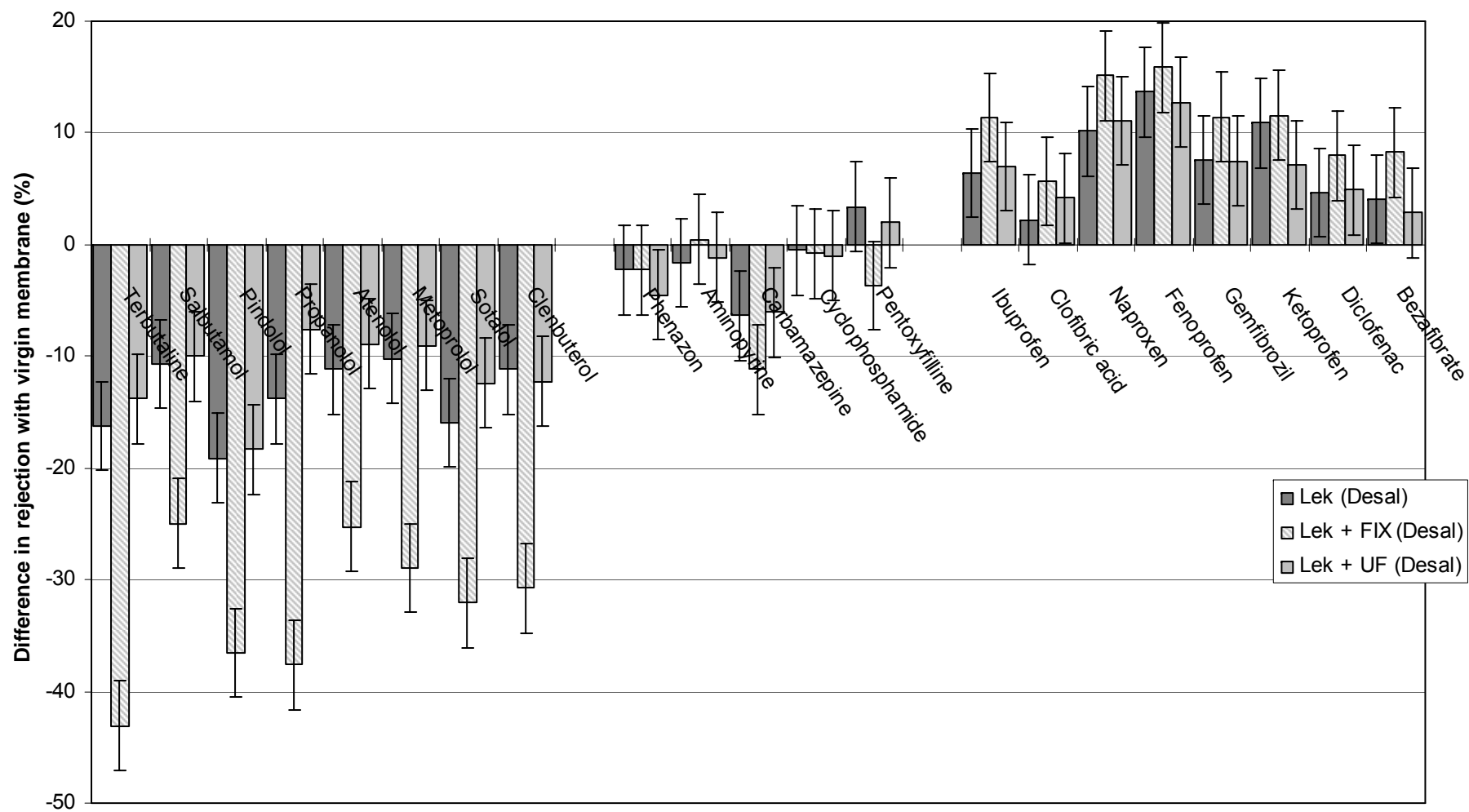


Figure 5.11 – Difference in rejection for different fouled Desal HL membranes in comparison with a clean Desal HL membrane

From the large increase in rejection of negatively charged pharmaceuticals, and the large decrease in rejection of positively charged pharmaceuticals, it can be hypothesized that the FIX fouled membrane is the most negatively charged. This is, however, not in agreement with the streaming potential/streaming current measurements, which show that the FIX fouled membrane has the lowest surface charge.

One possible explanation may lie in the morphology of the fouling layer: from the SEM-images (Figure 5.8), it is apparent that the Desal HL virgin membrane and the UF fouled Desal HL membrane are very smooth. For the FIX fouled membrane, however, the fouling layer is considerably less smooth (apparent from both SEM-pictures and visual observations). It is assumed that streaming potential/streaming current measurements only measure the macroscopic surface charge of the membranes, and are therefore affected by the surface morphology. As is schematically depicted in Figure 5.12, filtration flow is different from flow during (tangential) streaming potential measurements.

For the FIX fouled membrane, the rough surface and the evenly distributed charge on the surface of the colloids leads to a difference in apparent charge of the membrane surface between tangential streaming potential/current measurements and during filtration (perpendicular to the membrane surface). Figure 5.12 (a) shows how a charged solute is surrounded by more charges in filtration mode, leading to a higher apparent surface charge than during the streaming potential/current measurements. For the virgin and UF fouled membranes, however, the fouling layer is smooth, and solutes in a macroscopic, tangential flow can interact with the same amount of charges as solutes during the filtration process (Figure 5.12 (b)).

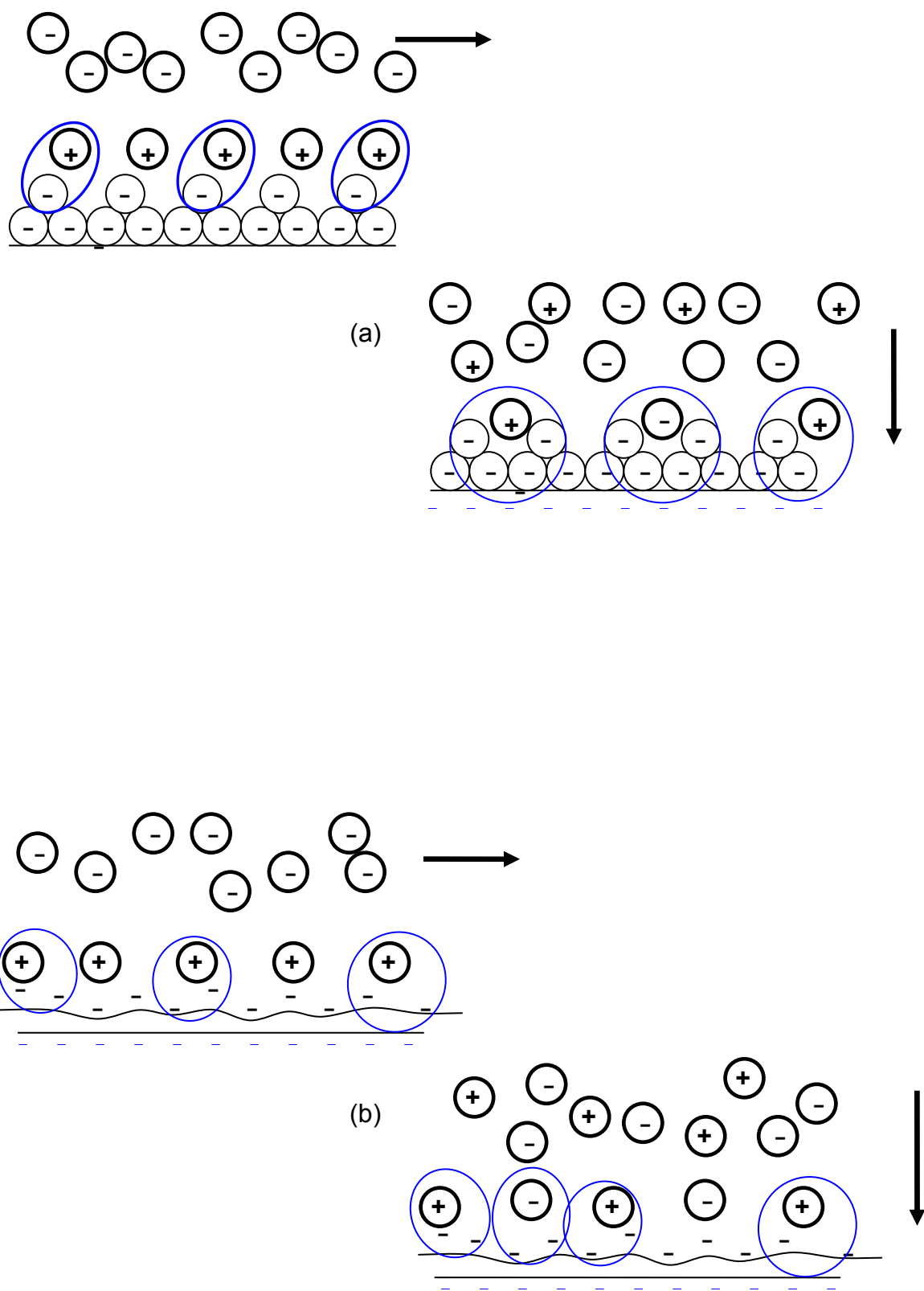


Figure 5.12 – Effective charge of membrane surface in tangential vs perpendicular flow for (a): rough colloidal fouling ; (b): smooth (NOM) fouling

A combination of these processes will occur for the membrane, fouled with the untreated Lek water.

For the FIX fouled Desal HL membrane, it can thus be concluded that the increased rejection of negatively charged solutes is due to charge repulsions with the fouled membrane surface, whereas the significant decrease in rejection of positively charged pharmaceuticals is due to the combination of charge attraction and hindered back-diffusion in the colloidal fouling layer [23,33]. Due to charge interactions with the negatively charged colloids, the positively charged pharmaceuticals are attracted towards the fouling layer. The concentration of positively charged pharmaceuticals at the membrane surface increases and the pharmaceuticals accumulate in the colloidal fouling layer. This leads to an even higher concentration increase due to a hindered back-diffusion in the colloidal fouling layer and therefore to a large decrease in rejection. Another indication for the influence of the hindered back-diffusion in the colloidal fouling layer is provided by the decrease in rejection of neutral pharmaceuticals for the FIX fouled membrane. Since charge interactions do not play a role there, the decrease in rejection is smaller.

From the streaming potential/streaming current measurements, it might be concluded that the UF fouled Desal HL membrane is the most negatively charged. This explains the higher rejection of negatively charged pharmaceuticals and the lower rejection of positively charged pharmaceuticals compared to the clean Desal HL membrane. The differences in rejection are nevertheless smaller than for the FIX fouled Desal HL membrane. The reason for this was previously explained (Figure 5.12). An additional explanation for the higher rejections of positively charged pharmaceuticals on the UF fouled Desal HL membrane compared to the FIX fouled Desal HL membrane, might be the formation of a more dense fouling layer by NOM fouling on the UF fouled

membrane, compared to the loose, colloidal fouling on the FIX fouled membrane. The more dense fouling layer would not lead to cake-enhanced concentration polarisation, but, in contrast, may even serve as an additional membrane layer, resulting in higher rejections for positively charged pharmaceuticals. The presence of this extra membrane layer should, however, also result in increased rejection values of the neutral pharmaceuticals. This increase in rejection for neutral pharmaceuticals is observed for the UF fouled Trisep TS80 membrane, but not for the UF fouled Desal HL membrane.

For the Desal HL membrane fouled with untreated Lek river water, rejection values follow approximately the same trends as for the UF fouled membrane. However, from the membrane characterisation, it becomes apparent that both membranes are significantly different. SEM images reveal differences in morphology, contact angle measurements indicate a slight difference in hydrophobicity and the XPS-measurements show a significant difference in fouling layer composition. Even with the naked eye, a significant difference between the membranes is seen (Figure 5.13). For the Desal HL membrane fouled with untreated Lek water, rejection values for the positively and negatively charged pharmaceuticals are between those for the UF and the FIX fouled membranes. However, rejection values are closer to those obtained with the UF fouled membrane, indicating a larger contribution of NOM fouling, compared to colloidal fouling, to the combined fouling with the untreated Lek water. This is also shown in the SEM-images, where the fouling layer on the Lek fouled membrane is smooth, with the inclusion of a few colloidal particles in the NOM cake layer.



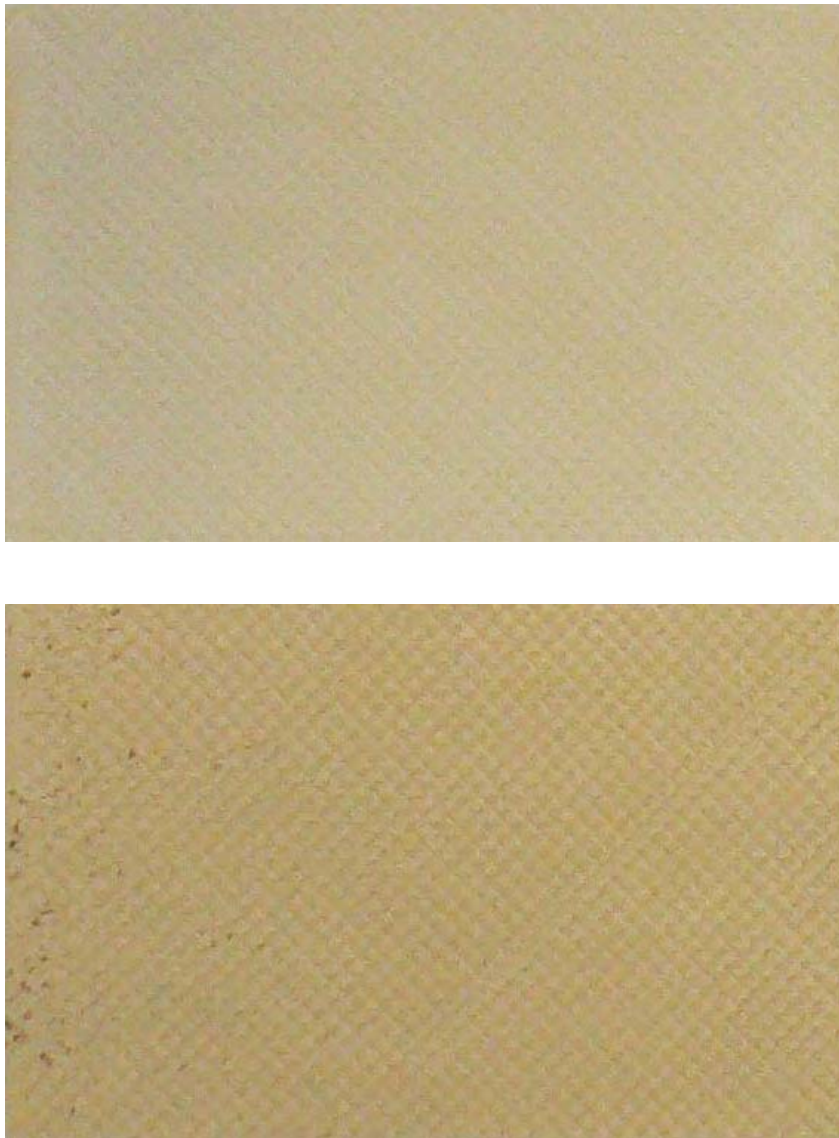


Figure 5.13 – Different fouled Trisep TS80 membranes. Top: Trisep TS80 fouled with Lek water after UF pretreatment ; bottom: Trisep TS80 fouled with untreated Lek water

For the fouled Trisep TS80 membranes, the same conclusions hold as for the Desal HL membrane. The only difference is that the differences in rejection between the fouled and the clean membranes are smaller than for the Desal HL membranes.

The reason for the smaller differences in rejection between the clean and the fouled Trisep TS80 membranes, compared with the Desal HL membranes, could be due to the difference in zeta-potential between the different membranes: the Trisep TS80 membrane has a higher negative surface charge than the Desal HL membrane, thus

making it less likely for negatively charged colloids or NOM-molecules to form a cake-layer on the surface. This is also confirmed when analyzing the flux data: the flux decline is lower for the Trisep TS80 membranes than for the Desal HL membranes, indicating that less material is probably deposited on the Trisep TS80 membrane surfaces.

Another explanation lies in the smaller pore size of the Trisep TS80: despite the presence of a fouling layer (and cake-enhanced concentration polarisation), the influence of the steric hindrance on the underlying membrane is still noticeable, even though charge and hydrophobicity properties have been altered. For the Desal HL membrane, this underlying steric hindrance is smaller, explaining the higher differences in rejection.

In conclusion, it can be said that the largest influence on the rejection of pharmaceuticals can be seen for the membranes with particulate fouling, for both the Trisep TS80 and the Desal HL. NOM fouling has a smaller effect on rejection, but also on the flux decline, as was mentioned before.

To gain more insight into the changes in rejection with fouled membranes, the rejection differences between the fouled Desal HL FIX and Trisep TS80 FIX membranes and the clean Desal HL and Trisep TS80 membranes are plotted in Figure 5.14 as a function of the pharmaceutical hydrophobicity. Only the data for the membranes fouled with the FIX pretreated Lek water are shown, since differences in rejection are the most obvious with these membranes. The rejection values with the other fouled membranes follow the same trends.

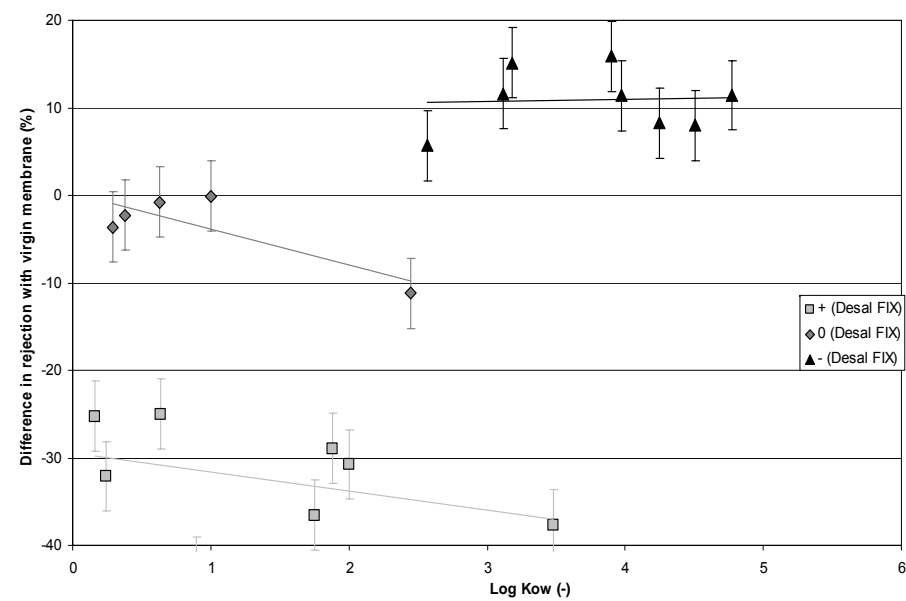
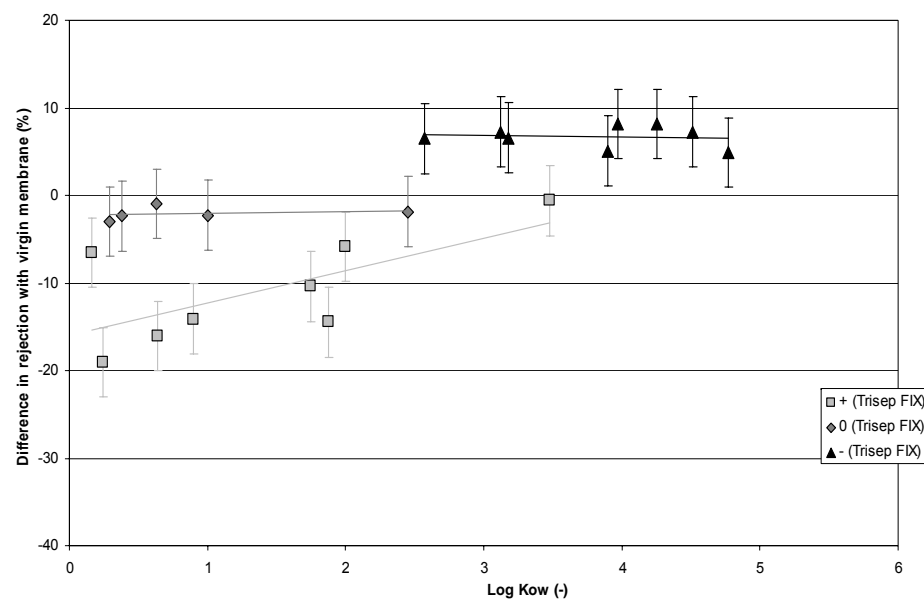


Figure 5.14 – Difference in rejection between FIX fouled and clean Trisep TS80 and Desal HL membranes as a function of solute hydrophobicity

For the Desal FIX membrane, it is apparent that the rejection decreases with increasing hydrophobicity of the solutes (at least for the positively charged and neutral pharmaceuticals). This is probably due to increased hydrophobic interactions between the more hydrophobic fouled membrane and hydrophobic solutes, in comparison with the more hydrophilic clean Desal HL membrane. These hydrophobic interactions cause an increased partitioning of hydrophobic solutes into the hydrophobic membrane matrix, which ultimately leads to lower observed rejection values (see Chapter 2). For negatively charged solutes, the change in rejection is independent of the solute hydrophobicity. This was observed before (see Chapter 3) and is due to the fact that negatively charged solutes can not approach the membrane surface due to electrostatic repulsion and thus can not experience hydrophobic interactions with it.

If the rejection values with the FIX fouled Trisep TS80 membrane are also plotted as a function of solute hydrophobicity, a different trend is seen than for the FIX fouled Desal HL membrane. For the FIX fouled Trisep TS80, the rejection decreases more for the hydrophilic pharmaceuticals, and less for the hydrophobic solutes (at least for the positively charged and neutral pharmaceuticals). This is due to decreased hydrophobic interactions with the membrane surface, caused by a decrease in membrane surface hydrophobicity. An increase in hydrophobicity is seen when the contact angle of the FIX fouled Trisep TS80 membrane is compared with the contact angle of the virgin Trisep TS80 membrane. However, when the FIX fouled Trisep TS80 membrane is compared with the compacted Trisep TS80 membrane (which is used in the clean membrane rejection experiments), the contact angle for the FIX membrane seems to be slightly lower, indicating a slightly more hydrophilic membrane surface.

The fouling layers on the Desal HL and the Trisep TS80 membrane are quite similar in composition (Table 5.3), which is also confirmed by the contact angle data. Since the Trisep TS80 membrane was initially more hydrophobic than the Desal HL membrane, the fouling layer leads to a decrease in hydrophobicity for the Trisep TS80 membrane, and an increase in hydrophobicity for the Desal HL membrane. Again, for the negatively charged pharmaceuticals, no influence of hydrophobicity on the rejection is seen with the FIX fouled Trisep TS80.

The flux decline trends obtained with this laboratory set-up are not representative for a full-scale installation. Firstly, full-scale installation are normally chemically cleaned when flux decline becomes larger than 10%. Secondly, the amount of membrane surface area in contact with the feed water is much smaller than for full-scale installations, resulting in a much larger load of organic matter towards the membrane surface. Thirdly, the hydrodynamic concentration polarisation in the flat-sheet cells is much higher than for spiral wound elements, which causes an additional increase of natural organic matter and colloid concentration at the membrane surface and possibly more membrane fouling. Therefore, the rejection values obtained in this chapter can not be used as quantitatively correct data to represent full-scale plants, The relative comparison between the different fouling types still remains valid. The insights gained in this chapter might therefore still be useful in explaining differences in rejection values between new and older plants, the latter of the two being more susceptible to membrane fouling.

In a previous publication [34] it was shown that the rejection values of the same set of pharmaceuticals only changed marginally after combined NOM- and colloidal

fouling with a 4-inch spiral wound Trisep TS80 membrane. The largest difference in rejection was about 5% and no clear conclusions on the fouling mechanism could be drawn. The flux decline was only about 20% after a period of 14 days, smaller than the flux declines obtained here. This could be due to the different source water used (surface water from the Weesperkarspel treatment plant (see Table 3.4), which was concentrated up to 75% recovery), or to the differences in hydrodynamic conditions between the small-scale set-up and the spiral wound elements.

#### **4. Conclusions**

The influence of feed water pretreatment on the flux decline and rejection performance was investigated for a mixture of neutral and negatively and positively charged pharmaceuticals of two nanofiltration membranes (Trisep TS80 and Desal HL). Raw, untreated river water was compared with the same river water, pretreated with a fluidized anionic ion exchange (FIX) and the river water, pretreated with an ultrafiltration unit. The FIX pretreatment removed a large part of the negatively charged natural organic matter from the feed water, but colloids/particles could pass the column freely. Therefore, the FIX pretreated water contained mostly colloids. The UF pretreatment removed most of the particles/colloids, but did not remove the natural organic matter from the water. Therefore, the UF pretreated water contained mainly NOM. The untreated water, contained both NOM and colloids.

The largest flux decline was observed with the feed water containing mainly colloids (FIX pretreated water). The (mainly colloidal) fouling layer had a rough morphology. The smallest flux decline was observed for the feed water containing mainly NOM

(UF pretreated water). The NOM fouling layer was more smooth. The flux decline behaviour of the untreated river water, containing both NOM and colloids, was between that of the two pretreated water types for both membranes used in this study.

Rejection of pharmaceuticals varied the most for the colloidal fouled membranes, (FIX pretreated water). The rejection of some positively charged pharmaceuticals decreased by more than 40% and rejection of some negatively charged pharmaceuticals increased by more than 15% for the Desal HL membrane. This variation in rejection was caused by a combination of cake-enhanced concentration polarisation and charge effects. Even though the zeta-potentials of the colloidal fouled membranes were lower than for the NOM fouled membranes, the morphology of the colloidal fouling layer on the colloidal fouled membranes seemed to enhance electrostatic interactions. For the NOM fouled membranes and the membranes fouled with untreated surface water, the variations in rejection were smaller and were caused by a combination of steric and electrostatic effects.

For the Trisep TS80 membrane, the fouling appeared to decrease the hydrophobicity of the membrane surface, resulting in smaller variations in rejections for hydrophobic solutes, compared to hydrophilic solutes, due to decreased hydrophobic interactions with the membrane surface. For the Desal HL membrane, fouling increased the membrane surface hydrophobicity, resulting in large variations in rejection for hydrophobic solutes, as a result of increased solute-membrane affinity/hydrophobic interactions. The influence of hydrophobicity on rejection was only observed for neutral and positively charged pharmaceuticals, since negatively charged pharmaceuticals could not approach the membrane surface due to electrostatic

repulsions and were thus disengaged from hydrophobic interactions with this membrane surface.

Rejection values before and after fouling obtained here with the small, flat-sheet membrane cell, can not be used as quantitatively representative data for spiral wound elements in full-scale units. This is due to differences in hydrodynamic flow conditions and the higher load of foulants towards the membrane surface in the small-scale cell. In spiral wound elements, flux declines and differences in rejection will be substantially lower, the differences in rejection before and after fouling will probably not exceed 5-10% (difference). However, the relative comparison between the different membranes and the different fouling layers caused by different feed water types, remains valid.



## References

- [1] H.-C. Flemming, G. Schaule, T. Griebel, J. Schmitt and A. Tamachkierowa, Biofouling-the Achilles heel of membrane processes, *Desalination*, 113 (2-3) (1997) 215.
- [2] Q. Li and M. Elimelech, Synergistic effects in combined fouling of a loose nanofiltration membrane by colloidal materials and natural organic matter, *Journal of Membrane Science*, 278 (2006), 72-82.
- [3] Q. Li and M. Elimelech, Organic fouling and chemical cleaning of nanofiltration membranes: measurements and mechanisms, *Environmental Science & Technology*, 38 (2004) 4683-4693.
- [4] X. Zhu and M. Elimelech, Colloidal fouling of reverse osmosis membranes: measurements and fouling mechanisms, *Environmental Science & Technology*, 31 (1997) 3654-3662.
- [5] S. Lee, J. Cho and M. Elimelech, Combined influence of natural organic matter (NOM) and colloidal particles on nanofiltration membrane fouling, *Journal of Membrane Science*, 262 (2005) 27-41.
- [6] E.M.V. Hoek, A.S. Kim and M. Elimelech, Influence of crossflow membrane filter geometry and shear rate on colloidal fouling in reverse osmosis and nanofiltration separations, *Environmental Engineering Science*, 19 (6) (2002) 357-372.
- [7] E.M. Vrijenhoek, S. Hong and M. Elimelech, Influence of membrane surface properties on initial rate of colloidal fouling of reverse osmosis and nanofiltration membranes, *Journal of Membrane Science*, 188 (2001) 115-128.
- [8] Q. Li and M. Elimelech, Natural organic matter fouling and chemical cleaning of nanofiltration membranes, *Water Science and Technology: Water Supply*, 4 (5-6) (2004) 245-251.
- [9] B. Van der Bruggen, J.H. Kim, F.A. DiGiano, J. Geens and C. Vandecasteele, Influence of MF pretreatment on NF performance for aqueous solutions containing particles and an organic foulant, *Separation and Purification Technology*, 36 (2004) 203-213.
- [10] M. Mänttari, L. Puro, J. Nuortila-Jokinen and M. Nyström, Fouling effects of polysaccharides and humic acid in nanofiltration, *Journal of Membrane Science*, 165 (2000) 1-17.
- [11] Y. Yoon, G. Amy, J. Cho and N. Her, Effects of retained natural organic matter (NOM) on NOM rejection and membrane flux decline with nanofiltration and ultrafiltration, *Desalination*, 173 (2005) 209-221.

- [12] J. Cho, G. Amy and J. Pellegrino, Membrane filtration of natural organic matter: initial comparison of rejection and flux decline characteristics with ultrafiltration and nanofiltration membranes, *Water Research*, 33 (11) (1999) 2517-2526.
- [13] D. Violleau, H. Essis-Tome, H. Habarou, J.P. Croué and M. Pontié, Fouling studies of a polyamide nanofiltration membrane by selected natural organic matter: an analytical approach, *Desalination*, 173 (2005) 223-238.
- [14] Z. Wang, Y. Zhao, J. Wang and S. Wang, Studies on nanofiltration membrane fouling in the treatment of water solutions containing humic acids, *Desalination*, 178 (2005) 171-178.
- [15] S. Lee, J. Cho and M. Elimelech, A novel method for investigating the influence of feed water recovery on colloidal and NOM fouling of RO and NF membranes, *Environmental Engineering Science*, 22 (4) (2005) 496-509.
- [16] J.E. Kilduff, S. Mattaraj and G. Belfort, Flux decline during nanofiltration of naturally-occurring dissolved organic matter: effects of osmotic pressure, membrane permeability, and cake formation, *Journal of Membrane Science*, 239 (2004) 39-53.
- [17] C.A.C. van de Lisdonk, B.M. Rietman, S.G.J. Heijman, G.R. Sterk and J.C. Schippers, Prediction of supersaturation and monitoring of scaling in reverse osmosis and nanofiltration membrane systems, *Desalination*, 138 (1-2) (2001) 259.
- [18] C.A.C. van de Lisdonk, J.A.M. van Paassen and J.C. Schippers, Monitoring scaling in nanofiltration and reverse osmosis membrane systems, *Desalination*, 132 (1-3) 101.
- [19] P. Xu, J.E. Drewes, T.-U. Kim, C. Bellona and G. Amy, Effect of membrane fouling on transport of organic contaminants in NF/RO membrane applications, *Journal of Membrane Science*, 279 (2006) 165-175.
- [20] L.D. Nghiem and S. Hawkes, Effects of membrane fouling on the nanofiltration of pharmaceutically active compounds (PhACs): Mechanisms and role of membrane pore size, *Separation and Purification Technology*, 57 (2007) 182-190.
- [21] K.O. Agenson and T. Urase, Change in membrane performance due to organic fouling in nanofiltration (NF)/reverse osmosis (RO) applications, *Separation and Purification Technology*, 55 (2007) 147-156.

- [22] K.V. Plakas, A.J. Karabelas, T. Wintgens and T. Melin, A study of selected herbicides retention by nanofiltration membranes – The role of organic fouling, *Journal of Membrane Science*, 284 (2006) 291-300.
- [23] H.Y. Ng and M. Elimelech, Influence of colloidal fouling on rejection of trace organic contaminants by reverse osmosis, *Journal of Membrane Science*, 244 (2004) 215-226.
- [24] E.R. Cornelissen, E.F. Beerendonk, M.N. Nederlof, J.P. van der Hoek and L.P. Wessels, The use of Fluidized Ion Exchange (FIX) to control NOM fouling in membrane filtration, *Desalination*, in press, doi: 10.1016/j.desal.
- [25] A.M. Comerton, R.C. Andrews, D.M. Bagley and C. Hao, The rejection of endocrine disrupting and pharmaceutically active compounds by NF and RO membranes as a function of compound and water matrix properties, *Journal of Membrane Science*, in press (2008).
- [26] G. Makdissy, S. Peldszus, R. McPhail and P.M. Huck, Towards a mechanistic understanding of the impact of fouling on the removal of EDCs/PPCPs by nanofiltration membranes, *American Water Works Association Water Quality Technology Conference and Exhibition (2007)*, American Water Works Association, Charlotte NC, USA.
- [27] K. Kimura, G. Amy, J. Drewes and Y. Watanabe, Adsorption of hydrophobic compounds onto NF/RO membranes: an artifact leading to overestimation of rejection. *Journal of Membrane Science*, 221 (2003) 89-101.
- [28] A. Magic-Knezev and D. van der Kooij, Optimisation and significance of ATP analysis for measuring active biomass in granular activated carbon filters used in water treatment, *Water Research*, 38 (2004) 3971-3979.
- [29] S.A. Huber and F.H. Frimmel, A new method for the characterization of organic carbon in aquatic systems, *International Journal of Environmental Analytical Chemistry*, 49 (1-2) (1992) 49-57.
- [30] J.S. Vrouwenvelder, J.W.N.M. Kappelhof, S.G.J. Heijman, J.C. Schippers and D. van der Kooij, Tools for fouling diagnosis of NF and RO membranes and assessment of the fouling potential of feed water, *Desalination*, 157 (1-3) (2003) 361.
- [31] S. Lee, J. Cho and M. Elimelech, Influence of colloidal fouling and feed water recovery on salt rejection of RO and NF membranes, *Desalination*, 160 (2004) 1-12.

- [32] A. Seidel and M. Elimelech, Coupling between chemical and physical interactions in natural organic matter (NOM) fouling of nanofiltration membranes: implications for fouling control, *Journal of Membrane Science*, 203 (2002) 245-255.
- [33] E.M.V. Hoek and M. Elimelech, Cake-enhanced concentration polarization: a new fouling mechanism for salt-rejecting membranes, *Environmental Science & Technology*, 37 (24) (2003) 5581-5588.
- [34] S.G.J. Heijman, A.R.D. Verliefde, E.R. Cornelissen, G. Amy and J.C. van Dijk, Influence of natural organic matter (NOM) fouling on the removal of pharmaceuticals by nanofiltration and activated carbon filtration, *Water Science & Technology: Water Supply*, 7 (4) (2007) 17.



# **Chapter 6:**

## **Practical applications**

Parts of this chapter were based on:

A.R.D. Verliefde, E.R. Cornelissen, S.G.J. Heijman, G.L. Amy, B. Van der Bruggen and J.C. van Dijk, Practical applications of the combination NF/RO with granular activated carbon for removal of organic micropollutants, to be submitted to Drinking Water Engineering & Science.

A.R.D. Verliefde, E.R. Cornelissen, S.G.J. Heijman, G.L. Amy, B. Van der Bruggen and J.C. van Dijk, Influence of electrostatic interactions on the rejection with NF and assessment of the removal efficiency during NF/GAC treatment of pharmaceutically active compounds in surface water, Water Research, 41 (15) (2007) 3227.

The previous chapters have discussed removal mechanisms of organic micropollutants by NF/RO and especially how these removal mechanisms are affected by solute properties, as well as membrane and feed water properties. The chapters all had a quite theoretical lay-out.

This chapter will focus more on practical applications of NF/RO and will thus be more dedicated to the mere observation and explanation of removal of organic micropollutants in practice (of course in relation to previously formulated theories), without formulating new theoretical concepts.

The chapter will be subdivided into two large parts. The first part will focus on the removal of organic micropollutants in two different source water applications, by the combination of NF/RO with granular activated carbon filtration. The second part will look at some newly developed RO membranes and will assess their removal potential for organic solutes, in comparison with a commercially available membrane.

## Chapter 6A: The combination of NF/RO with activated carbon filtration for removal of organic micropollutants from raw water

As was shown in the previous chapters, hydrophilic organic solutes are better removed with NF/RO membranes compared to hydrophobic organic solutes, due to the presence of hydrophobic (Van der Waals) interactions between the latter and the hydrophobic membrane matrix, resulting in an increased partitioning into the membrane matrix. From the literature [1,2], it is also known that activated carbon filtration preferentially removes hydrophobic organic solutes (adsorption is mainly influenced by Van der Waals interactions between the carbon and the solutes). Therefore, NF/RO and subsequent activated carbon filtration should be complementary and their combination should result in removal of a large part of the newly emerging organic micropollutants, since the whole range of solute hydrophobicity is covered.

This subchapter will investigate the removal of selected organic micropollutants with a combination of NF/RO and subsequent granular activated carbon (GAC) for two different raw water types.

### **4.1.High recovery NF combined with GAC for removal of organic micropollutants from surface water**

This study was part of a larger study on a new concept for surface water treatment. Surface water from the river Schie in Delft, the Netherlands, containing a high



concentration of dissolved organic carbon (DOC), was treated with a treatment train consisting of cationic ion exchange (IEX) – ultrafiltration (UF) – nanofiltration (NF) – granular activated carbon filtration (GAC).

The general idea behind this treatment concept was to remove divalent ions from the feed using the IEX (divalent ions are exchanged for  $\text{Na}^+$  ions), in order to reduce fouling of the UF membranes and prevent scaling on the NF (which was operated at high recovery). It is known from the literature [3] that reducing the  $\text{Ca}^{2+}$  and  $\text{Mg}^{2+}$  concentrations before ultrafiltration leads to a significant reduction in irreversible fouling of UF membranes. The current hypothesis is that the  $\text{Ca}^{2+}$  and  $\text{Mg}^{2+}$  ions may form a linkage between negatively charged NOM molecules and the negatively charged UF membrane surface, resulting in a dense, irreversible fouling layer on the membrane. Moreover, by removing  $\text{Ca}^{2+}$ , the recovery of the NF installation can be increased, since  $\text{CaCO}_3$ -scaling is prevented.

The IEX-UF-NF-GAC treatment train offers double barriers against pathogens (are removed by UF and NF), particles (UF and NF) and organic micropollutants (NF and GAC).

This study will only focus on the removal of organic micropollutants with the NF/GAC combination.

#### 4.1.1. Materials and methods

##### 4.1.1.1. *Surface water quality*

Some selected water quality parameters of the water fed to the NF unit are summarized in Table 6.1. The IEX pretreatment is carried out with a weak acidic

cationic exchange resin (Amberlite IRC86 (Rohm & Haas, Philadelphia PA, USA)). The multivalent scaling cations in the water ( $\text{Ca}^{2+}$ ,  $\text{Mg}^{2+}$  and Si) are partly exchanged for  $\text{Na}^+$  ions. Afterwards, the water is passed through an X-Flow UFC M5 ultrafiltration unit (X-Flow Norit, Enschede, the Netherlands) to lower turbidity and remove particles, before it is fed to the NF unit.

Schie water after ion exchange (IEX) and UF	
pH (-)	6.7
Dissolved Organic Carbon (DOC) (mg/l)	12.0
Conductivity ( $\mu\text{S}/\text{cm}$ )	980
$\text{Ca}^{2+}$ (mg/l)	19
$\text{Mg}^{2+}$ (mg/l)	16
Si (mg/l)	2.4
$\text{K}^+$ (mg/l)	14
$\text{Na}^+$ (mg/l)	153

Table 6.1 – Water quality parameters of Schie water after ion exchange (IEX) and UF (water fed to NF)

#### 4.1.1.2. NF/GAC equipment and filtration protocol

Figure 6.1 shows the schematic diagram of the equipment used in the nanofiltration- and the granulated activated carbon experiments. The pre-treated water from the river Schie is fed to a nanofiltration unit, operating at 80% recovery, with experiments carried out in a single-pass (once-through) mode. The granular activated carbon column is fed with the permeate of the nanofiltration unit.

The ultrafiltrated Schie water is delivered to a vertically placed pressure vessel, accommodating a single 2540-nanofiltration membrane element, by a multi-impellor centrifugal pump (Grundfos CRNE-1). The pump is capable of providing pressures of up to 20 bar at a flow rate of  $1.5 \text{ m}^3/\text{h}$ . Part of the produced concentrate is recycled to the feed stream to simulate higher system recoveries while still maintaining

sufficiently high cross-flow velocities. To provide the necessary recycle pressure, a Verder-Iwaki MDH 25 magnet pump is used. A tube-in-tube cooling system on the recycle stream (Tamson TLC 10B) is used to maintain a constant feed water temperature.

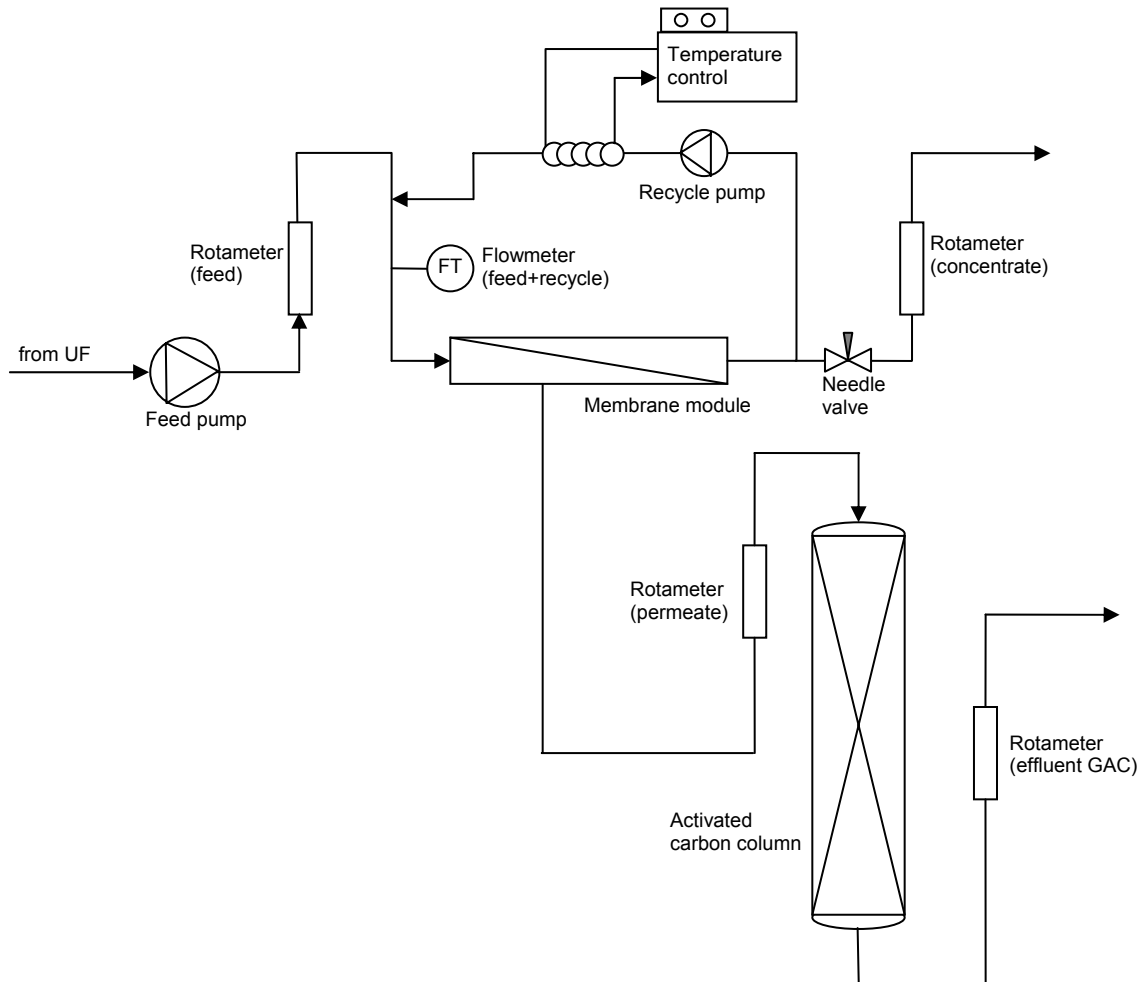


Figure 6.1 – Nanofiltration/granular activated carbon filtration set-up for experiments at 80% recovery with Schie water

Permeate, concentrate and system feed flow are monitored by rotameters (Heinrichs messgeräte), while the combined flow of feed and recycle is monitored by a digital flow meter (Endress and Hauser). Applied transmembrane pressure and system recovery are regulated using a needle valve in the concentrate stream. Feed pressure and differential pressure over the membrane element are measured with

precision manometers (Endress and Hauser). All test unit parts in contact with the solution are made of stainless steel to minimize adsorption of the organic compounds used. Spiking experiments were run for 4 days to allow adsorption of organic solutes onto the membrane to reach equilibrium and to ensure that steady-state rejection values were measured (see Paragraph 4.1, Chapter 2). Membrane filtration experiments are carried out at a constant cross-flow velocity of 0.2 m/s (which corresponds to a membrane feed flow of 400 l/h and a concentration polarization factor of about 1.07). During the rejection experiments, the system recovery is set to 80% to simulate the final element in the last stage of a full-scale plant. The feed temperature is set to  $20 \pm 1^\circ\text{C}$ .

The granular activated carbon column was placed in the permeate stream of the NF unit. Rotameters (Heinrichs messgeräte) were present to monitor feed and effluent streams of the column. A short empty bed contact time (EBCT) of 3 minutes was used. Pictures of both the NF and GAC are shown in Figure 6.2.

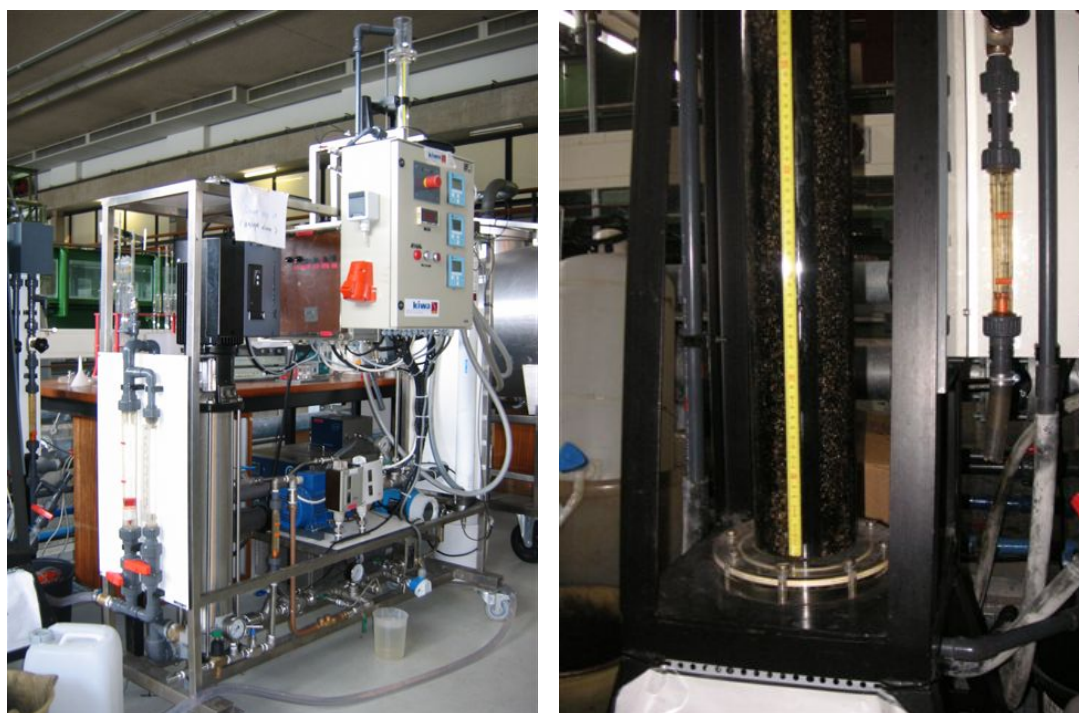


Figure 6.2 – Nanofiltration set-up (left) and granular activated carbon filtration set-up (right) for experiments at 80% recovery with Schie water

#### *4.1.1.3. NF membrane and activated carbon*

The membrane used in this study was a commercially available nanofiltration membrane that was also used in the experiments described in previous chapters: Trisep TS-80 TSF (Trisep Corp., Goleta CA, USA). Membrane properties are summarized in Table 2.1. For the experiments in this study, a single 2540 spiral wound element was used.

The granular activated carbon was supplied by Norit Nederland B.V. (Amersfoort, the Netherlands). The extruded grade Norit Row Supra 0.8 was chosen for its multi-purpose adsorption characteristics, low pressure drop and high resistance to attrition during regeneration. The bed density of the carbon is 345 kg/m<sup>3</sup> and the raw carbon material is peat. Freshly regenerated activated carbon was used in the experiments, so no preloading (of natural organic matter (NOM) or other organic pollutants) was present on the carbon.

#### *4.1.1.4. Organic solutes and analysis*

Two different spiking runs were carried out: one run with volatile organic solutes, and one with the same cocktail of pharmaceuticals as was dosed in previous experiments (see Chapters 3, 4 and 5). All solutes were spiked in high concentrations (up to 100 µg/l), so 99% rejection/removal could be measured for both NF and GAC. It was shown in Paragraph 3.3.3 in Chapter 3 that this higher feed concentration than the 2 µg/l-level used in most previous experiments, does not have a significant influence on solute rejection.

Since the organic solutes had to be dosed to the feed stream continuously from a concentrated solution, some pharmaceuticals could not be spiked in such high concentrations, due to their limited solubility. Lower spiking concentrations were chosen for these solutes.

	MW (g/mol)	log K <sub>ow</sub> (-)	pK <sub>a</sub> (-)	Charge at feed water pH (pH 7)	log D <sub>(pH 7)</sub> (-)	C <sub>feed</sub> (µg/l)
terbutaline	225.3	0.90	8.86	+	- 0.97	40
salbutamol	239.3	0.64	9.27	+	- 1.63	3
pindolol	248.3	1.75	9.26	+	- 0.52	50
propranolol	259.4	3.48	9.58	+	0.90	100
atenolol	266.3	0.16	9.43	+	- 2.27	50
metoprolol	267.4	1.88	9.49	+	- 0.61	80
sotalol	272.4	0.24	9.44	+	- 2.20	2.5
clenbuterol	277.2	2.00	9.29	+	- 0.29	2.5
phenazone	188.2	0.38	n.a.	neutral	n.a.	100
aminopyrine	231.3	1.00	n.a.	neutral	n.a.	100
carbamazepine	236.3	2.45	n.a.	neutral	n.a.	25
cyclophosphamide	261.1	0.63	n.a.	neutral	n.a.	100
pentoxifylline	278.3	0.29	n.a.	neutral	n.a.	100
ibuprofen	206.3	3.97	4.47	-	1.44	30
clofibric acid	214.7	2.57	3.35	-	- 1.08	100
fenoprofen	242.3	3.90	4.21	-	1.11	100
gemfibrozil	250.3	4.77	4.45	-	2.22	100
ketoprofen	254.3	3.12	4.29	-	0.41	50
diclofenac	296.2	4.51	4.08	-	1.59	5
tert butyl alcohol (TBA)	74.1	0.35	n.a.	neutral	n.a.	100
methyl tert butyl ether (MTBE)	88.1	0.94	n.a.	neutral	n.a.	20
ethyl tert butyl ether (ETBE)	102.2	1.92	n.a.	neutral	n.a.	20
tert amyl methyl ether (TAME)	102.2	1.92	n.a.	neutral	n.a.	20

Table 6.2 – Physico-chemical characteristics and feed concentrations for selected organic solutes for NF/GAC experiments (n.a.: not applicable)

Table 6.2 summarizes the concentrations of the organic solutes used in the two spiking rounds, together with their solute parameters.

Analysis of the pharmaceuticals was already described in Paragraph 2.3 in Chapter 3.

Analysis of the volatile solutes (MTBE, TBA, ETBE and TAME) was performed with gas chromatography/mass spectrometry. The solutes are analysed by purging with nitrogen gas and adsorption on Tenax rubber (purge and trap). More information on the analysis can be found in [4].

#### 4.1.2. Results and discussion

##### *4.1.2.1. NF flux decline during experiment*

The NF permeate flux decline during the experiment was studied in order to ensure an unbiased value, not influenced by membrane fouling, for the rejection of the organic solutes with the surface water studied. Since the experiments were only carried out for 4 days and all scaling ions and particles were removed in the pre-treatment (combination ion exchange-ultrafiltration), occurrence of biofouling, scaling and particle fouling are ruled out.

During the first 72 hours of the experiment no clear flux decline was observed, even though the experiment was carried out at a recovery of 80% and the DOC (dissolved organic carbon) content of the water was quite high. Therefore, it can be assumed that NOM fouling of the membrane surface is not discernable for this short time frame experiment and the measured rejection values are not influenced by fouling.

#### 4.1.2.2. *Removal of organic micropollutants with NF and GAC*

In Figure 6.3, the removal efficiencies after 4 days of adsorption equilibrium of the selected pharmaceuticals for the Trisep TS-80 membrane at 80% recovery and for the GAC filtration are shown, along with the total removal efficiency for the NF/GAC combination. The solute concentrations in the permeate of the NF unit are considered as the feed concentrations for the GAC. From the figure, it is clear that rejection levels for the Trisep membrane at 80% recovery are generally lower than for experiments with other water types with the Trisep membrane at 10% recovery (see Chapter 3). A decreasing rejection with increasing feed water recovery is a well-known phenomenon [5]: at higher system recoveries the average feed concentration in the system is higher, due to the internal recycle. This will result in lower observed rejections, when comparing the permeate concentrations to the feed of the complete NF system. Conclusions about charge effects on the rejection of the pharmaceuticals remain the same as in Chapter 3: positively charged pharmaceuticals are less efficiently removed compared to the neutral pharmaceuticals which, in turn, have lower rejections compared to the negatively charged pharmaceuticals. Again, rejection appears to be less determined by steric hindrance: in Figure 6.4, the three groups of pharmaceuticals are plotted as a function of their molar mass. For neutral and positively charged pharmaceuticals, no clear trends can be observed for the rejection as a function of molar mass. For negatively charged solutes, rejection appears to increase slowly with increasing molar mass, but there is no clear correlation. In general, the same rejection mechanisms appear to apply as for the rejection experiments at lower recovery. However, due to the higher recovery, solute concentrations in the system are higher, resulting in lower observed rejections.



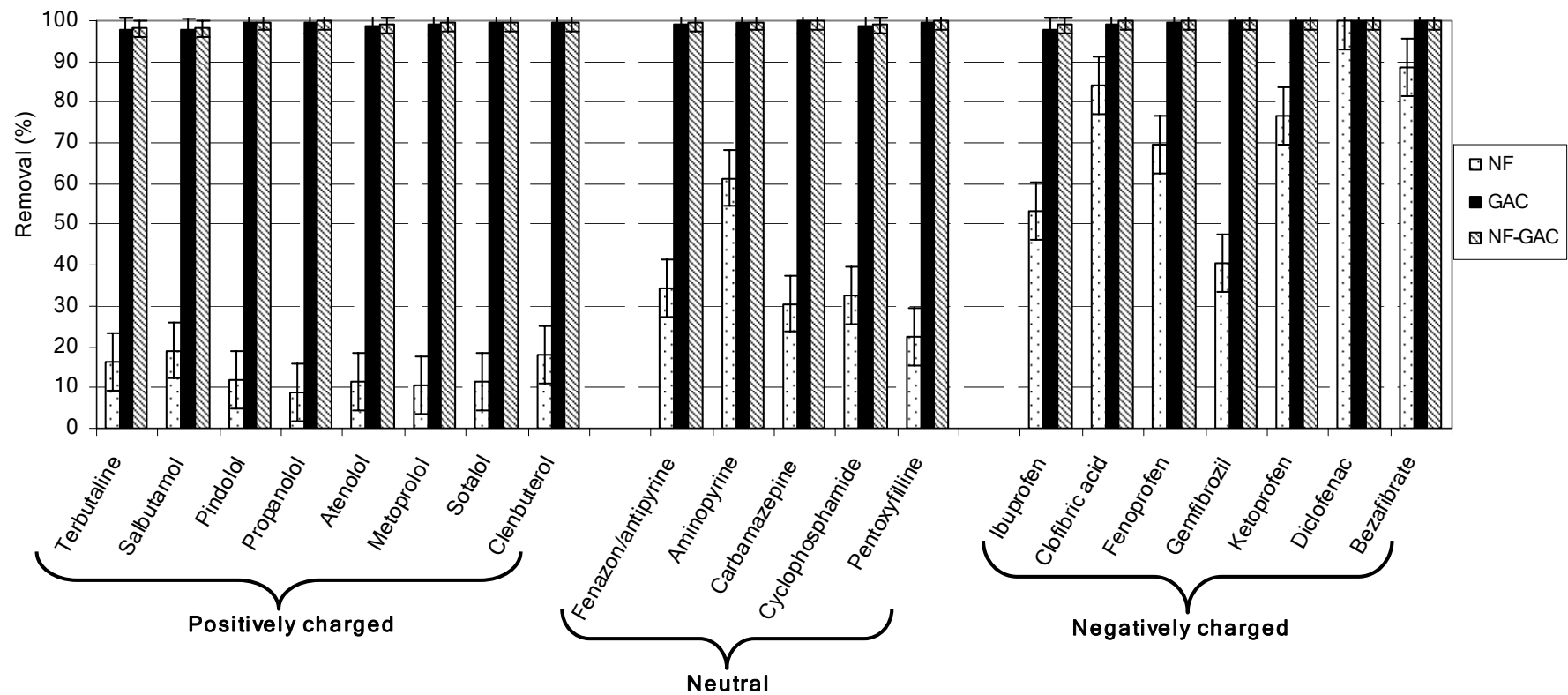


Figure 6.3 – Rejection of selected pharmaceuticals in Schie water for NF at 80% recovery (Trisep TS-80), removal efficiency for GAC filtration and total removal efficiency with NF/GAC combination

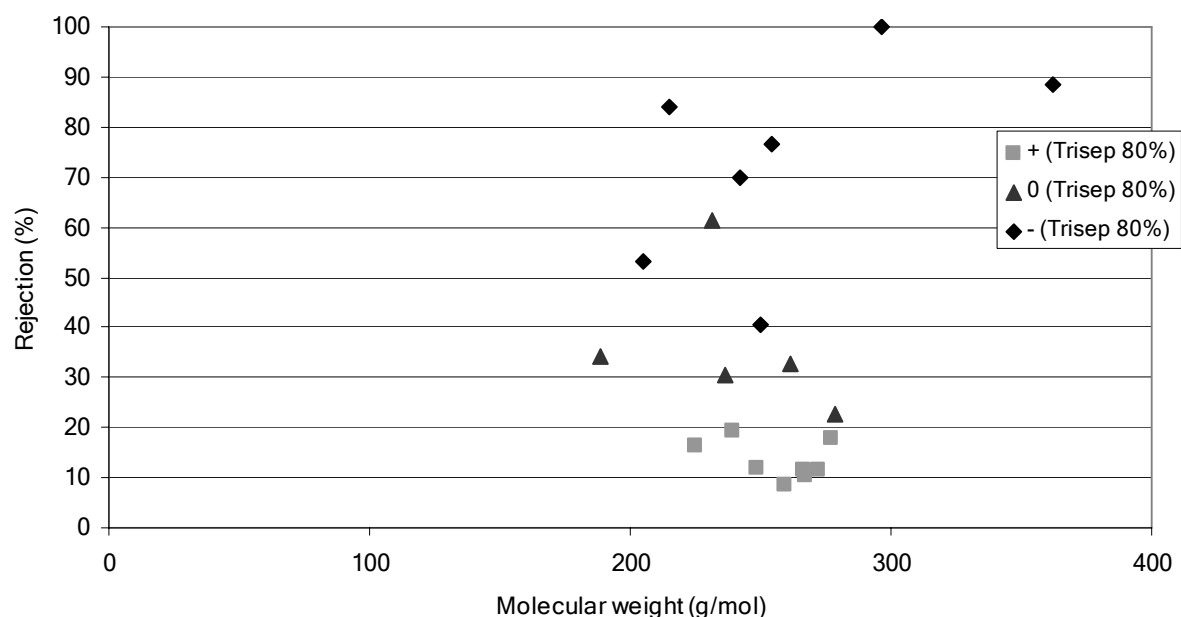


Figure 6.4 - Rejection versus molar mass for neutral (0) and positively (+) and negatively charged (-) pharmaceuticals for Trisep TS-80 membrane at 80% recovery in Schie water

Removal by adsorption on the GAC is high (> 98%) for all pharmaceuticals, even with the short empty bed contact time used (3 minutes). This is partly due to the use of freshly regenerated activated carbon, which should have a high adsorption capacity anyway, but also to the removal of NOM in the NF step. In normal GAC operation, pharmaceuticals would experience significant competition with the background NOM in the surface water for adsorption onto the organic carbon. Since, in this case, the nanofiltration step removes most of the higher molecular weight NOM, less NOM is present in the feed water to compete with the pharmaceuticals for adsorption sites on the activated carbon. Moreover, since only lower molecular weight NOM passes through the NF and enter the GAC step, less pore blocking will occur in the activated carbon. It has been observed in the literature [6] that especially this pore blocking by large NOM molecules is responsible for lowering the adsorption capacity of the activated carbon for small organic pollutants.

It can also be mentioned that the removal efficiency with GAC is slightly lower for smaller positively charged solutes, compared to the other solutes: this is probably due to the higher GAC influent concentrations for these solutes, caused by their less efficient removal in the preceding NF step.

Figure 6.3 also demonstrates that overall removal is extremely high for the NF/GAC combination. Thus, the combination of processes provides a robust dual barrier for the selected pharmaceuticals: as mentioned before, more hydrophilic (polar) solutes are better removed than hydrophobic (nonpolar) solutes in nanofiltration, whereas hydrophobic solutes are preferentially adsorbed on the activated carbon. Thus, the combination of the two processes should be able to remove most of the newly emerging organic micropollutants, since the whole range of solute hydrophobicity, as well as charge, is covered.

Moreover, due to the removal of NOM in the NF step, not only is the removal efficiency for the pharmaceuticals on the GAC higher, but GAC lifetime can be considerably prolonged, theoretically even up to a factor of 100 [6]. This decreases regeneration costs considerably. It is also possible to use a very short empty-bed contact time (EBCT) which decreases investment costs for GAC filtration.

The rejection values of the volatile organic solutes TBA, MTBE, ETBE and TAME with the NF unit after the third and fourth day are schematically shown in Figure 6.5.

Removal of all solutes is extremely low. TBA and MTBE are not removed at all (MTBE removal <2%); ETBE and TAME are removed to a slight percentage, probably due to their slightly larger size (the molar masses of ETBE and TAME are 102 g/mol, those of TBA and MTBE are 74 g/mol and 88 g/mol, respectively).

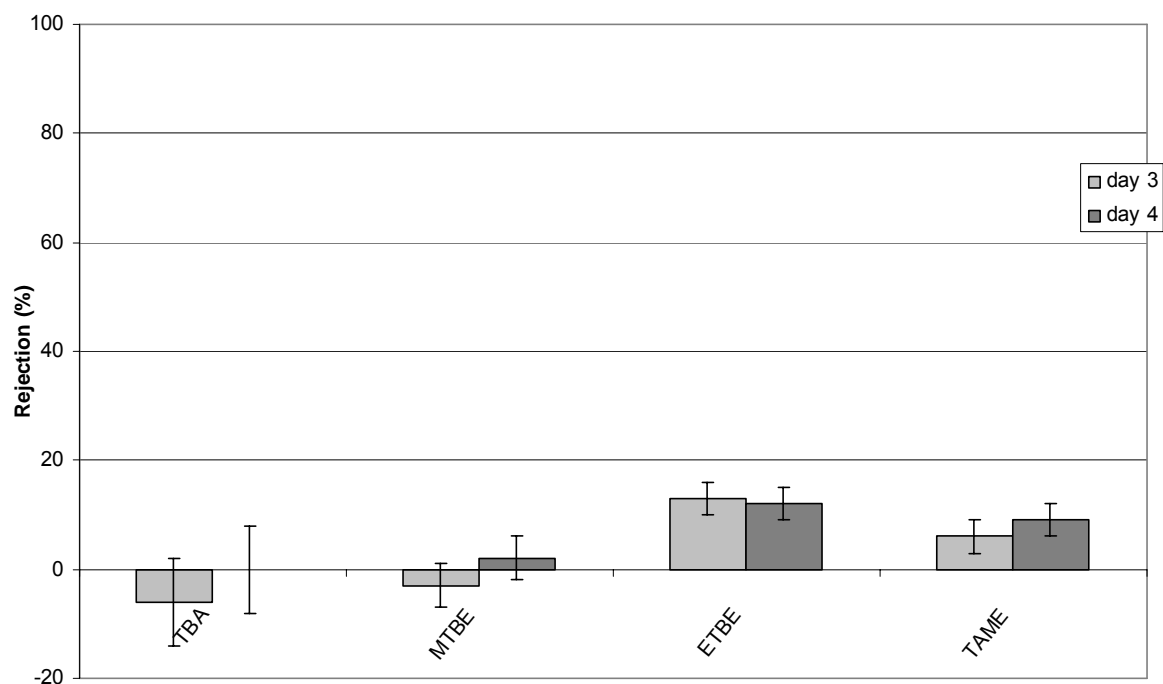


Figure 6.5 – Rejection of volatile organic micropollutants in Schie water for NF at 80% recovery

The observed rejection values are significantly lower than the values observed with the single membrane experiments at 10% recovery in Chapter 3. This is partly due to the higher recovery of the installation in this experiment, leading to a higher internal concentration and thus lower rejection values. However, 0% removal for MTBE indicates that the membrane does not remove MTBE at all in this study, whereas 94% removal was observed on a 4-inch spiral wound membrane at 10% recovery. This gigantic difference in rejection is not only due to the higher feed water recovery, but is also attributable to the difference in hydrodynamic conditions between the 2540-module used in these experiments, compared to the 4040-modules used in the experiments at 10% recovery, resulting in different concentration polarization conditions. Moreover, 2540 modules are still wrapped by hand, whereas 4040 modules are wrapped mechanically. This may lead to big quality differences between the different modules.

The removal of TBA, MTBE, ETBE and TAME on the granular activated carbon is shown as a function of time in Figure 6.6. After only 1 hour of filtration, a high concentration of TBA is already detected in the effluent of the carbon column. Apparently, almost no TBA is adsorbed during this short contact time experiment. The same holds, to a lower extent, for MTBE: after 1 hour of filtration, removal is already below optimal. After day 3 and day 4, MTBE removal has decreased to about 50%. The low removal of the hydrophilic TBA and MTBE could already be expected, based upon the literature [1,2]: adsorption of organic solutes onto activated carbon mainly occurs through hydrophobic interactions of the solute with the carbon. Therefore, hydrophilic solutes will be less preferentially removed by granular activated carbon than hydrophobic solutes.

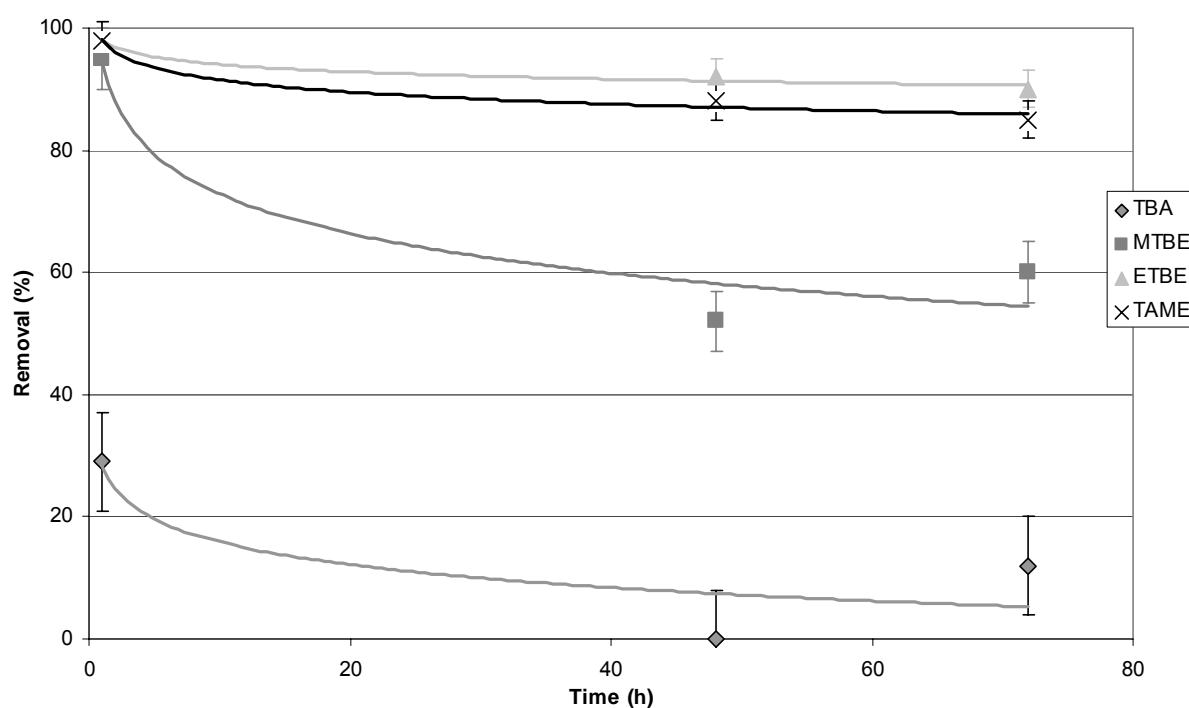


Figure 6.6 – Removal of volatile organic micropollutants for GAC filtration in Schie water pre-treated with NF at 80% recovery

For ETBE and TAME, removal is higher (and quite comparable), since both solutes are more hydrophobic than MTBE and TBA (expressed by their higher log  $K_{ow}$  (1.92 for ETBE and TAME, compared with 0.35 and 0.94 for TBA and MTBE, respectively).

## **4.2. Comparison of RO membranes and combination RO/GAC combination for removal of organic micropollutants from ground water**

The goal of this study was to compare four different RO membranes and select the one most suitable for the removal of organic micropollutants from a ground water source. Moreover, the combination of RO with subsequent activated carbon was investigated, since the combination yielded good results in the previous study and also in the literature [6].

### **4.2.1. Materials and methods**

#### *4.2.1.1. Ground water quality*

The ground water used for the RO experiments was sampled from the water treatment plant Engelse Werk (operated by the Dutch drinking water company Vitens) in Zwolle, the Netherlands. The ground water used for this study was pre-treated with rapid sand filtration (RSF) to remove the larger particles and part of the dissolved iron. Some general feed water quality parameters are summarized in Table 6.3.

For the activated carbon experiments, a batch of the permeate of the Hydranautics ESPA4 RO membrane was used as feed water. The water quality parameters of this water are also summarized in Table 6.3.

	Ground water pretreated with RSF	RO permeate
pH (-)	7.1	5.4
Dissolved Organic Carbon (DOC) (mg/l)	3	< 0.2
Conductivity ( $\mu$ S/cm)	633	11
Ca <sup>2+</sup> (mg/l)	78	<0.5
Mg <sup>2+</sup> (mg/l)	9.7	<0.1
Si (mg/l)	4.5	<0.5
K <sup>+</sup> (mg/l)	5	<1
Na <sup>+</sup> (mg/l)	50	2

Table 6.3 – Water quality parameters of Engelse Werk ground water in the feed and permeate of the RO (Trisep ACM5)

#### 4.2.1.2. *Equipment and filtration protocol*

The 4-inch, single spiral wound membrane element filtration set-up and protocol for the RO experiments was already described in Chapter 2. All experiments were carried out in a recycle mode with a single batch of water, with both permeate and concentrate recycled back into the feed reservoir.

Membrane filtration experiments were carried out at a constant cross-flow velocity of 0.2 m/s (which corresponds to a feed flow of 1500 l/h and a concentration polarization factor of 1.07) and at a constant recovery of approximately 10%. Transmembrane pressure and temperature were set to approximately 5 bar and 20  $\pm$  1°C, respectively. Feed, permeate and concentrate samples were taken after 4 days of filtration (which should be sufficient to reach adsorption equilibrium and ensure that steady-state rejection values are obtained) and analyzed for organic micropollutants.

The granular activated carbon column was 1m in height and had an inner diameter of 35mm. The column contained approximately 0.7L of carbon. The column was fed with a batch of RO permeate from a stainless steel tank and the empty bed contact time of the column was set to 3 minutes. Samples of feed and effluent of the column



were taken after treatment of 1200 bed volumes to see whether breakthrough of some micropollutants could already be observed after this time period.

#### 4.2.1.3. RO membranes and activated carbon

The membranes used in this study were all commercially available reverse osmosis membranes: Trisep X20 and ACM5 (Trisep Corp., Goleta CA, USA) and Hydranautics ESPA1 and ESPA4 (Nitto-Denko/Hydranautics, Oceanside CA, USA). All membranes are thin film composite membranes with an aromatic polyamide top layer. Before use, all membranes were rinsed with Milli-Q water for two hours in order to remove preservation liquids present in the membranes. Afterwards, the membranes were characterized for pure water permeability with Milli-Q water and for NaCl rejection with a 1500 ppm NaCl solution in Milli-Q water. Membrane properties are summarized in Table 6.4.

Membrane	Pure water permeability (m/(s.bar))	Contact angle (°)	% NaCl rejection	Zeta-potential at pH 7 (mV)
Trisep ACM5	$1.4 \times 10^{-6}$	35	98.5%	-20
Trisep X20	$9.9 \times 10^{-7}$	43	99.5%	-10
Hydr. ESPA1	$1.5 \times 10^{-6}$	25	99.3%	-27
Hydr. ESPA4	$2.1 \times 10^{-6}$	70	99.0%	n.d.

Table 6.4 – Membrane properties for selected membranes for comparison of organic micropollutant rejection (n.d.: not determined) [7-10]

Membrane contact angles were determined using the sessile drop method. The Zeta potentials were measured in a background solution containing 10 mM NaCl and 1 mM NaHCO<sub>3</sub>. Membranes with different membrane properties (especially with

different energy demands (pure water permeabilities)) were chosen, to be able to select the most suitable membrane for the application, based on both energy demand and organic micropollutant removal. Single 4-inch (4040) spiral wound elements were used.

The granular activated carbon was supplied by Norit Nederland B.V. (Amersfoort, the Netherlands). The properties of the carbon were already described before (Paragraph 6A.1.1.3).

#### *4.2.1.4. Selected organic pollutants and analysis*

The spiked organic pollutants were selected for two main reasons. Firstly, some emerging micropollutants, already occurring in Dutch surface- and ground waters were chosen. Examples include glyphosate, carbendazim, bentazon and MTBE. Since the dosing tests were carried out for a drinking water utility, assessment of the removal of problematic substances from the source waters was a necessity. Secondly, other organic solutes were also dosed, and these were mainly selected for their different physico-chemical properties. In the previous chapters, it was shown that solute charge, solute hydrophobicity and solute size may all have an influence on solute rejection by NF/RO treatment. Therefore, solutes were divided in different categories of increasing hydrophobicity (expressed as  $\log K_{ow}$ ). Within each category of hydrophobicity, different solutes were chosen with increasing size (expressed as molar mass). Moreover, some charged solutes (positively, as well as negatively charged) were included.

Table 6.5 summarizes the physico-chemical properties of the organic micropollutants and the concentrations in which they were spiked in the different source waters. All

micropollutants were dosed in concentrations that were 200 times higher than the limit of quantitation (LOQ) of the respective analysis method for that pollutant. 99.5% removal could thus be quantified.

Compound	MW (g/mol)	log Kow (-)	Charge at pH	C <sub>feed</sub> initial (µg/l)	C <sub>feed</sub> 4 days (µg/l)	analysis
NDMA	74	-0.57	neutral	0.2	0.2	A
1,4-dioxaan	88	-0.27	neutral	2000	1650	B
NMOR	116	-0.44	neutral	0.2	0.2	A
diglyme	134	-0.36	neutral	30	26	C
glyphosaat	169	-4.00	-	10	1.3	D
triglyme	178	-0.76	neutral	50	40	C
caffeine	194	-0.07	neutral	10	13.5	E
TBA	74	0.35	neutral	20000	7150	B
MTBE	88	0.94	neutral	10	0.05	B
fenazon	188	0.38	neutral	2	2.2	D
metamitron	202	0.83	neutral	10	9.7	E
terbutaline	225	0.90	+	2	1.4	D
sulfamethoxazol	253	0.89	neutral	2	1.9	D
sotalol	272	0.24	+	2	1.8	D
pentoxifylline	278	0.29	neutral	2	3.0	D
ETBE	102	1.92	neutral	10	<0.05	B
TAME	102	1.92	neutral	20	<0.05	B
2,4-dinitrophenol	184	1.67	-	20	19.5	B
carbendazim	191	1.52	neutral / +	3	2.9	E
monuron	199	1.94	neutral	10	5.7	F
metribuzin	214	1.70	neutral	10	10	F
metoxuron	229	1.64	neutral	10	10	F
pirimicarb	238	1.70	neutral	10	11	F
bisphenol-S	250	1.65	neutral	10	9.5	G
metoprolol	267	1.88	+	2	1.9	D
TCEP	285	1.44	neutral	10	<0.1	F
benzeen	78	2.13	neutral	100	<0.1	B
isoproturon	206	2.87	neutral	10	10.5	E
chlorotoluron	213	2.41	neutral	10	6.5	E
atrazine	216	2.61	neutral	10	11	E
diethylftalaat	222	2.42	neutral	100	<0.5	F
diuron	233	2.68	neutral	10	3.7	E
carbamazepine	236	2.45	neutral	2	2.5	D
bentazon	240	2.34	neutral	10	11.5	E
metobromuron	259	2.38	neutral	10	2	E
dimethenamide	276	2.15	neutral	5	5.2	E
ethylbenzeen	106	3.15	neutral	40	<0.2	B
naphtalene	128	3.30	neutral	50	<0.2	B
2-methylisoborneol	168	3.31	neutral	50	10.5	B
ibuprofen	206	3.97	-	2	2.2	D
mecoprop (MCP)	215	3.13	-	10	14.5	E
Bisphenol-A	228	3.32	neutral	2	2.1	G
linuron	249	3.20	neutral	10	1.8	E
oestron	270	3.13	neutral	2	1.7	G
dibutylftalaat	278	4.50	neutral	100	<0.5	F
diclofenac	296	4.51	-	2	1.9	D
bezafibraat	361	4.25	-	2	1.7	D

Table 6.5 – Physico-chemical characteristics, initial feed concentrations and concentrations after 4 days of recirculation in RO experiment for selected organic micropollutants (n.a.: not applicable)

All chemicals were obtained from Sigma-Aldrich (St Louis MO, USA), except for phenazone, ibuprofen, aminopyrine, carbamazepine and cyclophosphamide, which were obtained from Acros Organics (Geel, Belgium). All chemicals were at least reagent grade.

The cocktail of organic micropollutants was prepared as a concentrated stock in 10L of Milli-Q water. In order to prevent co-solvent effects and possible problems with biological growth in the system, no methanol was used to facilitate dissolution of the pharmaceuticals. For the RO rejection experiments, the desired volume of this stock solution was then added to the feed tank, containing the Engelse Werk ground water. For the activated carbon experiments, the desired volume of the stock solution was added to a tank containing 750L of RO permeate (the RO permeate did not contain any residuals of trace organic contaminants).

The analysis method used to determine solute concentration is mentioned in Table 6.5 for each separate solute. The corresponding codes are:

- A double-layer solid phase extraction (SPE) on reverse phased C18 and PAC followed by large volume injection (LVI) gas chromatography/chemical ionisation (GC/CI) with mass spectrometric detection (MS)
- B purge & trap GC/MS
- C direct injection on high-performance liquid chromatograph with electrospray ionisation (HPLC/ESI), with tandem mass spectrometric detection (MS-MS)
- D SPE on styrene-divinylbenzene (SDB) material at pH 3, followed by HPLC-MS-MS
- E SPE on RP-C18, followed by HPLC-ESI-MS-MS

F SPE on RP-C18, followed by GC-MS

G SPE on RP-C18, followed by derivation (silylation) and GC/MS

Since all micropollutants were dosed in concentrations that were 200 times higher than the limit of quantitation (LOQ), the limit of quantitation (LOQ) for each solute can be found from Table 6.5 by dividing the initial feed concentrations by a factor 200. More information on the analytical protocol can be found in [11].

#### 4.2.2. Results and discussion

Rejection values of the selected organic solutes for the reverse osmosis experiments are shown in Figures 6.7 and 6.8 for the Trisep and Hydranautics RO membranes, respectively. The rejection values of some solutes (e.g. dibutylphthalate) could not be determined on any of the membranes, due to the low feed concentrations on the fourth day. Table 6.5 compares the initial feed concentrations of all solutes to the feed concentrations on the fourth day. It is apparent that almost all feed concentrations are decreasing. This is partly due to the volatilisation of some volatile solutes (e.g. MTBE, TBA), but is mainly due to the adsorption of the solutes on the membrane polymer matrix. Adsorption on other test unit parts is ruled out, since almost all test parts were made out of stainless steel.

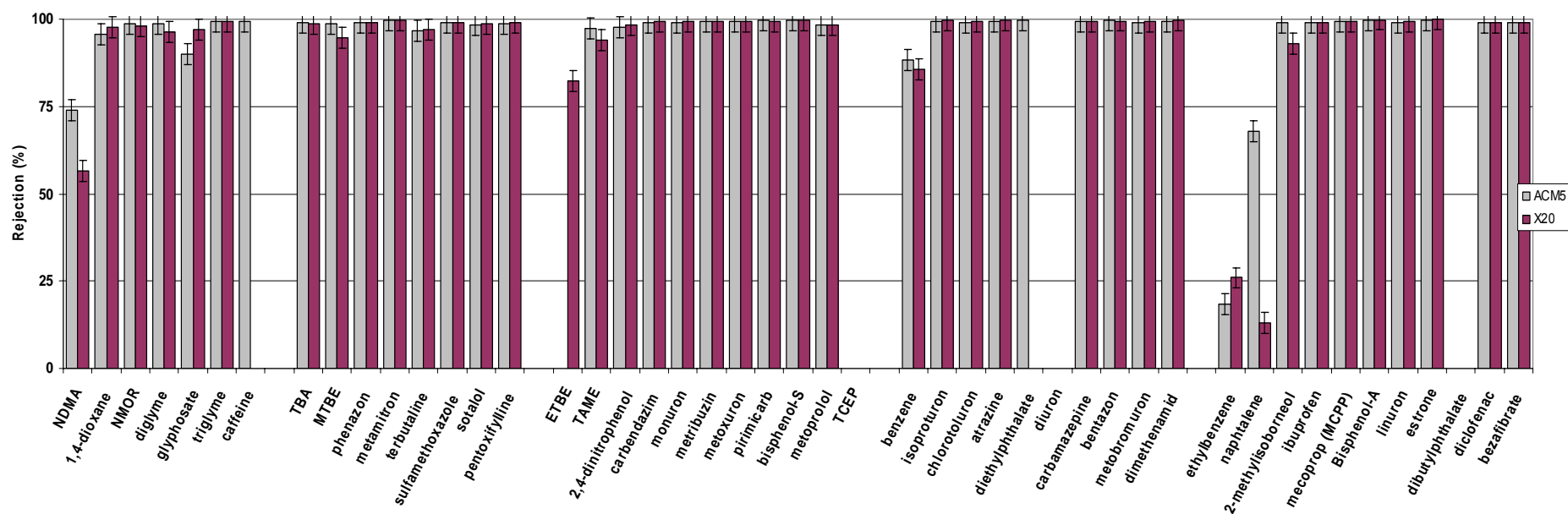


Figure 6.7 – Rejection values of selected organic micropollutants in Engelse Werk groundwater for Trisep RO membranes

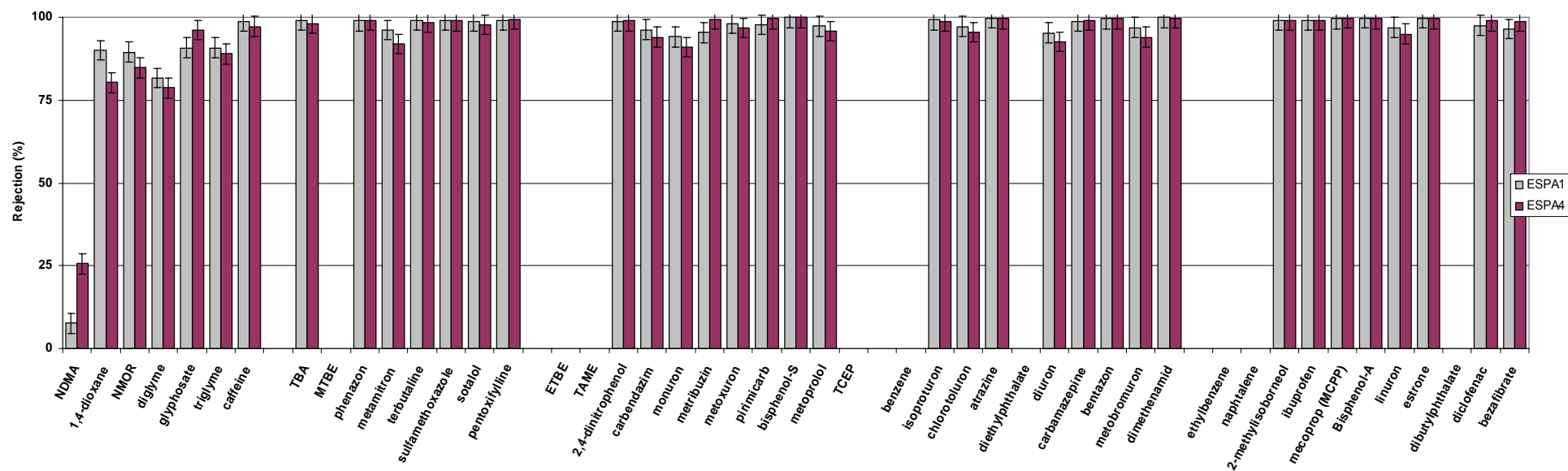


Figure 6.8 – Rejection values of selected organic micropollutants in Engelse Werk groundwater for Hydranautics RO membranes

Rejection values for the solutes in Figures 6.7 and 6.8 are summarized in categories in the order of increasing hydrophobicity. Within these categories, the solutes are shown as a function of increasing molar mass. It is apparent that for almost all solutes on all membranes in Figures 6.7 and 6.8, rejection values are very high (> 95%). However, some solutes do show low rejection, and this low rejection of these solutes is consistent for all four membranes. Especially the removal of NDMA seems to be extremely low. This is probably due to the very small size of NDMA, compared to the other molecules (the molar mass is 74 g/mol, but NDMA also has a very compact structure).

For both Trisep membranes (X20 and ACM5), the removal of the hydrophobic solutes ethylbenzene and naphthalene is very low, even though these solutes are larger than, for example, NDMA. This is probably due to hydrophobic interactions of these solutes with the hydrophobic membrane matrices, resulting in an increased partitioning of these solutes into the membranes and thus an increased transport through the membranes.

Upon comparison between the four membranes, it is apparent that the rejection values for most solutes are higher with the Trisep membranes than with the ESPA membranes. Both ESPA membranes probably have larger pore sizes than the Trisep membranes (apparent from the higher pure water permeabilities, pure water permeability is a linear function of membrane pore size).

In general, rejection values of the selected organic solutes are higher with the ESPA1 membrane than with the ESPA4 membrane. Even though the differences are only marginal on this small-scale units, differences will become bigger in full-scale plants operating at higher recovery.



Comparing rejection values between the two Trisep membranes, it is interesting to notice that rejection values are slightly higher for most solutes on the ACM5 membrane than on the X20 membrane, even though the ACM5 has a higher pure water permeability and thus probably a slightly larger pore size. The reason for this difference in rejection is probably the higher hydrophobicity of the X20 membrane (as shown in the contact angle measurements). The ACM5 membrane is more hydrophilic, which results in an increased transport of water and thus higher fluxes of this element at similar feed pressures, but also results in a decrease of hydrophobic interactions between hydrophobic solutes and the membrane matrix. This results in increased rejection values for hydrophobic solutes. The higher rejection value for the hydrophilic solute NDMA with the ACM5 membrane, compared to the X20 membrane is more difficult to explain. One possible explanation might again lie in the hydrophilic character of the ACM5 membrane. Due to the hydrophilic character and thus the high water flux through this membrane, most pores of the membrane will be filled with water molecules that are attached to the walls of the pores, hereby diminishing the space available for organic solute transport through these pores. Since the X20 is more hydrophobic, the water molecules will be less firmly attached to the walls of the pores, and the effective pore size will thus be bigger than for the ACM5.

Based on the results shown above, and by comparing the energy demands for all membranes, it is apparent that the Trisep ACM5 shows the most potential for use in a full-scale plant, due to its high removal capacity for organic micropollutants, in combination with its low energy demand.

Based on the rejection values obtained on the single ACM5 membrane element in the laboratory-scale unit, some rough estimations are made for a full-scale

installation, operating at 75% recovery. These rough estimations are based on the full-scale rejection model that was introduced in Chapter 4, but are probably a slight overestimation of the rejection of the full-scale plant, since the flux-dependency of the rejection was not incorporated in the calculation here. Table 6.6 summarizes the rejection values obtained on the single ACM5 element, and the rough predictions for the rejection in a full-scale plant.

It can be seen that the rejection of the positively charged pharmaceuticals terbutaline and sotalol is lower than expected, based on their size. This is again due to the presence of charge attraction with the negatively charged membrane surface, and thus an increased concentration at the membrane surface, resulting in a lower observed rejection.

Also the rejection value of glyphosate is lower than expected. Glyphosate is a very polar molecule that has several polar functional groups (positively, as well as negatively charged). At pH 7, there is a high positive charge density in the middle of the molecule, leading to a very high dipole moment (6.7 Debye) in the molecule and charge attraction towards the negatively charged membrane surface. Moreover, since glycerol is a stretched molecule, steric hindrance is also lower and glycerol permeates through the membrane quite easily.

Compound	Rejection at 10% recovery ( $\pm 2\%$ )	Estimated rejection at 75% recovery (%)
NDMA	74	63
1,4-dioxaan	96	94
NMOR	99	98
diglyme	99	98
glyphosaat	90	85
triglyme	99	98
caffeine	99	98
TBA	99	98
MTBE	99	98
fenazon	99	98
metamitron	100	100
terbutaline	97	95
sulfamethoxazol	99	98
sotalol	98	97
pentoxifylline	99	98
ETBE	n.d.	n.d.
TAME	97	95
2,4-dinitrophenol	98	97
carbendazim	99	98
monuron	99	98
metribuzin	99	98
metoxuron	99	98
pirimicarb	100	100
bisphenol-S	100	100
metoprolol	99	98
TCEP	n.d.	n.d.
benzeen	88	82
isoproturon	99	98
chlorotoluron	99	98
atrazine	99	98
diethylftalaat	100	100
diuron	n.d.	n.d.
carbamazepine	99	98
bentazon	100	100
metobromuron	99	98
dimethenamide	99	98
ethylbenzeen	18	10
naphtalene	68	56
2-methylisoborneol	99	98
ibuprofen	99	98
mecoprop (MCP)	99	98
Bisphenol-A	100	100
linuron	99	98
oestron	100	100
dibutylftalaat	n.d.	n.d.
diclofenac	99	98
bezafibraat	99	98

Table 6.6 – Rejection values for selected organic micropollutants on Trisep ACM5 membrane at 10% recovery and estimations for rejection values in full-scale installation operating at 75% recovery (n.d.: not determined)

It is apparent that the ACM5 element performs extremely well in organic micropollutant removal applications: except for NDMA, most problem organic pollutants (e.g. the pesticides diglyme, triglyme, atrazine, metamiltron, bentazon and glyphosate and the pharmaceuticals phenazon, carbamazepine and ibuprofen) are expected to be removed for more than 90%. However, 90% removal is still not complete removal, and a subsequent activated carbon filtration step might still be useful as polishing filter.

The removal of the selected organic pollutants after the treatment of 1200 bed volumes on the GAC column is schematically depicted in Figure 6.9. It is apparent that, even with the low contact times used, removal of most micropollutants is extremely high (> 95%). However, removal of some pollutants, such as NDMA; 1,4-dioxane and 2-methylisoborneol (2-MIB) is more problematic.

For NDMA and 1,4-dioxane, this low removal could be expected, due to the small size and the hydrophilic character of these substances. Moreover, NDMA, which was dosed in extremely low concentrations (200 ng/l), experienced significant competition from the other organic pollutants, which were dosed in much higher concentrations.

For 2-MIB, however, no breakthrough of the solute through the column was expected. 2-MIB is very hydrophobic, and since GAC adsorption occurs through hydrophobic Van der Waals interactions, a high removal was expected. Especially the small size of the molecule should make it easy for this molecule to diffuse into the small micropores of the carbon, where it should adsorb readily. Maybe the short contact time of 3 minutes is not enough to allow this pore-diffusion for 2-MIB. As was shown before, it can again be noted here that  $\log K_{ow}$  is not always the most suitable parameter to describe hydrophobic interactions.

Despite the low removal for NDMA; 1,4-dioxane and 2-MIB, no breakthrough of any other substance through the column is observed. As for the previous experiments, this is partly due to the freshly regenerated carbon, which should have a high adsorption capacity anyway. However, 1200 bed volumes have already been treated, so the carbon capacity will already be lower than for freshly regenerated carbon. The removal capacity of the carbon is also high, because of the removal of NOM which would normally compete with the organic micropollutants for adsorption sites on the carbon, in the reverse osmosis step. This NOM removal not only diminishes the competition between NOM and the micropollutants for adsorption sites on the activated carbon, but also reduces the carbon pore blocking by large NOM molecules [6]. As was mentioned before, pore blocking is one of the main mechanisms that causes a reduction in adsorption capacity of granular activated carbon. Again, as a consequence of the NOM removal in the RO process, short empty bed contact times can be used for the GAC, or the time before regeneration of the column can be extended. This reduces investment costs for the GAC considerably.

In conclusion, it can be said that the combination of reverse osmosis with subsequent granular activated carbon filtration will result in very high removal capacities for organic micropollutants. The only problematic substances will be the very small, polar solutes: these are not removed by the GAC, because of their polar character, and if they are small enough (e.g. NDMA), their removal efficiency with reverse osmosis will also be low.

Figure 6.9 also shows the combined removal efficiency for organic micropollutants of the best performing RO membrane (Trisep ACM5) and the subsequent activated carbon filter. Removal efficiency for all solutes is extremely high, except for the

smallest hydrophilic solutes (NDMA and 1,4-dioxane). Fortunately, however, the concentrations of these two pollutants in Dutch ground- and surface waters are still low, and thus a low removal efficiency is not yet problematic.

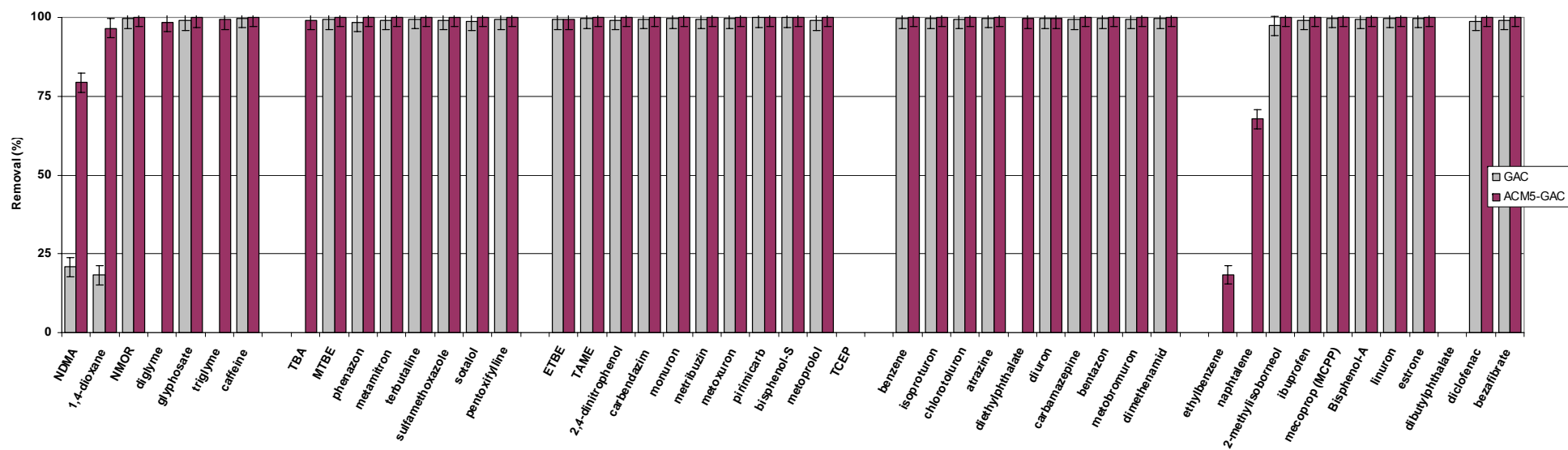


Figure 6.9 – Removal efficiency of selected organic micropollutants for GAC filtration and total removal efficiency with Trisep ACM5/GAC combination for Engelse Werk ground water

## Chapter 6B: Rejection performance of newly developed thin film nanocomposite reverse osmosis membranes for organic solutes in aqueous solutions

Nanofiltration and reverse osmosis have become wide-spread technologies over the last decades and are already extensively used in water treatment processes all over the world, mainly for desalination applications. However, they still remain relatively energy-intensive processes and no significant improvements in their energy-demand have been made recently. For the last 30 years, NF and RO membranes have been manufactured as thin-film composite membranes, mainly with polyamide top layers on polysulfone supports. Even though water flux and solute rejection of these membranes have continuously improved over the last decades, there is a growing need for new, more selective, more energy-efficient and less fouling-prone membranes, especially in seawater desalination applications.

The use of nanotechnology has led to new and exciting innovations, which can also be introduced in water treatment processes. Recently, researchers at the University of California in Los Angeles succeeded in incorporating super-hydrophilic, negatively charged NaA zeolite particles in the top layer of hand-cast thin film composite membranes, herewith almost doubling the pure water permeability of these membranes, while maintaining a high salt rejection capacity.

The inclusion of the zeolite particles causes a significant decrease in membrane surface hydrophobicity, which not only increases the permeate flux through the membranes, but which should also result in improved fouling resistance. For this study, the decrease in hydrophobicity might be important, since it might affect



hydrophobic solute rejection. The less hydrophobic the membrane surface, the less likely that hydrophobic interactions and partitioning into the membrane matrix will occur for hydrophobic solutes.

This study will focus on the rejection properties of the newly developed “thin film nanocomposite” (TFN) membranes for organic solutes, in comparison with a more traditional hand-cast thin film composite (TFC) membrane and a commercially available RO membrane. Rejection of hydrophobic, hydrophilic and charged solutes will be compared on all three membranes.

This study will therefore assess whether the improved permeability for the TFN membranes also leads to a reduction in organic solute separation performance (or an increased in rejection performance for hydrophobic solutes).

## **6B.1. Materials and methods**

### **6B.1.1. Equipment and filtration protocol**

The filtration equipment used in these rejection experiments was already described before (Paragraph 2.1, Chapter 5). The membranes, with an active membrane area of 140 cm<sup>2</sup>, were accommodated in a flat sheet cross-flow membrane cell (Sepa CF II, GE Osmonics, Fairfield CT, USA). Applied transmembrane pressure was regulated using a needle valve in the concentrate stream, with transmembrane pressure measured with a precision manometer (Wika fein-druckmessgerät).

Membrane filtration experiments were carried out at a constant cross-flow velocity of 0.2 m/s (corresponding to a feed flow of  $\pm$  60 l/h) and at a constant feed pressure of

20 bar. The cross-flow velocity of 0.2 m/s corresponds to cross-flow velocities used in full-scale nanofiltration plants. Feed water temperature was set to  $20 \pm 1^\circ\text{C}$ . All experiments were carried out in recycle mode with a single batch of water, with both permeate and concentrate recycled back into the feed reservoir.

Again, since adsorption of solutes onto the membrane surface, and sorption into the inner membrane structure, may influence measured rejection values, an accurate evaluation of the rejection of a given solute is not possible until saturation of the membrane with the solute of interest is accomplished [12]. In Paragraph 4.1 in Chapter 2, it was shown that an equilibration period of 4 days should be adequate to accomplish saturation and ensure that steady state rejection values are obtained at organic solute levels of  $2\text{ }\mu\text{g/l}$ . In this study, higher levels of organic solutes ( $20\text{ mg/l}$ ) were used. It was assumed that at these high concentration levels and with the limited amount of membrane surface area available, equilibrium would be reached faster. Rejection experiments were therefore carried out for 24 hours, and it is assumed that this time period is long enough to ensure that the final rejection values measured are not biased by an incomplete adsorption/saturation (this assumption was validated by Kimura et al. [12], who indicated that adsorption on the Sepa-cell set-up reached equilibrium after 24h for organic solutes at concentrations of  $200\text{ }\mu\text{g/l}$ . They also indicated that adsorption would be reached even faster for higher concentrations of organic solutes).

#### 6B.1.2. Membranes

Three different membranes were compared in this study. The first membrane was a commercially available reverse osmosis membrane with a thin-film polyamide top

layer (XLE, Dow-Filmtec). The second membrane was a thin-film composite membrane (TFC), handcast on a pre-formed polysulfone ultrafiltration (UF) membrane through interfacial polymerisation. The third membrane was made in a similar way as the the second membrane, but synthesized zeolite A particles were included in the top layer. More information on the formation of the TFC and TFN membranes was published before by Jeong et al. [13].

For the rejection experiments, flat sheet membrane specimens with an active membrane area of 140 cm<sup>2</sup> were used.

Before use, all membranes were rinsed with Milli-Q water for 24 hours at 20 bar to compact the membranes before the rejection experiments and remove preservation liquids present in the membrane. Afterwards, the membranes were characterized for pure water permeability with Milli-Q water and for MgSO<sub>4</sub> rejection with a 500 ppm MgSO<sub>4</sub> solution in Milli-Q water. Membrane properties are summarized in Table 6.7.

Membrane	Pure water permeability (m/(s.bar))	Contact angle (°)	% MgSO <sub>4</sub> -rejection	Zeta-potential at pH 7 (mV)
Dow-Filmtec XLE	$1.9 \times 10^{-6}$	$48 \pm 3$	95%	$-3 \pm 2$
TFC	$0.8 \times 10^{-6}$	$78 \pm 3$	90%	$-4 \pm 3$
TFN	$1.1 \times 10^{-6}$	$67 \pm 3$	88%	$-12 \pm 3$

Table 6.7 – Membrane properties of hand-cast and commercial membranes (n.d.: not determined)

According to the membrane manufacturer, the molecular weight cut-off (MWCO) for the XLE membrane is 100 g/mol. For the TFC and TFN membranes, no MWCO was determined.

Membrane zeta-potentials were determined in a background solution containing 10 mM KCl using commercially available streaming potential/current equipment

(SurPASS, Anton Paar, Graz, Austria). Membrane hydrophobicity was characterised by sessile drop contact angle measurements with Milli-Q water, using commercial contact angle measuring equipment and drop shape analysis software (Krüss, Hamburg, Germany). In order to minimise interference of surface morphology on the contact angle, at least 15 different measurements on 3 different places on each membrane sample were performed and the average of the measurements was taken. Membrane samples were dried during 24h in a dessicator before measuring contact angles.

### 6B.1.3. Solutes and analysis

Three different solutes were chosen for the rejection experiments: one hydrophobic, one hydrophilic and one negatively charged solute. This allows for comparison of the different membranes and their rejection mechanisms for organic solutes. The solutes and their physico-chemical properties are shown in Table 6.8.

	MW (g/mol)	log K <sub>ow</sub> (-)	pK <sub>a</sub> (-)
2-ethoxyethanol	90.1	-0.32	n.a.
dichlorobenzene	147.1	3.3	n.a.
oxalic acid	90.0	-2.22	pK <sub>a1</sub> = 1.27 ; pK <sub>a2</sub> = 4.28

Table 6.8 – Physico-chemical characteristics of selected organic solutes for rejection experiments (n.a.: not applicable)

All solutes were spiked separately in Milli-Q water and measured by analyzing the non-purgeable organic carbon (NPOC ~ total organic carbon (TOC)) -content of feed and permeate. The limit of detection for the NPOC-analysis is 0.2 mg/l. Therefore, all

solutes were spiked in concentrations of 20 mg carbon/l, in order to be able to measure at least 99% rejection (which corresponds to a permeate concentration of 0.2 mg/l). Duplicate feed, permeate and concentrate samples were taken and analysed after one hour and again after 24h of filtration. Comparison of the feed concentrations of the organic solutes after 1h and 24h, respectively, enables to study adsorption of the organic solutes onto the membranes.

## 6B.2. Results and discussion

The rejection values for the hydrophilic organic solute (2-ethoxyethanol) are summarized in Figure 6.10 for all three membranes, together with the feed concentrations at the beginning and end of the experiments.

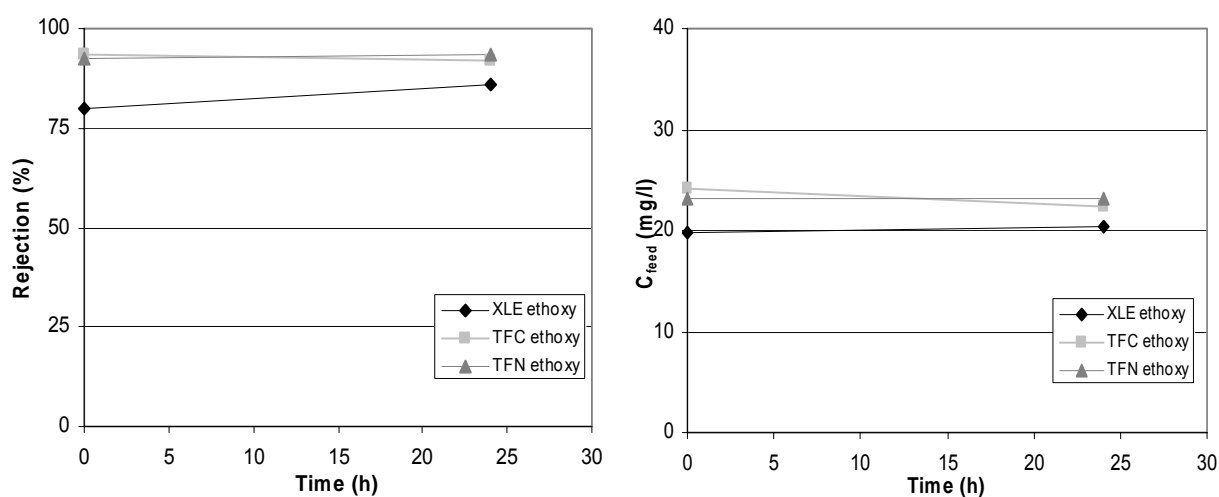


Figure 6.10 – Rejection values and feed concentrations for rejection experiments with 2-ethoxyethanol on XLE, TFC and TFN membranes

The rejection values for the solute on all membranes are relatively constant, and so are the feed concentrations. No significant adsorption of the hydrophilic solute on the

membrane matrix seems to occur. Rejection for 2-ethoxyethanol on the TFC and TFN membranes is quite comparable and is significantly higher than for the XLE membrane. This is probably due to the smaller pore sizes (and thus the increased steric hindrance) of both hand-cast membranes. A smaller pore size is expected for the hand-cast membranes, since their pure water permeabilities are lower. Even though the pure water permeability is higher for the TFN membrane, compared to the TFC membrane, the rejection of the hydrophilic solute 2-ethoxyethanol is equally high on both membranes. This is probably due to the more hydrophilic character of the TFN membrane, which leads to an increased friction due to the presence of more water molecules in the membrane pores, and thus an increased steric hindrance and higher rejection. This hypothesis was already formulated in Paragraph 6A.2.2.

For the negatively charged organic acid (oxalic acid), rejection values are also higher on the TFC and TFN membranes, compared to the commercial XLE membrane (Figure 6.11).

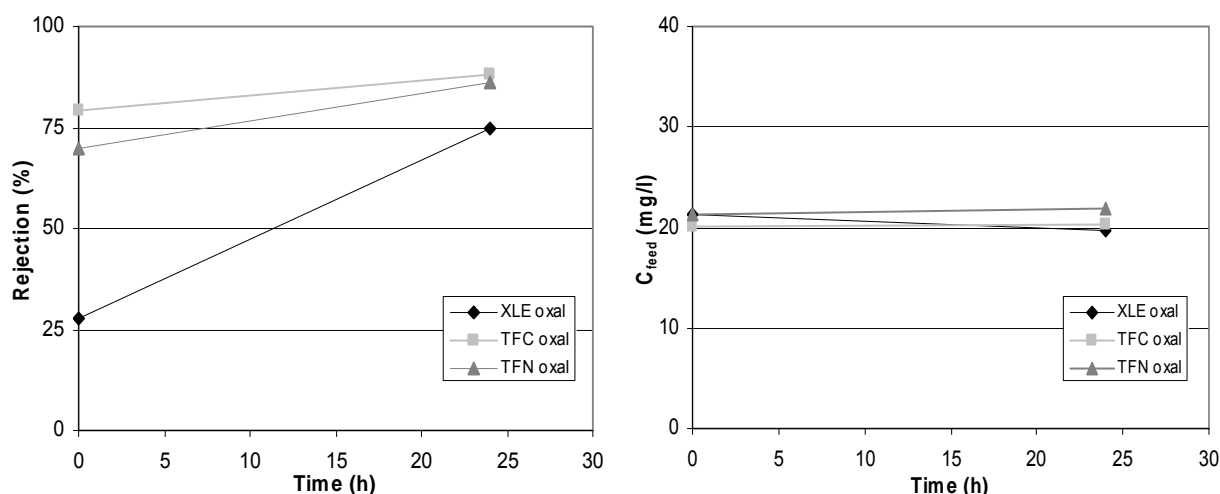


Figure 6.11 – Rejection values and feed concentrations for rejection experiments with oxalic acid on XLE, TFC and TFN membranes

This is mainly due to the more negative surface charge of both hand-cast membranes, resulting in more electrostatic repulsion with the negatively charged organic acid, and thus an increased rejection. Again, even though the TFN membrane has a higher pure water permeability, the rejection of oxalic acid at 24h is comparable to the TFC membrane rejection. This is probably due to the increased negative surface charge of the TFN membrane by the inclusion of the negatively charged zeolite particles. The feed concentration of the organic acid is stable for all 3 membranes, indicating that no adsorption of the acid on the membrane surface is occurring.

For the hydrophobic solute, dichlorobenzene, the picture is completely different. The highest rejection value here is observed for the XLE membrane. This is probably due to the lower contact angle (and thus the more hydrophilic surface) of the XLE membrane, compared to the other two membranes, resulting in less hydrophobic interactions of the hydrophobic solute with the XLE membrane, and thus an increased rejection.

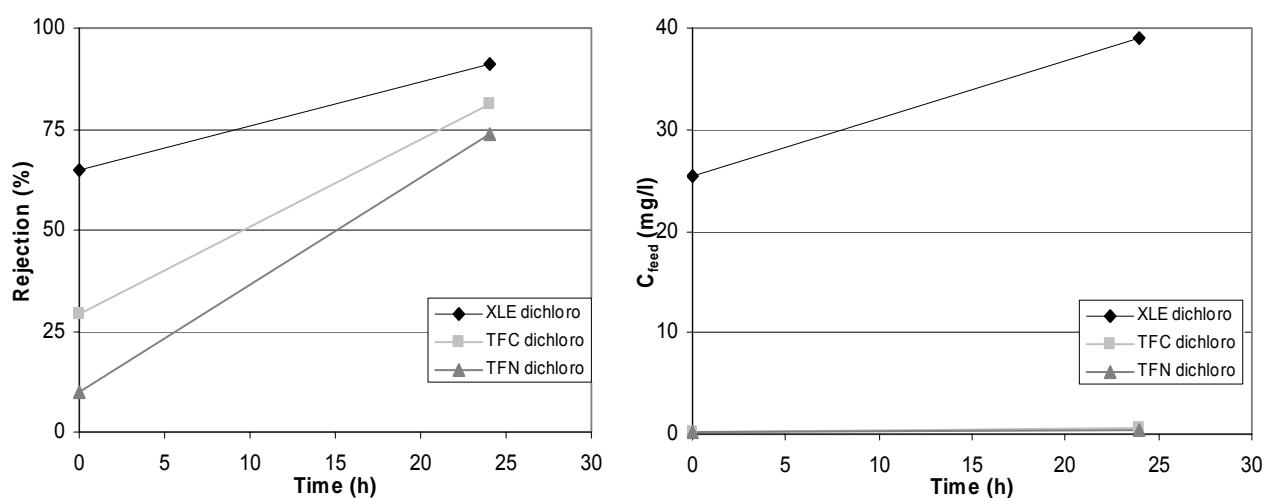


Figure 6.12 – Rejection values and feed concentrations for rejection experiments with dichlorobenzene on XLE, TFC and TFN membranes

When comparing rejection values on the TFC and TFN membranes, it is obvious that the rejection of the hydrophobic solute is slightly lower on the TFN membrane, even though it is more hydrophilic. Apparently, the difference in hydrophobicity by the inclusion of hydrophilic zeolites (and thus the difference in hydrophobic interactions), is not big enough to cause a significant change in rejection for hydrophobic solutes.

When looking at the feed concentration levels, the feed concentration (measured as total organic carbon (TOC)) seems to increase in time for the experiment with the XLE membrane, and the feed concentrations of the experiments with the TFC and TFN membranes are significantly lower than for the XLE membrane. An explanation for the lower feed concentrations in the TFC and TFN experiments might be adsorption of the hydrophobic solute onto the membrane surfaces. The increasing carbon-concentrations for the experiment with the XLE membrane, however, are more difficult to explain. One hypothesis might be that dichlorobenzene reacts with and dissolves a small part of the XLE membrane. However, this hypothesis has to be confirmed by performing a more accurate characterisation of the membrane surface.

In conclusion, it can be said that, concerning rejection properties for organic solutes, the TFC and TFN membranes perform extremely well in comparison with the commercial membrane. Rejection values of hydrophilic and charged solutes are higher on both hand-cast membranes, only the rejection of the hydrophobic solute is slightly lower.

Comparing the hand-cast TFC with the TFN membrane, it can be concluded that the inclusion of zeolite nanoparticles only has a minor (negligible) negative influence on



the separation performance for organic solutes and salts, which is largely countered by the enormous increase in pure water permeability (40% higher than the TFC membrane). Therefore, it can be said that the construction of nanocomposite membranes opens up new opportunities for future RO applications.

## References

- [1] L. Li, P. A. Quinlivan and D.R.U. Knappe. Effects of activated carbon surface chemistry and pore structure on the adsorption of organic contaminants from aqueous solution. *Carbon*, 40 (2002) 2085.
- [2] J.C. Crittenden, S. Sanongraj, J.L. Bulloch, D.W. Hand, T.N. Rogers, T.F. Speth and M. Ulmer. Correlation of aqueous-phase adsorption isotherms. *Environmental Science and Technology*, 33 (1999) 2926.
- [3] C. Lipreau and A. Abrahamse. Influence of cations on fouling of ultrafiltration membranes by NOM. BTO report 2006.043 (2006), Kiwa Water Research, Nieuwegein, the Netherlands.
- [4] I. Bobeldijk. Identificatiecriteria voor GC-MS analyse van milieucontaminanten in verschillende matrices. KOA report 98.222 (1998), Kiwa Water Research, Nieuwegein, the Netherlands.
- [5] S. Chellam and J.S. Taylor. Simplified analysis of contaminant rejection during ground- and surface water nanofiltration under the information collection rule. *Water Research*, 35 (10) (2001) 2460.
- [6] S.G.J. Heijman and R. Hopman. Activated carbon filtration in drinking water production: model prediction and new concepts. *Colloids and Surfaces A: Physicochemical and Engineering Aspects*, 151 (1999) 303.
- [7] L.D. Nghiem. Removal of emerging trace organic contaminants by nanofiltration and reverse osmosis. Ph.D. thesis (2004), University of Wollongong, Australia.
- [8] A. Subramani and E.M.V. Hoek. Direct observation of initial microbial deposition onto reverse osmosis and nanofiltration membranes. *Journal of Membrane Science*, 319 (2008) 111.
- [9] Q. Li, Z. Xu and I. Pinnau. Fouling of reverse osmosis membranes by biopolymers in wastewater secondary effluent: role of membrane surface properties and initial permeate flux. *Journal of Membrane Science*, 290 (2007) 173.
- [10] P. Xu, J.E. Drewes, T.-U. Kim, C. Bellona and G. Amy. Effect of membrane fouling on transport of organic contaminants in NF/RO membrane applications. *Journal of Membrane Science*, 279 (2006) 165.
- [11] F. Sacher, F.T. Lange, H.-J. Brauch and I. Blankenhorn. Pharmaceuticals in groundwaters: analytical methods and results of a monitoring program in Baden-Württemberg, Germany. *Journal of Chromatography A*, 938 (2001) 199.

- [12] K. Kimura, G. Amy, J. Drewes and Y. Watanabe. Adsorption of hydrophobic compounds onto NF/RO membranes: an artifact leading to overestimation of rejection. *Journal of Membrane Science*, 221 (2003) 89.
- [13] B.-H. Jeong, E.M.V. Hoek, Y. Yan, A. Subramani, X. Huang, G. Hurwitz, A.K. Ghosh and A. Jawor. Interfacial polymerization of thin film nanocomposites: A new concept for reverse osmosis membranes. *Journal of Membrane Science*, 294 (2007) 1.

# **Chapter 7:**

## **General conclusions and recommendations for future research**

## 1. General conclusions

One of the objectives of this study was to assess whether high pressure membrane filtration (NF/RO) was a good water treatment technique for the removal of organic micropollutants.

One membrane property often provided by membrane manufacturers is the Molecular Weight Cut-Off (MWCO) value: the MWCO of a membrane is equal to the molar mass of a certain organic solute that is removed for more than 90% by the membrane. The MWCO values, given by the manufacturers of NF/RO membranes, are often around 150-200 g/mol. Since most organic micropollutants are also in that size range, NF/RO should be viable techniques for the removal of organic micropollutants. It was observed, however (not only in this thesis, but also in the literature), that removal of some organic pollutants with a molar mass larger than 150-200 g/mol was still insufficient.

The main reason for this is that separation, based on the size of the solutes (size exclusion), is not the only mechanism that plays a role in removal of organic solutes in membrane filtration applications. Organic solute removal is also largely influenced by other interactions between solute and membrane, namely hydrophobic (Van der Waals) and electrostatic interactions.

Hydrophobic interactions between an organic solute and the membrane surface can result in an increased or decreased partitioning of the organic solute in the membrane matrix. Organic solutes that show affinity for the membrane can partition into the membrane more easily than solutes for which solute-membrane affinity is low. This results in a decreased rejection for organic solutes with high membrane affinity. In practice, hydrophobic solutes show the most affinity for the hydrophobic

membrane surface, which results in lower rejection for hydrophobic solutes in practical applications of NF/RO, compared to hydrophilic solutes. Two different models were constructed in Chapter 2 of this thesis to assess the influence of the hydrophobic interactions (in addition to steric interactions), on the rejection of organic solutes with NF/RO.

The first model was more empirical: using a log-normal pore distribution model, different rejection curves for solutes of different hydrophobicity (expressed as  $\log K_{ow}$ ) were modelled. Rejection of hydrophilic solutes ( $\log K_{ow} < 1$ ) appeared to be mainly (only) determined by steric interactions with the membrane, whereas for hydrophobic solutes ( $\log K_{ow} > 3$ ) solute-membrane affinity resulted in lower rejection values than could be expected purely based on steric interactions. The modelled MWCO for hydrophilic solutes was located at lower molar mass values and a sharp increase in rejection at molar mass values above the MWCO was observed, whereas for hydrophobic solutes, the MWCO was located at higher molar mass values and a more gradual increase in rejection was found. Construction of a rejection curve for hydrophobic solutes was more difficult than for hydrophilic solutes and more scattering of experimental data points around the modelled curve was seen, indicating that  $\log K_{ow}$  may not be the most suitable parameter to describe solute-membrane interactions.

Since  $\log K_{ow}$  could not be used as a tool to predict removal of organic solutes, a second model was derived. The second model used a novel approach in organic solute rejection, by introducing a solute-membrane affinity-dependent partition coefficient in the traditional Spiegler-Kedem transport equation. The partition coefficient consists of a term describing solute-membrane affinity and a term describing steric hindrance. The solute-membrane affinity could be determined by

contact angle measurements and solving a set of Young-Dupré equations. Solute-membrane affinity appeared to be more significant for the most hydrophobic membrane, but did not always show a good correlation with the  $\log K_{ow}$  of the solutes.

The use of a flux independent partition coefficient turned the advanced transport model into a predictive model (incorporating solute-membrane affinity) for the rejection of uncharged organic solutes. The transport model was able to predict rejection values quite well. This contrasts with a model, purely based on size exclusion effects, which overpredicted rejection values for solutes that showed significant affinity for the membrane. Moreover, the steric model underpredicted rejection values of solutes for which repulsive Van der Waals forces between solute and membrane were present (no spontaneous transfer of the solute from the water to the membrane phase). This indicates that the membrane pore size can not be determined using purely steric models and solute-membrane affinity has to be incorporated.

In addition to steric and hydrophobic interactions, charged organic solutes can also electrostatically interact with the membrane surface. At neutral feed water pH, most membranes are negatively charged, due to the dissociation of functional groups (carboxylic acid groups) on the membrane surface. This negative surface charge leads to high rejection values of negatively charged organic solutes, due to electrostatic repulsion between solute and membrane. However, rejection of positively charged organic solutes is lower than the rejection of neutral organic solutes, due to the electrostatic interactions: charge attraction between the positively charged organic solutes and the negatively charged membrane surface leads to an

increased concentration of positively charged solutes at the negatively charged membrane surface, and thus a decreased rejection. For negatively charged organic solutes, charge repulsion leads to a decrease in concentration at the negatively charged membrane surface.

This concept is called “charge concentration polarisation” and shows good potential as a simplified modelling tool to predict the rejection of charged solutes, based on the rejection of uncharged solutes with similar physico-chemical characteristics.

It can thus be concluded that nanofiltration and reverse osmosis are valuable techniques for removal of organic micropollutants from surface waters, but removal might be limited by certain factors. Removal is limited by size: solutes with a significantly smaller size than the pore size of the membranes will not show high removal efficiencies. Removal is also limited by solute-membrane affinity: in practice, this means that removal of hydrophobic organic solutes is often lower than the rejection of hydrophilic solutes of similar size. Finally, removal might also be limited by electrostatic interactions between charged organic solutes and the charged membrane surface: rejection of organic solutes bearing a charge, opposite to the membrane surface charge, is lower, due to electrostatic attractions of the solute towards the membrane surface, leading to increased concentrations at the membrane surface and thus lower rejections.

In practice, this boils down to a problematic removal for: extremely small polar solutes (e.g. the polar micropollutant NDMA), small to medium sized hydrophobic solutes (e.g. bisphenol-A) and small, positively charged solutes (e.g. the pharmaceutical terbutaline).



A recommendation of this study would be to combine NF/RO with subsequent activated carbon filtration: this counters the more problematic removal of hydrophobic organic solutes (these are preferentially removed by the activated carbon) and, as a result of the removal of natural organic matter (NOM) in the NF/RO step, the time before regeneration of the carbon column can be prolonged considerably, since the organic load is lower. This reduces operating costs for the activated carbon considerably.

The combination of NF/RO with subsequent granular activated carbon was also investigated in this thesis and yielded satisfactory results for the removal of a wide range of organic micropollutants from two different water sources.

Removal of organic solutes in practical applications (full-scale installations) is often lower than removal in lab-scale situations. This is due to the higher feed water recovery in full-scale installations, which leads to increased feed concentrations (and thus lower rejections) in the last stages of the full-scale plant. A model to describe the decrease in rejection with increasing feed water recovery (and thus a model to describe rejection in full-scale plants, or to translate rejections from lab-scale to full-scale units) was also derived in this thesis. The modelled/predicted rejection values seemed to correspond well to experimentally determined rejection values for a cocktail of 18 pharmaceuticals, 7 pesticides and 7 organic acids on a pilot plant, operated at feed water recoveries in the range from 75 to 90%.

One major drawback of all membrane filtration applications is membrane fouling and its impact on the plant operation. It was shown in this thesis that the occurrence of membrane fouling significantly alters the membrane surface properties and, as a

consequence, rejection of organic micropollutants changes drastically in comparison with clean membranes. It was observed that a fluidized anionic ion exchange pre-treatment to remove natural organic matter (that may cause organic fouling on the membrane surface) from surface water before being fed to the NF/RO unit, resulted in the formation of a colloidal fouling layer on the membrane surface, which increased the negative surface charge of the membrane, resulting in decreased rejections for positively charged organic solutes (up to 40% decrease) and increased rejections for negatively charged organic solutes. Moreover, the flux decline caused by this colloidal fouling layer was larger than the flux decline caused by untreated surface water. These observations were made on lab-scale units. In practical applications, the influence on the flux decline and rejection will be smaller, due to the larger surface area available (resulting in a smaller load of foulants to the membrane surface), and the better hydrodynamic flow conditions in spiral wound membranes.

Another major problem with membrane filtration is that a concentrated waste stream is generated. Even though NF/RO can be applied for the removal of organic micropollutants, the micropollutants are not really removed, but are concentrated in the concentrate (brine) stream. For drinking water utilities, it is necessary to know the concentration of organic micropollutants in this concentrate stream to know whether the stream can be discharged to the surrounding environment, or whether it has to be treated first. The models constructed in this thesis allow to determine removal of organic micropollutants in full-scale NF/RO applications and, once this removal is known, also the concentrations in the concentrate stream are known. Ongoing research is focusing on ways to increase the feed water recovery of full-scale NF/RO plants (e.g. by removing multivalent ions, that could cause scaling, from the feed

water (using ion exchange resins or other techniques)). It has to be kept in mind, however, that rejection of organic micropollutants decreases with increasing feed water recovery (due to the internal increase in concentration). In the end, utilities will have to find an optimal balance between a satisfactory removal of organic micropollutants and an increased feed water recovery (a smaller concentrate volume).

## **2. Recommendations for future research**

Even though all solute-membrane mechanisms that determine rejection of organic solutes with nanofiltration/reverse osmosis have been unravelled and mathematically described, some aspects of rejection still need some attention:

- It might be interesting to develop a new and fast method to describe solute-membrane affinity for solid organic solutes. For liquid organic solutes, solute-membrane affinity can easily be determined from contact angle measurements, but this is not feasible for solids. Determining interfacial tension from the solute's aqueous solubility might be an option.
- In order to gain even more insight on solute-membrane interactions (e.g. hydrophobic and electrostatic interactions), a better characterisation of the membranes is essential. The model to predict rejections of charged organic solutes uses the membrane zeta-potential as an approximation of the real membrane potential. Zeta-potential is not a real physical parameter, and determination of the zeta-potential from streaming potential/streaming current measurements is not always accurate and reproducible. Moreover, no standards exist for comparison. Also, determination of solute-membrane

affinity from contact angle measurements is feasible, but time-consuming. If the exact chemical composition of the membranes would be known, it would be easier to calculate molecular interactions between solute and membrane (e.g. with molecular modelling software) and predictions of solute rejection.

- Continuing on the previous point on better characterisation of membranes: synthesis of new, nano-engineered membranes provides unlimited possibilities to tweak membrane surface properties and provide membranes that are better suited for organic micropollutant removal (e.g. more hydrophilic membranes, as studied in Chapter 6). Lee et al. (2008) [1] also made an attempt to improve membrane rejection properties for organic solutes, while retaining a high pure water permeability and high selectivity for removal of salts. A better knowledge of the process of membrane formation allows to better know (and control) surface composition and surface properties.
- To better understand effects of membrane fouling on rejection of organic micropollutants, more insight in the interactions between foulant material and the membrane surface is necessary. If more knowledge is available on the type of foulant deposited on the membrane surface, it might be easier to predict the influence of these deposits on membrane surface properties and thus on rejection. Again, a better characterisation of the membrane surface, but also of the composition of the feed water is necessary. Especially a better characterisation of the natural organic matter in the feed water might help to gain more insight in which fractions of the NOM actually cause the fouling of the membrane surface and how the membrane surface properties will change with the deposition of these fractions. The construction of new membrane materials might help here as well, by choosing/constructing the right

membrane surface parameters to improve the fouling resistance or reduce the interactions between the foulants and the membrane surface.

- The effect of a fluidized anionic ion exchange pretreatment on the fouling of NF/RO membranes, and consequently the influence on organic solute/organic micropollutant rejection, needs to be studied in more detail. If the use of this pretreatment step also results in increased fouling for other water types with other membranes, it might not be useful to use this technique as pretreatment to remove natural organic matter before NF/RO installations.
- The influence of the feed water matrix on both fouling and removal of organic micropollutants is particularly important in waste water reuse applications for (in)direct potable reuse, which is becoming an increasingly popular application for NF/RO in drought-prone regions. Not only the complex (and sometimes varying) composition of the background organic matter matrix is of interest here, but also the higher feed concentrations of organic micropollutants (by an incomplete metabolism in the human body, these pollutants enter the sewage system) are a challenge and increase the need for high removal efficiencies.
- Finally, the concentrate problem remains one of the most important drawbacks of membrane filtration applications. Measures and techniques to reduce this concentrate stream thus deserve special attention. Especially concepts of zero liquid discharge (ZLD) might be of interest. One way to reduce concentrate volume is to increase the feed water recovery of the installation, by removing scaling ions prior to the NF/RO unit. This is already a challenge on its own, but the removal of organic micropollutants at high recoveries might also become problematic. Therefore, high recovery NF/RO and removal of organic micropollutants at these high recoveries should be studied in more detail.

## References

- [1] J.-H. Kim, P.-K. Park, C.-H. Lee and H.-H. Kwon, Surface modification of nanofiltration membranes to improve the removal of organic micropollutants (EDCs and PhACs) in drinking water treatment: Graft polymerization and cross-linking followed by functional group substitution, *Journal of Membrane Science*, in press (2008), doi:10.1016/j.memsci.2008.04.055.

# List of publications

## International refereed journals

- B. Van der Bruggen, A.R.D. Verliefde, L. Braeken, E.R. Cornelissen, K. Moons, J.Q.J.C. Verberk, J.C. van Dijk and G.L. Amy, Assesment of a semi-quantitative method for estimation of the rejection of organic compounds in aqueous solution in nanofiltration, *Journal of Chemical Technology and Biotechnology*, 81 (2006) 1166.
- A.R.D. Verliefde, N. Van Vliet, G.L. Amy, B. Van der Bruggen and J.C. van Dijk, A semi-quantitative method for prediction of the rejection of uncharged organic micropollutants with nanofiltration, *Water Practice & Technology*, 1 (4) (2006).
- A.R.D. Verliefde, E.R. Cornelissen, G.L. Amy, B. Van der Bruggen and J.C. van Dijk, Priority organic micro pollutants in water sources in Flanders and The Netherlands, and assessment of removal possibilities with nanofiltration, *Environmental Pollution*, 146 (1) (2006) 281.
- A.R.D. Verliefde, E.R. Cornelissen, S.G.J. Heijman, G.L. Amy, B. Van der Bruggen and J.C. van Dijk, Influence of electrostatic interactions on the rejection with NF and assessment of the removal efficiency during NF/GAC treatment of pharmaceutically active compounds in surface water, *Water Research*, 41 (15) (2007) 3227.
- A.R.D. Verliefde, E.R. Cornelissen, S.G.J. Heijman, G.L. Amy, B. Van der Bruggen and J.C. van Dijk, Rejection of trace organic pollutants with high pressure membranes (NF/RO), *Environmental Progress*, (2007) in press.
- S.G.J. Heijman, A.R.D. Verliefde, E.R. Cornelissen, G.L. Amy and J.C. van Dijk, Influence of NOM-fouling on the removal of pharmaceuticals by NF and activated carbon filtration, *Water Science & Technology: Water Supply*, 7 (4) (2008) 17.
- A.R.D. Verliefde, E.R. Cornelissen, S.G.J. Heijman, J.Q.J.C. Verberk, G.L. Amy, B. Van der Bruggen and J.C. van Dijk, The role of electrostatic interactions on the rejection of organic solutes in aqueous solutions with nanofiltration, *Journal of Membrane Science*, (2008) in press, doi:10.1016/j.memsci.2008.05.022

## Publications in preparation

- A.R.D. Verliefde, E.R. Cornelissen, S.G.J. Heijman, G.L. Amy, B. Van der Bruggen and J.C. van Dijk, The influence of hydrophobic interactions on the rejection of uncharged solutes by nanofiltration/reverse osmosis, to be submitted to Water Research.
- A.R.D. Verliefde, E.M.V. Hoek, E.R. Cornelissen, S.G.J. Heijman, G.L. Amy, B. Van der Bruggen and J.C. van Dijk, A predictive model for the rejection of uncharged solutes by nanofiltration/reverse osmosis – incorporation of solute-membrane (hydrophobic) interactions, in preparation for Environmental Science & Technology.
- A.R.D. Verliefde, E.R. Cornelissen, S.G.J. Heijman, G.L. Amy, I. Petrinic, T. Luxbacher, B. Van der Bruggen, and J.C. van Dijk, The influence of colloidal and organic fouling on the removal of trace organic pollutants with nanofiltration, to be submitted to Journal of Membrane Science.
- A.R.D. Verliefde, E.R. Cornelissen, S.G.J. Heijman, G.L. Amy, B. Van der Bruggen and J.C. van Dijk, Construction and validation of a predictive model for the rejection of trace organic pollutants in full-scale nanofiltration/reverse osmosis installations, to be submitted to Journal of Membrane Science.
- A.R.D. Verliefde, X. Huang, X. and E.M.V. Hoek, Rejection of organic solutes with nano-composite reverse osmosis membranes: comparison with a commercial reverse osmosis membrane, in preparation for Desalination.
- A.R.D. Verliefde, E.R. Cornelissen, S.G.J. Heijman, G.L. Amy, B. Van der Bruggen and J.C. van Dijk, Practical applications of the combination NF/RO with granular activated carbon for removal of organic micropollutants, to be submitted to Drinking Water Engineering & Science.

### **Conference proceedings**

- J.Q.J.C. Verberk, A.R.D. Verliefde, B. Van der Bruggen and J.C. van Dijk, Air sparging in capillary nanofiltration, Water Intelligence Online, 4 (2005).
- J.Q.J.C. Verberk, A.R.D. Verliefde, B. Van der Bruggen and J.C. van Dijk, Air sparging in capillary nanofiltration, M. Van Loosdrecht and J. Clemens (Eds.), A selection of papers from the 2nd IWA Leading-Edge Conference on Water and Wastewater Treatment Technologies, International Water Association, London, (2006) 32.
- A.R.D. Verliefde, E.R. Cornelissen, J.A.M.H. Hofman, B. Van der Bruggen and J.C. van Dijk, J.C., Modelling of removal of organic micropollutants by nanofiltration, T Melin & J Pinnekamp (Eds.), Membrantechnik in der wasseraufbereitung und abwasserbehandlung, 6 (2005) W15-1.



- A.R.D. Verliefde, E.R. Cornelissen, G.L. Amy, B. Van der Bruggen and J.C. van Dijk, A QSAR QSPR-Methodology for rejection of trace organic pollutants in nanofiltration, AWWA Water Quality Technology Conference, Quebec City, November 2005.
- E.R. Cornelissen, A.R.D. Verliefde, J.A.M.H. Hofman and S.G.J. Heijman, Verification of a NF retention model for organic contaminants in drinking water sources, AWWA Water Quality Technology Conference, Quebec City, November 2005.
- A.R.D. Verliefde, E.R. Cornelissen, S.G.J. Heijman, B. Van der Bruggen and J.C. van Dijk, Modelling of removal of organic micro pollutants by nanofiltration, Workshop Developments in Drinking water Treatment Modelling, TU Delft, June 2006.
- A.R.D. Verliefde, N. Van Vliet, G.L. Amy, B. Van der Bruggen and J.C. van Dijk, A Semi-Quantitative Method for Prediction of the Rejection of Uncharged Organic Micropollutants with Nanofiltration, IWA World Water Congress, Beijing, September 2006.
- A.R.D. Verliefde, S.G.J. Heijman, G.L. Amy, B. Van der Bruggen and J.C. van Dijk, Influence of hydrophobicity and charge on removal of trace organic pollutants with high pressure membranes, AWWA Water Quality Technology Conference, Denver, November 2006.
- A.R.D. Verliefde, S.G.J. Heijman, E.R. Cornelissen, G.L. Amy, B. Van der Bruggen and J.C. van Dijk, Removal of pharmaceutically active compounds from surface water, AWWA Membrane Technology Conference, Tampa Bay, March 2007.
- S.G.J. Heijman, A.R.D. Verliefde, E.R. Cornelissen, G.L. Amy and J.C. van Dijk, Influence of NOM-fouling on the removal of pharmaceuticals by NF and activated carbon filtration, IWA International Membrane Conference, Harrogate, May 2007.
- A.R.D. Verliefde, S.G.J. Heijman, E.R. Cornelissen, G.L. Amy, B. Van der Bruggen and J.C. van Dijk, Rejection of trace organic pollutants with high pressure membranes (NF/RO), North American Membrane Society, Orlando, Florida, May 2007.
- A.R.D. Verliefde, E.R. Cornelissen, S.G.J. Heijman, B. Van der Bruggen and J.C. van Dijk, Rejection of pharmaceutically active compounds with NF: influence of hydrophobicity, charge and fouling. T Melin & J Pinnekamp (Eds.), *Membrantechnik in der wasseraufbereitung und abwasserbehandlung*, 7 (2007) W9-1.

A.R.D. Verliefde, E.R. Cornelissen, S.G.J. Heijman, G.L. Amy, B. Van der Bruggen and J.C. van Dijk, Removal of trace organic pollutants with NF/RO membranes: construction and validation of a rejection model, Accepted for oral presentation at the International Conference on Membranes (ICOM), Honolulu, July 2008.

### **National publications**

Arne Verliefde, Leo Puijker, Bart Van der Bruggen en Hans van Dijk, Organische microverontreinigingen en de watervoorziening, H<sub>2</sub>O, tijdschrift voor water, 38 (7) (2005) 54.

Arne Verliefde, Bas Heijman, Wim Hijnen en Guus Ijpelaar, Relevante nieuwe kennis in Denver voor Nederlandse drinkwatersector, H<sub>2</sub>O, tijdschrift voor water, 39 (24) (2006) 6.

Arne Verliefde en Victor Yangali-Quintanilla, Removal of pharmaceuticals with NF and RO, Delft Cluster magazine (Drinking water: transfer of knowledge), 5 (2008).



# Curriculum vitae

Arne Roel Dirk Verliefde was born in Knokke-Heist; Belgium on September 22th, 1981. After finishing secondary school in the beautiful city of Bruges (Sint-Jozef Humaniora) in 1999, he started his studies of Chemical Engineering at the University of Leuven. From September to December 2003, he carried out research at Delft University of Technology for his Master's thesis, entitled "Air Sparging in capillary nanofiltration" under guidance of Jasper Verberk, Hans van Dijk and Bart Van der Bruggen. After graduating *cum laude* in July 2004, he started his Ph.D. research at Delft University of Technology on "Rejection of trace organic pollutants with high pressure membranes", in co-operation with Kiwa Water Research and the University of Leuven.

